2015

Olefin Metathesis by Supported Metal Oxide Catalysts

Soe Lwin
Lehigh University

Olefin Metathesis by Supported Metal Oxide Catalysts

by

Soe Lwin

Presented to the Graduate and Research Committee

Of Lehigh University

in Candidacy for the Degree of

Doctor of Philosophy

In

Chemical Engineering

May 2015

Copyright

CERTIFICATE OF APPROVAL

Approved and recommended for acceptance as a dissertation in partial fulfillment for the degree of Doctor of Philosophy

_____ _____

Acceptance Date

Professor Israel E. Wachs
Lehigh University
Committee Chair and Dissertation Advisor

Committee members:

_____ _____

Professor James T. Hsu
Lehigh University

Dr. Javier X. Guzman
ExxonMobil

_____ _____

Professor Hugo S. Caram
Lehigh University

Dr. Xingtao Gao
BASF

_____

Professor Jonas Baltrusaitis
Lehigh University

ACKNOWLEDGEMENTS

I would like to thank my adviser, Prof. Israel E. Wachs for accepting me into his group. Working with him is one of the best decisions I have made in my life and I am eternally grateful. He is not only a great mentor but also a good friend to me. He has been very patient with me in teaching how to do great research, how to live life well and how to improve my critical thinking skills. I would not be the same without ever meeting him.

I also gratefully acknowledge funding from the U.S. Department of Energy-Basic Energy Sciences (FG02-93ER14350) and the National Science Foundation (CHE 1301262). Those are results of the proposals that I wrote with Prof. Wachs and we are very proud of the success of these proposals.

I would like to thank my PhD committee members. Prof. Caram has been a good mentor to me since my undergraduate years. I cannot believe it is almost 10 years now since we first met. Prof. Hsu would not mind with me applying late to Lehigh and readily accepted me into the PhD program. Without his admission, I would not be where I am now. Prof. Baltrusaitis is also very patient with me to find time to be my committee member. Xingtao, according to Prof. Wachs, is the most accomplished member of our group, and I am much honored to have her in my committee. My first encounter with her was in 2011 during Chip Roberts' PhD defense and we have had great conversations ever since. My first meeting with Javier was in Kansas in 2008 and unexpected events of life fortunately brought us closer again as I got to meet him in 2012 during the annual NYCS

symposium. He would always stop by at my posters during not only NYCS but also operando and GRC conferences and made himself available to be on my committee.

I would like to thank my fellow group members. Dr. Chris Keturakis is my favorite member of the group and taught me how to use and fix equipment during my times here. He would readily provide his insights on every question that I have both on conducting experiments and interpretation of results. A special thank is also due to Minghui Zhu who would help me countless times with fixing the issues involving the TPSR system. I would also like to thank my other group lab mates, Dr. Chip Roberts, Dr. Kevin Doura, Dr. Julie Molinari, Dr. Somphonh Phivilay, Dr. Yadan Tang, Dr. Michael Ford, Anisha Chakrabarti and Dongchang Qin.

I would also like to thank my collaborators around the globe. It is unfortunate that some of their data did not make my thesis for a variety of reasons but I am very fortunate to have worked with them. Their stat-of-the-art experiments and theoretical calculations take me to unexplored areas of research that did not previously exist to me. An early collaboration with Dr. Nikolaos Soultanidis of ExxonMobil (formerly of Rice) made me get interested in this metathesis project and he has been a great friend to me ever since. The author would also like to thank Dr. Kazuhiko Amakawa of Mitsubishi Chemical (formerly of Fritz-Haber Institute) for donation of his MoO_x/SBA-15 catalysts and helpful discussions, Dr. Ned Marinkovic and Dr. Syed Khalid of Brookhaven National Laboratory and Prof. Anatoly Frenkel of Yeshiva University for *in situ* XAS (XANES/EXAFS) experiments, Prof. Philippe Sautet of Université de Lyon and Prof. Jaroslaw Handzlik of Cracow University of Technology for DFT calculations, Maxence Valla and Prof. Christophe Coperet of ETH Zurich for *in situ* NMR experiments, Dr.

Jurek Krzystek of National High Magnetic Field Laboratory and Prof. Albert Stiegman of Florida State University for HFHF EPR experiments and Prof. Franklin Tao of University of Notre Dame for *in situ* AP-XPS experiments.

Last but not least, I would like to thank my parents, brother, relatives and friends for their continued support, guidance and unconditional love over these long years. There will be a time when I make them proud and we have worked very hard for a long time to arrive at this moment in life. One brother, five cousins and four close friends passed away in the past decade. Tough times really do demand tough measures. Political conflicts, civil wars and fragile economies scattered my high school friends and some of them may not even be alive. Those were the best times of my life and I would like to meet them again before my last breadth.

TABLE OF CONTENTS

LIST OF TABLES

LIST OF FIGURES

(triphenylphosphine) rhenium(+5) (orange) and crystalline bulk ReO_3 (black) compounds.

Figure 2.4. *In situ* Raman spectra (442nm) of dehydrated supported 3% and 9.4% ReO_x/Al_2O_3 (H) catalysts at 100°C. The inset shows the 900-1100 cm^{-1} region.

Figure 2.5. *In situ* Raman spectra (442nm) of 3% ReO_x/Al_2O_3 (ReO_x-I) (H) at 200°C during ^{18}O-^{16}O isotope exchange by exposure to $H_2{}^{18}O$ vapor.

Figure 2.6. *In situ* Raman spectra (442nm) of supported 9.36% $ReO_x/10\%Ta_2O_5/Al_2O_3$ (ReO_x-II) (E) at 200°C during ^{18}O-^{16}O isotope exchange with $H_2{}^{18}O$ vapor.

Figure 2.7. *In situ* IR spectra of the surface hydroxyl region of dehydrated supported ReO_x/Al_2O_3 (E) catalysts as a function of rhenia loading at 200°C. The blue color represents ReO_x-I and the green color represents ReO_x-II.

Figure 2.8. *In situ* Raman spectra (442nm) of the (a) $3\%ReO_x/Al_2O_3$ (H), (b) $9.4\%ReO_x/Al_2O_3$ (H) and (c) $5\%ReO_x/15\%TaO_x/Al_2O_3$ (E) catalysts during propylene metathesis at 70°C up to 120 minutes. The catalyst was reoxidized in 10% O_2/Ar at 550°C after the reaction.

Figure 2.9. DFT optimized structures and relative energies for the surface Re^{+7} oxide species supported on (110) γ-alumina. Bond lengths are given in Å.

Figure 2.10. Steady-state catalytic performance for propylene metathesis at 70°C by supported ReO_x/Al_2O_3 (blue squares) and $ReO_x/\%15\%TaO_x/Al_2O_3$ (green squares) catalysts that were dehydrated in flowing O_2/Ar at 500°C for prior to reaction at 70°C. The reaction was performed with ReO_x catalysts supported on Al_2O_3 (E). The dashed line indicates the x-axis shift for ReTaAl catalysts to show the promotion effect of the surface

TaO_x species. The slight offset may be due to experimental error such as volatilization of ReO_x at higher loading.

Figure 2.11. Comparison of estimated surface ReO_4-II concentration as a function of Re loading for supported ReO_x/Al_2O_3 catalysts that have been reported in the literature. The solid line indicates the concentration of surface ReO_4-II species as a function of Re coverage on alumina determined in the present study. The concentration of surface ReO_x-II species for other experimental data is estimated from the solid line generated in the present study. The studies reporting surface rhenia coverage higher than maximum of 2.2Re/nm^2 did not account for volatility of rhenia above this loading and, thus, can only contain a maximum of ~2.2 Re/nm^2.

Figure S2.1. UV Vis spectra of the solid Re_2O_7 reference

Figure S2.2. DFT optimized structures and relative energies for the surface Re^{+7} oxide species supported on (100) γ-alumina. Bond lengths are given in Å.

Figure S2.3. Energy analysis for the surface Re species: deformation energies of the protonated alumina surface ($E_{def}((Al_2O_3)_nH^+)$) and ReO_4^- fragment ($E_{def}(ReO_4^-)$), in the surface complex structure, corresponding interaction energies (E_{int}) between these deformed fragments and $HReO_{4(g)}$ adsorption energies (E_{ads}) to form the surface Re oxide species on (100) and (110) planes of Al_2O_3.

Figure S2.4. Schematic structure of reference compounds. The short form indicates the number of Re=O bonds in the corresponding compound.

Figure S2.5. Raw data of (a) all the reference compounds and (b) dehydrated supported $ReOx/Al_2O_3$ catalysts in k-space

Figure 3.14. Production of $C_3^=$ from $C_2^=$ titration of surface intermediates resulting from $C_4^=$ adsorption (60 minutes at 30^{o}C) as a function of Ar flushing time (0-240 minutes) between $C_4^=$ adsorption and $C_2^=$ titration, (a) as a function of time at 30°C (x-axis corresponds to the time of $C_2^=$ flow) and (b) during TPSR.

Figure 3.15. Production of $C_3^=$ from $C_2^=$ titration of surface intermediates resulting from $C_4^=$ adsorption (60 minutes at 30^{o}C) as a function of $C_2^=$ partial pressure (a) as a function of time at 30°C (x-axis corresponds to the time of $C_2^=$ flow) and (b) during TPSR.

Figure 3.16. Evolution of $C_3^=$ during $C_2^=$ titration of surface intermediates resulting from $C_4^=$ adsorption (60 minutes at 30^{o}C) as a function of $C_4^=$ activation temperature (30-300^{o}C), (a) titration at 30°C (x-axis corresponds to the time of $C_2^=$ flow) and (b) titration during TPSR.

Figure 3.17. Evolution of $C_3^=$ during $C_2^=$ titration of surface intermediates resulting from $C_4^=$ adsorption (60 minutes at 30^{o}C) as a function of ReO_x loading. The x-axis corresponds to the time of $C_2^=$ flow at 30^{o}C.

Figure 3.18. Number of $C_3^=$ molecules produced from titration of surface intermediates created by $C_4^=$ adsorption with $C_2^=$ as a function of ReO_4 loading on Al_2O_3. The y-axis is normalized by taking the number of $C_3^=$ molecules produced and dividing by the total number of ReO_4 sites to yield a percentage.

Figure S3.1. C_4= desorption profile during 0-240 minutes of Ar flush. In the 0 minute experiment, 1%C_2=/Ar was flown immediately.

Figure S3.2. Time resolved evolution of products during metathesis of 1% $C_2^=$/Ar and 1% $C_4^=$/Ar to $C_3^=$ from the supported 15.6ReAl catalyst at 30°C.

Figure S4.1. TPSR signals of (a) C_3H_6 and (b) C_2H_4 in flowing Ar after 100, 125 and 150°C C_3H_6 pre-treatment and room temperature C_2H_4 adsorption (separate experiments).

Figure S4.2. TPSR signals of (a) C_2H_4 (top) and (b) C_4H_8 (bottom) in flowing Ar after various desorption temperature treatments. The full experimental procedure can be found in section 2.3.5.

Figure S4.3. Plot of ln ($C_0T_p^2$) against $1/T_p$ to give a slope of E_a/R for the second order desorption kinetics.

Figure S4.4. TPSR in flowing different gases after 100°C C_3H_6 pretreatment and cooling to room temperature in Ar: (a) in C_3H_6 and (b) in C_2H_4 (blue) and Ar (red).

LIST OF ILLUSTRATIONS (SCHEMES)

ABSTRACT

Olefin metathesis is considered to be a green route to production of olefins due to its high selectivity towards desired products. Due to their ease of preparation and catalyst lifetimes, heterogeneous supported metal oxide catalysts such as ReO_x, MoO_x and WO_x are used at large scale industrial applications. Despite decades of catalysis research, the exact nature of catalytic active sites, reaction intermediates and kinetics are not well understood because of lack of modern characterization techniques in the past and absence of detailed knowledge at the molecular level. Extensive *in situ* and *operando* spectroscopy (Raman, UV vis, XAS and IR) experiments, theoretical DFT calculations, steady-state kinetics and temperature programmed surface reaction (TPSR) studies were undertaken *for the first time* to obtain unprecedented insights about the catalytic active sites (their anchoring sites, coordination and oxidation states), reaction intermediates, olefin adsorption/desorption/reaction and kinetics to unravel the fundamental molecular structure-reactivity relationships.

The supported ReO_x/Al_2O_3 system is the most reactive among the heterogeneous supported metal oxide catalysts. The long standing debates surround the nature of ReOx species, number of reactive intermediates and kinetics of this catalytic system. *In situ* ^{18}O-^{16}O Raman experiments along with *in situ* XAS and theoretical DFT calculations of the initial catalyst show that rhenia exists on the Al_2O_3 support as two distinct isolated surface ReO_4 species with dioxo coordination. The two structures are related to their anchoring at different surface hydroxyl sites on the alumina support. The surface ReO_4-I species on basic alumina sites were found to be stable and difficult to activate with propylene while

the surface ReO_4-II species on acidic alumina sites were found to be easily activated with propylene. This information allowed *for the first time* the use of acidic promoters to block formation of the inactive surface ReO_4-I species and design catalysts with only active surface ReO_4-II species.

During activation with propylene, *in situ* UV-vis and XAS spectroscopy revealed that the surface ReO_4-II species become partially reduced, mostly to Re^{+5} species, by forming the oxygenated CH_3CHO and HCHO products (pseudo-Wittig mechanism). Subsequent reaction of the partially reduced Re^{+5} species with propylene oxidizes rhenia back to reactive Re^{+7}-carbenes ($Re{=}CH_2$, $Re{=}CHCH_3$, etc.). The surface Re^{+7}-carbenes are reactive at room temperature and in equilibrium with the gas phase olefins. Consequently, removal of the gas phase olefins significantly diminishes the concentration of reactive surface Re^{+7}-carbenes by about an order of magnitude. This accounts for the low number of reactive intermediates reported in earlier studies that evacuated the catalysts prior to titrating the reactive intermediates.

Two types of surface intermediates were found to be present: weakly adsorbed that reacts at room temperature and strongly adsorbed π-complexes that reacts at high temperatures (>100^{o}C). The weakly adsorbed Re-carbenes are dynamic and in equilibrium with the gas phase. The strongly adsorbed π-complexes are not dependent on the gas phase composition and only react with olefins at elevated temperatures. TPSR studies showed that the weakly bound Re-carbenes follows a unimolecular reaction mechanism while the strongly bound π-complexes follow a bimolecular reaction mechanism. The olefin metathesis steady-state kinetics is affected by these intermediates: first-order in propylene partial pressure at low temperatures (<70^{o}C) and second-order in propylene partial

pressure at high temperatures (>140^{o}C). C_3H_6/C_3D_6 TPSR studies also demonstrated that the rate-determining-step does not involve C-H bond breaking and all olefins share the same rate desorption rate.

These new unprecedented insights are able to resolve the confusing claims that existed for decades in literature.

CHAPTER 1

Literature Review of Olefin Metathesis by Supported Metal Oxide Catalysts

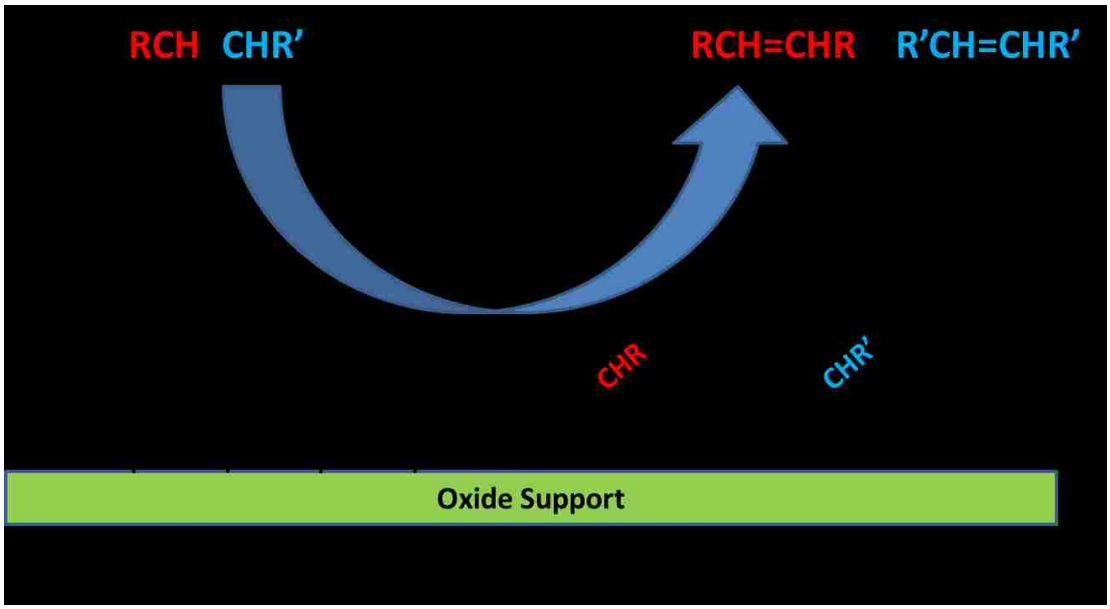

Abstract

The literature of olefin metathesis by heterogeneous supported catalysts, both industrial-type supported metal oxides (ReO_x/Al_2O_3, $ReO_x/(SiO_2$-$Al_2O_3)$, MoO_x/SiO_2, MoO_x/Al_2O_3, $MoO_x/(SiO_2$-$Al_2O_3)$, WO_x/SiO_2 and $WO_x/(SiO_2$-$Al_2O_3)$) and supported organometallic complexes, is comprehensively reviewed. The focus of the review is supported metal oxide catalysts, but the well-defined supported organometallic catalyst literature is also covered since such model catalysts have the potential to bridge heterogeneous and homogenous olefin metathesis catalysis. The recent world shortage of small olefin feedstocks has created renewed interest in olefin metathesis as a route to synthesizing small olefins and is reflected in the recent growth of the patent literature. In

spite of the extensive application of supported metal oxides in industry for metathesis of small and large olefins, the molecular structures and oxidation states of the catalytic active sites, surface reaction intermediates and reaction mechanisms of this important catalytic reaction have still not been resolved. The absence of reported *in situ* and *operando* spectroscopic studies from the olefin metathesis catalysis literature has hampered progress in this area. It appears from this literature review that the topic of olefin metathesis by heterogeneous supported metal oxide catalysts is still a relatively undeveloped research area and is poised for significant progress in understanding of the fundamental molecular details of these important catalytic systems in the coming years.

1. Introduction

The olefin metathesis reaction was discovered by Anderson and Merckling at Dupont in 1955 when norbornene was polymerized to polynorbornene using lithium aluminum tetraheptyl and titanium tetrachloride catalysts[1] and would later be known as ring opening metathesis polymerization.[2] Another Dupont researcher Eleuterio found in 1956 that ethylene, propylene and butenes were produced when propylene was passed over an alumina-supported molybdena catalyst.[2] Natta independently discovered the ring opening metathesis polymerization of cyclopentene with a molybdenum chloride catalyst.[3] Banks and Bailey of Philips Petroleum discovered that silica-supported tungsten oxide catalysts efficiently perform olefin metathesis of small olefins[4] and in 1964 pioneered the first large scale olefin metathesis industrial process called 'Phillips Triolefin Process' that converted propylene to ethylene and 2-butene.[4,5] That same year, a patent was awarded to British Petroleum (BP) for disproportionation of short and long chain olefins using supported Re_2O_7/Al_2O_3 catalysts.[6] Scientists at Shell discovered the

formation of liner alpha-olefins via ethylene oligomerization and olefin metathesis in 1968 that subsequently led to commercialization of the Shell Higher Olefin Process (SHOP) in 1977 by supported molybdenum oxide on alumina catalysts.[7] Calderon and coworkers at Goodyear introduced the term 'olefin metathesis' from the Greek words 'meta' (change) and 'thesis' (position)[8] after observing production of 3-hexene and 2-butene from the self-reaction of 2-pentene in the presence of a homogeneous tungsten hexachloride catalyst. There is much renewed interest in olefin metathesis to meet the world's shortage of propylene, via metathesis of ethylene and 2-butene, and production of sustainable, green products.[5,7,9,10-12]

The fascinating olefin metathesis reaction inter-converts C=C bonds in hydrocarbons and can be tailored to produce a hydrocarbon of any length. It can be summarized as[9]

$2RCH{=}CHR' \leftrightarrows RCH{=}CHR + R'CH{=}CHR'$

in which R and R' are (functionalized) alkyls or hydrogen atoms.

The three most common types of olefin metathesis reactions are (1) cross-metathesis (exchange of double bonds between linear olefins), (2) ring opening metathesis polymerization (opening of a closed olefin ring followed by polymerization) and (3) ring closing metathesis (opposite of ring opening metathesis).[9,10] The versatility of this novel reaction opened up new chemical routes that resulted in industrial applications of important petrochemicals, oleochemicals, polymers and specialty chemicals.[5,10-12] These commercial applications have sparked a tremendous growth in basic research of this field over the past few decades that culminated in the 2005 Nobel Prize in Chemistry to

Chauvin, Grubbs and Schrock for their fundamental contributions to the development of catalytic olefin metathesis in organic synthesis.[12]

The initial olefin metathesis catalysts developed in the early years were poorly defined multicomponent homogeneous and heterogeneous systems. To address this issue, extensive basic organometallic chemistry research was performed to obtain better fundamental insights into the olefin metathesis reaction.[2,4,11] Employing homogeneous well-defined single-component organometallic catalysts, it was elegantly shown that olefin metathesis proceeds via metal carbene complexes.[13] More recently, surface organometallic chemistry was also successfully employed to synthesize well-defined heterogeneous model supported tungsten, molybdenum and rhenium organometallic catalytic active sites that exhibit high catalytic activity.[14] Density Functional Theory (DFT) calculations have been performed on the model catalyst systems to understand the nature of the catalytic active sites and reaction mechanism at the molecular level.[15-19] In contrast to the progress achieved with well-defined organometallic catalysts, there has been only limited progress for heterogeneous metathesis catalysts because the nature of the catalytic active sites typically has not been identified. The major industrial olefin metathesis processes, however, employ heterogeneous supported metal oxide catalysts (supported rhenia, molybdena and tungsta on Al_2O_3, SiO_2 and SiO_2-Al_2O_3 catalyst systems).[2,4,7,9-11] This literature review will focus on olefin metathesis by heterogeneous catalysts to highlight what is currently known and what more needs to be done to fully understand the heterogeneous olefin metathesis catalytic systems.

Supported metal oxide catalysts consist of an active metal oxide component dispersed on an inactive oxide support.[20,21] The dispersed metal oxide, the active

component, can be present as isolated surface species, oligomeric surface species, clusters (< 1nm) or crystalline nanoparticles on a high surface area oxide support (~100-500 m^2/g).[21]

2. Initiation Mechanisms. Formation of the initial metal carbene species during olefin metathesis is claimed to proceed through one or more of the four initiation mechanisms as shown in scheme 1.1 for supported metal oxide catalysts.[22-24] All of the olefin metathesis initiation pathways except the pseudo-Wittig mechanism involve an oxidative addition reaction in which the catalytic active center is oxidized by losing two electrons.

3. Reaction Mechanism. The reaction mechanism for propylene metathesis was proposed by Chauvin based on the results of homogeneous catalysis.[13,25] It was subsequently supported by olefin titration results with supported rhenia/alumna catalysts. In these experiments, the supported rhenia/alumina catalyst was first activated with propylene or 2-butene. The surface intermediates were subsequently titrated with a second olefin (ethylene, propylene or 2-butene) to form mixed olefin reaction products with deuterated olefins confirming the mixed products. For example, 2-butene adsorption followed by ethylene adsorption produced propylene and some 2-butene reaction. The same number of sites were obtained by reacting either propylene or 2-butene with ethylene and would not have been the case if metal carbenes and metallacyclobutanes were not reaction intermediates, as shown in scheme 1.2.[25]

4. Supported ReO_x Systems

ReO_x/Al_2O_3

ReO_x in Initial Oxidized Catalyst. Supported ReO_x/Al_2O_3 heterogeneous catalysts are prepared by impregnation of an aqueous rhenia precursor ($HReO_4$, $(NH_4)ReO_4$, etc.) on the alumina support, then dried and calcined at elevated temperatures in an oxidizing environment. The crystalline Re_2O_7 low melting temperature of 297°C assures that rhenium oxide becomes homogeneously dispersed on the alumina support during calcination at ~500°C. The supported rhenia/alumina catalyst system has been studied in its initial oxidized state under oxidizing dehydrated conditions prior to activation and exposure to the olefin metathesis reaction conditions, but there is still not complete agreement about the structure of surface rhenium oxide species and oxidation states. Early characterization with electron microscopy did not detect crystalline Re_2O_7 nanoparticles and concluded that if crystallites were present they would have to be less than 2 nm.[26] Initial *in situ* Raman and IR studies of supported ReO_x/Al_2O_3 catalysts determined that crystalline Re_2O_7 nanoparticles were not present and assigned the detected vibrations to dimeric surface $(O=)_3$-Re-O-Re$(=O)_3$ species.[27,28] Subsequent *in situ* Raman and IR studies demonstrated that the vibrations correspond to two distinct isolated surface $(O=)_3$Re-O-Al trioxo sites on the alumina support, with the relative concentration of the second species increasing with surface rhenia coverage.[29,30] *In situ* IR spectroscopy measurements also revealed that at low rhenia loadings, surface ReO_x reacts first by consuming the most basic surface OH groups and at higher loadings the surface ReO_x consumes moderate and more acidic surface hydroxyls.[29,31,32] The different anchoring sites on the alumina surface account for the presence of two distinct surface ReO_x species on

alumina.[29] As a consequence of the volatilization of rhenia oligomers,[29-31] rhenia is completely dispersed as isolated species on the surface of oxide supports. The molecularly dispersed nature of supported rhenia sites on high surface area oxide supports assures that all characterization techniques, surface as well as bulk, only provide surface information about the supported ReO_x sites. *In situ* X-ray Absorption Near Edge Spectroscopy (XANES) studies concluded that surface rhenia on alumina under dehydrated, oxidizing conditions is present as Re^{+7} with trioxo $(O=)_3ReO$ coordination[33,34] as shown in Figure 1.1a. More recent *in situ* XANES/EXAFS and DFT calculations concluded that the fully oxidized surface rhenia species may possess dioxo $(O=)_2Re(\text{-}O\text{-}Support)_3$ penta-coordination[35] on Al_2O_3 as shown in Figure 1.2b. The fitting of EXAFS data with only one surface ReO_x structure when *in situ* Raman and IR spectroscopy show that there are two distinct surface ReO_x species is problematic since XAS only provides an average molecular structure. Additional studies are clearly required to resolve this molecular structural issue surrounding the fully oxidized surface rhenia species. In a recent review, Okal and Kepinski concluded that "even though significant progress has been made in the understanding of the chemistry of supported rhenium oxide catalysts a detailed description of the [rhenia] species is still lacking and requires further study".[36]

Activated ReO_x in Reducing Environments. Much less information is currently available about the partially reduced surface rhenia species on alumina. Both Shpiro *et al.* [37] and Yide *et al.* [38] studied the oxidation states of supported rhenia/γ-Al_2O_3 catalysts by XPS under vacuum conditions and concluded that after hydrogen reduction the initial Re^{+7} is transformed to a mixture of Re oxidation states. Balcar *et al.* concluded that activation of the catalyst in an inert environment results in a mixture of Re^{+7} and reduced surface

rhenia species.[39] Fung *et al.* reduced a low loaded supported rhenia/Al_2O_3 catalyst with H_2 at elevated temperatures and monitored the changes with *in situ* EXAFS and XANES and concluded that both oxidized and reduced rhenia species coexisted after the reduction treatment.[40] The Re L_3 XANES edge feature suggested that the oxidized rhenia resembled the Re^{+4} present in bulk ReO_2. Ronning *et al.* also concluded from *in situ* EXAFS analysis after H_2 reduction of low loaded supported rhenia/Al_2O_3 catalysts that both reduced and oxidized rhenia species were present with the former accounting for ~80% of total ReO_x.[41] Similar conclusions were reached by Bare *et al.* from *in situ* XANES Re L_3 and EXAFS measurements of low loaded supported rhenia/Al_2O_3 catalysts after reduction by H_2 at 500-700^{o}C.[34] *In situ* FT-IR spectra with CO as the probe molecule also demonstrated that the surface rhenia species were partially reduced (Re^{n+}, with $0 < n < 7$) upon exposure to olefins.[42-45] Stoyanova *et al.* reported the presence of Re(+6) species from *ex situ* UV-vis spectra of used catalysts.[46] The presence of reduced surface rhenia species during olefin metathesis by supported rhenia/Al_2O_3 is consistent with the known activation of supported rhenia/Al_2O_3 catalysts in reducing environments of H_2,[31] CO,[42] hydrocarbons[44] and photoreduction[47].

Surface Reaction Intermediates during Olefin Metathesis. Only limited information has appeared in the heterogeneous catalysis literature about the nature of the hydrocarbon surface reaction intermediates during the olefin metathesis reaction by supported rhenia/alumina catalysts. Exposure of supported rhenia/Al_2O_3 catalysts to isobutene[42] and n-butene[48] at around room temperature and after evacuation gave rise to hydrocarbon fragments with CH_3 vibrations in the FT-IR spectra. The same surface CH_3 vibrations, however, were also observed with Re-free Al_2O_3 suggesting that the CH_3 fragments may

be formed by the strong surface Lewis acid sites of the alumina support.[48] Furthermore, the catalyst was evacuated for one hour before the FT-IR spectra were recorded. Such treatment would be expected to result in reaction and desorption of any reactive surface intermediates. *In situ* FT-IR under flowing propylene at 60^{o}C gave rise to vibrations from adsorbed propylene, ethylene, 2-butene and a band at 1450 cm^{-1} characteristic of aliphatic C-H groups.[48]

Initiation and Reaction Mechanisms. The most detailed mechanistic studies of olefin metathesis by supported rhenia/Al_2O_3 catalysts with chemical probe reactions have been reported by Coperet and collaborators.[23] The 1-2 hydrogen shift and H-assisted metathesis reaction mechanisms were ruled out by the absence of 3-methyl-2-pentene from the self-metathesis of cis 2-butene. The allyl mechanism was ruled out by the metathesis of Z-stilbene with ethylene to form styrene, a transformation that does not require the participation of allyl H atoms. It was concluded from these chemical probe studies that the pseudo-Wittig metathesis mechanism is the most probable for formation of the necessary initial surface carbene species. Earlier studies by Farona *et al*., however, did not discard the allylic mechanism.[24] Both Coperet *et al.*[23] and Farona *et al*.[24] concluded that ethylene cannot initiate metathesis owing to the absence of $H_2C{=}CD_2$ as a product of the cross metathesis of C_2H_4 with C_2D_4. This is also in agreement with the IR studies of Boelhouwer *et al.* who claimed ethylene does not reduce a ReO_x/Al_2O_3 catalyst.[48] As mentioned in the previous section, Chauvin proposed carbene and metallacyclobutane reaction intermediates from homogenous catalysis and titration studies.[13,25] Direct determination of the proposed surface intermediates for this catalytic system still awaits confirmation.

Number of Catalytic Active Sites. There is a continued discussion in the metathesis catalysis literature about the number of activated sites present and participating during steady-state olefin metathesis since not all the supported ReO_x sites on alumina are claimed to be active for olefin metathesis.[5,25,31] *Indirect* measurements based on kinetic analysis of the olefin metathesis reaction over supported rhenia/alumina catalysts and quantitative titration with chemical probe molecules (NO, CO and bases) of activated catalysts suggest that only a small number of the supported rhenia sites participate in the metathesis reaction at room temperature.[5,25,31] Chauvin *et al*. quantitatively counted the number of catalytic active sites present after olefin metathesis at room temperature for supported ReO_x/Al_2O_3 catalysts by chemical titration. After initial chemisorption of one olefin, evacuation of the catalyst system for 4-6 hours and subsequent titration of the resulting surface reaction intermediates with a second olefin formed the mixed metathesis reaction products.[25] The same number of sites was reported to be involved in the reaction regardless of whether propylene or 2-butene was used as an activator.[25] The number of sites did not depend on the contact time of the second reactant, ethylene, but on its partial pressure. This titration method is most likely undercounting the number of participating sites because (*i*) the catalyst is evacuated for 4-6 hrs during which metathesis and desorption of the first olefin can take place and (*ii*) it assumes that the titration with the second olefin consumes all the surface reaction intermediates at rather mild temperatures. Without direct observation of the molecular events which take place during this titration method it is not known if these assumptions are indeed representative of the actual reaction pathway. Yide *et al*.[38], however, demonstrated that the number of activated surface ReO_x sites on alumina can be significantly increased by activation with olefins at

elevated temperatures which indicates that the number of activated sites strongly depends on the pretreatment conditions. Stoyanova *et al*. using high throughput methods claimed that the calcination procedure (temperature and time), pretreatment conditions (temperature and gas) and reaction temperatures affect both conversion and selectivity.[46] This indeed suggests that the number of activated sites determined with room temperature activation is only a lower limit and that a much higher number of activated sites can be accessed by activation at elevated temperatures and with inclusion of promoters.

Kinetics. Kinetic studies of propylene metathesis by Kapteijn and Mol[49] showed that the reaction is pseudo first-order in propylene partial pressure and that the reaction rate increases with ReO_x loadings due to surface heterogeneity of the alumina support. The olefin metathesis catalytic activity of supported ReO_x/Al_2O_3 catalysis is strongly dependent on the rhenia loading on the alumina support.[31] For loadings below ~6% ReO_x/Al_2O_3 (0.75 Re/nm^2), the activity is very low. Optimal catalytic activity is observed for ~14-18% ReO_x/Al_2O_3 (~2.4 Re/nm^2), which corresponds to the maximum loading of surface rhenium oxide that can be anchored on an alumina support.[31] The non-linear relationship between the surface rhenia loading and olefin metathesis activity is most probably related to the relative abundance of two different surface rhenia species at these loadings, which in turn suggests that the surface rhenia species anchored on the neutral and more acidic surface hydroxyl sites may be more active for metathesis than the surface rhenia species on the basic surface hydroxyls.[31] Propylene metathesis by supported ReO_x/Al_2O_3 catalyst exhibited an overall activation energy of 25-40 kJ/mol.[49] The exponential increase of the reaction rate as a function of the rhenia content was claimed to result from a combined increase of the reaction rate and equilibrium constants, k and K,

respectively.[49] However, as noted above, increasing the reaction temperature also increases the number of activated rhenia sites that further complicates the temperature dependence of the rate and equilibrium constants.[38,46]

Surface Acidity. The roles of surface Brønsted and Lewis acid sites on the alumina support upon olefin metathesis by supported rhenia/alumina catalysts have been studied extensively. Earlier researchers were of the opinion that the presence of surface Brønsted acid sites contributed to the metathesis activity of supported rhenia/Al_2O_3 catalysts.[50-54] Subsequently, attention has focused on the presence of neighboring Lewis acidic Al sites that are enhanced by the strength of the Brønsted acidity of silica-alumina.[55,56] This realization caused the metathesis literature to focus on the interaction of surface rhenia species with adjacent surface Lewis acid sites as being responsible for olefin induced activation of rhenia catalysts.[14,35,57] The entire role of acidity upon olefin metathesis still needs to be resolved.

Alumina Support Type. Several researchers have also examined the role of mesoporous Al_2O_3 supports for olefin metathesis by supported rhenia/alumina. The Balcar and Onaka research groups have claimed that use of mesoporous alumina supports results in higher activity (as much as 20x) due to a higher concentration of surface Lewis acid sites, lower concentration of basic surface OH groups and better stabilization of surface reaction intermediates.[39,58-64] Onaka *et al*. also reported EXAFS studies which found similar Re-O bonding for ReO_x supported on both mesoporous and regular alumina. This result suggests that the same surface rhenia species are present on both types of alumina supports, and that the enhanced performance derives from use of the mesoporous support.[62] The improvement, however, seems to be more significant in metathesis of functionalized

olefins rather than that of linear olefins.[57,62] Contrary to Balcar *et al*. and Onaka *et al*., Bregeault *et al*. reported that mesoporous supports do not have an advantage over conventional alumina supports.[65]

Promoters. Promoters are claimed to increase the activity of ReO_x/Al_2O_3 catalysts by either maintaining Re in a desirable oxidation state,[66] increasing support acidity,[9] or changing local Re structures[67]. Some of the promoters that have been reported are SiO_2,[9] $(CH_3)_4Sn$,[31,67] P_2O_5,[68] B_2O_3,[69] V_2O_5,[45,69] MoO_3[45,69] and WO_3.[45,52] Although the enhancement of catalytic activity by promoters is accepted, additional fundamental studies are still required to understand the promotion mechanism(s).

$ReO_x/(SiO_2$-$Al_2O_3)$

The same surface ReO_x structure is reported to be present on silica-alumina supports as on alumina, but a different structure is present on silica.[35] Studies by Mol *et al.* found that activity decreases with increasing ReO_x on SiO_2-Al_2O_3, contrary to the Al_2O_3 support.[31] At low rhenia loadings (<0.5 Re/nm^2), supported $ReO_x/(SiO_2$-$Al_2O_3)$ catalysts are 3-6 times more active than supported ReO_x/Al_2O_3 catalysts and supported ReO_x/SiO_2 catalysts are inactive for olefin metathesis.[31,35,70] At low rhenia loadings, ReO_x initially anchors by reacting with Si-(OH)-Al bridging hydroxyls resulting in electron poor rhenium sites that are claimed to be highly active sites.[31] With increasing rhenia loading, the additional ReO_x is stabilized at Si-OH hydroxyls that result in inactive ≡Si-O-ReO_3 sites.[31] A recent paper by Bouchmella and Debecker *et al.* used a non-hydrolytic sol-gel (NHSG) method with Cl precursors and diisopropyl ether to prepare mesoporous Re-Si-Al catalysts Bouchmella *et al.*[71] These catalysts displayed superior activity over catalysts prepared via the incipient wetness impregnation method due to their superior properties

such as acidic sites, well dispersed ReO_x species and high surface areas. Interestingly, the loss of rhenia is claimed to be prevented by adding more alumina. The maximum activity is observed at Si/Al ratio of 0.3.[71] The simultaneous variation of several experimental parameters complicates determination of the origin of the catalytic enhancement for olefin metathesis and systematic studies are required to fully understand the catalyst structure-activity relationships for supported $ReO_x/(SiO_2\text{-}Al_2O_3)$ catalysts.

Supported Organometallic Catalysts. Model ReO_x organometallic catalysts can provide fundamental insights about the reactive intermediates and reaction mechanism of olefin metathesis. Hermann *et al*. discovered that methyltrioxorhenium (MTO), CH_3ReO_3, supported on silica-alumina is very active for metathesis of functionalized olefins in 1991.[72] The same product selectivity is obtained for propylene metathesis by the model supported $MTO/Al_2O_3\text{-}SiO_2$ and conventional supported ReO_x/Al_2O_3 catalysts. Coperet *et al*. concluded from solid-state ^{13}C CPMAS NMR and DFT calculations for CH_3ReO_3 supported on alumina that the surface $Al_sCH_2ReO_3$ intermediate located at octahedral alumina sites represents the catalytic active species rather than the majority surface $Al_sReO_3CH_3$ species.[73,74] The active surface $Al_sCH_2ReO_3$ complex is structurally similar to the Tebbe reagent, which was the first well-defined metathesis catalysts and is used in carbonyl methylenation.[73,74] A different activated structure of CH_3ReO_3 was proposed by Scott *et al*. based on XAS measurements of $ZnCl_2$ modified CH_3ReO_3/Al_2O_3.[75] In this proposal, Lewis acidic Al centers are claimed to be the most favorable sites for CH_3ReO_3 chemisorption. The use of a mixed silica-alumina support instead of alumina is claimed to result in elongation of one of Re=O bonds in CH_3ReO_3 via an interaction with an Al site.[76] Coperet *et al*. also reported that modifying the Al_2O_3 support by treatment with

$Si(allyl)(CH_3)_3$ prior to impregnation with CH_3ReO_3 improves the cis/trans ratio of 2-butenes for propylene metathesis, mainly through the increase of the desorption kinetics.[77,78] Although the supported CH_3ReO_3/Al_2O_3 catalyst doesn't exhibit an induction period and is about 10 times more active than the conventional supported ReO_4/Al_2O_3 catalyst system, it deactivates much more rapidly, clear indications that supported organometallic catalysts are not identical to traditional supported ReO_x/Al_2O_3 catalysts.[79]

As mentioned above, silica supported rhenium complexes, rhenium oxide and MTO typically do not exhibit olefin metathesis activity.[5,9,11,35,72] The *first* successful synthesis of a highly active silica supported ≡SiO-Re(≡C-Bu-t)(=CH-Bu-t)(CH_2Bu-t) olefin metathesis catalyst was reported by Coperet and Basset *et al.* in 2001.[80] Structural knowledge of these grafted rhenium compounds having d^0 configurations and alkylidene ligands was drawn from the analogous homogeneous systems.[80] The silica support was partially dehydroxylated at high temperatures (700°C) before impregnation of the Re complex to both stabilize the ligands and remove surface hydroxyls that promote double bond isomerization.[80,81] The hydrocarbyl complex Re(≡C-Bu-t)(=CH-Bu-t)(CH_2Bu-t)$_2$ was used as a catalyst precursor and characterization with solid-state ^{13}C and ^{1}H NMR along with its ability to also metathesize alkynes allowed proposing the molecular structure as ≡SiO-Re(≡C-Bu-t)(=CH-Bu-t)(CH_2Bu-t) catalyst.[80] Given that these compounds already possess Re=carbenes, the silica supported Re(≡C-Bu-t)(=CH-Bu-t)(CH_2Bu-t) catalyst doesn't require activation since it already contains Re=carbenes and is even compatible with functionalized olefins without co-activator like Me_4Sn required for Re_2O_7/Al_2O_3.

Patents. The patent literature for olefin metathesis by supported rhenia/Al_2O_3 catalysts has been quite active since 2000.[82-119] Supports of choice are γ-alumina, [82,84-90,93,97,99,102-104,110] mesoporous alumina[98,99,101] and silica-alumina[96,112]. The alumina-based supports are sometimes treated with an inorganic halide (such as $FeCl_3$, $CuCl_2$, or $ZnCl_2$.)[90,99,102,113] and promoters that include B_2O_3,[96] SnO_2,[113] Bu_4Sn,[108] Cs_2O,[118] Nb_2O_5,[106,107] and Ta_2O_5 [86]. The function of the Cl is most probably to remove the surface hydroxyls that are claimed to have a negative effect on the olefin metathesis reaction.[75,120,121] There is also emphasis on maintaining a very low concentration of heteroatom hydrocarbons in the feed since they negatively impact the olefin metathesis catalytic activity, presumably by site blocking.[84] One patent claimed that co-feeding H_2 enhances metathesis catalytic activity and allows operation at lower temperatures. Inclusion of H_2 could either minimize coke deposition or increase the number of reduced catalytic active sites.[91] Regeneration of supported rhenia/alumina is achieved by heating in an O_2-containing gas to >400°C[107,122] and treatments with H_2O_2, NaOH, KOH, or NH_4OH[122]. The above olefin metathesis patent literature reveals the methodology employed by industry in preparing commercial supported rhenia/Al_2O_3 catalysts and some of their general concerns about how to optimize performance, but does not provide any fundamental insights about the supported rhenia catalytic active sites during the different stages of the catalyst evolution: (*i*) synthesis (effect of support characteristics, promoters, poisons and Re precursors), (*ii*) activation (effect of air, inert, H_2 and CO), (*iii*) olefin metathesis reaction conditions (effect of temperature and feed composition), and (*iv*) regeneration (effect of air, steam, H_2, etc.).

Summary of ReO_x/Al_2O_3 catalysts. Although supported ReO_x/Al_2O_3 catalysts are currently not employed for large industrial applications due to the high price of rhenium and its volatility, this catalyst system has been studied extensively due to its high selectivity and catalytic activity at room temperature. Progress has been made in the understanding of ReO_x/Al_2O_3-catalyzed olefin metathesis, but many key details continue to elude catalysis researchers in this field. These include the: (*i*) molecular structure of the initial oxidized isolated surface ReO_x species, (*ii*) molecular structure(s) and oxidation state(s) of activated surface ReO_x site(s) during olefin metathesis, (*iii*) number of activated catalytic sites during olefin metathesis, (*iv*) activation mechanism, (*v*) surface reaction intermediates, (*vi*) reaction mechanism and (*vii*) promotion mechanism(s). The absence of direct characterization studies of supported ReO_x/Al_2O_3 catalysts during olefin metathesis has hampered progress in the understanding of this catalytic system. The availability of modern *in situ* and *operando* spectroscopy instrumentation (XAS, ^{13}C NMR, High Field EPR, Near Atmospheric Pressure-XPS, Raman and IR vibrational studies with isotopes) complemented with DFT calculations should allow resolution of the above issues in the near future.

5. Supported MoO_x Systems

Supported molybdena catalysts are active for olefin metathesis at moderate reaction temperatures (25-200^oC) and are usually prepared from aqueous impregnation of ammonium salts such as ammonium heptamolybdate via incipient wetness impregnation.[123,124] Other preparative methods include sol-gel techniques,[125] flame spray pyrolysis[126] and even spontaneous thermal spreading of crystalline MoO_3[127]. The resulting

supported molybdena heterogeneous catalyst systems have been well characterized in their initial oxidized states under oxidizing dehydrated conditions prior to activation and exposure to the olefin metathesis reaction conditions. The molecular structures of the fully oxidized surface MoO_x sites have been shown to be independent of synthesis method below the maximum dispersion or monolayer coverage limit.[20,128,129] Non-aqueous impregnation techniques employing molybdenum organometallic complexes have also been used to prepare supported molybdena catalysts with a variety of well-defined surface functionalities which are analogous to those of homogeneous metathesis catalysts.[130-132]

MoO_3/SiO_2. Supported MoO_3/SiO_2 catalysts are about an order of magnitude less active for olefin metathesis than supported MoO_3/Al_2O_3 catalysts.[70] However, the dehydrated supported MoO_3/SiO_2 system is viewed as a model metathesis catalyst because only isolated surface MoO_x sites are generally thought to be present below the maximum dispersion limit of molybdenum.[133-136]

Supported MoO_x/SiO_2 in Initial Oxidized Catalyst. The dehydrated, fully oxidized surface MoO_x species on SiO_2 have experimentally been characterized with *in situ* UV-vis,[123,133,136] Raman,[20,123,133,136-139] XAS,[136-139] isotopic ^{18}O-^{16}O exchange[140] and IR spectroscopy[133,136] and found to be present as isolated dioxo $(O=)_2MoO_2$ and mono-oxo $O=MoO_4$ species as depicted in Figure 1.2. The surface dioxo $(O=)_2MoO_2$ structure represents the majority species (see Figures 1.2a and 1.2b, respectively).[128,129,133-136] Above the maximum dispersion limit, crystalline MoO_3 NPs also form (see Figure 1.2c).[128,133,136] One study has claimed that both isolated and oligomeric surface MoO_x sites are present on SiO_2 (SBA-15) from *in situ* Raman, UV-vis and XAS measurements.[139] The absence of pronounced Mo-Mo features in the 3.2-4.0 Å range in the EXAFS second

coordination sphere, present for crystalline MoO_3, does not support the assignment of a significant amount of surface oligomers. A more recent study with a similar MoO_3/SiO_2 catalyst employing SBA-15 employed more extensive structural characterization (*in situ* Raman, IR, UV-vis, XANES, EXAFS and NEXAFS), however, found no evidence for surface MoO_x oligomers and concluded that the surface MoO_x species on SiO_2 are primarily present as isolated surface dioxo MoO_4 species.[136] DFT calculations support the presence of two isolated surface MoO_x structures on SiO_2 and the greater stability of the isolated surface dioxo MoO_4 than the mono-oxo MoO_5 sites.[16,134]

Activated MoO_x/SiO_2 in Reducing Environments. The nature of surface MoO_x sites during olefin activation and metathesis reaction are still not known since *in situ* and *operando* spectroscopy studies during catalyst activation and olefin metathesis reaction conditions have not been reported.[141-146] Yermakov *et al.* examined a series of organometallic complexes on SiO_2, produced from Mo(π-allyl)$_4$ and containing different Mo oxidation states, for self- metathesis of propylene at 90^{o}C. They concluded that the initial Mo^{+4} complex leads to the highest metathesis activity whereas initial Mo^{+6} and Mo^{+2} are inactive for the metathesis of propylene at 90°C, but supporting evidence that the initial oxidation states were unchanged during the metathesis reaction was not provided.[130] Kazansky *et al*. activated a supported MoO_3/SiO_2 catalyst by photoreduction in the presence of CO, which allowed determination of the number of reduced sites by quantifying the CO_2 formed, with subsequent cyclopropane adsorption. Surface Mo^{+4} species were concluded to be the active metathesis sites since their concentrations, measured with *in situ* UV-vis spectroscopy, related relatively well with catalytic activity.[142,143] Zhang *et al.* examined the oxidation states of MoO_x/SiO_2 catalysts

pretreated under H_2, H_2-N_2 and H_2 conditions with *ex situ* XPS and EPR.[141] A correlation between the room temperature quenched EPR Mo^{+5} signals and propylene conversion suggested that the Mo^{+5} sites are the catalytic active sites. Two distinct Mo^{+5} sites were detected, a distorted MoO_5 square pyramidal and a distorted MoO_6 coordination, with the former coordination suggested to be the catalytic active site. The optimum H_2 pretreatment was found to be 400-450°C; over-reduction at higher temperatures was proposed to form Mo^{+4} which was thought to be responsible for the reduced activity.[141] DFT calculations have concluded that surface dioxo MoO_4, and not the surface mono-oxo MoO_5, species are the energetically favored precursors of the catalytic active sites for olefin metathesis.[16]

Surface Reaction Intermediates during Olefin Metathesis. No *in situ* and *operando* studies during olefin metathesis with supported MoO_x catalysts have been reported. Consequently, surface reaction intermediates have not yet been reported for MoO_x/SiO_2 catalysts. Kazansky *et al.* reported the first *in situ* IR detection of surface $Mo{=}CH_2$ intermediates from cyclopropane adsorption on photoreduced MoO_x/SiO_2 catalysts.[143,144] Adsorption of ethylene on a CO-treated photoreduced MoO_x/SiO_2 catalyst resulted in two UV-vis bands at ~480 and ~590 nm bands, as well as IR bands at 2985, 2955, 2930 and 2870 cm^{-1}. These bands were tentatively assigned to Mo-cyclobutane and π-bonded propylene complexes, respectively.[144,145] Catalyst deactivation was claimed to result from transformation of the active surface Mo-cyclobutane intermediates into inactive surface π-bonded propylene.[145] These very early *in situ* IR and UV-vis spectroscopy studies, however, were not taken during either catalyst activation with olefins or olefin metathesis reactions. More detailed fundamental insights came from DFT calculations that concluded that the IR bands reported by Kazansky *et al.* mostly correspond to a stable square-

pyramidal (SP) Mo-cyclobutane rather than a more reactive trigonal bipyramidal (TBP) Mo-cyclobutane.[16]

Initiation and Reaction Mechanisms. Surface isopropoxide species were recently claimed to be the major surface reaction intermediates during the initial stage of propylene metathesis by supported MoO_x/SBA-15 catalysts (activation of surface Mo^{+6} sites by reduction to Mo^{+4} and formation of a C_3 oxygenate).[22] This conclusion was based on the similarity of IR bands for the surface intermediates formed by adsorption of propylene and isopropanol as well as their similar heats of adsorption. The IR vibration for the surface isopropoxide C-O bond, however, was not detected for the photoreduced catalysts described in the previous section, which suggests differences between the photoreduction and initial olefin activation treatments.[143,144] Transient isotopic switching experiments, however, would allow for better discrimination between surface reaction intermediates and possible spectator species. To date, DFT calculations start with a surface $Mo{=}CH_2$ intermediate, do not address the initiation mechanism and suggest that olefin metathesis occurs via a mechanism that proceeds through a Mo-cyclobutane intermediate.[16]

Number of Catalytic Active Sites. For the MoO_x/SBA-15 system, the number of active sites after activation at 50^{o}C with propylene ($H_2C{=}CHCH_3$) was determined to be <2% of the total surface MoO_x sites. This conclusion was based on perdeuteroethylene titration of the surface intermediates which remained on the catalyst when the reaction was stopped.[22] Bykov *et al*. investigated the metathesis of α-olefins on heterogeneous supported binary ($MoCl_5/SiO_2$–Me_4Sn) and ternary ($MoCl_5/SiO_2$–Me_4Sn–ECl_4, E = Si or Ge) catalysts and concluded that up to 6% of the Mo atoms are active at 50°C without applying evacuation

or desorption steps.[146] Subsequently, these workers reported that 13% of the Mo sites present in ($MoOCl_4/SiO_2$)–$SnMe_4$ catalysts participate in the metathesis reaction.[147] As mentioned above, there are inherent assumptions in the chemical titration approach that may be undercounting the number of activated MoO_x catalytic sites.

Kinetics. The propylene metathesis reaction rate, normalized per unit of surface area and expressed as mmol/(m^2-s), for supported MoO_x/SBA-15 catalysts as a function of MoO_x loading exhibited an exponential rise with increasing surface MoO_x coverage until crystalline MoO_3 nanoparticles were present at high coverage.[136] This strongly increasing reactivity trend was attributed to increasing distortion of the isolated dioxo surface MoO_4 sites with higher surface MoO_x coverage on SBA-15. Such distortion is due to lateral interactions between the MoO_x sites, and is also related to the accessibility of anchoring on 6-, 8- or 10-membered rings. The surface MoO_x sites were also proposed to interact with adjacent Brønsted acid sites for activation,[136] but Brønsted acid sites are not significant for siliceous materials such as SBA-15. The reactivity rapidly decreased with increasing amounts of crystalline MoO_3 nanoparticles which reflects the low activity of MoO_3 nanoparticles and probably also agglomeration of a portion of the surface MoO_x catalytic active sites.[128] Earlier studies by Mol *et al.* observed a similar trend for the MoO_x/SiO_2 system with the catalytic activity reaching a maximum at 1.0 Mo atoms/nm^2 and decreasing at higher molybdena loadings.[70,136]

Supported Organometallic Catalysts. Coperet and Shrock *et al.* showed that silica supported organometallic Mo-based catalysts having the general formula [(Y)M (≡ER)(=CHtBu)(X)] (Y =≡SiO) (X=CH_2tBu, OR or NR2; with M = Mo with ER = NR) out-performed their homogenous analogues.[131] As mentioned in the previous section about

supported organometallic ReO_x catalysts, these supported organometallic complexes are grafted by replacing one of the anionic X ligand with a siloxy ligand[131,132] and normally remain intact on the SiO_2 support. *In situ* ^{13}C CPMAS NMR showed that the Mo supported organometallic complexes react via the same surface alkylidene and metallacyclobutane intermediates as observed in homogeneous catalysts.[131,132] Although the model silica-supported surface organometallic catalysts have provided many molecular details about olefin metathesis catalytic active sites and surface reaction intermediates, there is still a materials gap between the surface organometallic catalysts and industrial-type heterogeneous supported metal oxide catalysts because of the special ligands used to stabilize the surface organometallic catalysts on SiO_2.

MoO_3/Al_2O_3. Supported MoO_x/Al_2O_3 catalysts find industrial application in the Shell Higher Olefins Process (SHOP) for metathesis of long-chained olefins (C_2H_4-$C_{20}H_{40}$).[5,7,9] The supported MoO_x/Al_2O_3 catalysts are at least 10 times more active than the supported MoO_x/SiO_2 catalysts in the same temperature range reflecting their easier reduction or activation.[9,70]

MoO_x in Initial Oxidized Catalyst. The surface MoO_x structures present for fully oxidized, dehydrated supported MoO_3/Al_2O_3 catalysts have been established in the past few years from extensive *in situ* spectroscopic measurements (Raman,[123,137,148,149] UV-vis,[123] XAS[137,148,149]) and DFT calculations[150,151]. At low surface molybdena coverage (<20% of monolayer), isolated surface dioxo $(O=)_2MoO_2$ species dominate and at high surface coverage both isolated surface dioxo MoO_4 and oligomeric mono-oxo $O=MoO_4$ species coexist on the alumina support as indicated in Figure 1.3. Above monolayer

coverage (4.6 Mo atoms/nm^2), crystalline MoO_3 NPs are also present on top of the surface MoOx species since there are no anchoring surface Al-OH sites remaining.[152]

Activated MoO_x in Reducing Environments. Less is known, however, about the oxidation state and molecular structure of supported MoO_x/Al_2O_3 catalysts that have been activated or exposed to olefin metathesis reaction conditions. The earliest reported spectroscopic characterization for supported MoO_3/Al_2O_3 involved initially exposing the catalysts to the propylene metathesis reaction at 200^oC and, subsequently, examining the catalysts with *ex situ* XPS and EPR spectroscopy.[153,154] It was concluded that activated sites only formed from initial Mo^{6+} and Mo^{4+} species while other oxidation states were inactive, but measurements were performed after metathesis and exposure to air that can oxidize the catalysts. Carbon monoxide reduction of supported MoO_3/Al_2O_3 catalysts suggested that surface MoO_x sites anchored at basic surface hydroxyls do not reduce at 500^oC, but surface MoO_x sites anchored at non-basic surface hydroxyls reduce to approximately Mo^{4+}.[155] From *ex situ* solid-state ^{27}Al NMR of molybdena-supported mesoporous Al_2O_3, it was proposed that only surface MoO_x sites on surface AlO_6 sites are most active for olefin metathesis,[156] but ambient moisture may have affected the coordination of the surface AlO_x sites. The importance of the coordination of the surface alumina sites where the active surface MoO_x species are anchored is supported by DFT calculations.[15-18] The DFT calculations suggest that the most active surface MoO_x sites possess pseudo-MoO_4 coordination and are anchored to AlO_6 sites on the (100) surface of the Al_2O_3 support.

Surface Reaction Intermediates during Olefin Metathesis. DFT studies also suggest that the less stable surface Mo-cyclobutane intermediates anchored to the surface AlO_6

sites are responsible for their high reactivity.[15] Early *in situ* studies by Olsthoorn and Moulijn stated that propylene is π-bonded on both oxidized and CO-reduced MoO_x/Al_2O_3 catalysts.[157] From the position of the 1600 cm^{-1} C=C bond, which is lower than that (1645 cm^{-1}) observed in adsorption of propylene on pure Al_2O_3, it was concluded that adsorption is reversible on the MoO_x/Al_2O_3 catalyst and the resulting π-bonded complex could be an intermediate during the reaction.[157] The absence of transient experiments, however, did not allow for discrimination between surface reaction intermediates and possible spectator species.

Initiation and Reaction Mechanisms. From isotopic D-labelled studies, it was proposed that olefin metathesis of long chain olefins by supported MoO_x/Al_2O_3 catalysts is initiated and proceeds via surface π-allyl species,[158] suggesting that C-H bonds may be involved in metathesis by long chain olefins. Recent DFT calculations, however, suggest that allylic CH bonds are not required for catalyst activation for small olefins and that the pseudo-Wittig mechanism is the most likely activation mechanism.[159]

Number of Catalytic Active Sites. The percentage of catalytic active surface MoO_x sites on alumina that participate in olefin metathesis has received much attention by debates in the literature. Early studies by Burwell *et al*. for supported $Mo(CO)_6/Al_2O_3$ concluded less than 1% of surface MoO_x sites are involved in the metathesis reaction at 53°C.[160] This conclusion is in sharp contrast to the findings of Hightower *et al*. who found from NO poisoning experiments that for cobalt-promoted supported MoO_3/Al_2O_3 catalysts ~15% of surface MoO_x sites were active at room temperature.[161] Handzlik *et al.* counted the number of activated surface MoO_x sites present for supported MoO_x/Al_2O_3 catalysts during propylene metathesis by either slightly increasing the temperature or switching the

flow to argon for tens of minutes. They found that only ~1% of MoO_x sites were activated at ~50°C; however, ~4.5% of MoO_x sites were activated for a tin-promoted supported MoO_x/Al_2O_3-$SnMe_4$ (Mo/Sn = 1.2) catalyst at the same temperature.[162] The lack of consistency in the reported number of catalytic active surface MoO_x sites in each of the above studies is most likely related to the different catalysts and surface MoO_x coverages employed. Furthermore, all the measurements were performed close to room temperature; the influences of activation temperature and olefin partial pressure on the number of activated surface MoO_x sites were not examined. As mentioned above, there are inherent assumptions in the chemical titration approach that may be undercounting the number of activated MoO_x catalytic sites. Direct spectroscopic observations are needed to determine how much these assumptions deviate from the actual situation.

Kinetics. The supported MoO_x/Al_2O_3 catalysts exhibit a maximum in steady-state activity for metathesis of small olefins at approximately monolayer coverage of surface MoO_x sites.[70,127] This suggested to most investigators that the surface MoO_x sites, either isolated or oligomeric, are probably the precursors to the catalytic active sites and not crystalline MoO_3 or $Al_2(MoO_4)_3$ nanoparticles since the latter tend to form above monolayer coverage. [70,124-127,130,] The individual contributions of the isolated and oligomeric precursor surface MoO_x sites on alumina in generating activated sites for olefin metathesis, however, is still not known. Grunert and Minachev reported that the reaction order is 0.8 in propylene at 200°C.[154] The apparent activation energy was reported to be 37-30 kJ/mol and decreased slightly with increasing Mo loadings.[154]

Promoters. Some of the promoters added to the MoO_x/Al_2O_3 system include SiO_2,[124-127] , and ECl_4 (E=Si or Ge)[147] CoO[161] and $(CH_3)_4Sn$.[162] $(CH_3)_4Sn$ is claimed to increase the

number of Mo active sites.[162] The promotion mechanisms of the other promoters still require further studies for their understanding.

Patents. The industrial patent literature for olefin metathesis by supported molybdena catalysts has also seen activity in recent years.[82,84,91,93-97,104,108-112,114,163-188] The support of choice is γ-alumina,[82,163-167,174-183,186-188] but mesoporous alumina[84,98,100,184] and silica-alumina[185] supports have also been claimed. The alumina-based supports are sometimes treated with halides[178] and promoters that include B_2O_3,[184] CoO,[189] alkyl-Sn[190] and alkyl-Pb[179,190]. The patents are about equally divided between metathesis of small olefins (C_2H_4-C_4H_8)[82,84,165,169-172,174,178,189,191-196] and higher olefins(C_5H_{10}-$C_{20}H_{40}$).[94,95,100,108,115,175-177,181-183,186-188,197] The promotion mechanisms have not received attention in the catalysis literature.

$MoO_x/(SiO_2$-$Al_2O_3)$. Mixed Al_2O_3-SiO_2 supports and zeolite supports have been claimed to improve the olefin metathesis activity for supported $MoO_x/(Al_2O_3$-$SiO_2)$ catalysts, but only limited studies have appeared for such catalysts.[124-127,198-205] It was proposed that mixed SiO_2-Al_2O_3 supports achieve an appropriate level of Brønsted acidity that is crucial for efficient catalytic performance during olefin metathesis with optimal activity achieved at moderate molybdena loadings[126,127,198-201] and that excessive Brønsted acidity may be responsible for side reactions such as cracking and isomerization.[198-200] Surface Mo^{5+} sites, with MoO_5 or MoO_6 coordination, were detected for supported $MoO_x/(Al_2O_3$-$SiO_2)$ catalysts exposed to propylene metathesis with *ex situ* EPR after evacuation at 25 and 200°C.[201] Although surface Mo^{5+} sites were detected after metathesis, no information is provided about other Mo oxidation states that may possibly be more important (e.g., Mo^{4+}). The EPR measurements were complemented with *ex situ* L_3-XANES of fresh and

used catalysts that indicated that the activated surface MoO_x sites are present as poorly formed oligomeric species containing some partially reduced Mo cations.[201] The *ex situ* spectroscopy characterization studies leave much to be desired since they were performed after the reaction was terminated, and the samples evacuated and exposed to ambient conditions containing molecular oxygen and moisture. The spectroscopic findings tend to be dominated by one Mo oxidation state (e.g., EPR is dominated by the Mo^{5+} cations and XANES is dominated by Mo^{6+} cations since a majority of the surface MoO_x sites are not expected to be reduced, especially after exposure to air). Only direct spectroscopic characterization during olefin metathesis will reveal the nature of the actual surface MoO_x cations on alumina present during the reaction.

The metathesis of 2-butene and ethylene on silica, silica-alumina and alumina supported MoO_x catalysts was recently reported by Hahn *et al*.[202] The optimal reactivity is observed around 40wt% silica. On silica-alumina supports, Brønsted acidity increases with increasing silica and MoO_x loading whereas an inverse trend is observed for Lewis acidity. This increasing Brønsted acidity is claimed to be responsible for improved metathesis activity of isolated MoO_4 and polymeric MoO_6 species that were detected from Raman and UV-vis measurements under ambient and dehydrated conditions, respectively. Combining results from ambient (hydrated) and dehydrated conditions is problematic since the molecular structures of surface MoO_x species are strongly dependent on moisture content.[123] When MoO_3 crystals are present, the catalytic activity cannot be improved by the Brønsted acidity. Interestingly, in their later paper, butene reactions (self-metathesis of butenes and 2 to 1 isomerization) are reported to be faster on isolated species, where polymeric species catalyze metathesis of 2-butene and ethylene much faster.[203] This is a

bit surprising since increasing Brønsted acidity would be expected to contribute more to side reactions according to earlier studies.[198-200] Debecker *et al.* earlier claimed from self-metathesis of propylene with flame made $MoO_3/(SiO_2\text{-}Al_2O_3)$ that an inverse relationship exists between the number of Mo-O-Mo bonds and specific activity.[126] Therefore, Debecker *et al*. concluded that isolated MoO_x sites represent the most active sites, which is contrary to the findings of Hahn *et al*. that polymeric MoO_x sites are the most active sites for olefin metathesis. Debecker *et al*. also reported an one-pot aerosol synthesis method of $MoO_3\text{-}SiO_2\text{-}Al_2O_3$ from block copolymer (Brij58), $AlCl_3$, $12MoO_3H_3PO_4\ xH_2O$ or $MoCl_5$ with aqueous solution of tetraethyl orthosilicate and ethanol.[204,205] With an average pore size of 1.8-2.0 nm, these catalysts were free of $Al_2(MoO_4)_3$ and MoO_3 crystals and displayed activity 2-3 times higher than those prepared by using ammonium heptamolybdate on traditional $SiO_2\text{-}Al_2O_3$ supports.[204,205] As indicated above, a more systematic variation of synthesis parameters is needed to fully understand the relationships between synthesis and catalyst performance for olefin metathesis by supported $MoO_3/(SiO_2\text{-}Al_2O_3)$ catalysts.

Summary. The supported MoO_x olefin metathesis literature has attracted much attention because of the industrial importance of the SHOP olefin metathesis process.[5,7,9] Although the molecular structures of the fully oxidized surface MoO_x sites have been determined for unpromoted supported molybdena catalysts, the nature of the surface MoOx sites and surface reaction intermediates during olefin metathesis still need to be resolved. DFT calculations and model studies with supported organometallic catalysts have been very informative, but direct observation of the surface MoO_x sites and surface reaction intermediates during olefin metathesis of both small and long-chain olefins still awaits

further *in situ* and *operando* spectroscopy studies (e.g., XAS, ^{13}C NMR, High Field EPR, Near Atmospheric Pressure-XPS, Raman and vibrational IR studies with isotopes). Such studies are expected to resolve many of the key fundamental issues that surround supported MoO_x catalysts.

6. Supported WO_x Systems

Supported WO_x/SiO_2. The supported WO_x/SiO_2 catalyst has received much less attention in the olefin metathesis literature than either supported ReO_x and MoO_x catalysts, which is quite surprising since it is the major industrial olefin metathesis catalyst for the "Triolefin Process" that converts two propylene molecules to ethylene and 2-butene molecules.[4,5] The reverse process is called "Olefin Conversion Technology" and is now licensed by ABB Lummus.[5,11] One of the reasons for this relative inattention may be the need to employ higher temperatures (~350-450^oC) for activation of supported WO_x/SiO_2 catalysts. Use of such high temperatures precludes performing titration reactions since the surface reaction intermediates should have a very short lifetime and will react during the evacuation step. The supported WO_x/SiO_2 catalysts are typically prepared by impregnation of the aqueous $(NH_4)_6H_2W_{12}O_{40}$ precursor onto the SiO_2 support, followed by drying and calcination under oxidizing conditions at elevated temperatures (~500^oC).[206]

WO_x in Initial Oxidized Catalyst. The surface WO_x structures present for fully oxidized, dehydrated supported WO_x/SiO_2 catalysts have been established in the past few years from detailed *in situ* spectroscopic measurements (Raman[133,140,206] and UV-vis[133,140,206]). Both isolated surface dioxo, $(O=)_2W(-O)_2$, and mono-oxo $O=W(-O)_4$ species co-exist on

silica, depicted in Figure 1.4, with the dioxo species being the dominant site. Above the maximum dispersion limit, crystalline WO_3 nanoparticles are also present as shown in Figure 4. The oxidized supported WO_x/SiO_2 catalysts have analogous structures to the supported MoO_x/SiO_2 catalysts which reflects the similar structural inorganic chemistry of both oxides.[140]

Activated WO_x in Reducing Environments. The nature of the tungsten oxide structures present for supported WO_3/SiO_2 catalysts after catalyst activation and under olefin metathesis reaction conditions has not received any attention; no *in situ* or *operando* spectroscopy studies have been reported. Consequently, there is no agreement knowledge about the nature of the tungsten oxide active site(s) responsible for olefin metathesis by supported WO_x/SiO_2 catalysts.[207-227]

Initiation and Reaction Mechanisms. There is no direct characterization study of initiation and reaction mechanisms for olefin metathesis by WO_x/SiO_2 catalysts. Basrur *et al.* reported formation of traces of acetone and acetaldehyde during the induction period and claimed involvement of lattice oxygen in the mechanism.[224] The Pseudo-Wittig mechanism could be implied from their studies. Basrur *et al.* also claimed detection of nonstoichiometric oxidation states, such as $WO_{2.9}$ from *ex situ* ESR studies,[224] but provided no information about the nature of the surface WO_x sites. A recent Density Functional Theory (DFT) study of olefin metathesis employed the crystalline $WO_3(001)$ plane as the model for its catalytic active sites.[225] However, the oxidation state(s) of WO_x species were not mentioned. The crystalline $WO_3(001)$ plane is the most thermally stable plane and consists of polymeric WO_5 and WO_6 sites. This model, however, is not

representative of the surface WO_x sites anchored on SiO_2 (isolated WO_4 and WO_5 sites and WO_3 nanoparticles) in the heterogeneous supported WO_3/SiO_2 catalysts. Consequently, DFT studies with more realistic catalyst models still need to be performed.

Number of Catalytic Active Sites. No attempt to count the number of sites involved in olefin metathesis by supported WO_x/SiO_2 catalysts has been reported. As indicated above, it is highly unlikely that the short lived surface reaction intermediates could be titrated at the high activation temperatures of 300-500°C. Direct spectroscopic measurements during activation and olefin metathesis should be able to address the issue of number of participating catalytic active sites.

Kinetics. Detailed kinetic studies of olefin metathesis by supported WO_x/SiO_2 have not appeared in the literature, but several researchers attempted to relate the nature of the WO_x structures present on SiO_2 with the catalytic activity. Davazoglou *et al.* observed similar catalytic olefin metathesis performance for well-dispersed tungsten oxide at low loadings and on high loaded supported WO_3/SiO_2 catalysts. They concluded that the well dispersed tungsten oxide phase on SiO_2 is the catalytic active site since excess crystalline WO_3 did not influence the overall catalyst performance.[226] Wang *et al*. examined 1-butene isomerization and metathesis over two different supported WO_3/SiO_2 catalysts prepared with different silica supports.[227] Raman analysis[227] showed that the tungsten oxide was better dispersed on the lower surface area SiO_2 support, which is quite surprising since the opposite behavior would generally be expected. Whereas the lower surface area W-free SiO_2 support was not active for 1-butene isomerization, the higher surface area W-free SiO_2 support almost completely isomerized 1-butene suggesting that the higher surface area support contained significant amounts of acidic surface impurities. The catalyst with

higher surface area exhibited greater olefin metathesis activity suggesting that the surface impurities were also acting as promoters. Unfortunately, no surface analysis was performed to determine the nature of the surface impurities present on the high surface area silica support. For the cleaner supported WO_3/SiO_2 catalyst, the optimum metathesis performance was obtained at intermediate tungsten oxide loadings where both dispersed surface WO_x and crystalline WO_3 nanoparticles coexist. This observation suggests that WO_3 nanoparticles may also be responsible for 1-butene metathesis. Hua *et al*. investigated 1-butene self-metathesis with supported WO_x/MTS-9 (a titano-silica molecular sieve) and found that the metathesis performance was comparable over a wide range of tungsten oxide loadings which suggests that both dispersed surface WO_x species and WO_3 nanoparticles contribute to the olefin metathesis reaction.[215,216] Chaemchuen *et al*. investigated the influence of calcination temperature on the metathesis of ethylene and 2-butene to propylene over supported WO_x/SiO_2 catalysts. They concluded that the surface WO_x species were the catalytic active sites for olefin metathesis even though both surface WO_x species and crystalline WO_3 nanoparticles were always simultaneously present in their catalysts.[213] Most recently, the metathesis of 1-butene was studied over supported WO_x/SiO_2 catalysts with moderate dispersions of tungsten oxide, where both surface WO_x species and WO_3 nanoparticles coexist, yield the optimum metathesis performance.[218] The contributions of the surface WO_x sites and WO_3 nanoparticles on silica to the olefin metathesis reaction appear to be unresolved. Studies with well-defined supported WO_x/SiO_2 catalysts are required to determine the catalytic contributions of the different WO_x sites present in supported WO_x/SiO_2 catalysts.

Surface Acidity. Selectivity is claimed to be related to surface acidity in the WO_x/SiO_2 system.[207] Isomerization is claimed to occur through either alkoxide or allylic intermediates.[228] Sources of alkali metal ions such as Na_2O and K_2O can be added to suppress the Brønsted acidity which is claimed to be responsible for undesired isomerization products.[228] However, large amounts of alkali ions may adversely affect conversion since they can also reduce the Lewis acidity which is thought to be beneficial for metathesis activity.[208,209,228] The role of surface acidity on olefin metathesis by supported WO_x/SiO_2 still awaits resolution with well-defined catalysts.

$WO_x/(SiO_2$-$Al_2O_3)$

Supported WO_x/Al_2O_3 catalysts have received less attention in the literature than supported ReO_x/Al_2O_3 and MoO_3/Al_2O_3 catalysts due to their lower olefin metathesis activity.[9] This lower activity is related to its low ability to form reduced active site as seen in H_2-TPR spectra studies by Moulijn *et al*.[229] The olefin metathesis activity of supported WO_x/SiO_2 catalysts is reported to be higher than that of supported WO_x/Al_2O_3 [218,230], but other researchers found the opposite effect.[231] Andreini and Mol claimed that supported WO_x/Al_2O_3 catalysts deactivate above 397°C, whereas supported WO_x/SiO_2 catalysts are stable at such temperatures.[230] For the supported $WO_x/(SiO_2$-$Al_2O_3)$ system, the optimal SiO_2 loading is reported to be 20-30wt%.[218] Liu *et al*. claimed to only achieve moderate dispersion of surface WO_x species by impregnation of 3-aminopropyl-triethoxylsilane on the Al_2O_3 support from Raman and UV-vis experiments under ambient conditions.[218] These researchers concluded that the most active species are polymeric surface WO_x species and not isolated WO_x sites or WO_3 nanocrystallites.[218] Huang *et al*. attributed the improved self-metathesis activity of 1-butene to addition of 30% γ-Al_2O_3 to HY-zeolite

(Si/Al_2=10), which was enhanced relative to either γ-Al_2O_3 and HY-zeolite.[232] The improved performance was related to the Raman band for the surface WO_x species.[232] Debecker *et al*. reported W-Si-Al catalysts synthesized by an aerosol method outperformed traditional supported $WO_x/(SiO_2$-$Al_2O_3)$ by a factor of 1.5 at 250°C, which was attributed to an improved well-balanced acidity, pore size and better dispersion of WO_x species in the former samples.[231] As already mentioned earlier, simultaneous variation of the catalyst parameters prevents determining the origin of the catalyst structure-activity relationships for olefin metathesis, and more systematic studies are required to really understand the fundamentals of supported $WO_x/(SiO_2$-$Al_2O_3)$ catalysts.

Supported Organometallic Catalysts. Several model silica-supported surface WO_x-organometallic catalysts have been reported. Verpoort *et al*. anchored aryloxy tungsten complexes on an Nb_2O_5/SiO_2 support and subsequently converted the aryloxy ligands to phenoxy ligands by refluxing with phenol in n-hexane.[213] The resulting catalysts were extremely active for 2-pentene metathesis and also much more active than their corresponding homogeneous analogues. The enhanced activity was assigned to the anchoring of the tungsten complexes to the acidic dispersed NbO_x species on the silica support. Characterization of the supported complexes, however, was not performed and, thus, a molecular level understanding of such novel supported organometallic metathesis catalysts is lacking. Le Roux *et al*. successfully synthesized and molecularly characterized a well-defined surface tungsten hydride organometallic catalyst on SiO_2 that was active for alkane metathesis.[221] Gauvin *et al*. synthesized and extensively characterized a well-defined silica supported surface dinuclear tungsten amido organometallic catalyst, which

was not active for alkyne metathesis, but became active after it was reacted with tert-butanol to introduce tert-butoxide ligands.[222] The presence of alkylidene and metallacyclobutane surface reaction intermediates were detected with *in situ* solid state NMR by Schrock and Coperet *et al.* on a silica supported [W(≡NAr)(=CH*t*Bu)(2,5-$Me_2NC_4H_2)_2$] catalyst.[132] Mazoyer *et al*. synthesized and extensively characterized the first well-defined surface tungsten oxide oxo (W=O) alkyl organometallic catalysts on SiO_2, that were quite active for propylene metathesis.[223] It was hypothesized that metathesis catalytic active sites require W=O oxo bonds.[223] Recently Schrock and Coperet *et al.* grafted $(ArO)_2W(=O)(=CHtBu)$ (ArO = 2,6-mesitylphenoxide) on silica that had been partially dehydroxylated at 700^oC and was found to be one of the most active olefin metathesis catalysts to date.[233] IR and NMR analysis revealed the formation of [(≡SiO)W(=O)(=CHtBu)(OAr)] (80%) and [(≡SiO)W(=O)(CH_2tBu)-$(OAr)_2$] (20%) surface complexes.[233] Unlike the industrial supported WO_3/SiO_2 catalysts that require high temperatures and are inactive for metathesis of functionalized olefins, the silica supported [(≡SiO)W(=O)(=CHtBu)(OAr)] catalyst is able to perform metathesis of olefins containing oxygenated groups such as oleic acid esters.[233] The surface organometallic catalysts have an advantage in metathesis of functionalized olefins since these complexes better stabilize bulky compounds.[80,233] The significantly enhanced activity of the silica supported W organometallic complexes than industrial type supported WO_3/SiO_2 catalysts indicates that the structures and ease of activation of the catalytic active sites are different for these two catalyst systems.

Patents. Since 2000, the industrial patent literature for olefin metathesis by supported WO_x/SiO_2 catalysts has been receiving attention.

[83,84,86,97,103,104,109,114,115,163,169,172,191,193,194,234-243] Although most of the patented metathesis processes are devoted to the use of ethylene and 2-butene feedstocks to make propylene, some of the processes also employ unconventional feeds such as butenes (partially converted to ethylene),[109,114,165,168,238] isobutanol (dehydrated to butene),[172,191] and ethylene (partially dimerized to butene)[82,115]. Some of the metathesis patents focus on the nature of the SiO_2 support (amorphous SiO_2, MCM-22 or MCM-48)[106,197,235,236] and there is also emphasis on the purity of the SiO_2 support[109]. It has also been claimed that metathesis catalytic activity can be enhanced by initially acid washing the silica support to reduce levels of impurities (e.g., Mg, Ca, Na, Al and Fe, that must be maintained below several hundred ppm)[234,235] and that the metathesis activity can be increased by the addition of promoters such as Nb_2O_5 (0.01-10%).[171] Impregnation of the active tungsten oxide component on the silica support is always performed with the aqueous $(NH_4)_6H_2W_{12}O_{40}$ precursor followed by drying at ~120^oC to remove the water and subsequent treatment at elevated temperatures.[104] The standard elevated temperature treatment involves calcination in air, but some patents also report heating in inert environments (N_2) or olefins.[104,106,239,243] Patents on regeneration of coked catalysts describe regeneration with air and steam.[168,193]

Summary. Although the molecular structures of the multiple WO_x sites present on silica for the initially oxidized supported WO_x/SiO_2 catalysts are known, there is no information about the nature of these WO_x sites during catalyst activation and olefin metathesis. The absence of direct characterization during catalyst activation and olefin metathesis prevents accessing fundamental information about the surface reaction intermediates and reaction mechanism. Relevant DFT calculations for olefin metathesis by supported WO_x/SiO_2

catalysts that relate the specific reactivity of each of the WO_x sites have to be performed. In comparison to the other supported metal oxide olefin metathesis catalysts, the supported WO_x/SiO_2 catalyst system has received minimal attention in the catalysis literature that is surprising given the industrial importance of this olefin metathesis catalytic system.

7. Summary of Olefin Metathesis by Supported Metal Oxide Catalysts

The absence of direct observation measurements of the catalytic active sites and surface reaction intermediates during olefin metathesis is one of the primary reasons for the lack of scientific progress in this important field of heterogeneous catalysis. Systematic time-resolved *in situ* and *operando* molecular spectroscopy studies of supported rhenium, molybdenum and tungsten oxide catalysts during catalyst activation and olefin metathesis should significantly advance our fundamental understanding of the nature of the catalytic active sites, surface reaction intermediates, reaction mechanisms and structure-reactivity relationships of these important heterogeneous catalysts for olefin metathesis. A recent critical review of heterogeneous olefin metathesis by Coperet concluded that future research should be focused on (i) synthesis of well-defined supported catalysts, (ii) control of the surface structure of the oxide supports as a way to control the coordination sphere of the surface active species, (iii) development of advanced *in situ* and *operando* spectroscopic characterization methods to better understand the evolution of supported active sites and surface reaction intermediates under working conditions, (iv) correlation of the spectroscopic findings with kinetic studies (structure-activity relationships) and (v) elucidation of deactivation phenomena in order to prepare more robust catalysts and to provide novel methods of catalyst regeneration.[79] It

appears from this literature review that the topic of olefin metathesis by heterogeneous supported metal oxide catalysts is still a relatively undeveloped research area and is poised for significant progress in understanding of the fundamental molecular details of these important catalytic systems in the coming years.

8. Outline of Research

Thus, a unique research opportunity currently exists to unravel the molecular level nature of the catalytic active sites, especially during olefin metathesis, their activation and deactivation as well as promotion, surface reaction intermediates, surface reaction mechanism and structure-reactivity relationships for olefin metathesis by supported metal oxide catalysts. Successful execution of this research program is expected to unravel the fundamentals of heterogeneous supported metal oxide olefin metathesis catalysis, stimulate additional research in the field and impact commercial applications by molecular design of advanced catalyst materials. In accomplishing these objectives, two very important supported metal oxide systems, namely alumina supported rhenium oxide (ReO_x/Al_2O_3) and silica supported tungsten oxide (WO_x/SiO_2) are chosen for this thesis. The general scheme for this research is outlined as follows:

Chapter 1: Literature Review of Olefin Metathesis by Supported Metal Oxide Catalysts

This chapter provides a comprehensive review of existing literature from both academic and industrial publications/patents and outlines the foundation of the subsequent research.

Chapter 2: Surface ReO_x Sites on Al_2O_3 and their Molecular Structure-Reactivity Relationships for Olefin Metathesis

This chapter addresses the nature of ReO_x sites on the Al_2O_3 support and their olefin metathesis reactivity. The state-of-the-art *in situ* techniques and comprehensive DFT calculations are employed in achieving the objectives. The ability to identify more reactive ReO_x-II sites leads *for the first time* to the design of advanced $ReO_x/TaO_x/Al_2O_3$ catalysts.

Chapter 3: Activation of Surface ReO_x Species on Al_2O_3 for Olefin Metathesis

This chapter resolves the activation of ReO_x sites on the Al_2O_3 support for olefin metathesis. Long standing debates about the number of participating active sites/reactive intermediates are resolved by carefully designed temperature programmed surface reaction (TPSR) experiments.

Chapter 4: Mechanism and Kinetics of Olefin Metathesis by Supported ReO_x/Al_2O_3 Catalysts

This chapter discusses the reaction mechanism and kinetics of olefin metathesis by supported ReO_x/Al_2O_3 catalysts. Temperature dependent reaction orders and mechanisms are observed which allows for derivation of important kinetic and thermodynamic parameters.

Chapter 5: Conclusions and Proposed Future Studies

This chapter concludes with the main findings of the thesis and suggests new ideas to those interested in olefin metathesis by supported metal oxide catalysts.

Acknowledgements

The authors gratefully acknowledge funding from the U.S. Department of Energy-Basic Energy Sciences (FG02-93ER14350) and the National Science Foundation (CHE 1301262).

References

1. Anderson, A. W.; Merckling, N.G. Polymeric bicyclo-(2,2,1)-2-heptene. US Patent 2721189 (A), October 18, 1955.
2. Rouhi, A.M. *Chem. Eng. News* **2002**, *80*, 34–38.
3. Grubbs, R.; Tumas, W. Science (Washington, DC, US) **1989**, *243*, 907–915.
4. Banks, R.L; Bailey, G.C. *Ind. Eng. Chem. Prod. Res. Dev*. **1964**, *3*, 170–173.
5. Mol, J.C. *J. Mol. Catal. A. Chem*. **2004**, *213*, 39–45.
6. Disproportionation catalyst. British Petroleum Corporation. Great Britain Patent GB1054864 (A), September 8, 1964.
7. Keim, W. *Angew. Chem. Int. Ed*. **2013**, *52*, 12492–12496.
8. Calderon, N.; Chen, H.Y.; Scott, K.W. *Tetrahedron Lett.* **1967**, *34*, 3327–3329.
9. Mol, J. C.; van Leeuwen, P. W. N. M. 2008. Metathesis of Alkenes. Handbook of Heterogeneous Catalysis. 14:3240–3256.
10. Rouhi, A.M. *Chem. Eng. News* **2002**, *80*, 29–33.
11. Metathesis. *Kirk Othmer Encyclopedia of Chemical Technology*, 5th ed.; Wiley & Sons: New York, 2005, Vol. 20, pp 1–29.
12. The Nobel Prize in Chemistry. http://www.nobelprize.org/nobel_prizes/chemistry/laureates/2005/ (Accessed March 20, 2014).
13. Hérisson, J.-L.; Chauvin, Y. *Makromol. Chem*. **1971**, *141*, 161–176.
14. Coperet, C.; Chabanas, M.; Saint Arroman, R. P.; Basset, J.M. *Agnew. Chem. Int. Ed.* **2003**, *42*, 156–181.

15. Handzlik, J.; Sautet, P., *J. Catal*. **2008**, *256*, 1–14.

16. Handzlik, J. *J. Phys. Chem. B*, **2005**, *109*, 20794–20804.

17. Handzlik, J. *Surf. Sci.* **2007**, *601(9)*, 2054–2065.

18. Handzlik, J.; Ogonowski, J.; Tokarz-Sobieraj, R. *Catal. Today*, **2005**, *101*, 163–173.

19. Solans-Monfort, X.; Filhol, J.; Coperet, C.; Eisenstein, O. *New J. Chem.* **2006**, *30*, 842–850.

20. Wachs, I. E. *Catal. Today* **1996**, *27*, 437–455.

21. Wachs, I. E.; Keturakis, C. J. Monolayer Systems. In *Comprehensive Inorganic Chemistry II*; Schlogl, R., Ed.; Elsevier Publishing, 2013; pp 131–151.

22. Amakawa, K.; Wrabetz, S.; Kroehnert, J.; Tzolova-Mueller, G.; Schloegl, R.; Trunschke, A. *J. Am. Chem. Soc*. **2012**, *134*, 11462–11473.

23. Salameh, A.; Coperet, C.; Basset, J.; Bohm, V.P.W.; Roper, M. *Adv. Synth. Catal*. **2007**, *349*, 238–242.

24. McCoy, J.R.; Farona, M.F. *J. Mol. Catal*. **1991**, *66*, 51–58.

25. Chauvin, Y.; Commereuc, D. *J. Chem. Soc., Chem. Comm.*, **1992**, *6*, 462–464.

26. Olsthoorn, A. A.; Boelhouwer, C. *J. Catal*. **1976**, *44*, 197–206.

27. Nakamura, R.; Abe, F.; Echigoya, E. *Chem. Lett.* **1981**, 51–54.

28. Wang, L.; Hall, K. E. *J. Catal*. **1983**, *82*, 177–184.

29. Vuurman, M.A.; Stufkens, D.J.; Oskam, A.; Wachs, I.E. *J. Mol. Catal*. **1992**, *76*, 263–285.

30. Vuurman, M.A.; Wachs, I.E. *J. Phys. Chem*. **1992**, *96*, 5008–5016.

31. Mol, J.C. *Catal. Today*, **1999**, *51*, 289–299.

32. Turek, A.M.; Wachs, I.E.; DeCanio, E. *J. Phys. Chem*. **1992**, *96*, 5000–5007.

33. Hardcastle, F.D.; Wachs, I.E.; Horsley, J.A.; Via, G.H. *J. Mol. Catal*. **1988**, *46*, 15–36.

34. Bare, S.R.; Kelly, S.D.; Vila, F.D.; Boldingh,E.; Karapetrova,E.; Kas,J.; Mickelson, G.E.; Modica, F.S.; Yang, N.; Rehr, J. *J. Phys. Chem. C* **2011**, *115*, 5740–5755.

35. Vicente, B.C.; Nelson, R.C.; Moses, A.W.; Chattopadhyay, S.; Scott, S.L. *J. Phys. Chem. C* **2011**, *115*, 9012–9024.

36. Okal, J.; Kepinski, L. In Focus on Catalysis Research; Bevy, L. P., Ed.; Nova Science Publishers, Inc.: Hauppauge, N. Y., 2006; p 21.

37. Shpiro, E. S.; Avaev, V. I.; Antoshin, G. V.; Ryashentseva, M. A.; Minachev, K. M. *J. Catal*. **1978**, *55*, 402–406.

38. Yide, X.; Xinguang, W.; Yingzhen, S.; Yihua, Z.; Xiexian, G. *J. Mol. Catal*. **1986**, *36*, 79–89.

39. Balcar, H.; Zilkova, N.; Bastl, Z.; Dedecek, J.; Hamtil, R.; Brabec, L.; Zukal, A.; Cejka, J. *Studies in Surf. Sci. and Catal*., **2007**, *170*, 1145–1152.

40. Fung, A. S.; Tooley, P. A.; Kelley, M. J.; Koningsberger, D. C.; Gates, B. C. *J. Phys. Chem*. **1991**, *95*, 225–234.

41. Ronning, M.; Nicholson, D.G.; Holmen, A. *Catal. Lett.* **2001**, *72*, 141–146.

42. Daniell, W.; Weingard, T; Knozinger, H. *J. Mol. Catal. A: Chem*. **2003**, *204-205*, 519–526.

43. Duquette, L.G.; Cielinsky, R.C.; Jung, C.W.; Garrou, P.E. *J. Catal*. **1984**, *90*, 362–365.

44. Xu, Y.; Huang, J.; Lin, Z.; Guo, X. *J. Mol. Catal*. **1991**, *65*, 275–285.

45. Xiaoding, X.; Boelhouwer, C.; Vonk, D.; Benecke, J.I.; Mol, J.C. *J. Mol. Catal.* **1986**, *36*, 47–66.

46. Stoyanova, M.; Rodemerck, U.; Bentrup, U.; Dingerdissen, U.; Linke, D.; Mayer, R.-W.; Lansink Rotgerink, H.G.J.; Tacke, T. *App. Catal. A: Gen*. **2008**, *340*, 242–249.

47. Tarasov, A.L.; Shelimov, B.N.; Kazansky, V.B.; Mol, J.C. *J. Mol. Catal. A: Chem*. **1997**, *115*, 219–228.

48. Olsthoorn, A.A.; Boelhouwer, C. *J. Catal*. **1976**, *44*, 207–216.

49. Kapteijn, F.; Bredt, L.H.G.; Homburg, E.; Mol, J.C. *Ind. Eng. Chem. Prod. Res. Dev.* **1981**, *20*, 457–466.

50. Ellison, A.; Coverdale, A. K.; Dearing, P. F. *App. Catal.* **1983**, *8*, 109–121.

51. Ellison, A.; Coverdale, A. K.; Dearing, P. F. *J. Mol. Catal*. **1985**, *28*, 141–167.

52. Xiaoding, X; Mol, J. C. *J. Chem. Soc., Chem. Commun*. **1985**, *10*, 631–633.

53. Xiaoding, X; Mol, J.C.; Boelhouwer, C., *J. Chem. Soc* **1986**, *82*, 2707–-2718.

54. Amigues, P.; Chauvin, Y.; Commereuc, D.; Hong, C.T.; Lai, C.C.; Liu, Y.H. *J. Mol. Catal*. **1991**, *65*, 39–50.

55. Murrell, L. L.; Dispenziere, N. C. *Catal. Lett.* **1989**, *2*, 329–333.

56. Crepeau, G.; Montouillout, V.; Vimont, A.; Mariey, L.; Cseri, T.; Mauge, F. *J. Phys. Chem. B* **2006**, *110* , 15172–15185.

57. Schekler-Nahama, F.; Clause, O.; Commereuc, D.; Saussey, J. *Appl. Catal. A: Gen*. **1998**, *167*, 237–245.

58. Bek, D.; Balcar, H.; Zilkov, N.; Zukal, A.; Horacek, M.; Cejka, J. *ACS Catal*. **2011**, *1*, 709–718.

59. Hamtil, R.; Zilkova, N.; Balcar, H.; Cejka, J. Appl. Catal. A: Gen. **2006**, *302*, 193–200.

60. Balcar, H.; Hamtil, R.; Zilkova, N.; Cejka, J., *Catal. Lett.* **2004**, *97*, 25–29.

61. Balcar, H.; Hamtil, R.; Zilkova, N.; Zhang, Z, Pinnavaia, T.; Cejka, J. *Appl. Catal. A: Gen*. **2007**, *320*, 56–63.

62. Oikawa, T.; Ookoshi, T.; Tanaka, T.; Yamamoto, T.; Onaka, M. *Micro. Meso. Mat.* **2004**, *74*, 93–103.

63. Balcar, H.; Zilkova, N.; Zukal, A.; Cejka, J., *Studies in Surf. Sci. and Catal.* **2008**, *174 A*, 61–66.

64. Oikawa, T.; Masui, Y.; Tanaka, T.; Chujo, Y.; Onaka, M. *J. Organo. Chem*. **2007**, *692*, 554–561.

65. Bakala, P.C.; Briot, E.; Millot, Y.; Piquemal, J.; Brégeault, J., *J. Catal.* **2008**, *258*, 61–70.

66. Sheu, F.; Hong, C.; Hwang, W.; Shih, C.; W, J. *Catal. Lett*. **1992**, *14*, 297–304.

67. Williams, K.P.J.; Harrison, K. *J. Chem. Soc. Faraday Trans.* **1990**, *86*, 1603–1610.

68. Sibeijn, M.; Spronk, R.; Van Neen, J.A.R.; Mol, J.C. *Catal. Lett*. **1991**, *8*, 201–208.

69. Xiaoding, X.; Boelhouwer, C.; Benecke, J.I.; Vonk, D.; Mol, J.C. *J. Chem. Soc. Faraday Trans*. **1986**, *82*, 1945–1953.

70. Ivin, K.C.; Mol, J.C., “Olefin Metathesis and Metathesis Polymerization”, (Academic Press, London, **1997**).

71. Bouchmella, K.; Mutin, P.H.; Stoyanova, M.; Poleunis, C.; Eloy, P.; Rodemerch, U.; Gaigneaux, E.M.; Debecker, D.P. *J. Catal*. 2013, *301*, 233–241.

72. Herrmann, W.A.; Wagner, W.; Flessner, U.N.; Vokhardt, U.; Komber, H. *Angew. Chem. Int. Ed*. **1991**, *30*, 1636–1638.

73. Salameh, A.; Joubert, J.; Baudouin, A.; Lukens, W.; Delbecq, F.; Sautet, P.; Basset, J.; Coperet, C. *Angew. Chem. Int. Ed.* **2007**, *46*, 3870–3873.

74. Salameh, A.; Baudouin, A.; Soulivong, D.; Boehm, V.; Roeper, M.; Basset, J.; Copéret, C., *J. Catal*. , **2008**, *253*, 180–190.

75. Tovar, T.; Stewart, S.M.; Scott, S.L. *Top. Catal*. **2012**, *55*, 180–190.

76. Moses, A.W.; Ramsahye, N.A.; Raab, C.; Leifeste, H.D., Chattopadhyay, S.; Chmelka, B. F.; Eckert, J.; Scott, S.L. *Organometallics* **2006**, *25*, 2157–2165.

77. Salameh, A.; Baudouin, A.; Basset, J.; Coperet, C. *Angew. Chem. Int*. Ed. **2008**, *47*, 2117 –2120.

78. Coperet, C. *Beilstein J. Org. Chem*. **2011**, *7*, 13–21.

79. Coperet, C. *Dalton Trans*. **2007**, *47*, 5498–5504.

80. Chabanas, M.; Baudouin, A.; Coperet, C.; Basset, J. *J. Am. Chem. Soc*. **2001**, *123*, 2062– 2063.

81. Scott, S.L.; Basset, J. *J. Am. Chem. Soc*. **1994**, *116*, 12069–12070.

82. Coleman, S.T.; Sawyer, G. A.; Bridges, R. S. Production of 1-Butene and Propylene From Ethylene. US Patent 20120095275 A1, April 19, 2012.

83. Chahen, L.; Berthod, M.; Kelsen, V.; Chauvin, Y.; Olivier-Bourbigou, H.; Vallee, C. 20110098497 A1. US Patent 20110098497 A1, April 28, 2011.

84. Takai, T.; Ikenaga, H.; Kotani, M.; Miyazoe, S. Olefin manufacturing method. PCT Int. WO 2010024319 A1, March 4, 2010.

85. Szesni, N.; Sturm, S.; Fischer, R. Improved process for preparation of methyltrioxorhenium by chlorination of rhenium oxides and methylation by methylzinc acetate. DE 102008062687 A1, July 1, 2010.

86. Ramachandran, B.; Choi, S.; Gartside, R. J.; Kleindienst, S.; Ruettinger, W.; Alerasool, S. Olefin isomerization and metathesis catalyst for manufacture of propylene. US Patent 20100056839 A1, March 4, 2010.

87. Szesni, N.; Sturm, S.; Fischer, R.; Hermann, W. Improved process for preparing methyltrioxorhenium and organorhenium(vii) oxides. PCT Int. WO 2009036775 A1, March 26, 2009.

88. Gennaro, A.; Guerrini, R.; Panella, F.; Querci, C.; Russo, M. Process for the preparation of supported rhenium catalyst and its use in the metathesis reaction of olefins. IT 1347799 B1, October 2, 2008.

89. Sigl, M.; Schneider, D. Assignee: BASF SE, Germany. Carrier catalyst for metathesis. PCT Int. WO 2008077835 A2, July 3, 2008.

90. Bespalova, N. B.; Masloboishchikova, O. V.; Kozlova, G. A. Rhenium oxide catalyst for production of propylene by olefin metathesis. RU 2292951 C1, February 10, 2007.

91. Takai, T.; Kubota, T. Method for producing olefins by metathesis reaction of olefins under hydrogen using catalysts. PCT Int. WO 2006093058 A1, September 8, 2006.

92. Basset, J.M.; Thivolle Cazat, J.; Taoufik, M.; Le Roux, E.; Coperet, C. Process for the metathesis of alkenes using a catalyst comprising alumina which has been surface grafted with tungsten hydride moieties. FR 2872509 A1, January 6, 2006.

93. Herrmann, W.A.; Kuehn, F.E.; Fischer, R. A method for efficient production of methyltrioxorhenium (VII) (MTO) and organorhenium (VII) oxide. DE 102004062246 A1, March 2, 2006.

94. Brown, D.S.; Ginestra, J.M. Metathesis catalyst and process. US Patent 20060116542 A1, June 1, 2006.

95. Schubert, M.; Stephan, J.; Poplow, F.; Heidemann, T.; Diehlmann, U.; Maltry, M. Metathesis method for purifying starting products. PCT Int. WO 2006089957 A1, August 31, 2006.

96. Sigl, M.; Schubert, M.; Stephan, J.; Poplow, F. Method for producing propene from 2-butene and isobutene-rich feeding flows. PCT Int. WO 2006089956 A2, August 31, 2006.

97. Gartside, R. J.; Greene, M. I. Catalyst and process for the metathesis of ethylene and butenes in the manufacture of propylene. US Patent 20050124839 A1, June 9, 2005.

98. Schubert, M.; Stephan, J.; Boehm, V.; Brodhagen, A.; Poplow, F.; Weichert, C.; Borchert, H. Supported catalyst with a defined pore distribution in the mesopore range. PCT Int. WO 2005082532 A1, September 9, 2005.

99. Schubert, M.; Stephan, J.; Boehm, V.; Brodhagen, A.; Poplow, F. Metathesis catalysts supported on delta- or theta-modified alumina for nonaromatic unsaturated compound manufacture. PCT Int. WO 2005082526 A2, September 9, 2005.

100. Onaka, A.; Oikawa, T. MXy-meso Al2O3 catalyst support and metathesis catalyst. JP 2005152888 A, June 16, 2005.

101. Schubert, M.; Hesse, M.; Stephan, J.; Boehm, V.; Brodhagen, A.; Poplow, F.; Diehlmann, U.; Hellmann, M.; Loewenmuth, G. Porous, supported metathesis rhenium catalyst manufactured using porous building materials. DE 102004009804 A1, September 15, 2005.

102. Querci, C.; Bosetti, A.; Guerrini, R.; Panella, F.; Russo, M. Rhenium catalyst supported on modified alumina and use thereof in the metathesis reaction of olefins. PCT Int. Appl. WO 2005105286 A2, November 10, 2005.

103. Basset, J. M.; Coperet, C.; Soulivong, D.; Taoufik, M.; Thivolle, C.J. Metal compound fixed on a support, preparation process, and use of the compound in hydrocarbon metathesis reactions. FR 2852866 A1, October 1, 2004.

104. Schubert, M.; Hesse, M.; Stephan, J.; Boehm, V.; Brodhagen, A.; Poplow, F.; Sinner-Lang, Mschub Diehlmann, U.; Cox, G.; Pfeifer, J. Preparation of activated metathesis catalysts. EP 1473083 A1, November 3, 2004.

105. Turchetta, S.; Massardo, P.; Tuozzi, A. Improved process for preparation of trioxomethylrhenium by methylation of dirhenium heptaoxide by tetramethylstannane in the presence of chlorotrimethylsilane. PCT Int. WO 2004076469 A1, September 10, 2004.

106. Flego, C.; Pollesel, P.; Ricci, M.; Romano, U. Process for preparation of 2,3-dimethylbutane. IT 1324054 B1, October 28, 2004.

107. Stephan, J.; Schubert, M.; Weichert, C.; Ruppel, W.; Resch, P.; Zimdahl, S.; Mrzena, F.; Molitor, A.; Berg, S.; Fohrmann, M. Regeneration of supported rhenium oxide-doped olefin metathesis catalysts. DE 10309070 A1, September 16, 2004.

108. Euzen, P.; Guibert, S.; Kruger-Tissot, V.; Vidouta, G. Catalyst compound for the metathesis of olefins. US Patent 20030023125 A1, January 30, 2003.

109. Gartside, R. J.; Greene, M. I.; Jones, Q. J. Metathesis process for producing propylene and hexene from C4 olefin streams. US Patent 20030176754 A1, September 18, 2003.

110. Twu, F.; Christensen, S.A.; Hensey, S.; Rost, W.R. US Patent 20030224945 A1, December 4, 2003.

111. Querci, C.; Panella, F.; Guerrini, R.; Russo, M. EP 1350779 A1, October 8, 2003.

112. Matkovskii, P. E.; Startseva, G. P.; Aldoshin, S. M.; Mihailovic, D.; Stankovic, V. Process for production of olefinic oligomers by cationic oligomerization of isomeric decenes with nickel-aluminum catalyst systems. RU 2199516 C2, February 27, 2003.

113. Woehrle, I.; Reckziegel, A.; Esser, P.; Stuermann, M. Synthesis of cycloalkadiene by metathesis of cycloalkenes using Re_2O_7 catalyst supported over γ-Al_2O_3. EP 1287887 A1. March 5, 2003.

114. Gartside, R. J.; Greene, M. I.; Khonsari, A. M.; Murrell, L. L. Catalyst consisting of a transition metal supported on a high purity silica for the metathesis of olefins. PCT Int. WO 2002100535 A1, December 19, 2002.

115. Guerin, F.; Guo, S. X. Production of low molecular weight hydrogenated nitrile rubber involving metathesis of nitrile rubber and an olefin. PCT Int. WO 2002100905 A1, December 19, 2002.

116. Basset, J.; Chabanas, M.; Coperet, C. Supported catalysts for the metathesis of olefins. PCT Int. WO 2002022262 A2, March 21, 2002.

117. Schwab, P.; Breitscheidel, B.; Schulz, R.; Schulz, M.; Mueller, U. Catalysts based on rhenium heptoxide on a support and its manufacture for metathesis of olefins. DE 19837203 A1, February 24, 2000.

118. Metathesis catalyst based on rhenium and cesium, its preparation and its use in conversion of a C4 olefin fraction. DE 19947352 A1, April 6, 2000.

119. Commereuc, D.; Mikitenko, P. Process for the metathesis of olefins in the presence of a stabilizing agent for the catalyst. EP 1024123 A1, August 2, 2000.

120. Amigues, P.; Chauvin, Y.; Commereuc, D.; Hong, C.T.; Lai, C.C.; Liu, Y.H. *J. Mol. Catal*. **1991**, *65*, 39–50.

121. Bakala, P.C.; Briot, E.; Millot, Y.; Piquemal, J.; Brégeault, J. *J. Catal.* **2008**, *258*, 61–70.

122. Chauvin, Y.; Commereuc, D.; Saussine, L. Reprocessing of used rhenium catalyst. EP 568407 A1, November 03, 1993.

123. Tian, H.; Roberts, C.A.; Wachs, I.E. *J. Phys. Chem. C* **2010**, *114*, 14110–14120.

124. Debecker, D.P.; Stoyanovab, M.; Rodemerckb, U.; Gaigneaux, E.M. *J. Mol. Catal. A: Chem.* **2011**, *340*, 65–76.

125. Debecker, D.P; Bouchmella, K.; Poleunis, C.; Eloy, P.; Bertrand, P.; Gaigneaux, E.M; Mutin, P.M. *Chem. Mater.* **2009**, *21*, 2817–2824.

126. Debecker, D.P; Schimmoeller, B.; Stoyanova, M.; Poleunis, C.; Bertrand, P.; Rodemerck, U.; Gaigneaux, E.M. *J. Catal*. **2011**, *277*, 154–163.

127. Debecker, D.P.; Stoyanova, M.; Rodemerck,U.; Eloy, P.; Léonard, A.; Su, B.; Gaigneaux, E.M. *J. Phys. Chem. C* **2010**, *114 (43)*, 18664–18673.

128. Banares, M.; Hu, H.; Wachs, I.E. *J. Catal.* **1994**, *150(2)*, 407–420.

129. Williams, C.C.; Ekerdt, J.G.; Jehng, J. M.; Hardcastle, F.D.; Turek, A.M.; Wachs, I.E. *J. Phys. Chem.* **1991**, *95(22)*, 8781–8791.

130. Imamoglu, Y.; Zumeroglu-Karan, B.; Amass, A.J., "Olefin Metathesis and Polymerization Catalysts: Synthesis, Mechanism and Utilization", Kluwer Academic Publishers, Series C: Mathematical and Physical Sciences, **1989**, Vol. 326.

131. Blanc, F.; Rendon, N.; Berthoud, R.; Basset, J.; Coperet, C. Tonzetich, Z. J.; Schrock, R.R. *Dalton Trans*., **2008**, 3156-3158.

132. Blanc, F.; Berthoud, R.; Coperet, C.; Lesage, A.; Emsley, L.; Singh, R.; Kreickmann, T.; Schrock, R.R. *Proceedings of the National Academy of Sciences*, **2008**, *105*, 12123–12127.

133. Lee, E. L.; Wachs, I. E. *J. Phys. Chem. C* **2007**, *111*, 14410–14425.

134. Chempath, S.; Zhang, Y.; Bell, A.T. *J. Phys. Chem. C* **2007**, 111, 1291–1298.

135. Handzlik, J.; Ogonowski, J. *J. Phys. Chem. C* **2012**, *116*, 5571–5584.

136. Amakawa, K., Sun, L., Guo, C., Hävecker, M., Kube, P., Wachs, I. E., Lwin, S., Frenkel, A. I., Patlolla, A., Hermann, K., Schlögl, R. and Trunschke, A. *Angew. Chem. Int. Ed*. **2013**, *52*, 13553–13557.

137. Radhakrishnan, R.; Reed, C.; Oyama, S.T; Seman, M.; Kondo, J.N.; Domen, K.; Ohminami, Y.; Asakura, K. *J. Phys. Chem. B* **2001**, *105*, 8519–8530.

138. Ohler, N.; Bell, A.T. *J. Phys. Chem. B* **2006**, *110*, 2700–2709.

139. Thielemann, J. P.; Ressler, T.; Walter, A.; Tzolova-Müller, A.; Hess, C. *App. Catal. A: General* **2011**, *399*, 28–34.

140. Lee, E.L.; Wachs, I.E. *J. Phys. Chem.C* **2008**, *112*, 6487–6498.

141. Zhang, B.; Liu, N.; Lin, Q.; Jin, D. *J. Mol. Catal.* **1991**, *65*, 15–28.

142. Kazansky, V.B.; Shelimov, N.B.; Vikulov, K.A. *Studies in Surf. Sci & Catal*. **1993**, *75*, 515–527.

143. Vikulov, K. A.; Shelimov, B.N.; Kazansky, V.B.; Martra, G.; Marchese, L.; Coluccia, S., *Catal. Surf. Char*. **1992**, *114*, 87–96.

144. Vikulov, K.A.; Elev, I.V.; Shelimov, B.N.; Kazansky, V.B. *Catal. Lett.* **1989**, *2*, 121–123.

145. Vikulov, K.A.; Shelimov, B.N.; Kazansky, V.B; Mol, J.C. *J. Mol. Catal.* **1994**, *90*, 61–67.

146. Bykov, V.I.; Khmarin, E.M.; Belyaev, B.A.; Butenko, T.A.; Finkel'shtein, E.S. *Kin. Catal.* **2008**, *49*, 11–17.

147. Bykov, V.I.; Belyaev, B.A.; Butenko, T.A.; Finkel'shtein, E.S. *Kin. Catal.* **2012**, *53*, 353–356.

148. Hu, H.; Wachs, I.E.; Bare, S.R. *J. Phys. Chem*. **1995**, *99*, 10897–10910.

149. Chen, K.; Xie, S.; Bell, A.T.; Iglesia, E. *J. Catal.* **2001**, *198*, 232–242.

150. Handzlik, J.; Sautet, P. *J. Phys. Chem. C* **2008**, *112*, 14456–14463.

151. Handzlik, J.; Sautet, P. *J. Phys. Chem. C* **2010**, *114*, 19406–19414.

152. Masitkhin, V.M.; Nosov, A.V.; Zamaraev, K.I.; Wachs, I.E. *J. Phys. Chem C* **1994**, *98*, 13621–13624.

153. Grunert, W.; Stakheev, A.Y.; Morke, W.; Feldhaus, R.; Anders, K.; Shpiro, E. S.; Minachev, K. M. *J. Catal*. **1992**, *135*, 269–286.

154. Grunert, W.; Stakheev, A.Y.; Feldhaus, R.; Anders, K.; Shpiro, E. S.; Minachev, K. M. *J. Catal.* **1992**, 135, 287–299.

155. Kilmov, O. V.; Aleksev, O. S.; Startsev, A. N. *React. Kinet. Catal. Lett*. **1995**, *56*, 143–150.

156. Aguado, J.; Escola, J.M.; Castro, M.C. *Studies in Surf. Sci. & Catal*. **2005**, *156*, 835–842.

157. Olsthoorn, A. A.; Moulijn, J. A. *J. Mol. Catal*. **1980**, *8*, 147–160.

158. Grubbs, R. H.; Swetnick, S. J. *J. Mol. Catal*. **1980**, *8*, 25-36.

159. Guan, J.; Yang, G.; Zhou, D.; Zhang, W.; Liu, X.; Han, X.; Bao, X. *J. Mol. Catal: A. Chem*. **2009**, *300*, 41–47.

160. Brenner, A.; Burwell, R. L. *J. Catal.* **1978**, *52*, 364–374.

161. Hardee, J. R.; Hightower, J. W. *J. Catal*. **1983**, *83*, 182–191.

162. Handzlik, J.; Ogonowski, J. *Catal. Lett.* **2003**, *88*, 119–122.

163. Fuerstner, A.; Heppekausen, J. Molybdenum and tungsten metal complexes and use thereof as precatalysts for olefin metathesis. PCT Int. WO 2012116695 A1, September 7, 2012.

164. Taoufik, M.; Mazoyer, E.; Nicholas, C. P.; Basset, J. Olefin metathesis process and catalyst containing tungsten fluorine bonds for olefin. PCT Int. WO 2012092014 A2, July 5, 2012.

165. Van Hal, J. W.; Stevenson, S. A.; Allman, Jim; Sullivan, D. L.; Conant, T. A process for producing propylene and aromatics from butenes by metathesis and aromatization. PCT Int. WO 2011136983 A1, November 3, 2011. 20111103.

166. Nicholas, C.P.; Mazoyer, E.; Taoufik, M.; Basset, J.; Barger, P.T.; Rekoske, J.E. Conversion of butylene to propylene under olefin metathesis conditions. US Patent 20110245570 A1, October 6, 2011.

167. Miyazoe, S.; Ikenaga, H.; Kotani, M. Process for producing olefin", PCT Int. WO 2010113993 A1, October 7, 2010.

168. Po-Sum Shum. Catalyst regeneration with coke removal from pores. US Patent 20100167911 A1, July 1, 2010.

169. Halsey, R. B. Metathesis process using a moving phase reactor. US Patent 20090281364 A1, November 12, 2009.

170. Halsey, R. B.; Coleman, S.T. Olefin metathesis process using a fluidized bed reactor. US Patent 20090203950 A1, August 13, 2009.

171. Li, W.; Wang, Y.; Xie, Z.; Chen, Q.; Yang, W. Catalysts for metathesis of butylene for preparation of propylene. CN 1618515 A, May 25, 2005.

172. Bridges, R. S. Multi-step process for propylene and gasoline manufacture from tert-butanol and ethylene. US Patent 20050250969 A1, November 10, 2005.

173. Botha, J. M.; Spamer, A.; Mbatha, M.; Mthokozi, J.; Nkosi, B.S.; Reynhardt, J. P. K.; Jacobus, K. S.; Schwikkard, G. W. High-temperature metathesis process for

the conversion of C5-15 alkenes into C9-18 alkenes. PCT Int. WO 2001002324 A1, January 11, 2001.

174. Conant, T.; Stevenson, S. A. Mixed-phase operation of butenes metathesis process for maximizing propylene production using metathesis catalysts", US Patent 20130150643 A1. June 13, 2013.

175. Xuan, D.; Wang, Y.; Liu, S. Method for preparing 2,3-dimethyl-2-butene by metathesis of isobutylene. CN 102464552. May 23, 2012.

176. Kinkead, S. A. Olefin metathesis for kerogen upgrading. US Patent 20090133935 A. May 28, 2009.

177. Basset, J.; Merle, N.; Stoffelbach, F.; Taoufik, M.; Thivolle-Cazat, J. Solid metal compound, preparations and uses thereof. PCT Int. WO 2009044107. April 15, 2010.

178. Bridges, R.S.; Coleman, S. T. Integrated cracking and metathesis process for the manufacture of propylene from ethane. US Patent 20070112236. May 17, 2007.

179. Kruger, T. V.; Guibert, S.; Commereuc, D. Method for improving the regeneration of a metathesis catalyst. US Patent 20030008766. January 9, 2003.

180. Maas, H.; Wiebelhaus, D.; Stephan, J.; Paciello, R. Method for producing C6-20 linear α-olefins using transalkylation with isomerization and metathesis. DE 10103309. August 1, 2002.

181. Mukerjee, S. L.; Kyllingstad, V. L. Ring-opening metathesis polymerization (ROMP) of cycloolefins with molybdenum catalysts with outstanding reactivity. US Patent 20020111446. August 15, 2002.

182. Lutz, E. F. Metathesis process and catalysts for the preparation of α-olefins from internal olefins and ethylene. US Patent 5672802. September 30, 1997.

183. Endo, Z.; Yamada, T. Metathesis polymerization catalyst solution and system for preparing cross-linked polymers. EP0815155 B1. August 7, 2002.

184. Inagaki, S.; Fukushima, Y.; Ichikawa, M.; Oonishi, R. Olefin metathesis catalysts. JP 08215565. August 27, 1996.

185. Noweck, K.; Hoffmann, A. Aluminosilicate-supported rhenium oxide catalysts and their use in olefin metathesis. US Patent 5883272 A. March 16, 2009.

186. Kelly, J. Preparation of C4-alkene streams by olefin metathesis", EP 691318 A1. January 10, 1996.

187. Nicolaides, C. P. Production of C4-6 olefins for manufacture of gasoline octane boosters using a metathesis catalyst. ZA 9207693. April 15, 1993.

188. Quann, R. J. Alpha-olefins from light olefins. US Patent 4665245 A. May 12, 1987.

189. Motz, K. L.; Poe, R. L.; Washecheck, P.H.; Yates, J. E. Olefins. EP 139774. May 8, 1985.

190. Tanaka, K. Catalyst for metathesis reaction. JP 61125438. June 13, 1986.

191. Vermeiren, W.; Adam, C.; Minoux, D .Production of propylene via simultaneous dehydration and skeletal isomerization of isobutanol on acid catalysts followed by metathesis. PCT Int. WO 2011113836 A1, September 22, 2011.

192. Bespalova, N. B.; Masloboyshchikova, O. V.; Kozlova, G. A. High selectivity dimerization and metathesis catalyst for producing propylene from ethylene in petrochemical industry. RU 2370314 C1. October 20, 2009.

193. Ikenaga, H. Process for reactivation of metathesis catalysts and process for production of olefins comprising the reactivation. PCT Int. WO 2009013964 A1, January 29, 2009.

194. Liu, S.; Wang, Y.; Xu, W.; Xu, Z.; Yang, W. Olefin metathesis catalyst for preparing propylene. CN 1915510 A. February 21, 2007.

195. Kukes, S.G.; Banks, R. L. Olefin metathesis and catalyst. US Patent 4517401. May 14, 1985.

196. Kukes, S.G.; Banks, R. L. Metathesis process and catalyst. US 4465890 A. August 14, 1984.

197. Tupy, M. J.; Amore, F.; Kaido, H; Meng, X. Method of making hydrogenated metathesis products. PCT Int. WO 2007081987 A2, July 19, 2007.

198. Li, X.; Zhang, W.; Liu, S.; Han, X.; Xu, L.;Bao, X. *J. Mol. Catal. A: Chem*. **2006**, *250*, 94–99.

199. Li, X.; Zhang, W.; Liu, S.; Xu, L.; Han, X.; Bao, X. *J. Catal*. **2007**, *250*, 55–66.

200. Li, X.; Zhang, W.; Liu, S.; Xu, L.; Han, X.; Bao, X. *J. Phys. Chem. C* **2008**, *112*, 5955–5960.

201. Aritani, H.; Fukuda, O.; Miyaji, A.; Hasegawa, S. *App. Surf. Sci.* **2001**, *180*, 261–269.

202. Hahn, T.; Bentrup, U.; Armbrüster, M.; Kondratenko, E. V.; Linke, D. *ChemCatChem* **2014**, *6*, 1664–1672.

203. Hahn, T.; Kondratenko, E.V.; Linke, D. *ChemCommun*. **2014,** Advance Article doi: 10.1039/C4CC01827C.

204. Debecker, D.P.; Stoyanova, M.; Colbeau-Justin, F.; Rodemerck, U.; Boissière, C.; Gaigneaux, E. M.; Sanchez, C. *Angew. Chem. Int. Ed*. **2012**, *51*, 2129 –2131.

205. Debecker, D.P.; Colbeau-Justin, F.; Sanchez, C.; Chaumonnot, A.; Berthod, M. Method of olefin metathesis using a catalyst based on a spherical material comprising oxidised metal particles trapped in a mesostructured matrix. PCT Int. WO2013011209 A1, January 24, 2013.

206. Ross-Medgaarden, E.I.; Wachs, I.E. *J. Phys. Chem. C* **2007**, *111*, 15089–15099.

207. van Schalkwyk, C.; Spamer, A.; Moodley, D.J.; Dube, T.; Reynhardt, J.; Botha, J.M.; Vosloo, H.C.M. *Appl. Catal. A: Gen.* **2003**, *255*, 143–152.

208. Spamer, A.; Dube, T.I.; Moodley, D.J.;van Schalkwyk, C.; Botha, J.M. *Appl. Catal. A: Gen*. **2003**, *255*, 133–142.

209. van Roosmalen, A. J.; Mol, J.C. *J. Catal.* **1982**, 78, 17–23.

210. Thomas, R.; Moulijn, J. A.; De Beer, V. H. J.; Medema, J. *J. Mol. Catal* **1980**, *8*, 161–174.

211. van Roosmalen, A. J.; Koster, D.; Mol, J. C. *J. Phys. Chem.* **1980**, *84*, 3075–3079.

212. Verpoort, F.; Fiermans, L.; Bossuyt, A. R.; Verdonck, L. *J. Mol. Catal.* **1994**, *90*, 43–52.

213. Verpoort, F.; Bossuyt, A.; Verdonck, L. *Chem. Comm*. **1996**, *3*, 417–418.

214. Verpoort, F.; Bossuyt, A. R.; Verdonck, L. *J. Elec. Spec. Phenom.* **1996**, *82*, 151–163.

215. Hua, D.; Chen, S.; Yuan, G.; Wang, Y.; Zhang, L. *Trans. Metal Chem.* **2011**, *36*, 245–248.

216. Hua, D.; Chen, S.; Yuan, G.; Wang, Y.; Zhao, Q.; Wang, X.; Fu, B., *Micro. Meso. Mat.* **2011**, *143*, 320–325.

217. Chaemchuen, S.; Phatanasri, S.; Verpoort, F.; Sae-ma, N.; Suriye, K. *Kin. Catal.* **2012**, *53(2)*, 247–252.

218. Liu, N.; Ding, S.; Cui, Y.; Xue, N.; Luming Peng, L.; Guo, X.; Ding, W. *Chem. Eng. Resea. Des.* **2013**, *91*, 573–580.

219. Huang, S.; Liu, S.; Zhu, Q.; Zhu, X.; Xin, W.; Liu, H.; Feng, Z.; Li, C.; Xie, S.; Wang, Q.; Xu, L. *App. Catal., A: Gen*. **2007**, *323*, 94–103.

220. Maksasithorn, S.; Debecker, D.P.; Praserthdam, P.; Panpranot, J.; Suriye, K.; Ayudhya, S.K.N. *Chin. J. Catal*. **2014**. *35*, 232–241.

221. Le Roux, E.; Taoufik, M.; Baudouin, A.; Coperet, C.; Thivolle-Cazat, J.; Basset, J.; Maunders, B. M.; Sunley, G. J. *Adv. Syn. & Catal.* **2007**, *349* , 231–237.

222. Gauvin, R.M.; Coutelier, O.; Berrier, E.; Mortreux, A.; Delevoye, L.; Paul, J.; Mamede, A.; Payen, E. *Dalton Trans*. **2007**, 3127–3130.

223. Mazoyer, E.; Merle, N.; de Mallmann, A.; Basset, J.; Berrier, E.; Delevoye, L.; Paul, J.; Nicholas, C. P.; Gauvin, R. M.; Taoufik, M. *Chem. Comm.* **2010**, *46(47)*, 8944–8946.

224. Basrur, A. G.; Patwardhan, S. R.; Vyas, S. N. *J. Catal*. **199**1, *127(1)*, 86–95.

225. Cheng, Z.; Lo, C. *ACS Catal*. **2012**, *2*, 341−349.

226. Davazoglou, D.; Moutsakis, A.; Valamontes, V.; Psycharis, V.; Tsamakis, D. *J. Electrochem. Society* **1997**, *144*, 595–599.

227. Wang, Y.; Chena, Q.; Yang, W.; Xie, Z.; Xua, W.; Huang, D. *App. Catal. A. Gen.* **2003**, *250*, 25–37.

228. Spamer, A.; Dube, T.I.; Moodley, D.J.; van Schalkwyk, C.; Botha, J.M. *App. Catal. A. Gen.* **2003**, *255*, 153–167.

229. Thomas, R.; Moulijn, J. A. *J. Mol Catal*. **1982**, *15*, 157–172.

230. Andreini, A.; Mol, J. C. *J. Col. Inter. Sci.* **1981**, *84*, 57–65.

231. Debecker, D.P.; Stoyanova, M.; Rodemerck, U.; Colbeau-Justin, F. Boissere, C.; Chaumonnot, A.; Bonduelle, A.; Sanchez, C. *App. Catal. A: Gen*. **2014**, *470*, 458–466.

232. Huang, S.; Chen, F.; Liu, S.; Zhu, Q.; Zhu, X.; Xin, W.; Feng, Z.; Li, C.; Wang, Q.; Xu, L. *J. Mol. Chem. A: Chem.* **2007**, *267*, 224–233.

233. Conley, M.P.; Mougel, V.; Peryshov, D.V.; Forrest, Jr., W.P.; Gajan, D.; Lesage, A.; Emsley, L.; Coperet, C.; Schrock, R.R. *J. Am. Chem. Soc*. **2013**, *135*, 19068–19070.

234. Popp, K. E.; Krawczyk, M. A.; Nicholas, C. P.; Abrahamian, J. F. US Patent 20110196184 A1. August 11, 2011.

235. Krawczyk, M. A.; Popp, K. E.; Nicholas, C. P.; Abrahamian, J. F. US Patent 20110196185 A1. August 11, 2011.

236. Mueller, K.; Dyllick-Brenzinger, R.; Limbach, M.; Sturm, B. Method for producing an aqueous polymer dispersion using water-soluble metal carbene complexes as catalysts. PCT Int. WO 2011051374 A1, May 5, 2011.

237. Schrock, R.R.; King, A.J.; Zhao, Y.; Flook, M. M.; Hoveyda, A. H. US Patent 20110077421 A1. March 31, 2011.

238. Butler, J. R. Isomerization catalyst supported metathesis catalyst for olefin production from feedstock containing blend of terminal and internal olefins. US Patent 20110077444 A1. March 31, 2011.

239. Botha, J. M.; Dube, T.I; Moodley, D. J.; Spamer, A.; Van Schalkwyk, C. Silica-supported tungsten oxide catalysts for metathesis of α-olefins for production of linear internal C8-20-olefins. PCT Int. WO 2004016351 A1. February 26, 2004.

240. Xuan, D.; Wang, Y.; Liu, S.; Yang, W. Method for synthesis of hexane by metathesis of butylene. CN 102040454 A. August 14, 2013.

241. Basset, J.; Stoffelbach, F.; Taoufik, M.; Thivolle-Cazat, J. PCT Int. WO 2008001040 A1. January 3, 2008.

242. Sugawara, T. Manufacture of cyclo-olefin polymers by metathesis polymerization for monomer-free moldings without causing corrosion of molds. JP 2001131264 A. May 15, 2011.

243. Schubert, M.; Gerlach, T.; Hesse, M.; Stephan, J.; Bohm, V.; Brodhagen, A.; Poplow, F. Preparation of olefins or alkynes by metathesis of alkenes or alkynes over a transition metal carbide or oxycarbide catalyst. US Patent 20040220441 A1. November 4, 2004.

Scheme 1.1. Proposed olefin metathesis activation mechanisms. M represents the catalytic active site and S represents the oxide support [22-24]

(A) 1-2 hydrogen shift mechanism

(B) π-allyl mechanism

(C) H-assisted mechanism

(D) Pseudo-Wittig mechanism

Scheme 1.2. Chauvin's reaction mechanism for olefin metathesis[13] for the self-metathesis of propylene to ethylene and 2-butene.

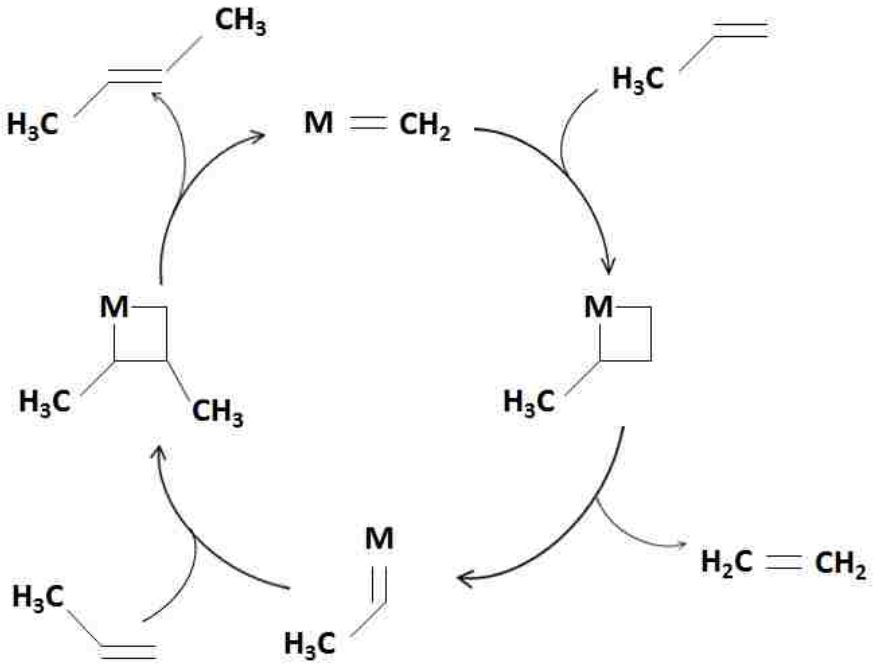

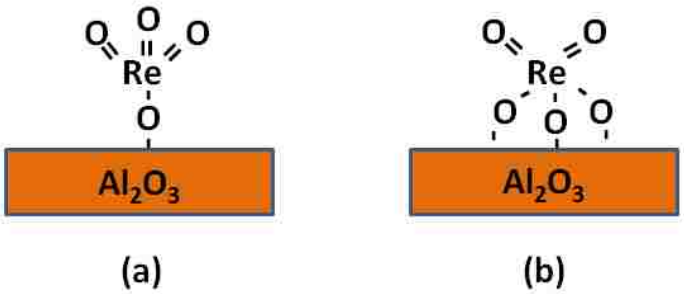

Figure 1.1. Proposed molecular structures of surface ReO_x species with (a) trioxo ReO_4 and (b) dioxo ReO_5 coordination on Al_2O_3.

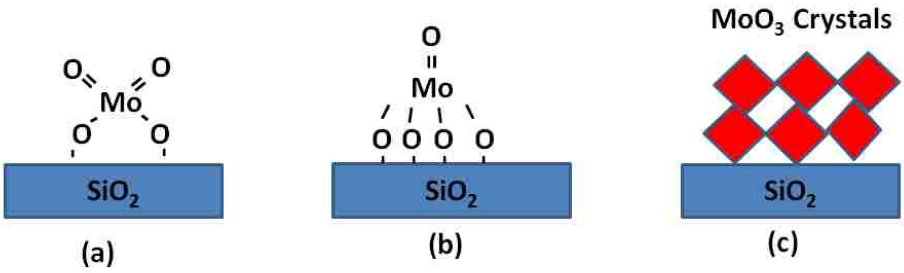

Figure 1.2. Structures of MoO_x species on SiO_2. Surface MoO_x dioxo (a), and mono-oxo (b) species coexist with MoO_3 crystals (c) at high coverage.

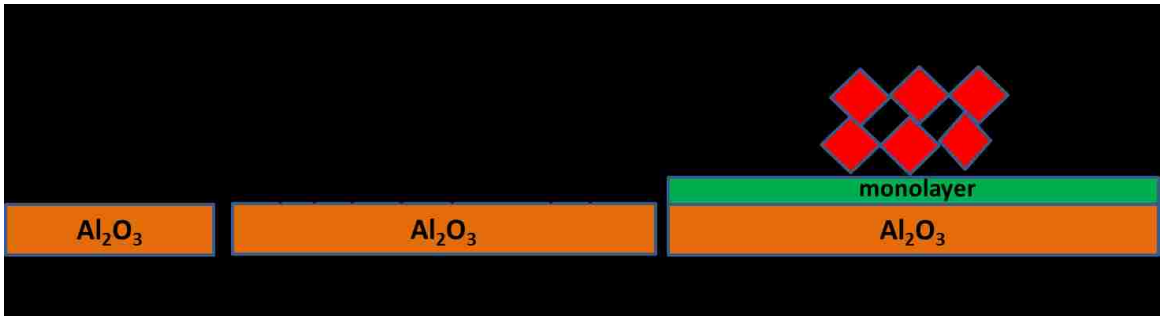

Figure 1.3. Structures of surface MoO_x species on Al_2O_3. (a) isolated dioxo MoO_4, (b) oligomeric mono-oxo MoO_5 and (c) crystalline MoO_3 NPs on surface MoO_x monolayer.

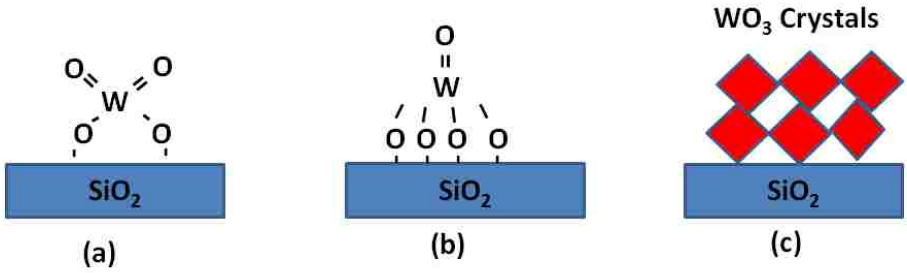

Figure 1.4. Structures of WO_x species on SiO_2. Surface WO_x species coexist with WO_3 crystals at high coverage. (a) dioxo WO_4, (b) mono-oxo WO_5 and (c) crystalline WO_3 nanoparticles.

CHAPTER 2

Surface ReO_x Sites on Al_2O_3 and their Molecular Structure-Reactivity Relationships for Olefin Metathesis

Abstract

Supported ReO_x/Al_2O_3 catalysts were investigated for propylene metathesis as a function of surface rhenia loading and extensively characterized with *in situ* UV-vis, Raman, IR, XANES/EXAFS and isotopic ^{18}O-^{16}O exchange studies. The experimental studies were complemented with DFT calculations using realistic models of the alumina surface. The surface ReO_x sites were found to be isolated surface dioxo $(O=)_2ReO_2$ species, which represent the most stable surface rhenia structures on alumina as shown by DFT. Two distinct surface ReO_4 species, however, were found to be present and only slightly differ in their bridging Re-O-Al bond lengths brought about by anchoring at different sites of the Al_2O_3 support. The deformed surface ReO_4-I species preferentially anchor at more basic μ_1 Al_{IV} and μ_1 Al_{VI} sites and are difficult to activate for propylene metathesis. The surface ReO_4-II species are formed at more acidic μ_2 Al_{VI} and μ_3 Al_{VI} sites and are the catalytic active sites for propylene metathesis. The surface ReO_4-II sites were readily activated by propylene while the deformed surface ReO_4-I sites were almost not affected by propylene, with only a few sites being activated. The steady-state propylene metathesis reaction rates are much higher for the surface ReO_4-II sites than the deformed surface ReO_4-I sites. The formation of the less reactive deformed surface ReO_4-I species could be blocked by occupation of the μ_1 Al_{IV} sites with sacrificial surface TaO_x species that resulted in catalysts exclusively containing the more active surface ReO_4-II

sites on alumina. This is *the first study* to demonstrate that the surface ReO_4-II sites are the precursors for the catalytic active sites for propylene metathesis by supported ReO_4/Al_2O_3 catalysts and to molecularly design olefin metathesis catalysts that exclusively contain isolated surface ReO_4-II sites.

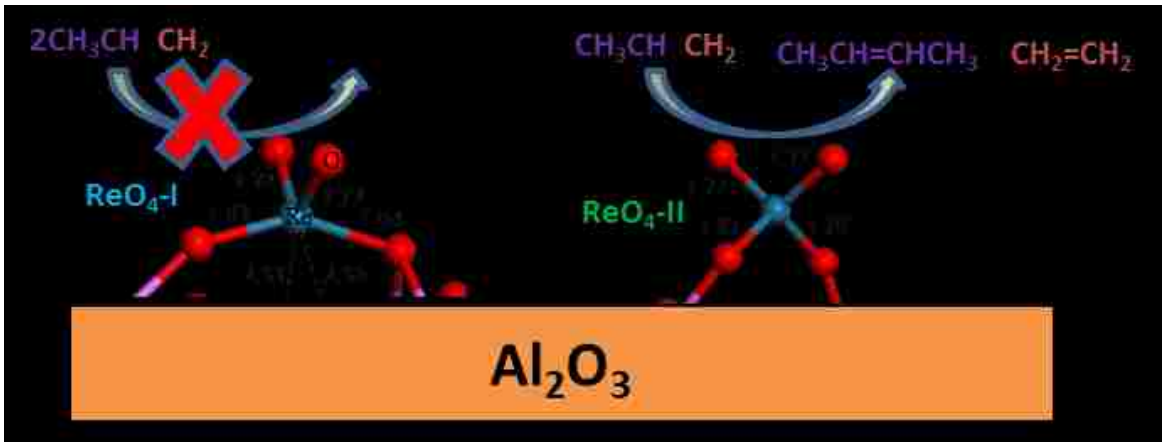

1. Introduction

Supported rhenium oxide catalysts find wide applications in numerous chemical processes.[1-3] For olefin metathesis, rhenium oxide supported on Al_2O_3 stands out since it is active and selective at low temperatures.[1] The industrial importance of olefin metathesis reactions, especially to meet the current global shortage of propylene by on purpose propylene production,[4] has stimulated numerous fundamental studies about the nature of the Re^{+7} oxide catalyst precursor supported on alumina. In particular, multiple *in situ* characterization studies (Raman, IR and XAS) and DFT calculations have confirmed that the surface rhenium oxide species are present as isolated sites on alumina.[5-13] The most commonly assigned molecular structure for the dehydrated Re^{+7} oxide on Al_2O_3 has been the trioxo $(O=)_3Re$-O-Al site (C_{3v} symmetry).[5-12] The nature of the surface Re^{+7} oxide species on alumina has recently come into question because of reported contradictory

conclusions.[12,13] Bare *et al.* concluded that isolated trioxo $(O=)_3Re$-O-Al species are present for calcined supported rhenia/alumina catalysts[12] mainly from EXAFS analysis. In contrast, Scott *et al*. postulated isolated penta-coordinated dioxo $(O=)_2Re(-O-Al)_3$ from XANES/EXAFS measurements and DFT calculations employing cluster models.[13] The precise coordination of the isolated surface Re^{+7} oxide species on alumina is of great importance to understand the remarkable low temperature olefin metathesis activity of this catalyst system. Indeed, it was shown for alumina supported Mo-oxo-carbene reactive intermediate complexes that the strain induced by multiple interactions with the support can strongly enhance the catalytic properties.[14] The structural analysis of surface Re^{+7} oxide species on alumina is further complicated since two slightly different dehydrated surface rhenia species have been observed by *in situ* Raman spectroscopy as a function of rhenia loading.[5,6] It is, thus, of paramount importance to settle the previously mentioned Re^{+7} oxide structural debate and understand the catalytic structure-reactivity relationships for the supported ReO_x/Al_2O_3 catalyst system for olefin metathesis as a function of rhenia loading and anchoring sites on the alumina support.

In the present study, comprehensive *in situ* Raman, IR, UV-vis and XANES/EXAFS experimental studies and DFT calculations are undertaken to determine the nature of surface ReO_x species on the Al_2O_3 support and their structure-reactivity relationships for olefin metathesis. The domain size or nuclearity of the surface ReO_x species are examined with *in situ* UV-vis spectroscopy. The average coordination of the surface ReO_x species is accessed with *in situ* XANES and the radial distribution of the atoms surrounding Re with *in situ* EXAFS. The molecular structure(s) and anchoring site(s) of the surface ReO_x species on alumina are probed with *in situ* Raman and IR

spectroscopy, respectively, and isotopic $^{18}O/^{16}O$ exchange Raman measurements. A number of possible DFT surface models are compared for multiple surface Re^{+7}oxide sites (trioxo, dioxo and mono-oxo coordinated rhenium oxide centers) on the (100) and (110) surfaces of γ-alumina. The alumina surfaces are described by a periodic slab.[15,16] The experimental *in situ* isotopic $^{18}O/^{16}O$ Raman band splitting patterns for supported ReO_x on alumina are compared with those obtained from theoretical calculations for the possible ReO_x species on the most dominant (110) alumina surface. Structure-reactivity relationships are developed for olefin metathesis of the supported ReO_x/Al_2O_3 catalysts by comparing the relationships between the initial surface ReO_x structures and their olefin metathesis reactivity.

2. Experimental

2.1. Catalyst Synthesis

2.1.1. Supported ReO_x/Al_2O_3 Catalysts

A series of 1-18wt% supported ReO_x/Al_2O_3 catalysts were prepared by incipient wetness impregnation of a 65-70 wt% aqueous solution of perrhenic acid, $HReO_4$ (Sigma Aldrich), onto two different Al_2O_3 supports (Harshaw batch#DD351, denoted as 'H' and Engelhard batch#H5433C, denoted as 'E') with BET surface areas of 180 m^2/g and 170 m^2/g, respectively. Using estimations from previous studies and taking consideration of ReO_x volatility, the actual Re loadings are approximated to be 1-15.6%.[6] The supported rhenia phase did not volatilize below 6.5% and the amount of volatilization increased non-linearly with rhenia loading above this value. The Al_2O_3 (Harshaw) support was used for some of the studies because the low fluorescence from this alumina gave rise to higher

quality *in situ* Raman spectra. An incipient wetness point of 1.0 mL H_2O/g was used for both supports. The alumina supports were impregnated with the aqueous perrhenic acid solution and the powders stirred for 30 minutes. After impregnation, the samples were initially dried overnight under ambient conditions, further dried at 120^oC for 2 hrs in flowing air (AirGas, ultrahigh purity (UHP)) and calcined in the flowing air by heating at 1^oC/min and held at 500^oC for 4 hrs (Thermodyne, furnace model 48000).

2.1.2. Promoted Supported $ReO_x/TaO_x/Al_2O_3$ Catalysts

The supported ReO_x/Al_2O_3 catalysts were also promoted with TaO_x via incipient wetness impregnation. The supported Ta_2O_5/Al_2O_3 was prepared from a solution of tantalum ethoxide (Ta-$(OC_2H_5)_5$, Alfa Aesar, 99.999%) dissolved in toluene (Sigma Aldrich, 99%) inside a glovebox (Vacuum Atmospheres, Omni-Lab VAC 101965) under a N_2 environment because of the air sensitivity of the Ta-ethoxide precursor. The supported Ta-ethoxide/Al_2O_3 sample was initially dried overnight in the glovebox and subsequently subjected to the same calcination procedure as applied to the supported ReO_x/Al_2O_3 catalysts. The supported Ta_2O_5/Al_2O_3 catalyst was impregnated with an aqueous $HReO_4$ solution, with the aforementioned preparation and calcination procedures, to synthesize the supported $ReO_x/Ta_2O_5/Al_2O_3$ catalysts. A reverse preparation procedure was also used to make a supported $Ta_2O_5/ReO_x/Al_2O_3$ catalyst in which the rhenia was initially impregnated and calcined prior to the addition of the tantalum oxide.

2.2. *In situ* Diffuse Reflectance Ultraviolet-visible (UV-vis) Spectroscopy

The UV-vis spectra of the catalysts were collected with a Varian Cary 5E UV-vis-NIR spectrophotometer with the Harrick Praying Mantis accessory. Approximately 5-25 mg of each catalyst in finely ground powder form was loaded into an *in situ* environmental cell (Harrick, HVC-DR2). The catalysts were dehydrated *in situ* at 500^{o}C under oxidizing conditions (10%O_2/Ar) and spectra of the dehydrated samples were collected in the 200-800nm range at 100^{o}C, using a scan rate of 15 nm/min and a signal averaging time of 0.6 seconds. A magnesium oxide sample was used as a standard for obtaining the background absorbance. The spectra of reference compounds, $KReO_4$ (Sigma Aldrich, 99.98%), $NaReO_4$ (Sigma Aldrich, 99.99%), NH_4ReO_4 (Sigma Aldrich, >99%) and Re_2O_7 (Alfa Aesar, 99.995%) were collected under ambient conditions. The spectrum of the moisture sensitive Re_2O_7 solid was collected with the sample in its original sealed glass vial. The Kubelka-Munk function $F(R_\infty)$ was calculated from the absorbance of the UV-vis spectra. The edge energy (E_g), or band gap, was determined by finding the intercept of the straight line for the low-energy rise of a plot of $[F(R_\infty)h\nu]^2$ versus $h\nu$, where $h\nu$ is the incident photon energy. A detailed example of this calculation can be found elsewhere.[17]

2.3. *In situ* XAS (XANES/EXAFS) Spectroscopy

The *in situ* Re L_1-edge X-ray absorption spectroscopy (XAS) experiments were performed in transmission mode at beam lines X19A and X18B at the National Synchrotron Light Source (NSLS) at the Brookhaven National Laboratory, using ionization chamber detectors for measuring incident and transmitted beam intensities. In addition, a third ionization chamber was used to detect the beam through a reference Re foil for energy calibration and alignment purposes. A plug flow reactor cell with a quartz

capillary tube (I.D./O.D. = 0.8 /1.0 mm) was used for *in situ* dehydrated measurements. The supported ReO_x/Al_2O_3 catalysts were dehydrated at 500^oC using the same dehydration procedure mentioned above and cooled to 70^oC before the spectra were recorded. Reference compounds, trioxo(triphenylsilyloxy) rhenium(VII) (Sigma Aldrich, 99.9%), iododioxobis (triphenylphosphine) rhenium(V) (Sigma Aldrich, 99.98%), trichlorooxobis (triphenylphosphine) rhenium(V) (Sigma Aldrich, 99.99%) and rhenium (VI) oxide, ReO_3 (Alfa Aesar, 99%) were diluted with Boron Nitride (Sigma Aldrich, 99%) to give a Re concentration of ~5-10 wt% and measured under ambient conditions. Data processing and analysis were performed using Athena and Artemis softwares.

2.4. *In situ* Raman spectroscopy

2.4.1. *In situ* Raman of dehydrated catalysts

The Raman spectra the supported ReO_x/Al_2O_3 catalysts were obtained with a Horiba-Jobin Ybon LabRam HR instrument equipped with three laser excitations (532, 442 and 325nm) and a liquid N_2-cooled CCD detector (Horiba-Jobin Yvon CCD-3000V). The 442nm laser was chosen since it minimized sample fluorescence. Spectral resolution was approximately 1 cm^{-1} and the wavenumber calibration was checked using the silica standard line at 520.7 cm^{-1}. The lasers were focused on the samples with a confocal microscope using a 50X objective (Olympus BX-30-LWD). Typically, the spectra were collected at 30 s/scan and 5 scans with a 200 μm hole.

Approximately 5-25 mg of each catalyst in powder form was loaded into an environmental cell (Harrick, HVC-DR2) with a SiO_2 window and O-ring seals which was kept cool by flowing water. The catalysts were initially dehydrated at a heating rate of

10°C/min up to 600°C and held for an hour under a 30 mL/min flow of 10% O_2/Ar (Airgas, certified, 9.989% O_2/Ar balance). Spectra were collected at the lowest possible temperatures as allowed by the fluorescence limitation, typically about 100 or 200°C. 1% C_3=/He or Ar (inert) is used for in situ Raman experiments during the reaction.

2.4.2. *In situ* Raman spectroscopy during ^{18}O-^{16}O Isotopic Exchange

After the aforementioned pretreatment/dehydration procedure, the ^{18}O-^{16}O isotope switching of the ReO_x was performed at 200°C with $H_2{}^{18}O$ (Sigma-Aldrich, Water-^{18}O, 95 atom% ^{18}O, CAS# 14314-42-2). The $H_2{}^{18}O$ water was manually injected into a flowing gas of 3 mL/min of 10% $^{16}O_2$/Ar and 27 mL/min of Ar (Airgas, Ar UHP 300) through a T-shaped pipe fitting with an open port using a 5 mL syringe. The minute presence of $^{16}O_2$ prevented darkening of the samples, improved the quality of the Raman spectra and was minimally involved in the oxygen isotope exchange. Plastic tubing connected the syringe to the pipe fitting and was connected throughout the experiment to prevent exposure to the ambient atmosphere. The gas lines were wrapped in heating tape and kept at ~150°C, at the point of injection to the cell inlet, to vaporize the $H_2{}^{18}O$ water. The injection doses were manually varied depending on the amount of exchanged ReO_x observed during the real-time monitoring with online Raman spectroscopy.

2.5. *In situ* Diffuse Reflectance Infrared Fourier Transform Spectroscopy (DRIFTS)

The *in situ* DRIFT spectra were collected with a Thermo Nicolet 8700 FT-IR spectrometer equipped with a Harrick Praying Mantis attachment (model DRA-2) for diffuse reflectance spectroscopy. Spectra were taken using a MCT detector with a

resolution of 4 cm^{-1} and an accumulation of 72 scans. Approximately 5-25 mg of each catalyst in powder form was loaded into an environmental cell (Harrick, HVC-DR2). The collection of the initial background was performed by first optimizing the beam path and IR absorption signal using the height of the full Harrick sample cup, then removing the Harrick cell and placing a reflective mirror in the laser path. A spectrum was collected using the reflective mirror and was used as the background spectrum throughout the experiment. The catalysts were dehydrated at 500^{o}C using the same dehydration procedure mentioned above. Spectra were collected at 500, 400, 300, and 200°C after dehydration to minimize spectral thermal broadening. Spectra at 200^{o}C are reported, unless otherwise noted.

2.6. DFT Calculations

The periodic DFT calculations have been performed in the framework of the generalized gradient approximation with the PW91 functional[18], using the Vienna Ab Initio Simulation Package (VASP).[19-21] The one electron wave functions are developed on a basis set of plane waves. Atomic cores are described with the projector-augmented wave method (PAW)[22] using a cutoff energy of 400 eV.

The previously validated periodic models of the γ-Al_2O_3 surface[15,16] are based on the non-spinel bulk structure.[23] The most exposed (110) plane, having an area of 74% and the minority (100) surface, having an area of 16%, were considered for calculations.[15] The (100) and (110) surfaces have been modeled by a four- and six-layer slabs, respectively. The bottom two and three layers are frozen in the geometry of the bulk. Frequency calculations have been carried out by numerical differentiation of the force matrix. All the

optimised degrees of freedom were used for the frequency calculations. The surface unit cell dimensions (Å) are a=8.414, b=11.180 for the (100) plane (unit formula $Al_{32}O_{48}$) and a=8.069, b=8.398 for the (110) plane (unit formula $Al_{24}O_{36}$). The Γ-centered 331 Monkhorst-Pack mesh provides a converged energy with respect to Brillouin-zone sampling.[24] All models consider the Re atom in the +7 oxidation state. For the graphic presentation of the structures, Materials Studio 5.5 software is used.[25]

5.7. Steady-State Propylene Metathesis Reaction

The catalytic activity measurements were performed in a fixed-bed catalytic reactor under differential conditions (propylene conversion <15%). A separate molecular sieve moisture trap was installed in the inlet propylene gas line to purify the reactants. Both inlet and outlet gas lines were heated using external electric heaters to ~200°C to prevent condensation of the reactants and products. The catalysts were pretreated in 10% O_2/Ar at 500°C for 30 minutes before cooling down in Ar to the reaction temperature of 70°C. Then a gas mixture of 1% propylene/1% Ar (internal standard)/He (balance) was introduced to the reactor at the flow rate of ~100mL/min. The products were analyzed using an online gas chromatograph (Agilent GC 6890) equipped with flame ionization (Agilent Serial #: USC250823H) and thermal conductivity (Restek Product #: PC3533) detectors. Conversion was normalized with propylene flow rate and catalyst weight to obtain reactivity, reported in mmol/g/hr. The reported activity values are averages of three measurements and the error bars indicate the upper and lower confidence levels.

2. Results

2.1. *In situ* UV-vis Spectroscopy

The *in situ* UV-vis edge energy (Eg) values for the dehydrated supported ReO_x/Al_2O_3 catalysts are presented in Figure 2.1 and exhibit a constant Eg value of ~4.2 eV for all surface rhenia coverage (0.14-2.2 Re atoms/nm^2). The high UV-vis Eg value reflects the presence of only isolated surface rhenia species on alumina because the Eg values are comparable to those for the isolated ReO_4-containing $NaReO_4$ (3.9 eV), $KReO_4$ (4.0 eV) and NH_4ReO_4 (4.0 eV) reference compounds and significantly higher than the Eg value for the oligomeric Re_2O_7 reference compound (2.8 eV) (see Figure S2.1). The absence of surface oligomeric and crystalline Re_2O_7 nanoparticles is a consequence of the volatility of dimeric and polymeric Re_2O_7 species, which assures that only isolated surface rhenia species are present on alumina.[5,6]

2.2. *In situ* XANES and EXAFS Spectroscopies

The *in situ* XANES spectra of the supported ReO_x/Al_2O_3 catalysts under dehydrated conditions are shown in Figure 2.2. The coordination of the ReO_x site is reflected by the Re L_1 XANES pre-edge feature. For metal oxides with MO_6 coordination, O_h and inversion symmetry, the s-d transitions are dipole forbidden and, thus, there is no K or L_1 pre-edge.[26,27] Bulk ReO_3 possesses ReO_6 coordination (Figure S2.4) and the slight L_1 pre-edge is related to its minor distortion. Strong deviations from the MO_6 O_h symmetry result in a sharp pre-edge feature in the Re L_1 edge XANES reflecting the absence of inversion symmetry.[26] The trioxo(triphenylsilyloxy) rhenium(+7) reference compound consists of ReO_4 coordinated isolated $(O=)_3ReO\text{-}Si\text{-}(phenyl)_3$ units containing

C_{3v} symmetry (Figure S2.4) and exhibits a sharp Re L_1 XANES pre-edge because of the absence of inversion symmetry. The other rhenia reference compounds do not exhibit a strong Re L_1 XANES pre-edge. The *in situ* Re L_1 XANES spectra for the dehydrated supported 3% and 15.6% ReO_x/Al_2O_3 catalysts possess a strong pre-edge feature approaching that of the trioxo(triphenylsilyloxy) Re^{+7} reference compound with C_{3v} symmetry. The slightly lower intensity of the pre-edge for the catalysts suggests that the ReO_x symmetry is slightly lower than C_{3v}, which may also be affected by some adsorption of residual moisture. The almost same XANES pre-edge intensity for both dehydrated supported ReO_x/Al_2O_3 catalysts also indicates that the surface ReO_x coordination does not change much with rhenia loading on the Al_2O_3 support.

The k^2 weighted Re L_1-edge EXAFS data of the corresponding samples are presented in Figure 2.3. The $(O=)_3ReO\text{-}Si\text{-}(phenyl)_3$ reference compound with isolated rhenia sites exhibits a strong peak at ~1.2Å from the terminal Re=O bonds. The absence of strong peaks at high R distance is consistent with the isolated nature of the $(O=)_3ReO\text{-}Si\text{-}(phenyl)_3$ reference compound. With the decrease in the number of Re=O bonds (3 in trioxo $(O=)_3ReO\text{-}Si\text{-}(phenyl)_3$, 2 in iododioxobis (triphenylphosphine) rhenium and 1 in trichlorooxobis (triphenylphosphine) rhenium), the intensity of the EXAFS peak at ~1.2 Å decreases. The crystalline bulk ReO_3 reference compound contains its Re-O peak at ~1.5 Å reflecting the longer metal-oxygen bond length in ReO_3 and absence of Re=O bonds in this structure. The bulk crystalline ReO_3 reference also possesses strong peaks in the 2-5Å range, originating from the Re-Re single scattering path and several multiple scattering paths of this solid compound. The dehydrated supported ReO_x/Al_2O_3 catalysts have a pronounced peak at ~1.2Å, similar to the location of the peak corresponding to Re=O

bonds in the references. For both catalysts, the intensity of the peak at ~1.2 Å is almost the same and is in between the intensities of the corresponding peaks in the standard compounds with 3 and 2 Re=O bonds. This type of change is consistent with the change of the number of Re=O pairs in the catalysts, and agrees well with the changes in the pre-edge peak of the corresponding XANES spectra. These two independent observations suggest that the catalysts possess mainly terminal Re=O bonds and their coordination numbers can be estimated between 2 and 3 with symmetry less than C_{3v}. The absence of high R peaks in the spectra of catalysts reflects the isolated nature of the surface rhenia species on alumina, which is consistent with the above *in situ* UV-vis findings. Quantitative analysis yields the effective Re=O bond lengths of 1.72-1.75Å for both species (SI). This is in agreement with the Re=O bond length values published in the recent literature,[12,13] but the actual number of Re=O bonds cannot be reliably obtained from EXAFS analysis because those contributions to EXAFS also correlate strongly with the single Re-O bonds at longer distances (e.g., 1.76Å, as discussed later in the DFT section). The description of fitting models compared for the quantitative data analysis is presented in the Supplementary Information section.

2.3. *In situ* Raman Spectroscopy

2.3.1. Supported ReO_x/Al_2O_3 catalysts under dehydrated conditions

The *in situ* Raman spectra of the dehydrated supported ReO_x/Al_2O_3 catalysts are presented in Figure 2.4. The supported 3% ReO_x/Al_2O_3 catalyst, with a low surface rhenia coverage of 0.44 Re/nm^2, exhibits Raman bands at ~1002 ν_s(Re=O) (s), ~970 ν_{as}(Re=O) (w), ~879 ν_s(Re-O-Al) (m) and ~340 δ(O-Re-O) (m) cm^{-1} for the surface rhenia species (labeled ReO_x-I). Supported catalysts with 5% ReO_4 ($\geq$ 0.74 Re/nm^2) and higher rhenia

loading, as shown for 9.4% ReO_x/Al_2O_3 in Figure 2.4, possess a new ν_s(Re=O) (s) band at ~1012 cm^{-1} from a second surface rhenia species (labeled ReO_x-II) since each structure can only give rise to one symmetric stretch according to vibrational spectroscopy selection rules.[28] The surface ReO_x-II species possess vibrations at 1012 ν_s(Re=O) (s), ~976 ν_{as}(Re=O) (w), ~890 ν_s(Re-O-Al) (m), and ~340 δ(O-Re-O) (m) cm^{-1}.The absence of vibrations from bending δ_s(Re-O-Re) (m) at ~150-250 cm^{-1}, stretching ν_s(Re-O-Re) (w) at ~400-600 cm^{-1} and stretching ν_{as}(Re-O-Re) (vw) at ~600-800 cm^{-1} (see Figure S7 for the Raman spectrum of solid Re_2O_7) is further consistent with the isolated nature of the surface ReO_x species on alumina.[5,6]

2.3.2. Supported $ReO_x/TaOx/Al_2O_3$ under dehydrated conditions

The simultaneous presence of two dehydrated surface ReO_x species at high surface rhenia coverage on alumina greatly complicates molecular structural analysis of the surface ReO_x-II site. To resolve this problem, it was chosen to use a second surface metal oxide that may behave similarly to surface ReO_x-I and does not give rise to strong Raman bands that would interfere with the rhenia vibrations (the motivation for this strategy is given below in section 4.4.2). Surface TaO_x was selected as the second metal oxide because previous studies showed that the supported TaO_x/Al_2O_3 system doesn't give strong Raman bands (as shown in Figure S2.8 for 15% Ta_2O_5/Al_2O_3, which is about half a monolayer of surface TaO_x on alumina).[29] The influence of the secondary surface TaO_x species on the supported ReO_x/Al_2O_3 catalyst system is also shown in Figure S2.8, and only the Raman vibrations corresponding to the surface ReO_x-II species on alumina are found at ~1010 ν_s(Re=O) (s), ~980 ν_{as}(Re=O) (w), 890 ν_s(Re-O-Al) (m) and 345 δ(O-Re-

O) (m) cm^{-1}. [5,6] The order of impregnation and calcination of TaO_x or ReO_x does not affect the final results (compare ReTaAl and TaReAl spectra in Figure S2.8) suggesting that surface TaO_x is able to block formation surface ReO_x-I species and, thus, increase the number of surface ReO_x-II sites. This is *the first time* that the surface ReO_x-II species have been successfully isolated on the alumina support.

2.3.3. Isotopic ^{16}O-^{18}O Exchange of supported ReO_x/Al_2O_3 catalysts

Time-resolved *in situ* Raman spectroscopy isotopic ^{18}O-^{16}O exchange studies were undertaken with $H_2{}^{18}O$ to assist in the discrimination between surface trioxo $(O=)_3ReO_x$, dioxo $(O=)_2ReO_x$ and mono-oxo $O=ReO_x$ species on alumina. During isotopic oxygen exchange, (*i*) trioxo species are expected to split into 4 Raman bands ($(=^{16}O)_3$, $(=^{16}O)_2(=^{18}O)$, $(=^{16}O)(=^{18}O)_2$ and $(=^{18}O)_3$), dioxo species should split into 3 Raman bands ($(=^{16}O)_2$, $(=^{16}O)(=^{18}O)$ and $(=^{18}O)_2$), and mono-oxo species will split into 2 Raman bands ($(=O^{16})$ and $(=O^{18})$).

The time resolved isotopic oxygen exchange Raman spectra for the supported 3% ReO_x/Al_2O_3 (H) catalyst that only possesses the surface ReO_x-I species are presented in Figure 2.5. The time-resolved Raman spectra indicate three ν_s(Re=O) vibrations that are only consistent with dioxo surface ReO_x species at ~1000 ($^{16}O=Re=^{16}O$), 992 ($^{18}O=Re=^{16}O$) and 943 cm^{-1} ($^{18}O=Re=^{18}O$). The corresponding δ(O-Re-O) mode shifts from 337 to 321 cm^{-1} during the isotopic exchange process while the broad ν_s(Re-O-Al) band at 880 cm^{-1} and weak ν_{as}(Re(=O) band at 969 cm^{-1} stretching vibrations become too weak to detect.

The time resolved isotopic oxygen exchange Raman spectra for the supported 10% ReO_x/10% Ta_2O_5/Al_2O_3 (E) catalyst that only possesses the surface ReO_x-II species are presented in Figure 2.6. The time-resolved Raman spectra indicate three ν_s(Re=O) vibrations that are only consistent with dioxo surface ReO_x species at ~1010 (^{16}O=Re=^{16}O), 995 (^{18}O=Re=^{16}O) and 950 cm^{-1} (^{18}O=Re=^{18}O). The corresponding δ(O-Re-O) mode shifts from 345 to 327 cm^{-1} during the isotopic exchange while the broad ν_s(Re-O-Al) band at 897 cm^{-1} and the very weak ν_{as}(Re(=O) band at ~980 cm^{-1} become too weak to detect with the isotopic oxygen exchange.

2.4. *In situ* IR Spectroscopy under dehydrated conditions

2.4.1. Overtone Region

The strong absorption of the IR radiation by the Al_2O_3 support prevents observation of the Re=O and Re-O vibrations in the fundamental frequency region (~1000 cm^{-1} and below). The Re=O vibrations, however, can be observed in the overtone region and the *in situ* IR spectra of the dehydrated supported ReO_x/Al_2O_3 catalysts in the overtone region are shown in Figure S2.9. The supported 3% ReO_x/Al_2O_3 catalyst that only contains the surface ReO_x-I species gives rise to two broad bands in the overtone region at ~1996 (s) and ~1962 (s) cm^{-1} from the ν_s(Re=O) and ν_{as}(Re=O) vibrations, respectively. At higher surface rhenia coverage, two additional shoulders appear at ~2020 (m) and ~1971 (m) cm^{-1} are also present from the ν_s(Re=O) and ν_{as}(Re=O) vibrations of the surface ReO_x-II species, respectively. These observations and assignments are in agreement with prior IR studies of supported ReO_x/Al_2O_3 catalysts and further support the presence of two distinct surface ReO_x species on alumina.[6] The IR bands, however, are

very broad and significantly overlap compared to the sharper Raman bands, which makes Raman the preferred method to monitor the surface ReO_x species on alumina.

2.4.2. Surface Hydroxyl (OH) groups

2.4.2.1. Supported ReO_x/Al_2O_3 Catalysts under Dehydrated Conditions

The alumina surface hydroxyls of under dehydrated conditions have been extensively studied in the catalysis literature and at least 5 types of surface hydroxyls are present and their coordination to the different surface alumina sites are given in Table 2.1.[15,16,30,31] The *in situ* IR spectra of the surface hydroxyl region of the dehydrated supported ReO_x/Al_2O_3 catalysts as a function of rhenia loading are presented in Figure 2.7. At low surface ReO_x coverage (3% ReO_x/Al_2O_3), mainly the μ_1-Al_{IV} , μ_1-Al_{VI} and μ_1-Al_V surface hydroxyls at 3787, 3768 and 3743 cm^{-1}, respectively, are consumed due to anchoring of the surface rhenia species on alumina. Minor amounts of μ_3- Al_{VI} surface hydroxyls at 3670 cm^{-1} also appear to be consumed. At intermediate surface ReO_4 coverage (9.4% ReO_x/Al_2O_3), the consumption of the μ_1-Al_V hydroxyl at 3728 cm^{-1} becomes significant, the 3694 cm^{-1} μ_2-Al_V hydroxyl are only slightly consumed and there does not appear to be any significant amount of μ_1 surface hydroxyls (3730-3800 cm^{-1}) remaining. At the highest surface ReO_x coverage (15.6% ReO_x/Al_2O_3), almost all of the IR observable alumina surface hydroxyls have been consumed. There is no indication for the formation of Re-OH hydroxyls under the dehydrated conditions. The *in situ* IR spectra reveal that different alumina surface hydroxyls are employed in anchoring the surface ReO_x species on the alumina support and explain why more than one surface ReO_x species is present on the alumina support with rhenia coverage.

2.4.2.1. Supported $ReO_x/Ta_2O_5/Al_2O_3$ Catalysts

The surface TaO_x species anchor at the same basic surface hydroxyl sites consumed by surface ReO_x-I species (see Figure S2.10). Consequently, the surface rhenia species can only anchor at the surface hydroxyl sites available for forming surface ReO_x-II species.

2.5. *In Situ* Raman spectroscopy during propylene metathesis

In situ Raman spectra were also collected during propylene metathesis (1% C_3=/He at 70°C), and the spectra for the supported 3%ReO_x/Al_2O_3 (H), 9.4%ReO_x/Al_2O_3 (H) and 5%ReO_x/15%TaO_x/Al_2O_3 (E) are presented in Figures 8 (a), (b) and (c), respectively. The surface ReO_x-I species (~1003 cm^{-1}) are minimally perturbed by the reaction environment, only decreasing its Raman intensity by ~3-7% up to 120 minutes as shown in Figures 2.8(a) and (b). The surface ReO_x-II species (~1011 cm^{-1}), however, clearly undergo preferential interaction with propylene over the surface ReO_x-I species during propylene metathesis as shown in Figure 2.8(c). The strong interaction of propylene with the surface ReO_x-II sites, formed by addition of 15% TaO_x to 5% ReO_x/Al_2O_3 that suppresses formation of surface ReO_x-I sites, is clearly indicated in Figure 2.8(c) as the intensity of the Raman band is almost completely diminished after 120 minutes of reaction. Recovery of the initial surface ReO_x Raman bands after reaction by reoxidation of the catalysts indicates that the decreased Raman intensity during propylene metathesis was not caused by volatilization of surface rhenia from the catalyst.

2.6. Density Functional Theory Calculations

2.6.1. Surface ReO_x Structures on the Al_2O_3 support

Comparison of the adsorption energy of a model $HReO_4$ compound shows that the Al_2O_3(110) termination has a higher reactivity towards the surface ReO_x species compared to the more stable Al_2O_3(100) facet (see SI). This is a general feature for many Lewis base molecules and is related to the presence at the (110) surface of low coordinated Al_{III} and Al_{IV} sites, that present efficient acceptor orbitals of low energy (especially the Al_{III} site) while the (100) termination show less reactive Al_V surface atoms.[32] Hence occupation of the Al_2O_3(110) surface by ReO_x species is most probable and the DFT calculations below will be limited to the Al_2O_3(110) facet. An extensive discussion of the DFT calculations of surface ReO_x species on the less reactive Al_2O_3(100) surface can be found in SI (Figure S2). The Al_{III} sites result from the truncation at the (110) surface of tetra-coordinated Al atoms that are specific to the γ-alumina structure and are absent in α-alumina. The calculations here are performed in the limit of low hydroxyl content of the surface, however, at moderate hydration level accessible metastable structures with strong Lewis acid are also seen on the (110) alumina surface.[33]

The supported rhenia structures obtained for the majority (110) γ-alumina surface are shown in Figure 2.9. The optimized rhenia structures obtained for the (110) γ-alumina surface are especially important since this is the most exposed surface on alumina nanoparticles and is also more unsaturated, consequently, more reactive than the (100) surface.[15,16] This produces a larger variety of surface rhenium oxide species compared to the (100) plane and the surface rhenium oxide species are also more strongly bonded to the alumina support. The optimized ReO_x structures in Figure 2.9 possess trioxo, dioxo

and mono-oxo rhenium oxide coordination. The predicted Re=O bond lengths for the free Re=O bonds are typically 1.72 Å for the mono-oxo and dioxo structures, and 1.73 Å for the trioxo species 110_10, again in accordance with the EXAFS results.[12,13] An interaction between the oxo ligand and surface hydroxyl group causes an elongation of the double bond to 1.75 Å (110_8). The formally single Re-O bonds involved in Re-O-Al linkages are non-equivalent with their lengths varying over a wide range from 1.76-2.01 Å.

The relative energies of the obtained structures sometimes differ dramatically. The trioxo species with the C_{3v} symmetry (110_10) is clearly predicted to be unstable and other attempts to obtain trioxo Re^{+7} structures resulted in dioxo species. The formation of mono-oxo Re^{+7} species was also considered (110_3, 110_5 and 110_6) because of the high reactivity of the alumina surface. Each of the rhenium mono-oxo structures is 4-fold bonded to the alumina surface with three bridging Re-O-Al bonds and one additional dative bond from a surface oxygen atom to the rhenium atom. The most stable structures, however, are the surface dioxo species (110_1 and 110_2). Although they are very close in energies, their geometries are not identical. For the 110_1 structure, the ReO_4 unit is strongly deformed towards a C_{2v} symmetry with two additional weak and long Re…O bonds (2.35 Å) forming with surface O atoms. Such interactions, where the Re atom plays the role of a Lewis acid, complete the Re coordination and only form on the Al_2O_3 (110) surface since they require more basic oxygen atoms. There are two bridging oxygen atoms in this species, connected respectively to one AlO_4 and two AlO_5 aluminum atoms (here we refer to the final coordination of these Al atoms after interaction with Re). The surface 110_2 species appears as a ReO_4 coordinated unit. The rhenium atom is connected via two oxygen bridges with one AlO_4 and one AlO_5 site. The surface rhenia structures obtained

here, stabilized by multiple interactions with the surface, are consistent with earlier computational study on methyltrioxorhenium adsorbed on (110) γ–Al_2O_3.[23] A detailed discussion concerning the stability of the surface rhenium species in terms of deformation and interaction energy is included in SI.

The present DFT optimization study with realistic alumina surface models strongly supports the proposal that surface rhenium oxide species on γ-alumina exhibit a dioxo ReO_4 structure, and do not reproduce the proposed penta-coordinated dioxo Re species.[13] Since this (110) termination shows two structures with very similar energy, calculations suggest that the supported catalyst may be a mixture of different binding modes of the ReO_4 on γ-alumina, most likely having the surface (110_1) and (110_2) structures. It should, however, be noted that species of similar geometry can significantly differ in their stability, depending on their specific location on the surface (for instance, compare 110_1 and 110_9). Hence, surface stability of the ReO_x species might be strongly dependent on the detailed geometry of the alumina surface. The presence of defects or of different levels of hydration may also affect the complex geometry and stability.[33] Additional information is, thus, mandatory to confirm the trend proposed by the energy calculations.

2.6.2. Predicted Raman Vibrations from DFT Calculations

A key link with experiment is established by the calculation of vibrational frequencies. A benchmark study of Re=O frequencies with a well-characterized family of gas phase rhenium oxide compounds (data obtained from literature[34,35-37]) indicates that for optimum accuracy a scale factor of 0.9900 needs to be applied (Table 2.2). Note that the correction with respect to raw calculated data is small. The very good agreement

between theoretical and experimental values is another validation of the adopted methodology in this study.

The calculated Raman vibrations of each of the supported ReO_x structures on the alumina surface are presented in Table S2.1. It should be noted that Re=O and Re-O-Al vibrations are often coupled to each other. Furthermore, the vibrations of the mono-oxo, dioxo and trioxo surface ReO_x structures overlap and it is not possible to discriminate between the different structures just on the positions of the bands. For example, all the surface ReO_x structures on the $Al_2O_3(100)$ surface exhibit their strong ν_s (Re=O) stretch in the narrow region: between 987-997 cm^{-1} and on the $Al_2O_3(110)$ surface mono-oxo 110_3 and 110_5 (996 and 992 cm^{-1}), dioxo 110_7 (990 cm^{-1}) and trioxo 110_10 (997 cm^{-1}) are too close to be able to distinguish between them.

Isotopic oxygen exchange studies give key additional information in order to discriminate between mono-oxo, dioxo and trioxo surface ReO_x species on the most dominant $Al_2O_3(110)$ surface as shown experimentally above with Raman spectroscopy. The calculated isotopic ^{18}O-^{16}O shifts in the Re=O stretching frequencies for the most stable dioxo Re species on the (110) γ-alumina surface (110_1 and 110_2) are shown in Table 2.3. Additionally, the theoretical frequencies for the mono-oxo (110_3) and trioxo (110_10) Re models after the isotopic exchange are also presented. In the calculations, the ^{18}O-^{16}O substitution has been considered only for the oxo ligands (Re=O bonds) that dominate these vibrations. In the case of the partially substituted dioxo and trioxo species, all possible substitution patterns are taken into account for the determination of the theoretical frequencies. The calculated Re(=^{18}O)(=^{16}O), Re(=^{18}O)(=^{16}O)$_2$ and

$Re(=^{18}O)_2(=^{16}O)$ frequencies hardly depend on the substitution sequence. In most cases, the Re=O stretching modes are coupled with the Re-O-Al vibrations.

The calculated isotopic shifts for the 110_1 and 110_2 dioxo surface ReO_4 species are consistent with the experimental data for the supported ReO_x/Al_2O_3 catalysts (Table 2.4), especially for the symmetric Re=O modes. The theoretically predicted frequencies for the fully-substituted trioxo Re species (962, 922 and 915 cm^{-1} in Table 2.3) are different from the corresponding experimental values assigned to the species ReO_x-I and ReO_x-II (950-942 cm^{-1} in Table 4), confirming that surface ReO_x species are not trioxo. The calculated $\nu_s(Re=^{16}O)$ (996 cm^{-1}) and ν_{as} $(Re=^{18}O)$ (945 cm^{-1}) frequencies for the mono-oxo species 110_3 (Table 4) are close to the observed bands of the symmetric modes for the non-substituted (1000 cm^{-1}) and fully-substituted (943 cm^{-1}) species ReO_x-I, respectively (Table 4). However, in contrast to (110_1), the mono-oxo ReO_x species does not match all the observed bands and its existence is not confirmed experimentally. Such mono-oxo species as (110_3) cannot entirely be excluded as minority species by the DFT calculations because their vibrational stretching modes may be screened by the symmetric vibrations of the major dioxo species. Therefore, the combination of total energy calculations and of frequency calculations including isotopic exchange show that the two most energetically favored species on the most dominant 110 planes, 110_1 and 110_2, are observed experimentally as surface ReO_4-I and ReO_4-II, respectively.

2.7. Steady-State Propylene Metathesis

The steady-state catalytic performance of the supported ReO_x/Al_2O_3 catalysts for propylene metathesis to ethylene and 2-butene is shown in Figure 2.10. The same trend is

also obtained independent of the activity normalization (g of catalyst or m^2 since all the catalysts possess similar BET values). For the supported ReO_x/Al_2O_3 catalyst, there is almost no propylene metathesis activity below ~5% ReO_x/Al_2O_3 (0.74 Re/nm^2) loading and the only metathesis activity increases continuously with ReO_x loading above ~5% ReO_x (0.74 Re/nm^2). Comparison of the propylene metathesis activity with the surface ReO_x-I and ReO_x-II structures on alumina determined above suggests that the surface ReO_x–I sites possess minimal activity for metathesis. Although the Ta_2O_5/Al_2O_3 support is not active for propylene metathesis, the addition of surface TaO_x species significantly promotes the activity of supported ReO_x/Al_2O_3 catalyst by increasing the propylene metathesis at all surface rhenia coverage on alumina (e.g., by a factor of ~10x for 3% ReO_x and ~4x for 9.4% ReO_x). Furthermore, it appears that the surface TaO_x species only replace the surface ReO_x-I sites since the $ReO_x/TaO_x/Al_2O_3$ activity curve matches the activity of ReO_x/Al_2O_3 by shifting the curve to higher rhenia loadings as shown by the dashed line in Figure 2.10. This suggests that the surface TaO_x sites on alumina do not participate in the propylene metathesis reaction.

3. Discussion

3.1. Molecular Structures and Anchoring Sites of the Surface ReO_x Species on Al_2O_3

Only isolated surface ReO_x species are present on the alumina support since dimeric Re_2O_7 or higher rhenia oligomers are volatile. This is the reason for the volatilization of rhenia from alumina at high surface rhenia coverage. [5,6] The isolated nature of the surface ReO_x site on alumina is supported by the very high UV-vis Eg values

and the absence of observable Re-Re distances in the second coordination sphere at ~3-4 Å in the EXAFS radial distribution of the dehydrated supported ReO_x/Al_2O_3 catalysts.[12,13] ToF-SIMS analysis of calcined supported ReO_x/Al_2O_3 catalysts also demonstrated that the surface ReO_x species are essentially isolated on the alumina support.[38]

The intense Re L_1 XANES pre-edge feature of the supported ReO_x/Al_2O_3 catalysts approaches that of the $(O=)_3ReO\text{-}Si\text{-}(phenyl)_3$ reference compound in (see Figure 2.2), which strongly suggests that the surface ReO_x sites possess ReO_4 coordinated with only slightly different symmetry than C_{3v} from the reference compound. The presence of the two long Re…O bonds (2.35 Å) bonds for the deformed (110_1) surface ReO_4 structure does not appear to influence its first coordination shell and, thus, its XANES pre-edge features. Structures with other symmetries such ReO_6 or ReO_5 would give rise to very weak or intermediate XANES Re L_1 pre-edges, respectively. The somewhat weaker Re=O peak in the Re L_1 EXAFS of the dehydrated supported ReO_x/Al_2O_3 relative to the trioxo $(O=)_3ReO\text{-}Si\text{-}(phenyl)_3$ reference compound suggests less Re=O character and more Re-O character for the surface ReO_4 sites on the Al_2O_3 support. The isotopic $^{18}O\text{-}^{16}O$ oxygen exchange measurements confirm that the surface ReO_4 sites contain two oxo ligands (O=Re=O) (see Figure 2.5). This molecular structure is also supported by the DFT calculations indicating that the most stable surface rhenia structures on alumina are dioxo surface ReO_4 species. Moreover, spectroscopy and theory demonstrate that two distinct dioxo species are present. Dioxo surface ReO_4-I is assigned to the 110_1 in Figure 9, where, besides the two Re=O bonds, there are also two bridging Re-O-Al bonds and two much longer Re- - -O-Al bonds to the support with the latter outside of the first coordination sphere of the surface ReO_4-I site. The dioxo surface ReO_4-II is assigned to

the slightly less stable DFT calculated structure 110_2 in Figure 9 with two oxo bonds (O=Re=O) and two longer bridging Re-O-Al bonds. For the Re=O vibrational stretch frequencies, DFT calculations also predict the observed isotopic shift from ~1003/976 to ~1014/985 cm^{-1} for the surface ReO_4-I and ReO_4-II sites, respectively, on the alumina (110) surface (see Table 2.4).

The slight structural differences between the surface ReO_4-I and ReO_4-II sites is directly related to the bridging Re-O-Al bonds (1.83/1.94Å and 1.79/1.81Å on the Al_2O_3 (110) surface, respectively) and to an angular distortion of the tetrahedral Re center in ReO_4-I, since both rhenia sites have the same Re=O bond lengths of 1.72Å. The surface ReO_4-I site on alumina (110) is connected to one Al_{IV} site and two Al_V sites, in agreement with the observed preferential consumption of basic alumina μ_1 surface hydroxyls for 1-5% ReO_4/Al_2O_3 in the IR spectra (see Figure 2.7). The surface ReO_4-I site requires Lewis acid Al sites and additional surface basic O atoms for its stabilization on the alumina (110) surface. In the DFT model (110_2), the ReO_4 species is supported by a vacant alumina surface, and hence is a metastable case. In the experiment, surface ReO_4-II only appears after a loading of 5% and hence is anchored at μ_2-Al_{VI} and μ_3-Al_{VI} sites in agreement with the observed preferential consumption of the corresponding μ_2-Al_V and μ_3-Al_{VI} surface hydroxyls on alumina (110) for 5-15.6% ReO_4/Al_2O_3 (see Figure 2.7). The impregnation of Ta_2O_5 consumes Al_{IV} and Al_V sites which are involved in anchoring surface ReO_4-I species and, hence, only allows selective formation of surface ReO_x-II at low Re loading (see Figure S2.10). Regardless of the order of impregnation, the surface ReO_4-II species are always dominant on the Al_2O_3 support in the presence of Ta_2O_5 due to the higher mobility of surface ReO_x species.

As seen above, the most stable surface ReO_x sites on Al_2O_3 are the surface dioxo $(O=)_2ReO_2$ sites as predicted by DFT calculations based on the stability of different surface ReO_x structures on realistic models of the Al_2O_3 surface and confirmed experimentally with *in situ* XANES and isotopic ^{18}O-^{16}O exchange Raman spectroscopy. The current DFT optimizations do not reproduce the proposed penta-coordinated dioxo $(O=)_2ReO_3$ species as a stable surface ReO_x structure.[13] The most common proposed structure in the literature for surface ReO_x sites on alumina has been the trioxo $(O=)_3Re$-O-Al structure.[5-12] The ^{18}O-^{16}O exchange Raman findings are not consistent with trioxo species and the DFT calculations clearly indicate that the trioxo ReO_4 structure is not stable on the alumina (110) surface. The formation of mono-oxo $O=ReO_4$ species was also considered (see structures 110_3, 110_5 and 110_6 in Figure 9), but the presence of mono-oxo $O=ReO_4$ species is also not supported by the ^{18}O-^{16}O exchange findings and DFT calculations predict the mono-oxo ReO_x structure to be less stable than dioxo on the alumina (110) surface. The two previous structural assignments of surface trioxo $(O=)_3ReO$ and penta-coordinated dioxo $(O=)_2ReO_3$ were based on fitting of the EXAFS radial distributions of the oxygen atoms surrounding the Re^{+7} site.[12,13] The current EXAFS analysis indicates that it is not possible to determine the exact number of Re=O bonds with EXAFS alone since both the Re=O and Re-O bonds have similar bond lengths that complicates analysis. In addition, EXAFS analysis, which averages over the two surface ReO_4 sites on Al_2O_3, further complicates molecular structural analysis. Although the surface dioxo $(O=)_2ReO_2$ structure has previously not been proposed in the literature, the current experimental and theoretical calculations strongly indicate that it is the stable surface rhenia species on dehydrated supported ReO_x/Al_2O_3 catalysts.

3.2 Influence of the Propylene Metathesis Reaction Conditions on the Surface ReO_4-I and ReO_4-II Sites on Al_2O_3

The *in situ* Raman studies of the supported ReO_4/Al_2O_3 catalysts (3% ReO_4/Al_2O_3 with only surface ReO_4-I sites, 15.6% ReO_4/Al_2O_3 with both surface ReO_4-I and surface ReO_4-II sites, and 3% ReO_4/15% TaO_x/Al_2O_3 with only surface ReO_4-II sites) during propylene metathesis clearly demonstrate that the surface ReO_4-I sites are minimally perturbed by propylene and that all the surface ReO_4-II sites readily interact with propylene (see Figures 2.8 (a), (b) and (c), respectively). The nature of the surface ReO_x-II sites interacting with propylene is the subject of a subsequent study and will not be currently addressed.

The interaction of all the surface ReO_4-II sites on Al_2O_3 with propylene is unexpected since the olefin metathesis literature has been under the impression that only a very small number of sites, ~1% ReO_4, are active sites for metathesis.[29] This conclusion was reached from olefin metathesis titration studies at ambient temperatures (25-50^oC). The titration measurements were conducted at ambient temperatures after several hours of olefin metathesis and exposing the catalyst to vacuum for several hours to remove residual physically adsorbed olefins from the catalysts before titration with a second olefin. The presence of a significant amount of inactive surface ReO_4-I species on alumina in these studies further contributed to the estimated low apparent number of active sites. The estimated fraction of surface ReO_4-II sites on alumina in prior studies is indicated in Figure 2.11 revealing that the surface ReO_4-II sites were the minority species and the surface ReO_4-I sites were the majority (but inactive) species for half of the studies.[1,13,39-50]

The current study, however, demonstrates that the number of active surface ReO_4-II sites for olefin metathesis is a variable number that depends on the surface ReO_4 coverage on alumina as well as the presence of acidic surface metal oxides that block the formation of the less reactive surface ReO_4-I sites. Furthermore, "titration" with olefin is not a titration process, but actually is an activated chemical reaction that strongly depends on temperature. Thus, "titration" of the surface intermediates with olefins at ambient temperatures can't react away all or even a significant fraction of the surface intermediates. The present investigation is the first direct observation that propylene selectively interacts with surface ReO_4-II sites on Al_2O_3 during propylene metathesis. With the assistance of the surface TaO_x promoter, it is even possible to design catalysts approaching 100% ReO_4-II that are all interacting with propylene. Such higher concentrations of activated sites for supported ReO_4/Al_2O_3 catalysts, as well as other supported metal oxide olefin metathesis catalysts, finally opens the opportunity to characterize the activated surface ReO_4 sites on alumina.

3.3. Molecular Structure-Reactivity Relationships of Surface ReO_4-I and ReO_4-II Sites on Al_2O_3 for Propylene Metathesis

The steady-state catalytic studies indicate that the surface ReO_4-II sites are the catalytic active sites for propylene metathesis since the surface ReO_4-I sites do not exhibit significant catalytic activity . The surface ReO_4-I sites may even be inactive and the residual minimal activity may originate from trace amounts of surface ReO_4-II sites. The propylene metathesis steady-state catalytic trend as a function of surface rhenia loading on alumina has been observed in previous kinetic studies,[1,13,40,51] but this is *the first time* that

the surface dioxo ReO_4-II site on alumina has been isolated and identified as the precursor to the catalytic active site for propylene metathesis by supported ReO_4/Al_2O_3 catalysts. The major structural differences between surface ReO_4-I and ReO_4-II sites are their anchoring sites on the alumina surface and the resulting (Al-O)-Re-(O-Al) angle. The alumina anchoring sites act as potent multidentate ligands that moderate the activation of the surface ReO_4 sites for propylene metathesis. The weak interaction of surface ReO_4-I with two additional surface O atoms also certainly decreases its Lewis acidity compared to ReO_4-II.

The addition of surface TaO_x sites promotes the supported ReO_4/Al_2O_3 catalyst for propylene metathesis by occupying the surface Al_{IV} sites on the alumina support and, consequently, blocks formation of the less active surface ReO_4-I sites. As a result, the surface rhenia sites are forced to occupy the Al_V and Al_{VI} sites that result in selective formation of surface ReO_4-II sites. This is further emphasized by shifting the propylene activity curve for the supported $ReO_4/TaO_x/Al_2O_3$ catalyst by 4-5% ReO_4 towards the activity curve for Ta-free supported ReO_4/Al_2O_3 catalyst as shown in Figure 2.10. The overlap of the Ta-promoted and -unpromoted activity curves demonstrates that indeed the surface TaO_x sites are occupying the sites normally occupied by surface ReO_4-I and that surface TaO_x is not promoting the supported ReO_4/Al_2O_3 by chemical or electronic means, but just responsible for the formation of mostly surface ReO_4-II sites on alumina. It has been repeatedly proposed in the literature that the olefin metathesis activity is enhanced by introduction of acidic surface metal oxides (WO_x,[52] TaO_x,[53] MoO_x,[53,55] NbO_x[54,56]and VO_x[53,54]), but the current findings demonstrate that surface Brønsted acidity does not affect the intrinsic olefin metathesis reaction and the only function of acidic surface metal

oxides is to block the formation of inactive ReO_4-I sites on the most reactive alumina Al_{IV} sites, which has the effect of increasing the total number of active surface ReO_4-II sites for a given Re loading.

It was estimated that the maximum amount of surface ReO_4-I species on alumina corresponds to 5% ReO_4. The lack of propylene metathesis activity for the supported 1-5% ReO_x/Al_2O_3 catalysts suggests that the maximum amount of surface ReO_4-I species corresponds to 5% ReO_4 (see Figure 2.10). This is also consistent with the consumption of the basic Al-OH hydroxyls (μ_1-Al_{IV} , μ_1-Al_{VI} and μ_1-Al_V at 3787, 3768 and 3743 cm^{-1}, respectively) in the IR spectrum for supported 5% ReO_4/Al_2O_3 (see Figure 2.7) and appearance of a ReO_4-II Raman band above 5%ReO_4 (see Figure 2.4).

4. Conclusions

Supported ReO_x/Al_2O_3 catalysts were found to contain two distinct isolated tetra-coordinated dioxo surface ReO_4 species on alumina (deformed ReO_4-I on basic μ_1-Al_{IV} sites and ReO_4-II on acidic μ_2-Al_{VI} and μ_3-Al_{VI} sites). DFT optimization calculations found that other surface rhenia structures were less or not stable on Al_2O_3 (tetra-coordinated mono-oxo, penta-coordinated dioxo and tetra-coordinated trioxo). The deformed surface ReO_4-I species were not activated by propylene, but the surface ReO_4-II species were readily activated by exposure to propylene. The number of activated surface ReO_4-II species can be markedly increased by adding sacrificial surface TaO_x species that block the formation of the low activity deformed surface ReO_4-I species. These new insights allow for fundamental understanding how the (*i*) oxide support ligand controls the local surface rhenia structure and activation of the surface ReO_4 species, and (*ii*) surface

metal oxide promoters increase metathesis activity by allowing for the selective formation blocking of inactive surface ReO_4-I species that increases the number of active surface ReO_4-II species. The new molecular level insights are able to resolve many confusing claims about olefin metathesis by supported ReO_4/Al_2O_3 catalysts over the years.

Acknowledgements

S. Lwin and I.E. Wachs acknowledge financial support from U.S. DOE Basic Energy Sciences (Grant No. FG02-93ER14350). Y. Li and A. I. Frenkel acknowledge the U. S. DOE Grant No. DE- FG02-03ER15476 for supporting XAS data analysis. A.I. Frenkel acknowledges the U.S.DOE Grant No. DE-FG02-05ER15688 for supporting the X18B beamline operations. J. Handzlik acknowledges the computing resources from Academic Computer Centre CYFRONET AGH (grants MNiSW/SGI3700/PK/003/2013, MNiSW/SGI4700/PK/003/2013, MNiSW/IBM_BC_HS21/PK/003/2013) and PL-Grid Infrastructure.

References

1. Mol, J. C. *Catal. Today* **1999**, *51*, 289–299.

2. Secordel, X; Berrier, E.; Capron, M.; Cristol, S.; Paul, J.-F.; Fournier, M.; Payen, E. *Catal. Today* **2010**, *155*, 177–183.

3. Yoboué, A.; Susset, A.; Tougerti, A.; Gallego, D.; Ramani, S. V.; Kalyanikar, M.; Dolzhnikov, D. S.; Wubshet, S. G.; Wang, Y.; Cristol, S.; Briois, V.; La Fontaine, C.; Gauvin, R. M.; Paul, J.-F.; Berrier, E. *Chem. Commun*. **2011**, *47*, 4285–4287.

4. <http://www.cbi.com/technologies/propylene>. Accessed August 28, 2014.

5. Vuurman, M. A.; Wachs, I. E. *J. Phys. Chem.* **1992**, *96*, 5008–5016.

6. Vuurman, M. A.; Stufkens, D. J.; Oskam, A.; Wachs, I. E. *J. Mol. Catal.* **1992**, *76*, 263–285.

7. Kim, D. S.; Wachs, I. E. *J. Catal.* **1993**, *141*, 419–429.

8. Mitra, B.; Gao, X.; Wachs, I. E.; Hirt, A. M.; Deo, G. *Phys. Chem. Chem. Phys.* **2001**, *3*, 1144–1152.

9. Okal, J.; Kępiński, L.; Krajczyk, L.; Drozd, M. *J. Catal.* **1999**, *188*, 140–153.

10. Okal, J.; Baran, J. *J. Catal.* **2001**, *203*, 466–476.

11. Okal, J. *Appl. Catal. A* **2005**, *287*, 214–220.

12. Bare, S. R.; Kelly, S. D.; Vila, F. D.; Boldingh, E.; Karapetrova, E.; Kas, J.; Mickelson, G. E.; Modica, F. S.; Yang, N.; Rehr, J. J. *J. Phys. Chem. C* **2011**, *115*, 5740-5755.

13. Vicente, B. C.; Nelson, R. C.; Moses, A. W.; Chattopadhyay, S.; Scott, S. L. *J. Phys. Chem. C* **2011**, *115*, 9012–9024.

14. Handzlik, J.; Sautet, P. *J. Catal.* **2008**, *256*, 1–14.

15. Digne, M.; Sautet, P.; Raybaud, P.; Euzen, P.; Toulhoat, H. *J. Catal.* **2002**, *211*, 1–5.

16. Digne, M.; Sautet, P.; Raybaud, P.; Euzen, P.; Toulhoat, H. *J. Catal*. **2004**, *226*, 54–68.

17. Tian, H.; Roberts, C.A.; Wachs, I.E. *J. Phys. Chem. C* **2010**, *114*, 14110–14120.

18. Perdew, J. P.; Chevary, J. A.; Vosko, S. H.; Jackson, K. A.; Pederson, M. R.; Singh, D. J.; Fiolhais, C. *Phys. Rev. B* **1992**, *46*, 6671–6687.

19. Kresse, G.; Hafner, J. *Phys. Rev. B* **1993**, *47*, 558–561.

20. Kresse, G.; Furthmüller, J. *Comput. Mater. Sci*. **1996**, *6*, 15–50.

21. Kresse, G.; Furthmüller, J. *Phys. Rev. B* **1996**, *54*, 11169–11186.

22. Kresse, G.; Joubert, D. *Phys. Rev. B* **1999**, *59*, 1758-1775.

23. Krokidis, X.; Raybaud, P.; Gobichon, A.-E.; Rebours, B.; Euzen, P.; Toulhoat, H. *J. Phys. Chem. B* **2001**, *105*, 5121–5130.

24. Monkhorst, H. J.; Pack, J. D. *Phys. Rev. B* **1976**, *13*, 5188–5192.

25. *Materials Studio* v. 5.5; Accelrys Software Inc.: San Diego, CA, **2010**.

26. Horsley, J. A.; Wachs, I. E.; Brown, J. M.; Via, G. H.; Hardcastle, F. D. *J. Phys. Chem.* **1987**, *91*, 4014–4020.

27. Balerna, A.; Bernieri, E.; Burattini, E.; Kuz'min, A.; Lusis, A.; Purans, J.; Cikmacs, P., *Nuc. Instru. & Met. Phys. Res., Section A: Accelerators, Spectrometers, Detectors, and Associated Equipment* **1991**, *308*, 240–242.

28. Nakamoto, K. *Infrared and Raman Spectra of Inorganic and Coordination Compounds*, 4th ed.; Wiley: New York, **1986**; pp 68–75.

29. Chen, Y.; Fierro, J. L. G.; Tanaka, T.; Wachs, I. E. *J. Phys. Chem. B* **2003**, *107*, 5243–5250.

30. Knozinger, H.; Ratnasamy, P. *Catal. Rev. -Sci. Eng.* **1978**, *17*, 31–70.

31. Coperet, C. *Pure Appl. Chem.* **2009**, *81*, 585-896.

32. Wischert, R.; Copéret, C.; Delbecq, F.; Sautet, P. *ChemCatChem* **2010**, *2*, 1–4.

33. Wischert, R.; Laurent, P.; Copéret, C.; Delbecq, F.; Sautet, P. *J. Am. Chem. Soc.* **2012**, *134*, 14430–14449.

34. Beattie, I. R.; Gilson, T. R.; Jones P. J. *Inorg. Chem.* **1996**, *35*, 1301–1304.

35. Beattie, I. R.; Crocombe, R. A.; Ogden, J. S. *J. Chem .Soc. Dalton Trans.* **1977**, 1481–1489.

36. Beattie, I. R.; Jones, P. J. *Inorg. Chem.* **1979**, *18*, 2318–2319.

37. Zhou, M.; Citra, A.; Liang, B.; Andrews, L. *J. Phys. Chem. A* **2000**, *104*, 3457–3465.

38. Bouchmella, K.; Mutin, P. H.; Stoyanova, M.; Poleunis, C.; Eloy, P.; Rodemerck, U.; Gaigneaux, E. M.; Debecker, D.P. *J. Catal.* **2013**, *301*, 233–241.

39. Chauvin, Y.; Commereuc, D. *J. Chem. Soc., Chem. Comm.* **1992**, *6*, 462–464.

40. Balcar, H.; Zilkova, N.; Zukal, A.; Cejka, J., *Studies in Surf. Sci. Catal.* **2008**, *174 A*, 61–66.

41. Salameh, A.; Coperet, C.; Basset, J.; Bohm, V.P.W.; Roper, M. *Adv. Synth. Catal*. **2007**, *349*, 238–242.

42. Kawai, T.; Kudo, H.; Suzuki, T.; Iyoda, T. *J. Mol. Catal. A: Chem*. **2000**, 158, 533–540.

43. McCoy, J.R.; Farona, M.F. *J. Mol. Catal*. **1991**, *66*, 51–58.

44. Daniell, W.; Weingard, T; Knozinger, H. *J. Mol. Catal. A: Chem*. **2003**, *204-205*, 519–526.

45. Oikawa, T.; Ookoshi, T.; Tanaka, T.; Yamamoto, T.; Onaka, M. *Micro. Meso. Mat.* **2004**, *74*, 93–103.

46. Schekler-Nahama, F.; Clause, O.; Commereuc, D.; Saussey, J. *Appl. Catal. A: Gen*. **1998**, *167*, 237–245.

47. Bregeault, J-M.; Ali, B.E.; Martin, J.; Martin, C.; Derdar, F.; Bugli, G. *J. Mol. Catal.* **1988**, 46, 37–60.

48. Olsthoorn, A. A.; Boelhouwer, C. *J. Catal*. **1976**, *44*, 197–206.

49. Aldag, A. W.; Lin, C.J.; Clark, A. *J. Catal*. **1978**, *51*, 278–285.

50. Mahmood, C.S.; Yarmo, M.A.; Hamid, S.B.D.-A.. *J. Mol. Catal*. A. *Chem*. **2000**, *161*, 11–16.

51. Stoyanova, M.; Rodemerck, U.; Bentrup, U.; Dingerdissen, U.; Linke, D.; Mayer, R.-W.; Lansink Rotgerink, H.G.J.; Tacke, T. *App. Catal. A: Gen*. **2008**, *340*, 242–249.

52. Xiaoding, X.; Boelhouwer, C.; Vonk, D.; Benecke, J.I.; Mol, J.C. *J. Mol. Catal.* **1986**, *36*, 47–66.

53. Ramachandran, B.; Choi, S.; Gartside, R. J.; Kleindienst, S.; Ruettinger, W.; Alerasool, S. Olefin isomerization and metathesis catalyst for manufacture of propylene. US Patent 20100056839 A1, March 4, 2010.

54. Xiaoding, X.; Boelhouwer, C.; Benecke, J.I.; Vonk, D.; Mol, J.C. *J. Chem. Soc. Faraday Trans*. **1986**, *82*, 1945–1953.

55. Flego, C.; Pollesel, P.; Ricci, M.; Romano, U. Process for preparation of 2,3-dimethylbutane. IT 1324054 B1, October 28, 2004.

56. Stephan, J.; Schubert, M.; Weichert, C.; Ruppel, W.; Resch, P.; Zimdahl, S.; Mrzena, F.; Molitor, A.; Berg, S.; Fohrmann, M. Regeneration of supported rhenium oxide-doped olefin metathesis catalysts. DE 10309070 A1, September 16, 2004.

Figures

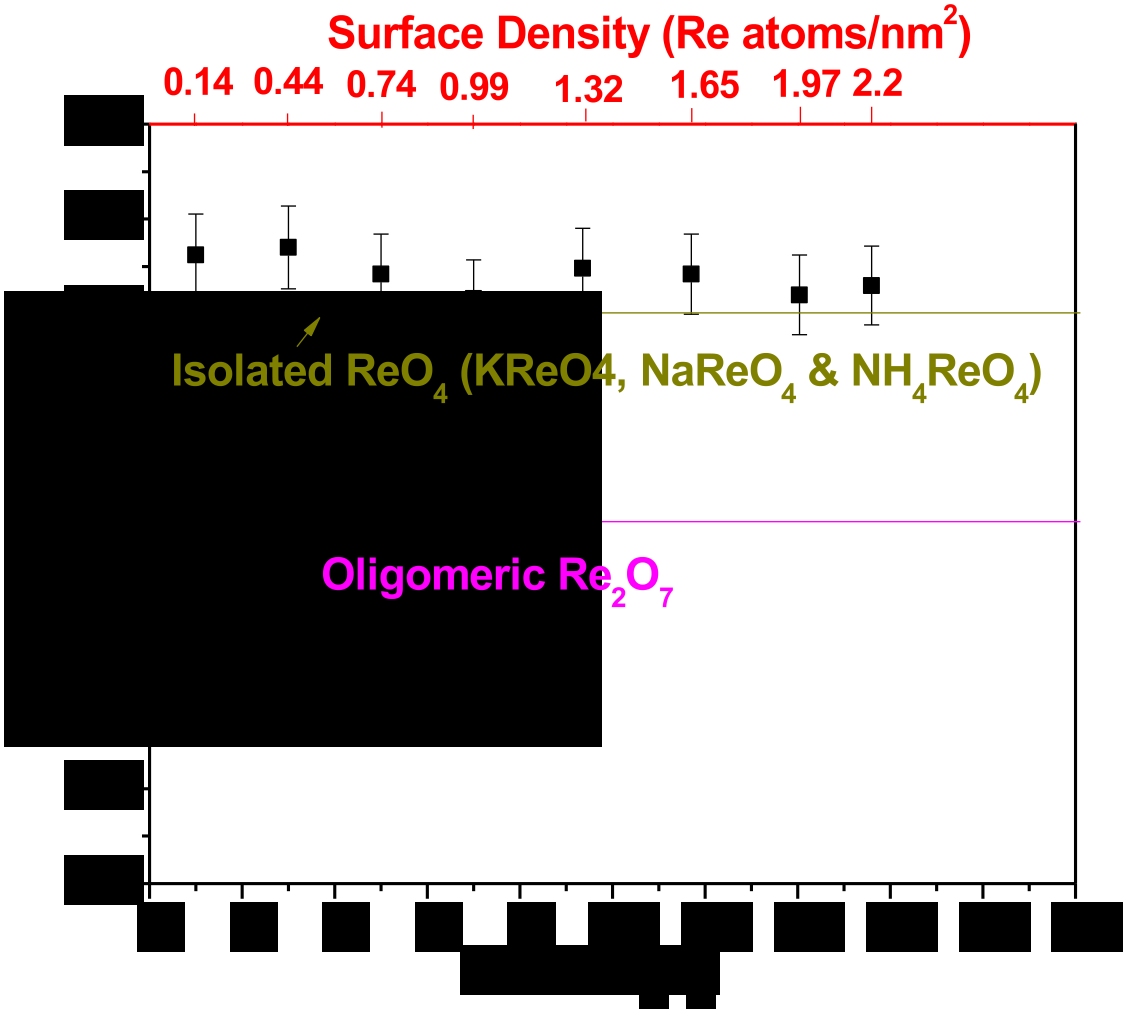

Figure 2.1. *In situ* UV-vis Eg values for dehydrated supported ReO_x/Al_2O_3 (E) catalysts as a function of rhenia surface coverage.

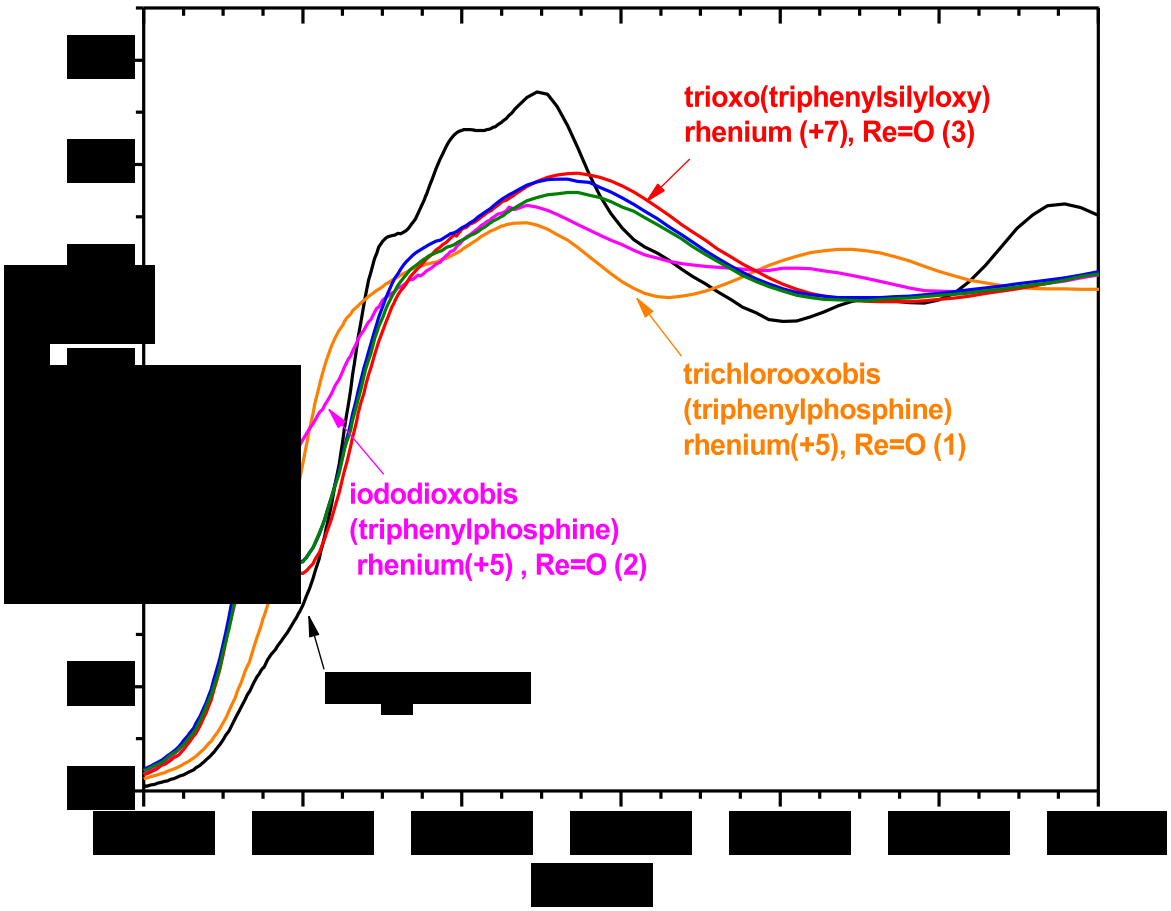

Figure 2.2. *In situ* Re L_1 XANES spectra for the dehydrated supported 3% (blue) and 15.6% (olive) ReO_x/Al_2O_3 catalysts. The XANES spectra of the reference compounds, trioxo(triphenylsilyloxy) rhenium (+7) (red), iododioxobis (triphenylphosphine) rhenium(+5) (magenta), trichlorooxobis (triphenylphosphine) rhenium(+5) (orange) and ReO_3 rhenium (+6) oxide (black) are taken under ambient conditions.

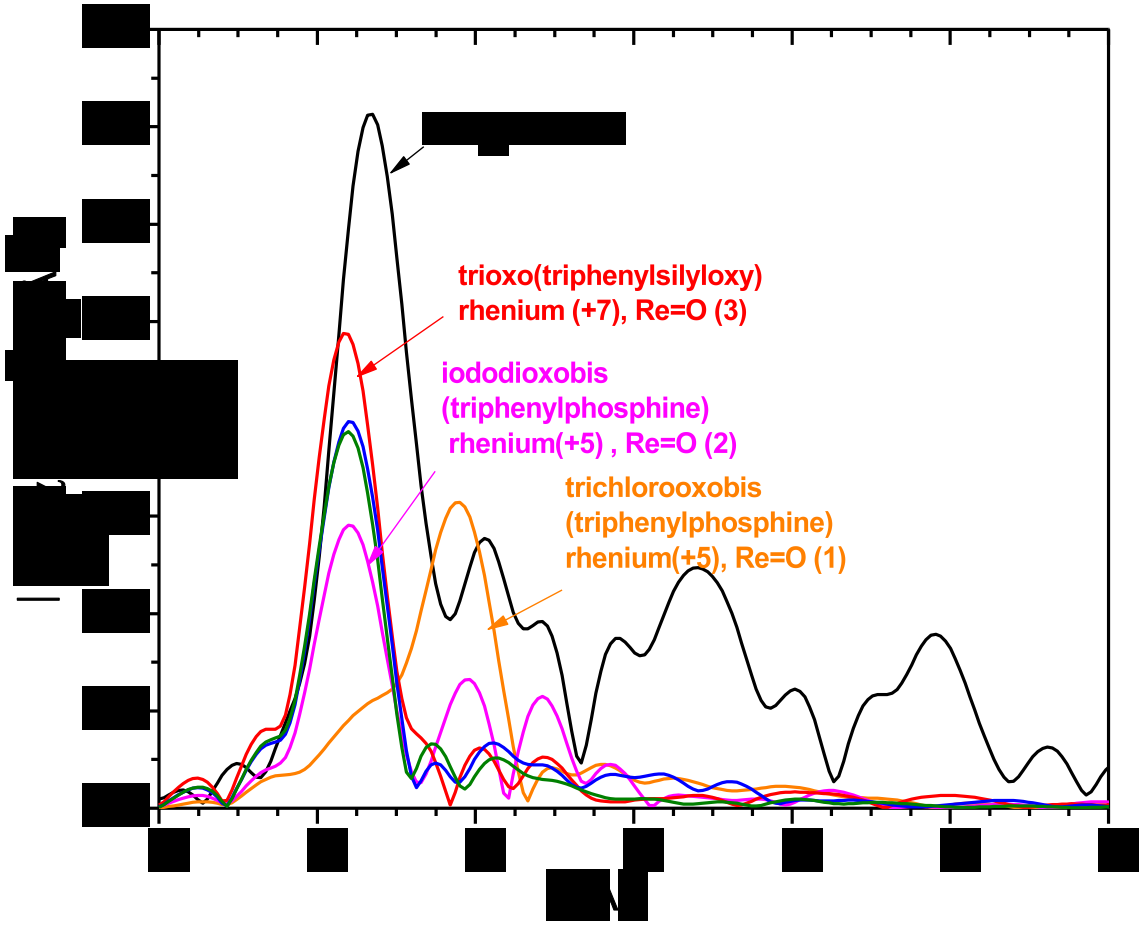

Figure 2.3. Magnitudes of Fourier-transformed, not-phase-corrected, k^2-weighted Re L_1-edge EXAFS spectra in the *R* space for the dehydrated supported 3%ReO_x/Al_2O_3 (blue) and 15.6%ReO_x/Al_2O_3 (olive) catalysts with the reference trioxo $(O=)_3ReO$-Si-$(phenyl)_3$ (red) , iododioxobis (triphenylphosphine) rhenium(+5) (magenta), trichlorooxobis (triphenylphosphine) rhenium(+5) (orange) and crystalline bulk ReO_3 (black) compounds.

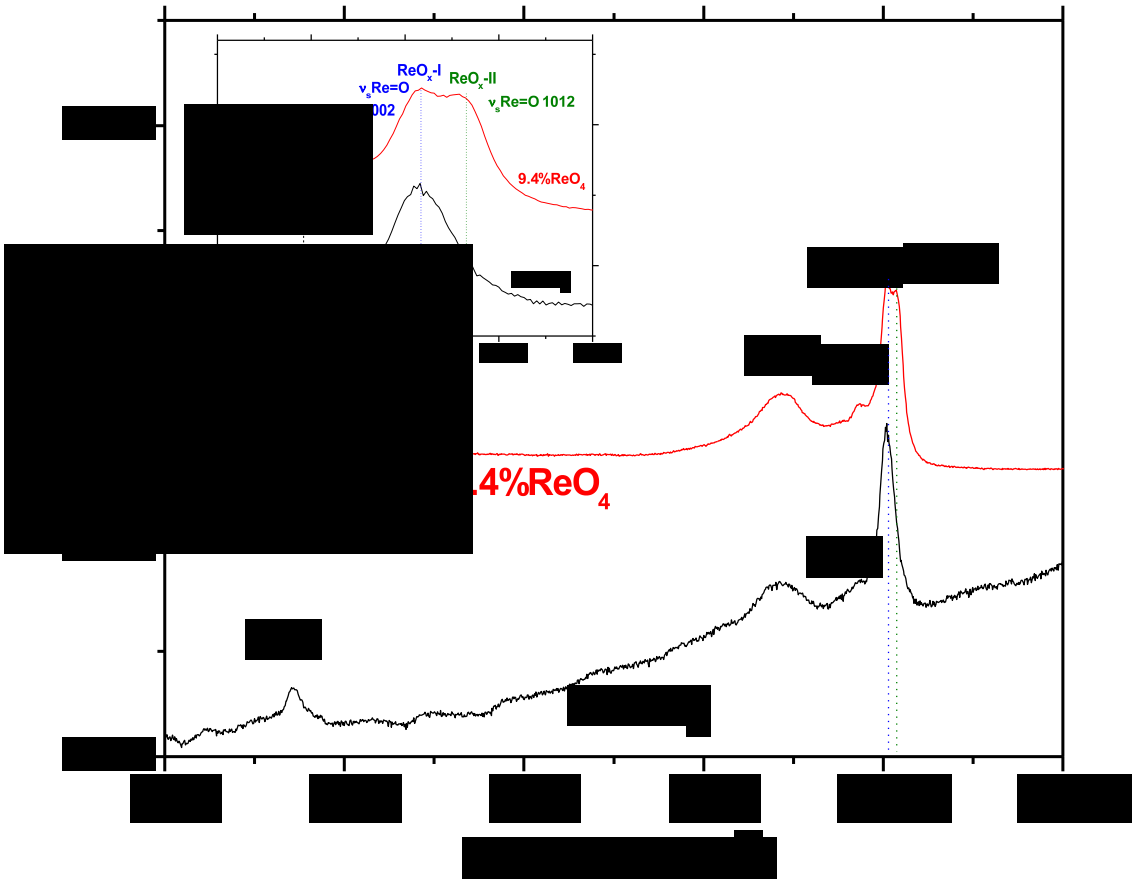

Figure 2.4. *In situ* Raman spectra (442nm) of dehydrated supported 3% and 9.4% ReO_x/Al_2O_3 (H) catalysts at 100^{o}C. The inset shows the 900-1100 cm^{-1} region.

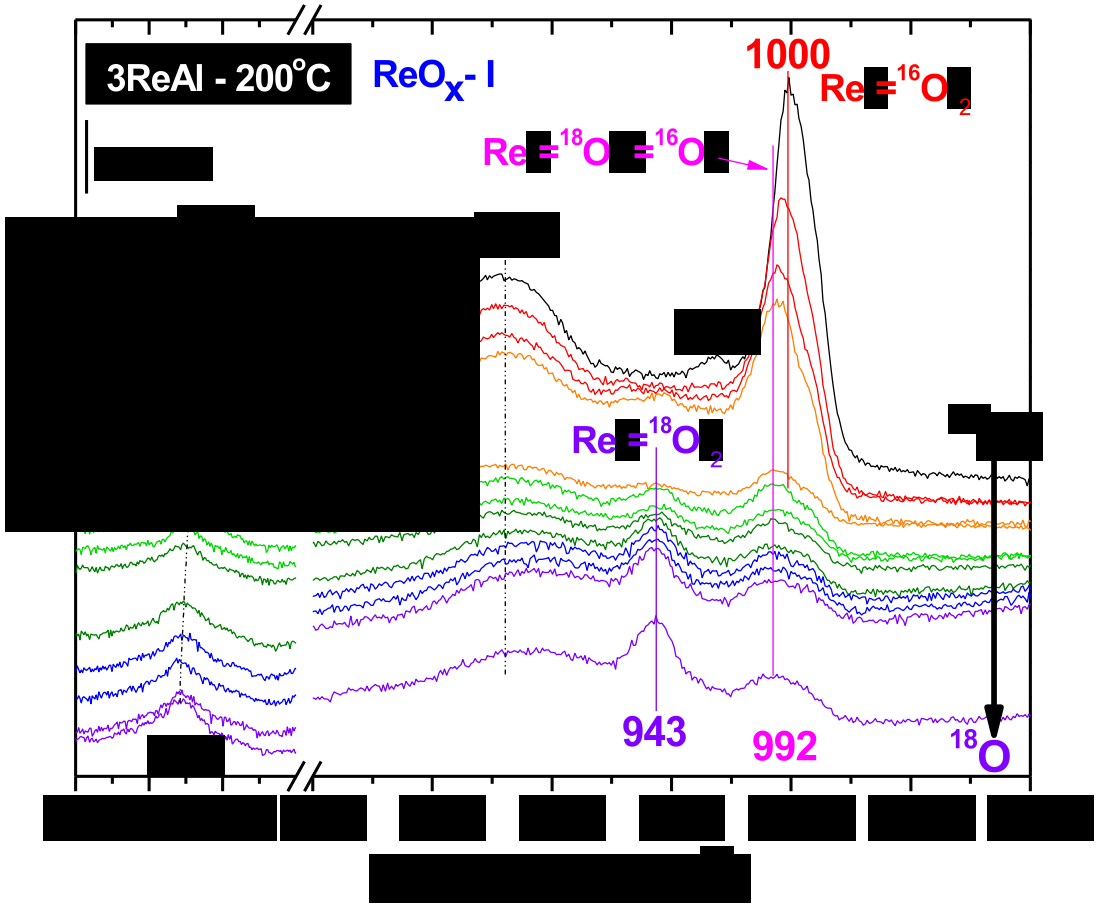

Figure 2.5. *In situ* Raman spectra (442nm) of 3% ReO_x/Al_2O_3 (ReO_x-I) (H) at 200°C during ^{18}O-^{16}O isotope exchange by exposure to $H_2{}^{18}O$ vapor.

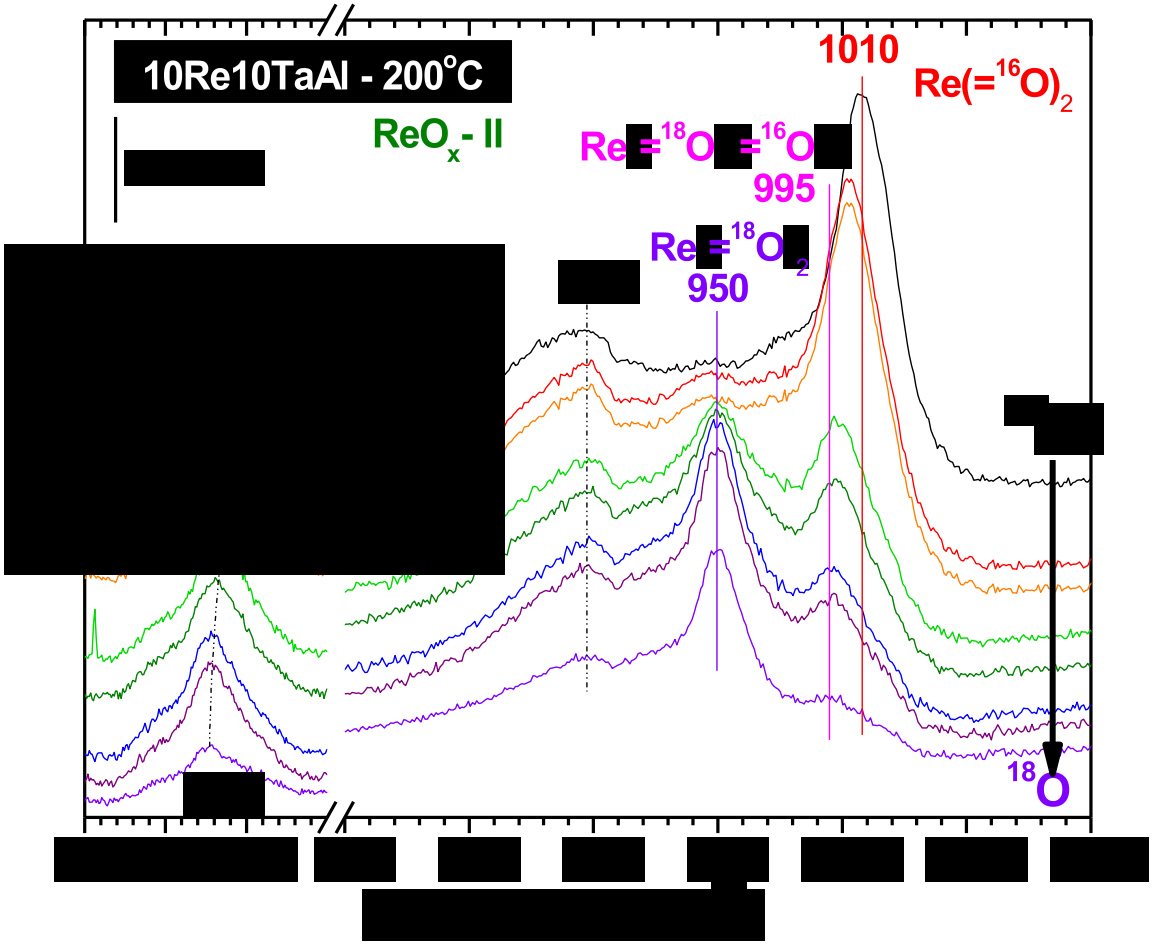

Figure 2.6. *In situ* Raman spectra (442nm) of supported 9.36% $ReO_x/10\%Ta_2O_5/Al_2O_3$ (ReO_x-II) (E) at 200°C during ^{18}O-^{16}O isotope exchange with $H_2{}^{18}O$ vapor.

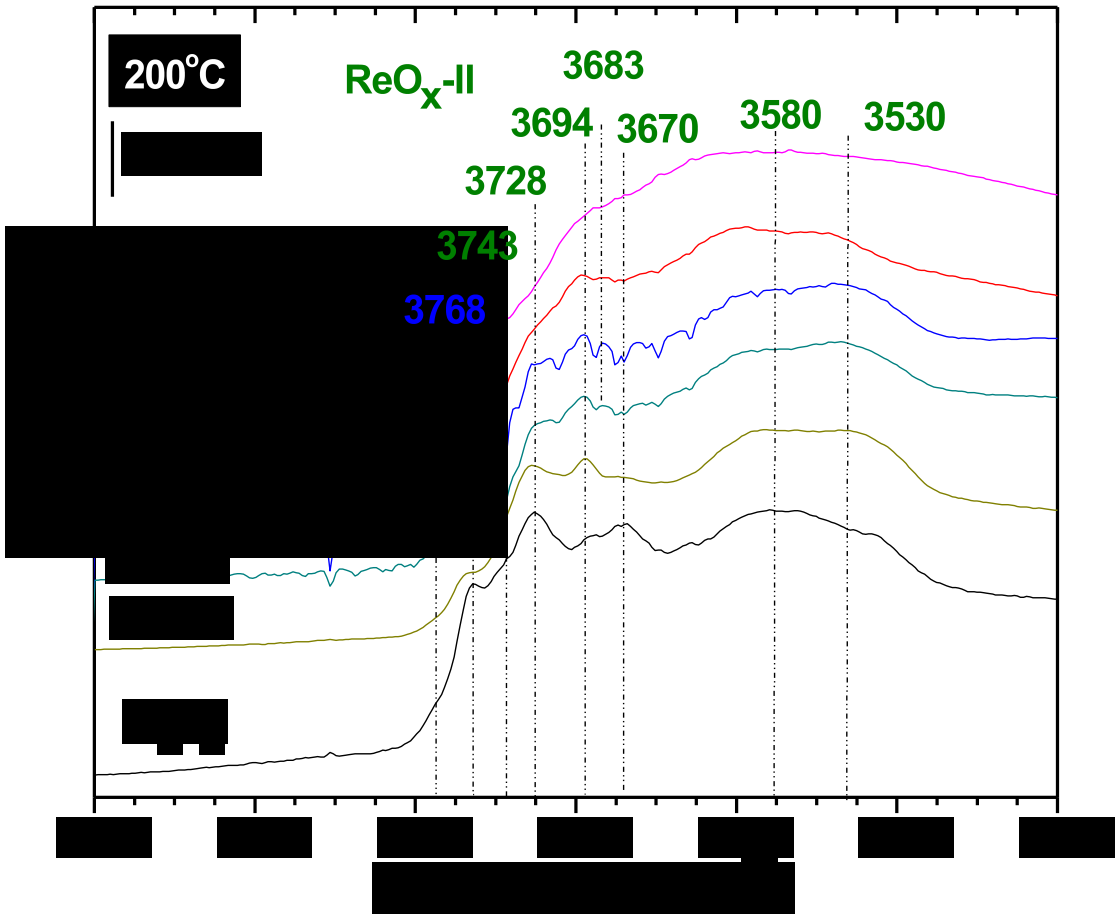

Figure 2.7. *In situ* IR spectra of the surface hydroxyl region of dehydrated supported ReO_x/Al_2O_3 (E) catalysts as a function of rhenia loading at 200°C. The blue color represents ReOx-I and the green color represents ReO_x-II.

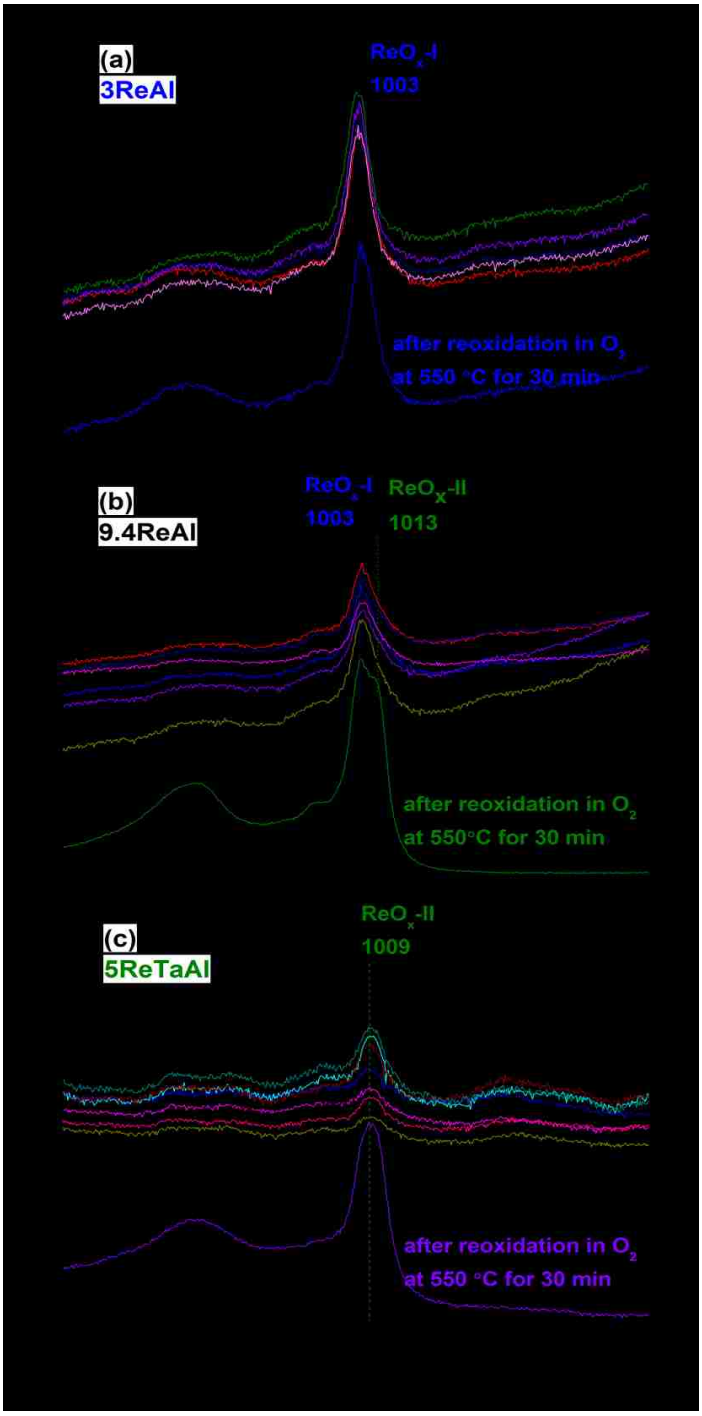

Figure 2.8. *In situ* Raman spectra (442nm) of the (a) 3%ReO_x/Al_2O_3 (H), (b) 9.4%ReO_x/Al_2O_3 (H) and (c) 5%ReO_x/15%TaO_x/Al_2O_3 (E) catalysts during propylene metathesis at 70°C up to 120 minutes. The catalyst was reoxidized in 10% O_2/Ar at 550°C after the reaction.

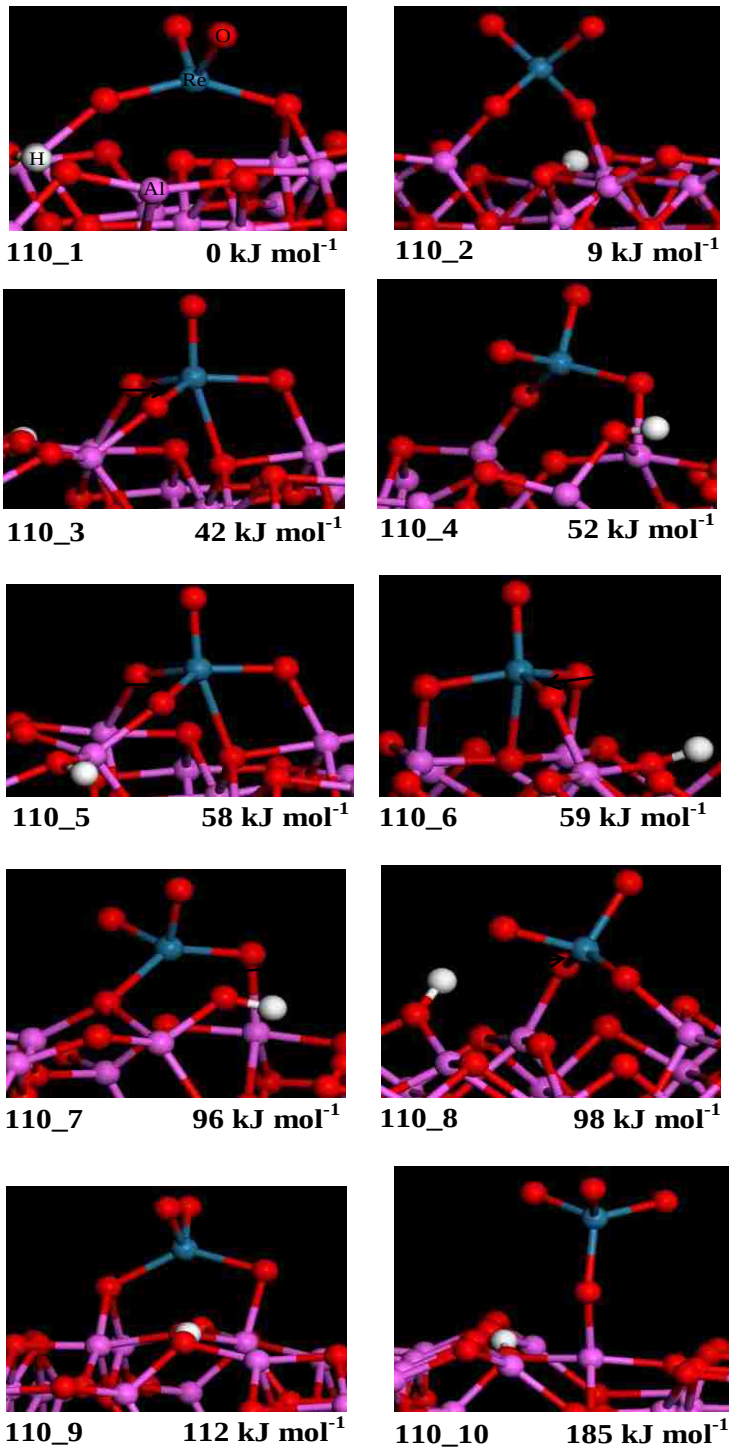

Figure 2.9. DFT optimized structures and relative energies for the surface Re^{+7} oxide species supported on (110) γ-alumina. Bond lengths are given in Å.

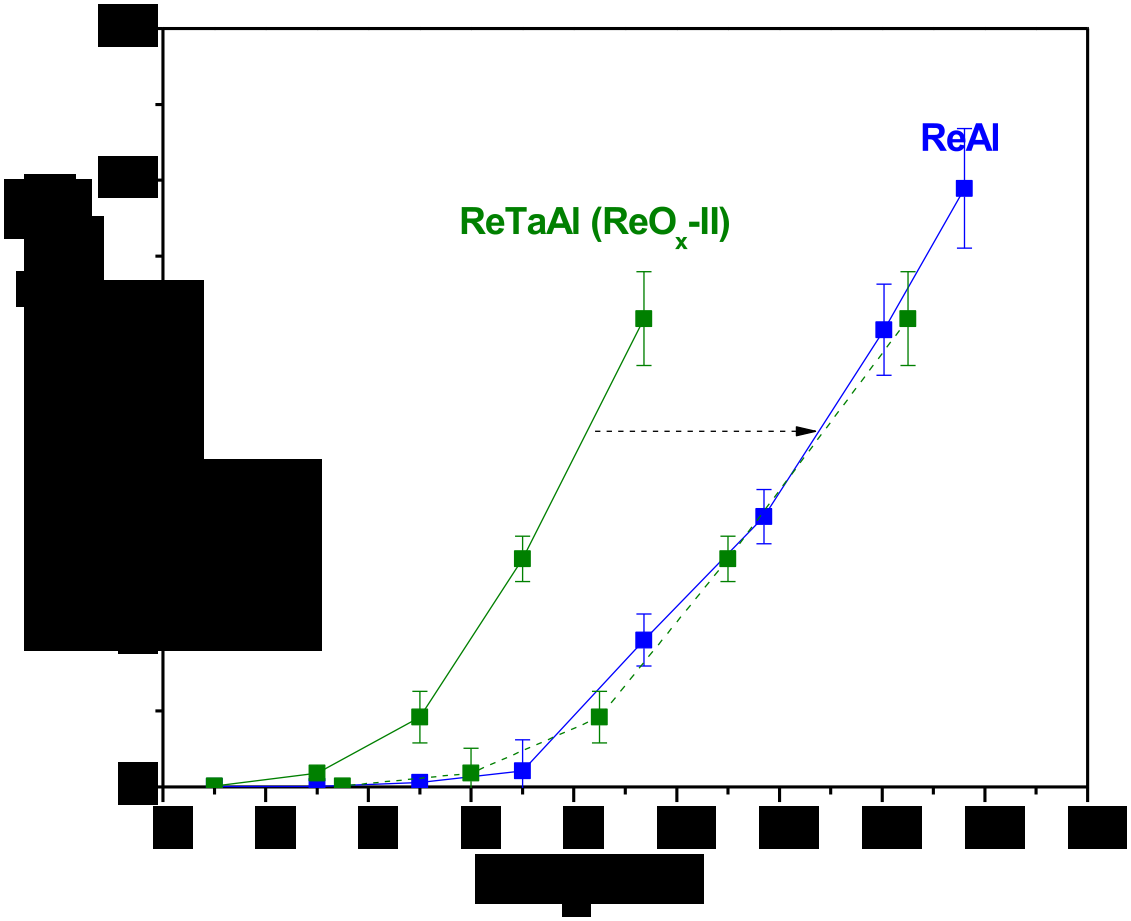

Figure 2.10. Steady-state catalytic performance for propylene metathesis at 70°C by supported ReO_x/Al_2O_3 (blue squares) and ReO_x/%15%TaO_x/Al_2O_3 (green squares) catalysts that were dehydrated in flowing O_2/Ar at 500°C for prior to reaction at 70°C. The reaction was performed with ReO_x catalysts supported on Al_2O_3 (E). The dashed line indicates the x-axis shift for ReTaAl catalysts to show the promotion effect of the surface TaO_x species. The slight offset may be due to experimental error such as volatilization of ReO_x at higher loading.

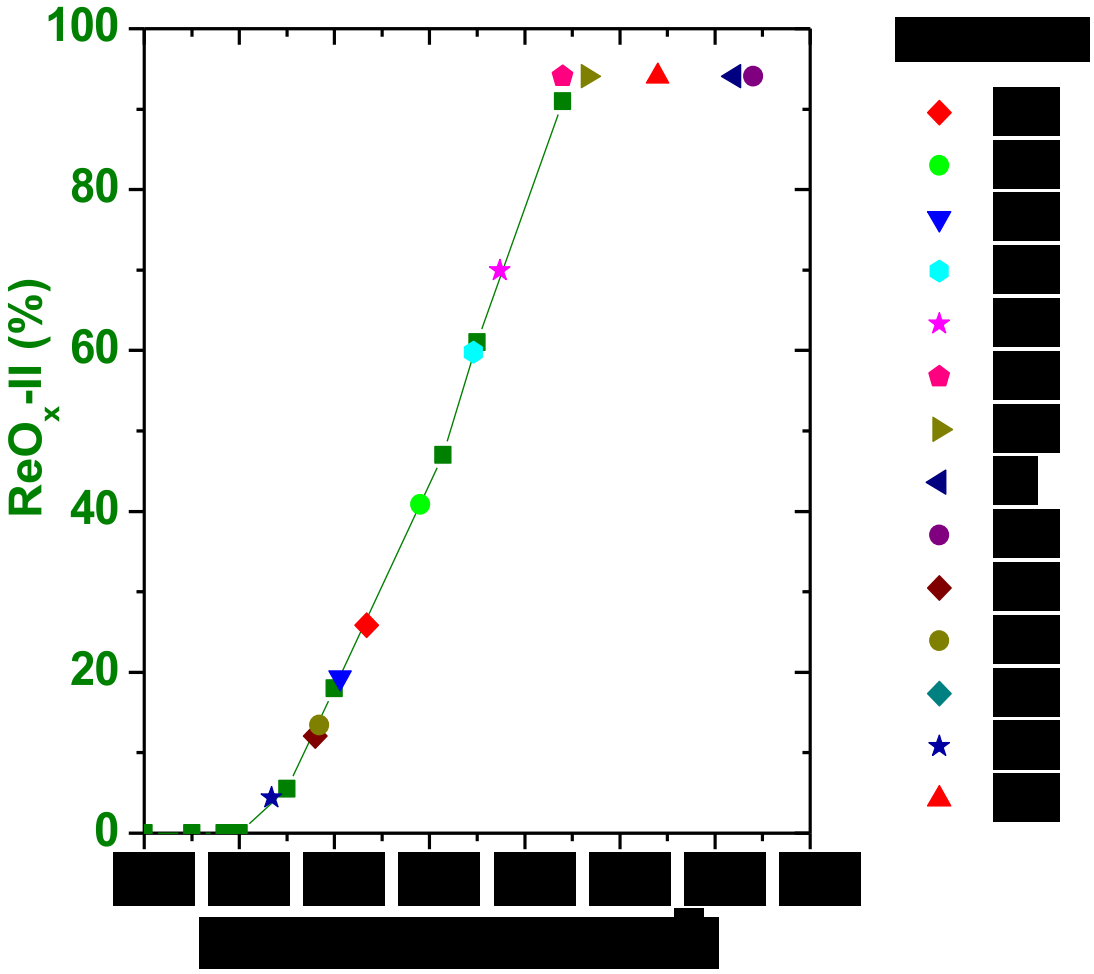

Figure 2.11. Comparison of estimated surface ReO_4-II concentration as a function of Re loading for supported ReO_x/Al_2O_3 catalysts that have been reported in the literature. The solid line indicates the concentration of surface ReO_4-II species as a function of Re coverage on alumina determined in the present study. The concentration of surface ReO_x-II species for other experimental data is estimated from the solid line generated in the present study. The studies reporting surface rhenia coverage higher than maximum of 2.2Re/nm^2 did not account for volatility of rhenia above this loading and, thus, can only contain a maximum of ~2.2 Re/nm^2.

Tables

Table 2.1. Al_2O_3 hydroxyl types and band positions (cm^{-1}) reported in the literature

Band Positions	Crystal Faces[15,16]	Structure of Hydroxyl Sites (from DFT)[15,16]
3785-3800	(110)	HO-μ_1-Al_{IV}
3760-3780	(100)	HO- μ_1-Al_{VI}
3730-3735	(110)	HO-μ_1-Al_V
3690-3710	(110)	HO-μ_2-Al_V
3590-3650	(100)	HO-μ_3-Al_{VI}

Table 2.2. Calculated and experimental Re=O stretching frequencies (cm^{-1}) for reference rhenium oxide reference compounds, after the determination of the optimum scaling factor of 0.9900.

	calc.[a]		exp.	
	ν_s(Re=O)	ν_{as}(Re=O)	ν_s(Re=O)	ν_{as}(Re=O)
$Re_2O_{7(g)}$	1006	975	1008[b]	975[b]
$HReO_{4(g)}$	1000	973	-	972[b]
$ReO_3F_{(g)}$	1011	979	1013[c]	978[c]
$CH_3ReO_{3(g)}$	1000	974	1003[d]	975[d]
$ReO_{2(g)}$	984	936	981-984[e]	931-934[e]

[a] a scale factor of 0.9900 is used. [b] Ref. 25. [c] Ref. 26. [d] Ref 27. [e] Ref 28.

Table 2.3. The effect of the isotopic ^{18}O-^{16}O exchange on the calculated[a] Re=O stretching frequencies (cm^{-1}) for the rhenium oxide species supported on the γ-alumina surface.

110_3 (monooxo)	Sites	**110_1** (dioxo)	**110_2** (dioxo)	sites	**110_10** (trioxo)	sites
996	$\nu(Re=^{16}O)$	1003	1014	$\nu_s(Re(=^{16}O)_2)$	997	$\nu_s(Re(=^{16}O)_3)$
945	$\nu(Re=^{18}O)$	992-991	1004-1001	$\nu_s(Re(=^{18}O)(=^{16}O))$	991-989	$\nu_s(Re(=^{18}O)(=^{16}O)_2)$
		952	967	$\nu_s(Re(=^{18}O)_2)$	981-978	$\nu_s(Re(=^{18}O)_2(=^{16}O))$
		976	985	$\nu_{as}(Re(=^{16}O)_2)$	962[d], 922, 915	$\nu_s(Re(=^{18}O)_3)$
		938-937, 915[b]	953-950, 937-935[b]	$\nu_{as}(Re(=^{18}O)(=^{16}O))$	956-955	$\nu_{as}(Re(=^{16}O)_3)$
		927	939[c], 933	$\nu_{as}(Re(=^{18}O)_2)$	957-955, 942-940[d], 912-909	$\nu_{as}(Re(=^{18}O)(=^{16}O)_2)$
					946-942, 918, 914-913[b], 907-906	$\nu_{as}(Re(=^{18}O)_2(=^{16}O))$
					908-906	$\nu_{as}(Re(=^{18}O)_3)$

[a] A scale factor of 0.9900 is used. [b] Strongly coupled with ν(Re-O-Al). [c] ν(O=Re-O-Al) coupled with ν(Al-O-Re-O-Al). [d] ν(Re-O-Al) coupled with $\nu((Re=O)_3)$.

Table 2.4. Comparison of DFT calculated Re=O stretching frequencies for the surface dioxo ReO_x species with experimentally measured Re=O vibrations for supported ReO_x/Al_2O_3 catalysts

DFT (110_1)	Experiment (ReO_x-I)	Sites	DFT (110_2)	Experiment (ReO_x-II)	Sites
1003	1000	$\nu_s(Re(=^{16}O)_2)$	1014	1010	$\nu_s(Re(=^{16}O)_2)$
992-991	992	$\nu_s(Re(=^{18}O)(=^{16}O))$	1004-1001	995	$\nu_s(Re(=^{18}O)(=^{16}O))$
952	946-942	$\nu_s(Re(=^{18}O)_2)$	967	950	$\nu_s(Re(=^{18}O)_2)$
976	970	$\nu_{as}(Re(=^{16}O)_2)$	985	980	$\nu_{as}(Re(=^{16}O)_2)$
938-937, 915[a]		$\nu_{as}(Re(=^{18}O)(=^{16}O))$	953-950, 937-935[a]		$\nu_{as}(Re(=^{18}O)(=^{16}O))$
927	915[c]	$\nu_{as}(Re(=^{18}O)_2)$	939[b], 933	915[c]	$\nu_{as}(Re(=^{18}O)_2)$

[a] Strongly coupled with ν(Re-O-Al). [b] ν(O=Re-O-Al) coupled with ν(Al-O-Re-O-Al).

[c] It was not possible to isolate and assign this vibration to an individual species.

Supplemental Information

1. *In situ* UV Vis Spectroscopy

An Eg value of 2.8 eV is obtained for the solid Re_2O_7 reference, sealed in vile to avoid air exposure, using the method reported in the literature.[S1]

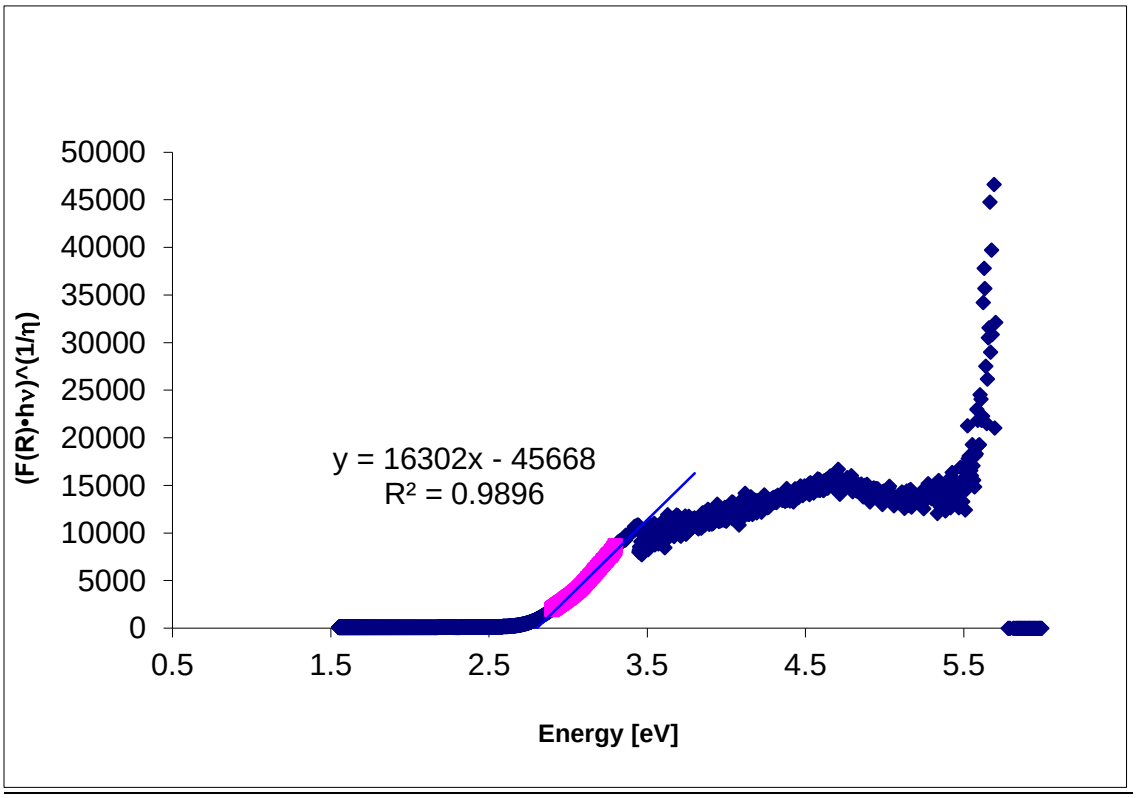

Figure S2.1. UV Vis spectra of the solid Re_2O_7 reference

2. DFT Calculations

Optimized structures for the surface Re^{+7} species attached to the minority (100) surface of γ-alumina are shown in Figure S2.2, ranked from the most stable (100_1) to the least stable (100_8).

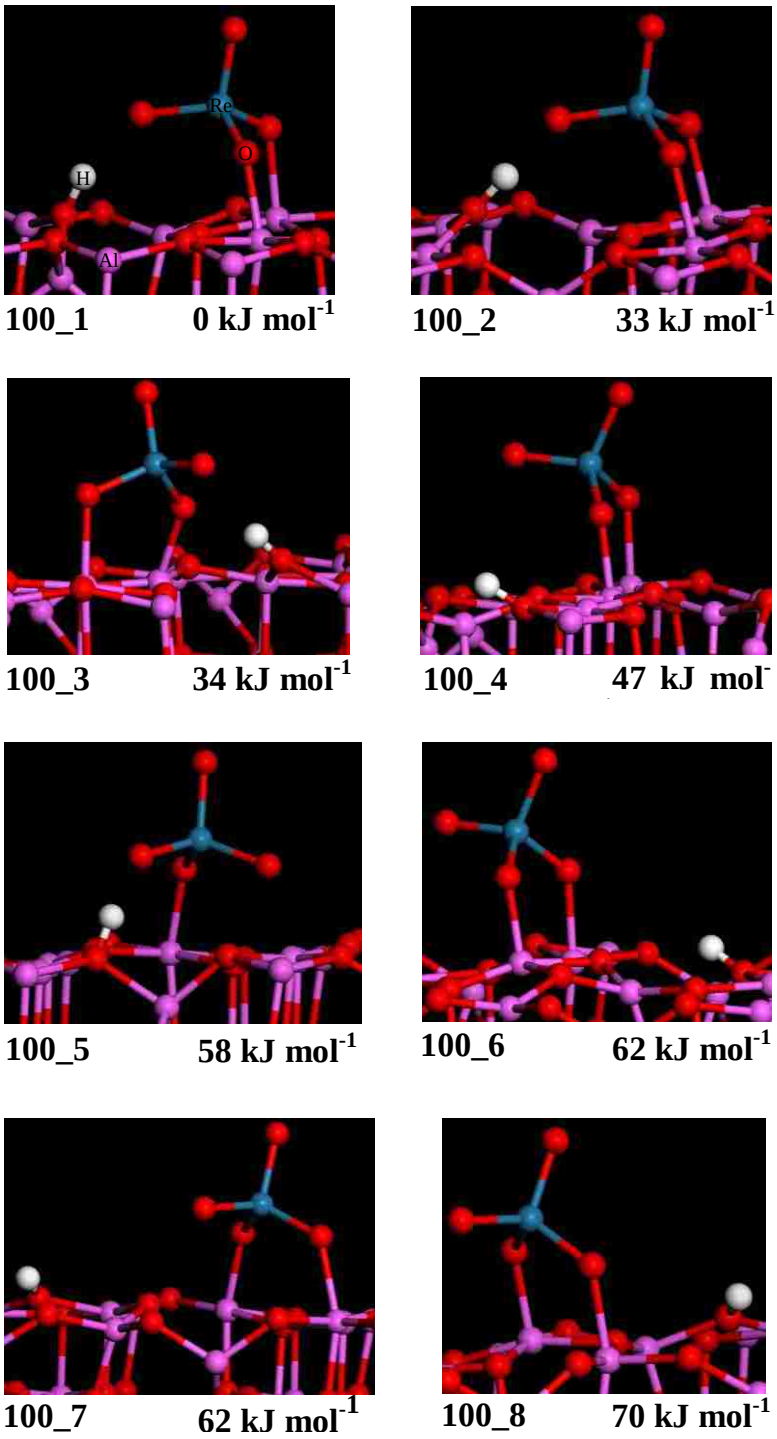

Figure S2.2. DFT optimized structures and relative energies for the surface Re^{+7} oxide species supported on (100) γ-alumina. Bond lengths are given in Å.

Almost all of the stable structures were pseudo-tetrahedral dioxo with Re=O bond lengths of ~1.7 Å. These structures were connected to the Al_2O_3 support through two Re-O-Al linkages having Re-O lengths of ~1.8 Å and Al-O lengths of 1.9-2.1 Å. The calculated Re=O bond length for typical free Re=O ligands is about 1.72-1.73 Å in perfect agreement with the recently reported EXAFS data of 1.73 Å.[S2,S3] The same values are theoretically predicted for gas-phase rhenium oxide compounds such as dimeric $Re_2O_{7(g)}$ (1.72 Å) or monomeric $HReO_{4(g)}$ (1.73 Å). In the case of the most stable configuration, 100_1, one Re=O bond is free and the second Re=O bond forms a hydrogen bond with a surface OH. The 100_5 structure is the only trioxo-like species obtained, but its geometry is also tetrahedral. Moreover, one Re=O bond is significantly elongated (1.77 Å) since it interacts at longer distance (2.16 Å) with a surface Lewis Al_V site, whereas, again, another Re=O bond is strongly hydrogen-bonded to a surface hydroxyl group. In addition, this species is significantly less stable than the lowest energy dioxo surface Re^{+7} species. Thus, Re=O bonds tend to form the maximum number of interactions with either Al Lewis centers or OH groups so that only one or two remain free oxo ligands in stable configurations. The length calculated for the non-oxo Re-O bonds in rhenium oxide gas compounds (1.89 Å) is much larger than in the case of the anchoring bridging Re-O-Al bonds (1.76-1.82 Å). This indicates partial Re=O bond character of the formally single Re-O bonds which explains the Re^{+7} oxidation state of the rhenium atom in the dioxo surface rhenium oxide species.

Table S2.1. Calculated[a] stretching frequencies (cm^{-1}) for the rhenium oxide species supported on the γ-alumina surface.

Structure	ν_s (Re=O)	ν_{as}(Re=O)	ν(Re-O-Al)
100_1	987	931	901, 878, 867
100_2	989	917	894, 852, 846
100_3	997	975, 964	909, 837, 768
100_4	988	961	915, 880
100_5	994	948, 908,	830
100_6	986	874	903, 849
100_7	995	960	867, 832
100_8	988	968	904, 847
110_1	1003	962	923, 914, 901, 720
110_2	1014	976	945, 842
110_3	996	985	896, 848, 816, 720
110_4	1008	-	948, 812
110_5	992	978	889, 830, 805, 720
110_6	985	-	867, 761, 736
110_7	990	-	874, 830, 784, 774, 706
110_8	986	964	837, 806, 797, 784, 762,
110_9	1001	904	719, 704
110_10	997	974	787, 734, 711
		956, 955	939

[a] a scale factor of 0.9900 is used.

The calculated frequencies shown in Table S2.1 for the most stable di-oxo species on the (100) surface are too low compared to the measured spectra, with a difference of at least 13 cm^{-1}, and hence significantly larger than the deviation between experiment and theory seen on the model compounds of Table 2 and, thus, the structures on the (100) terminated plane are subsequently omitted in the paper.

In order to obtain a deeper insight of the factors governing the structure and stability of the grafted perrhenate species, we performed a decomposition of the energy in interaction and deformation terms. In this approach the ReO_4^- species is detached from the support, leaving a protonated $(Al_2O_3)_nH^+$ surface. This separation is performed with a frozen geometry, enabling to evaluate the interaction energy between the deformed

fragments and their deformation energies with respect to their equilibrium structure.

Surface deformation energies have been calculated as the energy difference between the protonated alumina part frozen in the geometry of the supported ReO_x/Al_2O_3 system and the free protonated alumina surface in its relaxed geometry:

$$E_{def}((Al_2O_3)_nH^+) = E((Al_2O_3)_nH^+)_{frozen} - E((Al_2O_3)_nH^+)_{relaxed} \quad (1)$$

Deformation energies for the surface Re oxide species have been calculated for the ReO_4^- anion:

$$E_{def}(ReO_4^-) = E(ReO_4^-)_{frozen} - E(ReO_4^-{}_{(g)}) \quad (2)$$

Interaction energies are defined as the difference between the energy of the whole system and the energies of the respective fragments frozen in the geometry they have in the supported ReO_x/Al_2O_3 system:

$$E_{int} = E(system) - E((Al_2O_3)_nH^+)_{frozen} - E(ReO_4^-)_{frozen} \quad (3)$$

Adsorption energies of $HReO_4$ to form the surface Re oxide species on the γ-Al_2O_3 surface have been calculated as:

$$E_{ads} = E(system) - E((Al_2O_3)_n)_{relaxed} - E(HReO_{4\,(g)}) \quad (4)$$

The calculated deformation energies for the protonated alumina surface and ReO_4^- fragment and the corresponding interaction energies are presented in Figure S2.3. Values are compared with the associated $HReO_4$ adsorption energies on the neutral surface. A constant energy shift is produced by the deprotonation and protonation energies of the species, but this does not affect the trend between various surface structures. Not surprisingly, the ReO_4^- deformation energies for the (100) surface are very low (lower

than 15 kJ.mol^{-1}), because the geometry of the Re species is close to the ReO_4 coordination of the gas phase ReO_4^- anion. The deformation energies of the surface and the interaction energies are in the same range for all the Re oxide species, excluding 100_3, where a higher interaction energy is counterbalanced by a strong deformation energy. In the case of the (110) surface, the situation is quite different. With the exception of 110_2 and 110_10, the ReO_4^- deformation energies are much higher, compared to the (100) surface, reflecting significant variation from the ReO_4 geometry. The deformation energies of the (110) surface are also higher, on average, than those calculated for the (100) surface and, consequently, the interaction energies are increased as well. Actually, the global increase of interaction energies is even larger than it would result from the differences in the deformation energies, just confirming higher reactivity of the (110) surface. This is also seen from the values of the $HReO_4$ adsorption energies, much larger for the (110) surface, compared to the (100) one. Thus, the rhenium oxide species on the (110) γ-alumina are more stable than the species attached to the (100) surface.

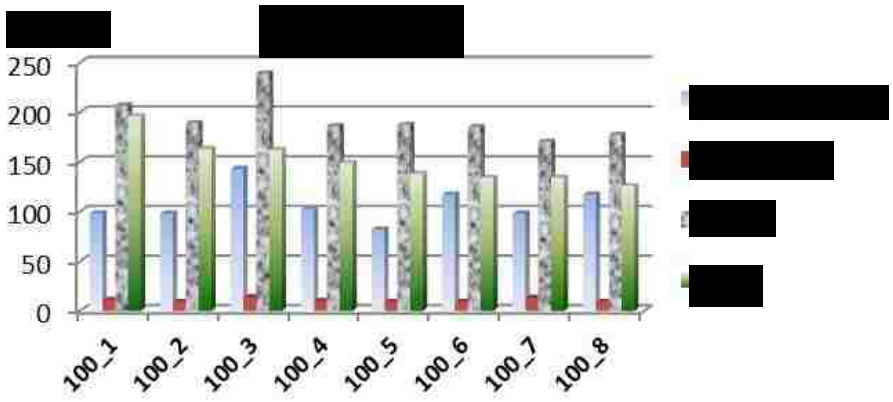

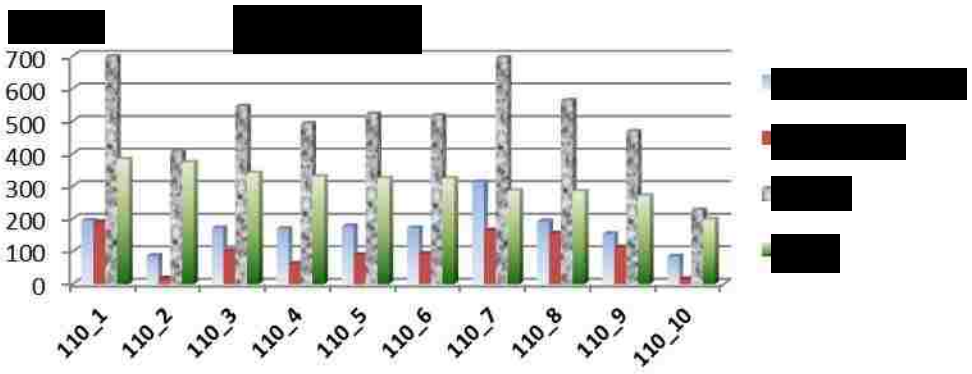

Figure S2.3. Energy analysis for the surface Re species: deformation energies of the protonated alumina surface ($E_{def}((Al_2O_3)_nH^+)$) and ReO_4^- fragment ($E_{def}(ReO_4^-)$), in the surface complex structure, corresponding interaction energies (E_{int}) between these deformed fragments and $HReO_{4(g)}$ adsorption energies (E_{ads}) to form the surface Re oxide species on (100) and (110) planes of Al_2O_3.

For the most stable 110_1 structure, a high ReO_4^- deformation energy for the quasi-ReO_6 configuration is compensated by the very large interaction energy. The overall balance is stabilizing, resulting in the best interaction-deformation compromise. Approximately the same interaction energy for 110_7 is accompanied by a much stronger distortion of the alumina surface, significantly lowering the stability of this surface rhenium oxide species. On the other hand, very weak deformations for the surface ReO_4 110_2 species explain the lowest interaction energy in this case, still high enough, however, to enable stable species formation. Approximately the same deformation energies for the trioxo 110_10 species correspond to dramatically lower interaction energy, because only one Re-O-Al bridge is formed. This is a low interaction-low deformation grafting mode that is significantly less stable than other surface Re oxide structures considered. Hence, the formation of at least two bridging Re-O-Al bonds between the Re center and the surface is mandatory for the generation of markedly stable surface rhenium oxide species.

2. Details of EXAFS Analysis

Before analyzing the structures of the dehydrated supported ReO_x/Al_2O_3 catalysts, the known structure of the reference compounds listed in Figure S2.4 with varying number of Re=O bonds was analyzed to obtain the information about the lengths of the Re=O and Re-O bonds. The passive electron reduction factor, S_0^2, was obtained by fitting the EXAFS spectrum of the ReO_3 reference and was fixed to the determined value in analysis of other reference compounds and catalysts. The models for fitting the experimental data of the reference compounds were constructed based on their known structural information (as listed in Table S2.2). The coordination numbers of nearest neighbor bonds were fixed to the values from the known structural data.

Re oxide (+6)[S4] short form: Re=O(0)

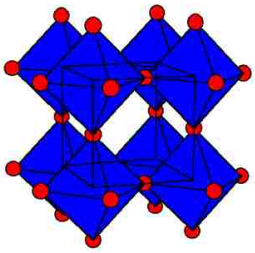

Trichlorooxobis(triphenylphosphine)rhenium(+5)[S5] short form: Re=O(1)

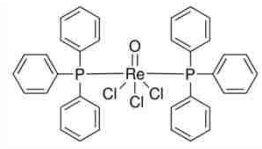

Iododioxobis(triphenylphosphine) rhenium (+5)[S6] short form: Re=O(2)

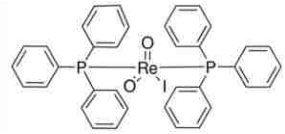

Trioxo(triphenylsilyloxy)rhenium(+7)[S7] short form: Re=O(3)

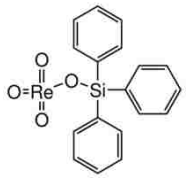

Figure S2.4. Schematic structure of reference compounds. The short form indicates the number of Re=O bonds in the corresponding compound.

Table S2.2. Local structure of Re in reference compounds

Standard	bond	N
Re=O(0)	Re-O	6
Re=O(1)	Re=O	1
	Re-Cl	3
Re=O(2)	Re=O	2
	Re-I	1
Re=O(3)	Re=O	3
	Re-O	1

Three models were tested to find the best model for fitting the experimental data of the catalysts with unknown local structures. In all three models, only the single scattering paths connecting the nearest neighbor Re and O atoms were considered. The simplest model (1) treated different types of Re-O bonds (single and double bonds) as one effective Re-O path with multiplicity N, the effective coordination number. Other models accounted for the split of the first shell in several types of Re-O paths with different half path lengths, as suggested by the possibility that both single and double Re-O bonds may be present in the catalysts. The other two models were constructed containing two or three unique Re-O paths, respectively. The details of each model are given below.

Model 1: one “effective” Re-O path

The energy origin shift, the Re-O bond length correction, the Re-O bond length disorder factor and the Re-O coordination number were varied in the fit.

Model 2: two Re-O paths

The two Re-O paths shared the same energy origin correction shift and the same disorder factor. The total coordination number of Re-O was constrained to be 4: $N(Re\text{-}O_1) + N(Re\text{-}O_2) = 4$.

Model 3: three Re-O paths

This model accounts for two identical Re=O (short double bond), one elongated Re=O(-Al) bond and one Re-O bond bridging to the support.

Results obtained with the models 2 and 3 were not meaningful in the context of the possible range of distances for the Re-O bonds expected in the unknown catalyst structure. For example, in the results obtained using model 2, some Re-O distance values were too large (around 2Å), and they fluctuated strongly between different samples. The fit quality obtained using model 2 was not better than for model 1. Analysis with model 3 was not successful possibly because it required too many constraints in order to lower the number of variables below the total number of relevant independent data points (5).

Of the three models compared, only model 1 provided physically reasonable and stable results (Table S3). Data (in k-space) of all the standard compounds and catalysts are shown in Figure S2.5 and the data and fits are shown in Figure S2.6.

Table S2.3. EXAFS Fit Results for the dehydrated supported ReO_x/Al_2O_3 catalysts with those of the reference compounds

Reference Compounds						
	bond	N	S_0^2	R(Å)	σ^2 (Å^2)	ΔE (eV)
Re=O(0)	Re-O	6	1.03±0.21	1.89±0.03	0.000	6.6±5.0
Re=O(1)	Re=O	1	1.03	1.70±0.03	0.003±0.005	2.4±2.9
	Re-Cl	3	1.03	2.44±0.02	0.002±0.001	2.4±2.9
Re=O(2)	Re=O	2	1.03	1.73±0.02	0.000	3.3±4.7
Re=O(3)	Re=O	3	1.03	1.71±0.02	0.000	2.4±3.1
	Re-O	1	1.03	1.84±0.04	0.000	2.4±3.1
Dehydrated Catalysts						
3ReAl	Re=O	3.1±0.6	1.03	1.74±0.01	0.001±0.002	2.1±2.7
15.6ReAl	Re=O	3.5±0.3	1.03	1.73±0.01	0.003±0.001	-0.3±1.2

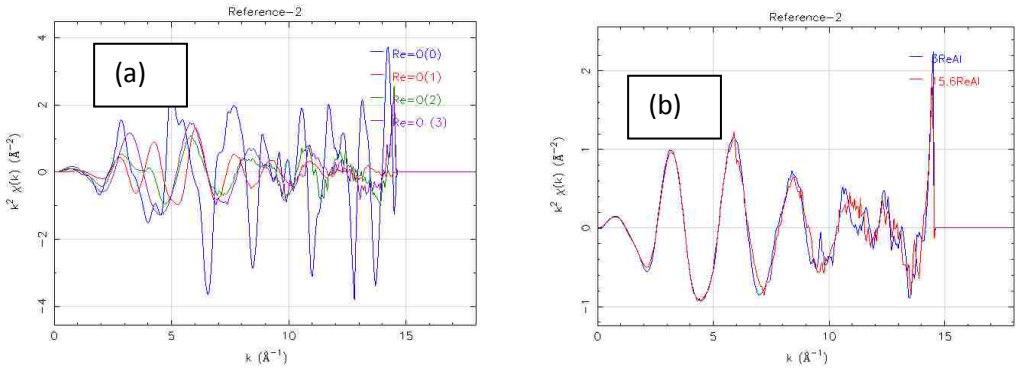

Figure S2.5. Raw data of (a) all the reference compounds and (b) dehydrated supported $ReOx/Al_2O_3$ catalysts in k-space

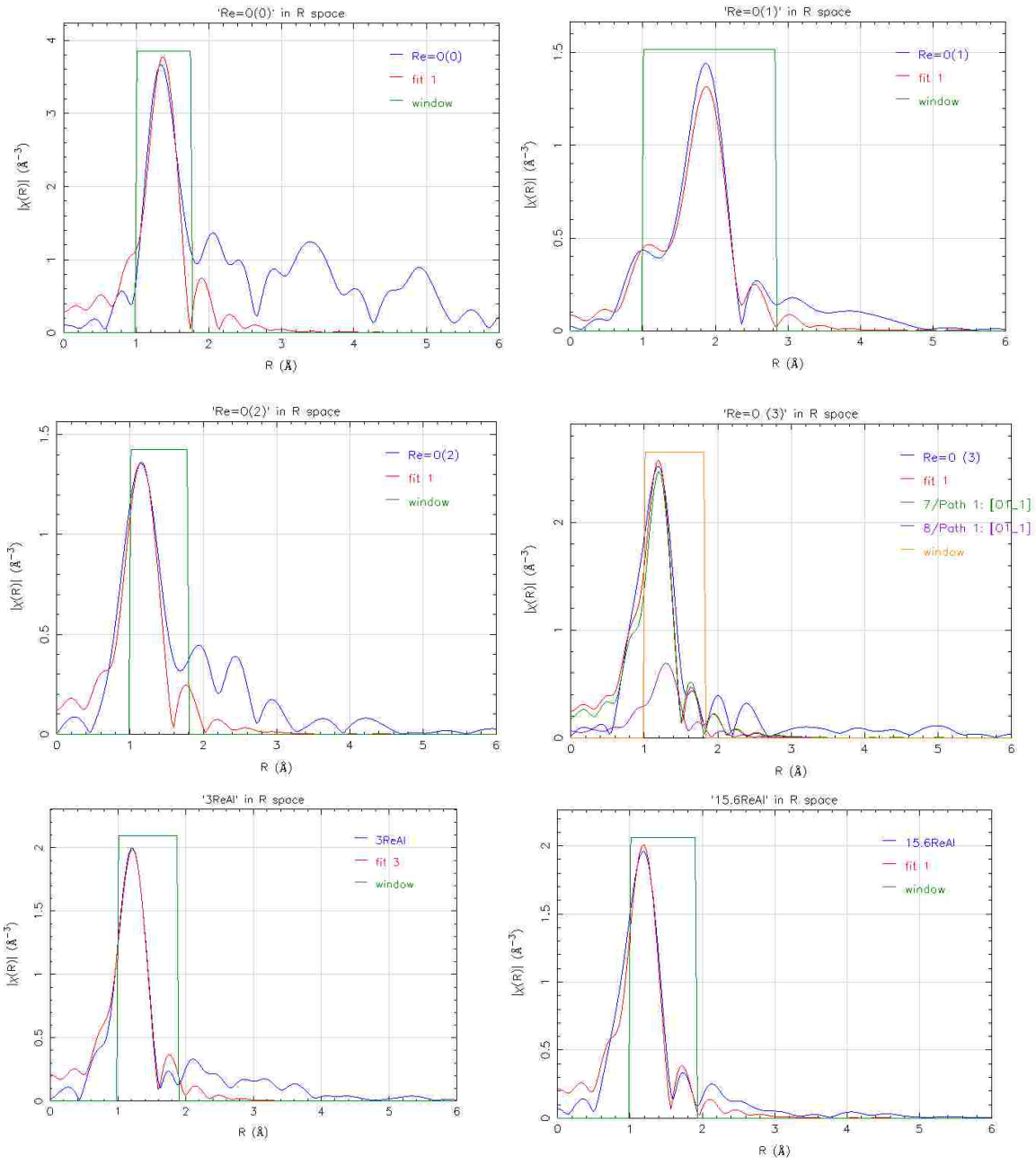

Figure S2.6. EXAFS fit results for dehydrated supported ReO_x/Al_2O_3 catalysts and reference compounds with those obtained experimentally (Fitting range: 2-11Å^{-1} in k-space and 1-1.8/1.9Å in R-space)

3. *In situ* Raman spectroscopy

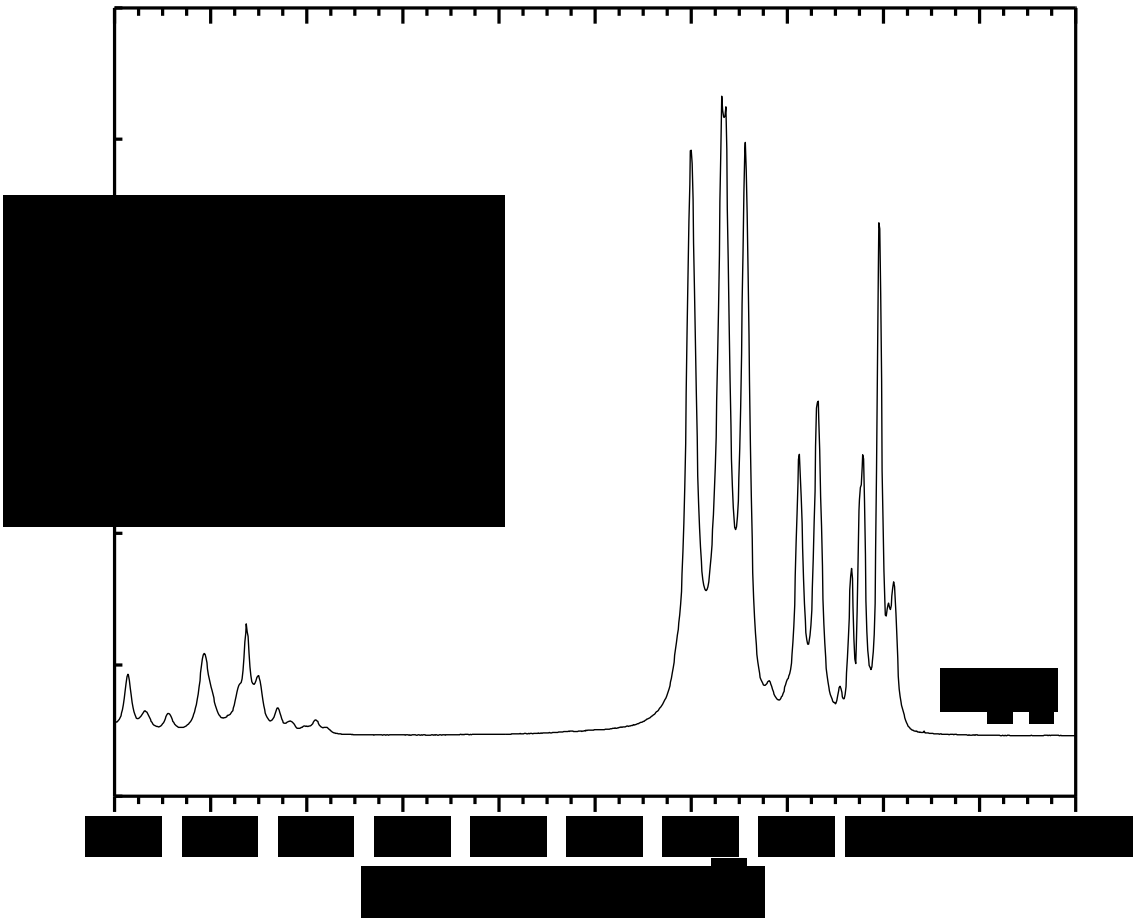

Figure S2.7. Raman spectrum of solid Re_2O_7 reference sealed in vile to avoid air exposure.

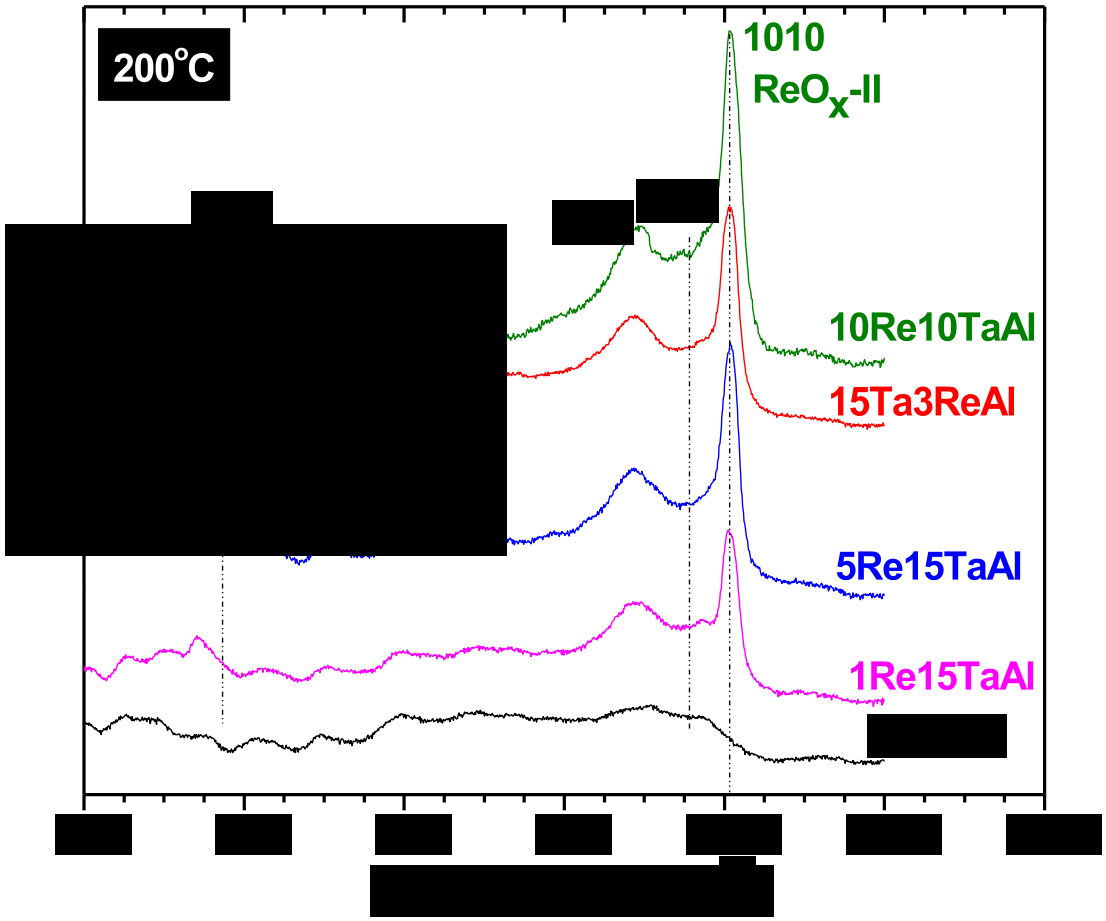

Figure S2.8. *In situ* Raman spectra (442nm) of dehydrated supported $ReO_x/Ta_2O_5/Al_2O_3$ (E). Note: the notation of 15Ta3ReAl corresponds to 15% Ta_2O_5/3% ReO_x/Al_2O_3 and indicates that Re was impregnated first, followed by Ta. All other samples were impregnated with Ta first and followed by Re.

3. *In situ* IR spectroscopy

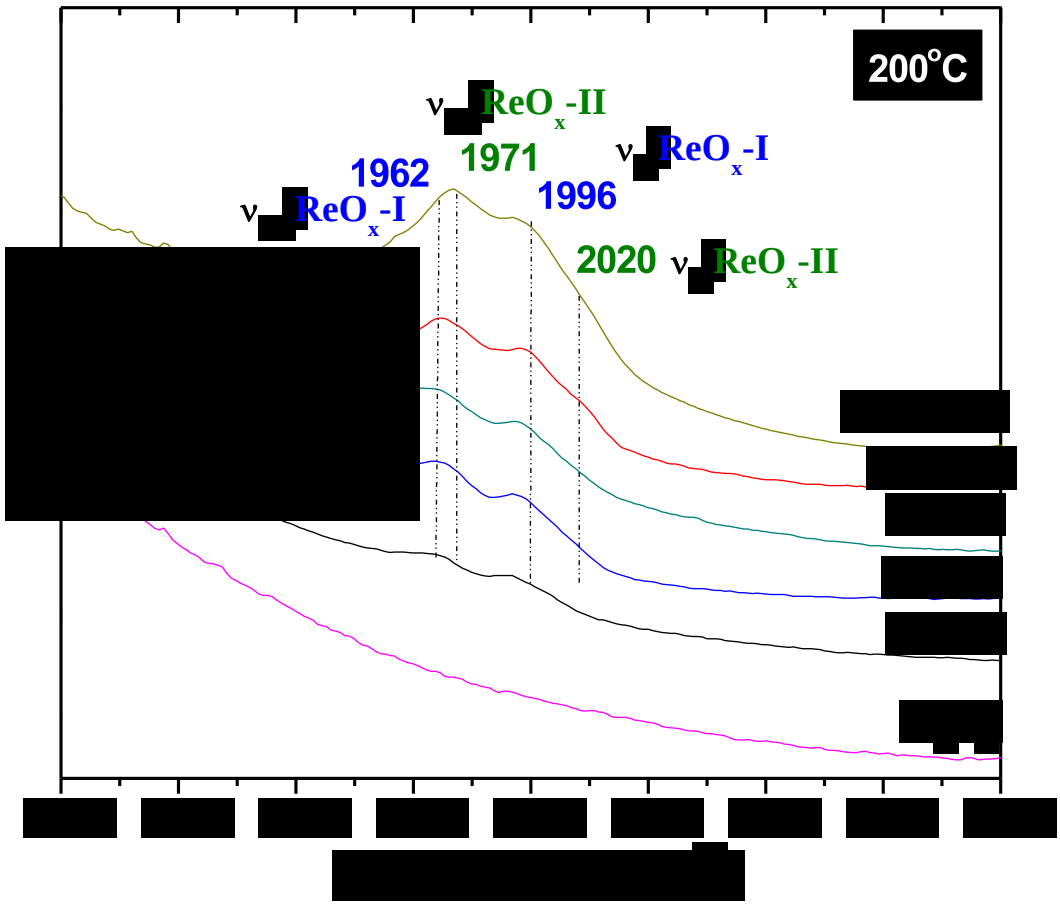

Figure S2.9. *In situ* IR spectra of dehydrated supported ReO_x/Al_2O_3 (E) catalysts at 200°C in the overtone region.

The interaction of surface TaOx species with the alumina surface hydroxyls is shown by the *in situ* IR spectra of supported TaO_x/Al_2O_3 in Figure S2.10. The addition of 15% Ta_2O_5 to Al_2O_3 mainly consumes the μ_1-Al_{VI} surface hydroxyls at 3768 cm^{-1} and minor amounts of μ_1-Al_V and μ_3-Al_{VI} hydroxyls at 3787, 3728 and 3670 cm^{-1}, respectively, also appear to be consumed. These are the same surface hydroxyls consumed by surface ReO_x-I as indicated in Figure 7. The addition of 5% ReO_x to the 15% Ta_2O_5/Al_2O_3 catalyst primarily consumes the residual μ_1-Al_V hydroxyls at 3768 cm^{-1} and

begins to also consume the μ_1-Al_V hydroxyls at 3728 cm^{-1}. Minor amounts of μ_1-Al_{IV} hydroxyls at 3787 cm^{-1} also appear to be consumed .The consumed surface μ_1-Al_V hydroxyls at 3728 cm^{-1} are the same surface hydroxyls consumed by the surface ReO_x species (see Figure 7).

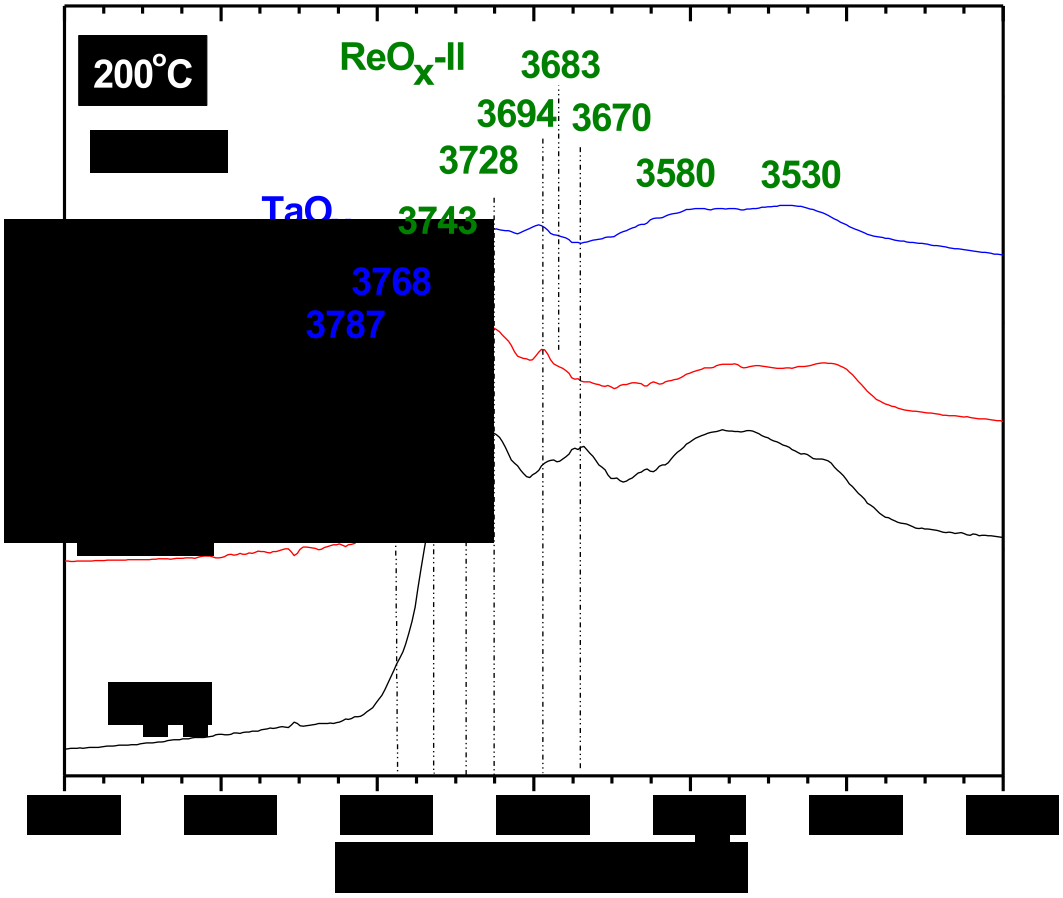

Figure S2.10. *In situ* IR spectra of the surface hydroxyl region of dehydrated supported $ReO_x/Ta_2O_5/Al_2O_3$ (E) catalysts at 200°C.

References

S1. Tian, H.; Roberts, C.A.; Wachs, I.E. *J. Phys. Chem. C* **2010**, *114*, 14110–14120.

S2. Bare, S. R.; Kelly, S. D.; Vila, F. D.; Boldingh, E.; Karapetrova, E.; Kas, J.;

Mickelson, G. E.; Modica, F. S.; Yang, N.; Rehr, J. J. *J. Phys. Chem. C* **2011**, *115*, 5740-5755.

S3. Vicente, B. C.; Nelson, R. C.; Moses, A. W.; Chattopadhyay, S.; Scott, S. L. *J. Phys. Chem. C* **2011**, *115*, 9012-9024.

S4. https://chemistry.osu.edu/~woodward/ch754/struct/ReO3.htm (accessed Jan 21, 2015).

S5. http://www.sigmaaldrich.com/catalog/product/aldrich/370193?lang=en&region=US (accessed Jan 21, 2015).

S6. http://www.sigmaaldrich.com/catalog/product/aldrich/362212?lang=en&region=US (accessed Jan 21, 2015).

S7. http://www.sigmaaldrich.com/catalog/product/aldrich/674192?lang=en&region=US (accessed Jan 21, 2015).

CHAPTER 3

Activation of Surface ReO_x Species on Al_2O_3 Catalysts for Olefin Metathesis

Abstract

The nature and number of active ReO_x species in the ReO_x/Al_2O_3 system used in olefin metathesis are systematically investigated using *in situ* Raman, UV Vis, XAS (XANES/EXAFS) and IR along with temperature programmed surface reaction (TPSR) spectroscopy experiments. The metathesis catalytic activity in ReO_x/Al_2O_3 is shown experimentally *for the first time* to stem from reduction of ReO_x species to Re(+6) and Re(+5) species through formation of CH_3CHO and HCHO. A reacting olefin then reoxidizes the active reduced species back to Re(+7). The number of sites is found to be dependent on ReO_x loadings and types, evacuation time between the reacting gases, partial pressure of the titrant and activation temperature. The delay time of reactants from Ar flush (evacuation) is *for the first time* shown to result in active sites leaving the surface resulting in lower number of active sites. The reactive intermediates are present along with π-complexes. The total number of active sites almost linearly increases as a function of ReO_x loadings although the percentage of active sites is low when only less reactive ReO_x-I sites are present. Pretreating the catalyst at slightly higher temperatures or addition of TaO_x promotors increases the number of total active sites up to 10%.

1. Introduction

The oxidation states of surface rhenia species on Al_2O_3 under non-metathesis conditions have been examined, but the nature of the activated surface rhenia species on Al_2O_3 during olefin metathesis is still not known because of the absence of supporting spectroscopic data.[1-6] Balcar *et al*. and Yide *et al*.[3,4] detected the presence of Re^{+4} and Re^{+3} with XPS after pretreatment with He, but possible XPS-induced reduction under the ultrahigh vacuum pressure clouds these findings for the initial state of the unactivated catalyst. *In situ* FT-IR measurements with CO as a probe molecule showed that rhenia is both partially and fully reduced upon from the carbon monoxide band positions.[5] Several researchers found that reduction of supported rhenia/Al_2O_3 catalysts with H_2 resulted in both partially oxidized (Re^{+4}) and metallic (Re^0) rhenia *in situ* XANES and EXAFS features for low rhenia loadings .[6-8] Stoyanova *et al.* reported detection of Re^{+6} species after olefin metathesis with *ex situ* UV-vis studies.[6] The UV-vis measurements, however, were taken under ambient conditions where the oxidation state of the rhenia is known to be altered by exposure to molecular O_2 and moisture.[7] The nature of the rhenia sites on alumina upon activation with olefins and during olefin metathesis are still not known since *in situ* and *operando* spectroscopic characterization studies have not been reported.

There is also a debate in the literature about the number of activated rhenia sites during olefin metathesis by supported rhenia/Al_2O_3 catalysts. Some studies report the number of active sites to only be ~1-2% of the total Re atoms after activation with olefins at room temperature and after evacuation for 4-6 hours.[8,9] In contrast, ~35% of Re sites have been reported to be activated for supported rhenia/Al_2O_3 catalysts prepared in hydrochloric acid medium.[10] The lack of agreement in literature for the number of

activated rhenia sites on alumina is not only due to different catalyst synthesis methodologies and surface rhenia coverage, but also to experimental conditions (e.g., temperature, pressure, evacuation time, etc.).

The objectives of this study are to understand the nature of activated rhenia species during olefin metathesis and determine the number of activated rhenia sites on alumina under different olefin experimental conditions. State-of-the-art spectroscopic characterization techniques of *in situ* Raman, UV Vis, IR and XAS spectroscopy allowed for direct monitoring of the activated rhenia species on alumina. Quantification of the surface reaction intermediates present was achieved by olefin titration (room and elevated temperatures). The titration studies revealed that there are two types of surface reaction intermediates, weakly bound and strongly bound. The weakly bound surface intermediates easily desorb at room temperature and can be titrated with olefins at room temperature. The strongly bound surface intermediates can only be titrated and reacted/desorbed at elevated temperatures (>100^{o}C).

2. Experimental

2.1. Catalyst synthesis

The supported ReO_x/Al_2O_3 and $ReO_x/TaO_x/Al_2O_3$ were prepared by impregnation of 65-70 wt% aqueous solution of perrhenic acid, $HReO_4$ (Sigma Aldrich) and ethanol toluene solution of tantalum ethoxide (Ta-$(OC_2H_5)_5$, Alfa Aesar, 99.999%) onto the Al_2O_3 support (Engelhard batch#H5433C), respectively. The full procedure of incipient-wetness impregnation, drying and calcination can be found in the previous chapter.

2.2. *In situ* UV-vis spectroscopy during propylene metathesis

The *in situ* UV-vis spectra of the catalysts were collected with a Varian Cary 5E UV-vis-NIR spectrophotometer with the Harrick Praying Mantis accessory. A magnesium oxide sample was used as a standard for obtaining the background absorbance. Approximately 5-25 mg of each catalyst in finely ground powder form was loaded into the *in situ* environmental cell (Harrick, HVC-DR2). The catalysts were initially dehydrated at 500^{o}C under oxidizing conditions (10%O_2/Ar) and the UV-vis spectra (200-800nm) of the dehydrated samples were subsequently collected after 30 minutes in flowing propylene (0.2-1% $C_3^{=}$/He) at 70 and 150^{o}C, using a scan rate of 15 nm/min and a signal averaging time of 0.6 seconds. The UV-vis spectra of reference compounds (iododioxobis (triphenylphosphine) rhenium(V) (Sigma Aldrich, 99.98%), trichlorooxobis (triphenylphosphine) rhenium(V) (Sigma Aldrich, 99.99%), ReO_3 (Alfa Aesar, 99%) and ReO_2 (Alfa Aesar, 99.995%)) were collected under ambient conditions.

2.3. *In situ* Raman spectroscopy during propylene adsorption/desorption experiments

The Raman spectra the supported ReO_x/Al_2O_3 catalysts were obtained with a Horiba-Jobin Ybon LabRam HR instrument equipped with three laser excitations (532, 442 and 325nm) and a liquid N_2-cooled CCD detector (Horiba-Jobin Yvon CCD-3000V). The 442nm laser was chosen since it minimized sample fluorescence. Spectral resolution was ~1 cm^{-1} and the wavenumber calibration was checked using the silica standard line 520.7 cm^{-1}. The lasers were focused on the samples with a confocal microscope using a 50X objective (Olympus BX-30-LWD). The spectra were typically collected at 30 s/scan

for 5 scans with a 200 μm hole. Approximately 5-25 mg of each catalyst in powder form was loaded into the *in situ* environmental cell (Harrick, HVC-DR2) possessing a SiO_2 window and O-ring seals which were kept cool by flowing water. The catalysts were initially dehydrated at 500°C by heating at 10°C/min after an hour inflowing 10% O_2/Ar (Airgas, certified, 9.989% O_2/Ar balance) at 30 mL/min. The cell was cooled in Ar to 30°C before introducing the reactive 1%propylene (C_3=)/He flow. The *in situ* Raman spectra were collected after the following treatment: 60 minutes of flowing 1% propylene (C_3=)/He, followed by flushing with Ar for another 60 minutes and then increasing the catalyst temperature to 200°C in the flowing Ar atmosphere.

2.4. *In situ* X-Ray absorption spectroscopy

The *in situ* Re L_1-edge X-ray absorption spectroscopy (XAS) experiments were performed in transmission mode at beam lines X19A and X18B of the National Synchrotron Light Source (NSLS) at the Brookhaven National Laboratory with ionization chamber detectors for measuring incident and transmitted beam intensities. A third ionization chamber was also used to detect the beam through a reference Re foil for energy calibration and alignment purposes. A plug flow reactor cell with a quartz capillary tube (I.D./O.D. = 0.8 / 1.0 mm) was used for *in situ* XAS measurements. The catalysts were pretreated at 500°C in flowing 10%O_2/He and cooled to the reaction temperature of interest (70 or 150°C) in He. A flowing 1% propylene (C_3=)/He mixture was used to activate the catalysts and perform olefin metathesis. Data processing and analysis were performed using Athena and Artemis software.[11]

2.5. *In situ* diffuse reflectance infrared-Fourier transform spectroscopy (DRIFTS)

The *in situ* DRIFT spectra were collected with a Thermo Nicolet 8700 FT-IR spectrometer equipped with a Harrick Praying Mantis attachment (model DRA-2) for diffuse reflectance spectroscopy. Spectra were taken using a MCT detector with a resolution of 4 cm^{-1} and an accumulation of 72 scans. Approximately 5-25 mg of each catalyst in powder form was loaded into the *in situ* environmental cell (Harrick, HVC-DR2). The collection of the initial background was performed by first optimizing the beam path and IR absorption signal using the height of the full Harrick sample cup, then removing the Harrick cell and placing a reflective mirror in the laser path. A spectrum was collected using the reflective mirror and was used as the background spectrum throughout the experiment. The catalysts were initially dehydrated at 500^{o}C in flowing 10%O_2/Ar and cooled down in Ar to 30°C. The catalysts were subsequently exposed to flowing 1% propylene (C_3=)/He for 45 minutes at 30 mL/min and finally flushed with Ar for 45 minutes to remove any residual physically adsorbed species before collecting the spectra. The *in situ* DRIFTS difference spectra were obtained by subtracting the spectrum of the dehydrated catalyst from that obtained after reaction with both collected at the same temperature. For the temperature programmed experiments, the catalyst was initially dehydrated as indicated above, exposed to the reactive flow of 1%C_3=/He (30 mL/min) 30°C to adsorb propylene, flushed with Ar (30 mL/min) for another 45 minutes and the temperature was then increased at 10°C/min with spectra collected every 30°C. For the C_4= adsorption/C_2= titration studies, the catalyst was initially exposed to flowing 1% C_4= (trans-2-butene)/Ar (30 mL/min) for 60 minutes at 30°C followed by titration with flowing 1%C_2=/Ar (30 mL/min) at 30^{o}C for 30 minutes. The catalyst temperature was

subsequently raised at 10°C/min in flowing 1%C_2=/Ar to 200°C (30 mL/min) and spectra taken every 50°C.

2.6. Temperature programmed surface reaction (TPSR) spectroscopy

The temperature programmed surface reaction experiments were performed using an Altamira Instruments (AMI-200) system. The outlet gases were connected to an online Dymaxicon Dycor mass spectrometer (DME200MS) and a TCD detector for analysis. Typically, ~100-300 mg of catalyst was loaded into the U-tube reactor. Blank tests with known concentrations of olefins were run for MS calibration before the experiments involving quantification of number of surface intermediates. The signals for the mass spectra were also normalized with catalyst weight for comparison. The m/z numbers used for detection of various reactants were as follows: propylene (m/z= 42), ethylene (m/z= 27), butene (m/z=56), acetaldehyde (m/z=43), formaldehyde (m/z=30), carbon dioxide (m/z=44), acetone (m/z= 58), O_2 (m/z=32), methane (m/z=16) and H_2O (m/z=18). The MS cracking patterns were carefully adjusted with blank runs using the calibration gases. Unless otherwise noted, the catalysts were dehydrated in 10%O_2/Ar at 500°C (30 mL/min) for 30 minutes and cooled in flowing Ar (30 mL/min) to the conditions of interest.

2.6.1. TPSR in flowing $C_3^=$/Ar

The same pretreatment and cooling steps as in the above experiments were utilized. After the pretreatment and cooling steps, the catalyst was allowed to interact with flowing $C_3^=$ for ~20 minutes at room temperature. A separate experiment was also

performed wherein the catalyst was immediately heated at 10°C/min to 500°C in flowing $C_3^=$/Ar (0.2-1% $C_3^=$).

2.6.2. O_2-TPO after adsorption and desorption of $C_3^=$

Similar procedures as in the Raman experiments were employed. Propylene was adsorbed on the catalyst at 30°C from flowing 1% $C_3^=$/Ar for 60 minutes, followed by flushing with Ar for another 60 minutes and increasing the temperature in flowing Ar to 200°C to desorb any remaining physically adsorbed species. After cooling to 30°C in flowing Ar, the TPO experiment was performed by introducing a flow of 2%O_2/Ar, increasing the catalyst temperature to 500°C at 10°C/min and monitoring the combustion products with the online MS to give the TPO spectra.

2.6.3. Delay time between reactants (Time of Ar flush)

Butene was adsorbed on the catalyst at 30^{o}C from flowing 1%$C_4^=$ (trans-2-butene)/Ar(30 mL/min)for 60 minutes. The catalyst was then flushed with flowing Ar (30 mL/min) at the same temperature for x minutes (x=0, 30, 60 or 240). The surface intermediates formed by 2-butene adsorption were then titrated to $C_3^=$ with flowing 1%$C_2^=$ (ethylene)/Ar initially for 60 minutes at 30^{o}C and then with TPSR (10°C/min) in flowing 1%$C_2^=$/Ar up to 500°C. The olefin reaction products were monitored with the online MS during the above titration studies.

2.6.4. Simultaneous flow of $C_4^=$ and $C_2^=$ at 30°C

The amount of $C_3^=$ produced from reaction of 1%$C_4^=$/Ar and 1%$C_2^=$/Ar at 30°C was determined with the online MS.

2.6.5. Effect of $C_2^=$ partial pressure during titration

The catalyst was exposed to flowing 1%$C_4^=$/Ar (30 mL/min) at 30°C to adsorb 2-butene for 60 minutes. The surface intermediates formed during 2-butene adsorption were then immediately titrated with varying amounts of flowing$C_2^=$/Ar mixtures (0, 0.33, 0.67 and 1% $C_2^=$) (30 mL/min) initially at 30°C and then during TPSR to 500°C (10°C/min).

2.6.6. Effect of $C_4^=$ activation temperature

After catalyst dehydration, the catalyst was activated with flowing 1%$C_4^=$/Ar (30 mL/min) at either 70, 150 or 300°C for 60 minutes in order to examine the effect of activation temperature. The catalyst was subsequently cooled down in flowing Ar (30 mL/min) to 30°C before again switching to flowing 1%$C_4^=$/Ar to adsorb 2-butene for another 60 minutes. Titration with flowing 1%C_2/Ar (30 mL/min) was immediately performed at 30°C for 60 minutes and followed by TPSR in the same $C_2^=$ gas mixture up to 500°C (10°C/min) and the propylene product was monitored with online MS.

3. Results

3.1. Propylene Activation of Supported ReO_4/Al_2O_3 Catalysts

3.1.1 *In situ* Raman spectroscopy during propylene adsorption/desorption

The *in situ* Raman spectra of supported 9.4%ReO_4/Al_2O_3 before and during $C_3^=$ adsorption/desorption experiments are shown in Figure 3.1. Prior to propylene exposure,

the Raman spectrum of the dehydrated catalyst exhibits two bands at 1003 and 1013 cm^{-1} that have been shown to originate from two distinct isolated surface ReO_4 species on the Al_2O_3 support.[12] The Raman bands labeled ReO_4-I and ReO_4-II correspond to surface ReO_4 species anchored at basic μ_1 Al_{IV} and Al_{VI} and acidic μ_2 and μ_3 Al_{VI} surface sites of the Al_2O_3 support, respectively (the Roman subscript refers to the number of O atoms surrounding the Al cation). Adsorption of propylene on the catalyst preferentially decreases the intensity of the surface ReO_4-II species indicating selective adsorption on these rhenia sites. Heating the catalyst to 200^oC in flowing Ar in an attempt to react or desorb the organic surface intermediate(s), however, does not restore the ReO_4-II band at 1013 cm^{-1} suggesting either retention of coordinated organic surface intermediates or removal of oxygen from the surface ReO_4-II species. The Raman band for the surface ReO_4-II species is only restored upon heating the catalyst in O_2/Ar. The presence of organic surface intermediates after the propylene adsorption/desorption cycle is confirmed by formation of CO_2 and H_2O during Temperature Programmed Oxidation (TPO) as shown in Figure 3.2. The oxidation state of the surface rhenia species after propylene adsorption/reaction/desorption and will be addressed below.

3.1.2 Propylene adsorption/metathesis and TPSR spectroscopy

Exposure of the supported 15.6% ReO_x/Al_2O_3 catalyst to flowing $C_3^=$/Ar at room temperature exhibits an induction period of several minutes for formation of $C_2^=$ and $C_4^=$, and initially yields acetaldehyde (CH_3CHO) (m/z=43) and formaldehyde (HCHO) (m/z=30) as the main oxygenated products presented in Figure 3.3. Neither acetone (m/z=58), alcohols (methanol, ethanol and propanol) or CO_2 are detected. Water (H_2O)

initially appears and is related to displacement of a small amount of residual adsorbed moisture by the stronger adsorption of propylene on the catalyst. Subsequent temperature programming of the catalyst in the flowing $C_3^=$/Ar, shown in Figure 3.4, continues to form $C_2^=$ and $C_4^=$ until ~300^{o}C, as well as acetaldehyde. Above 300^{o}C, extensive propylene combustion (CO_2, H_2O and some CH_3CHO, HCHO and CH_4) takes place with oxygen from the surface ReO_x sites. Formation of the CH_3CHO and HCHO oxygenates upon propylene adsorption at 30^{o}C reveals that surface rhenia species are being activated by removal of some of its oxygen atoms at mild temperatures. More extensive oxygen removal takes place above 300^{o}C since significant combustion products form at these temperatures.

3.1.3 *In situ* XAS (XANES/EXAFS) during $C_3^=$ adsorption/metathesis

The oxidation state of the surface ReO_4 species during exposure to propylene was monitored with *in situ* XANES at 70°C and 150°C and the spectra are presented in Figure 3.5. The strong XANES feature at 12533eV reflects the ReO_4 coordination of the surface rhenia species.[12] The XANES pre-edge is barely perturbed by adsorption and metathesis of propylene at 70^{o}C, which contains the Re^{+7} oxidation state for the surface rhenia species. It should be noted that $Re{=}CH_2$ and $Re{=}CHCH_3$ intermediates can also oxidize reduced surface rhenia sites with their two electrons by replacement of Re=O with $Re{=}CH_2$/$Re{=}CHCH_3$ bonds that can maintain the Re^{+7} oxidation state. At 150^{o}C, however, the XANES pre-edge is slightly decreased by adsorption and metathesis of propylene reflecting the presence of some reduced surface rhenia species.

The corresponding *in situ* EXAFS spectra during propylene adsorption and metathesis at 70°C and 150°C are presented in Figure 3.6. The peak at 1.1Å in the fresh catalysts is from the terminal Re=O bond of the surface rhenia species. The absence of Re-Re features at 3-4 Å reflects the isolated nature of the surface ReO_4 sites even during the reaction. At 70^{o}C, the EXAFS spectrum is not perturbed by propylene adsorption and metathesis. At 150^{o}C, however, the intensity of the EXAFS Re=O peak is slightly diminished reflecting the removal of some oxygen atoms from the surface rhenia species during propylene adsorption and metathesis.

3.1.4 *In situ* UV-vis during propylene adsorption/metathesis

The UV-vis spectra of rhenia reference compounds are presented in Figure 3.7 and consist of reduced Re^{+6}, Re^{+5} and Re^{+4} compounds. The ReO_3 reference consists of Re^{+6} sites that give rise to a sharp band at ~540nm. The iododioxobis (triphenylphosphine) Re^{+5} dioxo reference exhibits bands at 260, 300-353 and 560 nm while the mono-oxo trichlorooxobis (triphenylphosphine) Re^{+5} mono-oxo reference contains its bands at 260, 300-353 and 445 nm. The difference in the location of the 445 and 560nm bands from these two Re^{+5} reference compounds is most likely related to their different Re=O oxo bonds (dioxo *vs*. mono-oxo). The ReO_2 reference compound possesses Re^{+4} sites and only yields a very broad band at ~400nm and doesn't give rise to detectable UV-vis d-d transition bands.

The *in situ* UV-vis spectrum of the dehydrated supported 15.6% ReAl catalyst in flowing He is also shown in Figure 3.7 and does not possess any d-d transition bands in the 300-800nm region from reduced rhenia species reflecting the presence of only Re^{+7}

species for the dehydrated catalyst with a strong band at 240nm. The 15.6% ReAl catalyst was chosen because of its high Re content, which allows for the easier detection of reduced rhenia species. The *in situ* UV-vis spectra of the supported 15.6% ReAl catalyst in flowing He and propylene at 70 and 150°C are shown in Figure 3.8(a). Weak d-d transitions from reduced rhenia species are present after exposure to propylene in the 300-800nm region. In order to enhance the typically weak d-d transition bands from the reduced rhenia species, the spectrum of the dehydrated catalyst was subtracted from the spectra during propylene metathesis as shown as Figure 3.8(b). The UV-vis d-d bands in the difference spectra increase with temperature reflecting the greater number of reduced rhenia species. The observation of reduced rhenia species is a consequence of the lower concentration of coordinated surface reaction intermediates at higher temperatures that oxidize reduced rhenia species back to Re^{+7}. This is supported by the *in situ* UV-vis spectra that demonstrates desorption of surface intermediates at 200^{o}C in flowing He enhances the intensity of the d-d transitions as shown in Figure 3.9.

Increasing the partial pressure of propylene further increases the concentration of the reduced rhenia species on alumina as shown in Figure 3.10. The *in situ* UV-vis spectra at 70 and 150°C in the flowing propylene environment closely match those of the Re^{+6} and dioxo/mono-oxo Re^{+5} reference compounds. This suggests that the reduced rhenia species are most likely present as Re^{+6} and Re^{+5} species on the Al_2O_3 support during the propylene metathesis reaction conditions. This is also in agreement with High Field High Frequency (HFHF) EPR studies that confirm the presence of paramagnetic Re^{+6} and the absence of EPR-active Re^{+4} species.[13 The] Re^{+5} species are EPR silent since they are not paramagnetic.

3.1.6. *In situ* IR spectroscopy

The *in situ* IR spectra for propylene adsorption at 25°C on the Re-free pure Al_2O_3 support and 15.6% ReO_x/Al_2O_3 catalyst are shown in Figure 3.11. For the alumina support exposed to flowing $C_3^=$/Ar, the IR bands are characteristic of surface propylene complexes ($\delta_s(CH_3)$ [1390 cm^{-1}], ν(C=C) [1590 and 1670 cm^{-1}], $\nu_s(CH_2)$ [2870 cm^{-1}], $\nu_{as}(CH_2)$ [2940 cm^{-1}] and $\nu_{as}(CH_3)$ [2965 and 2980 cm^{-1}]), but lack the characteristic =C-H stretching bands above 3000 cm^{-1}. The 1670 cm^{-1} ν(C=C) band is similar to gas phase propylene (*i.e.*, weakly bound), while the very weak 1590 cm^{-1} shoulder could indicate a trace of surface propylene allyl complex. For the supported 15.6% ReO_x/Al_2O_3 catalyst in flowing $C_3^=$/Ar, IR bands from both gas phase propylene (2920, 2935, 2950, 3080, and 3105 cm^{-1}) and an adsorbed species at δ(=CH) [1300 cm^{-1}], $\delta_s(CH_3)$ [1390 cm^{-1}], $\delta_s(CH_2)$ of vinyl group (-CH=CH_2) [1400 and 1415 cm^{-1}], $\delta_{as}(CH_3)$ [1450 cm^{-1}], $\delta_s(CH_2)$ [1470 cm^{-1}], ν(C=C) [1650 cm^{-1}], $\nu_s(CH_2)$ [2870 cm^{-1}], $\nu_{as}(CH_2)$ [2940 cm^{-1}], and $\nu_{as}(CH_3)$ [2980 cm^{-1}].[14,15] The bands are generally in agreement with an adsorbed surface propylene π-complex (*vs*. weakly bound and allyl for Al_2O_3) except for the appearance of a 1400 cm^{-1} vinyl group band and the absence of =C-H stretches above 3000 cm^{-1}.[16]

The thermal stability of the surface intermediates on the supported 15.6 ReAl catalyst resulting from propylene adsorption at room temperature was monitored in flowing Ar with TP-IR spectroscopy and the spectra are presented in Figure 3.12. The spectrum at 30^{o}C under flowing propylene exhibits bands from gas phase propylene and an adsorbed propylene π-complex (see above for vibrations).[14-16] All bands related to the surface propylene π-complex decrease in intensity with temperature and disappear by

120^{o}C. Some minor bands at 2870, 2925, 2960 cm^{-1} remain at 150^{o}C and may indicate the presence of another minor adsorbed surface complex.

The difference IR spectra of the adsorption of trans-2-butene on the supported 15.6 ReAl catalyst, followed by titration of the surface intermediates by ethylene, are given in Figure 3.13. After 60 mins of trans-2-butene adsorption bands appear from gas phase trans-2-butene (875, 2945, 3015, and 3035 cm^{-1}) and adsorbed species $\delta_s(CH_3)$ [1375 and 1390 cm^{-1}], $\delta_s(CH_2)$ of vinyl group (-CH=CH_2) [1415 cm^{-1}], $\delta_{as}(CH_3)$ [1445 cm^{-1}], $\delta_s(CH_2)$ [1470 cm^{-1}], ν(C=C) [1650 cm^{-1}], $\nu_s(CH_2)$ [2865 cm^{-1}], $\nu_s(CH_3)$ [2890 cm^{-1}], $\nu_{as}(CH_2)$ [2925 and 2935 cm^{-1}], and $\nu_{as}(CH_3)$ [2960 and 2980 cm^{-1}].[14,15] Upon introduction of ethylene, new bands from gas phase ethylene appear at 2990, 3080, and 3125 cm^{-1}.[14] Oddly, bands from the vinyl group and C=C still exist, but no bands at >3000 cm^{-1} are detected for their corresponding =C-H stretching vibrations. The IR spectra do not change with increasing contact time with ethylene and no noticeable change is observed when increasing the temperature to 50^{o}C under ethylene. Increasing the temperature to 100^{o}C under ethylene causes a large decrease in bands at 1390, 1415, 1470, 1650, 2890, 2935, and 2980 cm^{-1}. This suggests that two adsorbed surface species exist: Species I (the decrease bands) which desorbs at ~100^{o}C and Species II (remaining bands: 1375, 1390, 1445, ~1680, 1470, 2870, 2935, and 2960 cm^{-1}) which is stable up to 150^{o}C. The exact identity of the adsorbed surface species cannot be determined, but the presence of ν(C=C) bands indicates that both are alkenes.

3.2. Titration of surface intermediates

To quantify the number and reactivity of the surface intermediates present on the catalyst after olefin adsorption, one olefin was first adsorbed ($C_3^=$ or 2-$C_4^=$) followed by

titration with a second olefin ($C_2^=$, $C_3^=$ or 2-$C_4^=$). For example, 2-butene was initially adsorbed and then titrated with ethylene to yield propylene. An advantage of this protocol is that weakly adsorbed 2-buetne on the catalyst would not participate in the metathesis reaction to form propylene.

3.2.1 Effect of delay time between $C_4^=$ adsorption and $C_2^=$ titration

Titration of the surface intermediate(s) formed by $C_4^=$ adsorption with $C_2^=$ produces propylene in two temperature ranges, 30^{o}C and ~50-150^{o}C, as shown in Figure 3.14 for the 15.6% ReAl catalyst. The two temperature ranges suggest that two distinct types of surface intermediates are present on the catalyst after 2-butene adsorption, weakly and strongly bound surface intermediates. Increasing the time between $C_4^=$ adsorption and $C_2^=$ titration with an Ar purge (from 0 to 240 minutes), dramatically decreased the number of weakly bound surface intermediates, but doesn't affect the number of strongly bound surface intermediates. Without a delay between $C_4^=$ adsorption and $C_2^=$ titration (0 minutes), the ratio of propylene produced at low temperature to high temperature was ~7.5 (corresponding to a $C_3^=$/Re ratio of 8.7). After 240 minutes of an Ar purge between $C_4^=$ adsorption and $C_2^=$ titration, the ratio of propylene produced at low temperature to high temperature was ~0.7 (corresponding to a $C_3^=$/Re ratio of 0.8). This demonstrates that the weakly adsorbed intermediates at 30^{o}C are in equilibrium with the gas phase 2-butene and that removal of $C_4^=$ from the gas phase results in recombination of surface intermediates that readily desorb to form 2-butene.

In addition to the production of propylene during ethylene titration of the surface intermediates resulting from 2-butene adsorption, desorption of $C_4^=$ also takes place. Upon switching from a $C_4^=$/Ar flow to an Ar flow, $C_4^=$ continues to elude for several minutes

reflecting the equilibrium between the surface intermediates and gas phase $C_4^=$ (see Figure S3.1). A minor amount of $C_4^=$ desorbs again from the catalyst upon switching to a flow of $C_2^=$/Ar (see 0 min experiment of Figure S3.1). This is especially evident when $C_2^=$ is introduced after flowing inert Ar and the amount of desorbed $C_4^=$ decreases with the Ar purge time. Desorption of $C_4^=$ upon exposure to $C_2^=$ was not observed for the Re-free Al_2O_3 support and, thus, the desorbed $C_4^=$ is associated with the ReO_x sites.

3.2.2. Number of propylene molecules formed from reaction of 1% $C_2^=$/Ar and 1% $C_4^=$/Ar at 30°C

The simultaneous presence of 2-butene and ethylene in the gas phase in the absence of an Ar purge at 30°C necessitated determining the catalytic activity between these two reactants by the supported ReO_4/Al_2O_3 catalyst. To determine the number of propylene molecules formed by reaction of 2-butene and ethylene at 30°C, 1% $C_2^=$/Ar and 1% C_4/Ar were simultaneously flown into the reactor and the results (see Figure S3.2). The simultaneous presence of 2-butene and ethylene in the gas phase only accounts for ~14% of the propylene formed during the titration experiment, and shows that propylene formed by $C_2^=$ titration of the surface intermediates from $C_4^=$ adsorption dominates the titration experiment.

3.2.3. Effect of $C_2^=$ partial pressure on number of surface reaction intermediates

The influence of the $C_2^=$ partial pressure on the formation of $C_3^=$ by reaction with the surface intermediates formed from $C_4^=$ adsorption is shown in Figure 3.15. The number of propylene molecules formed at 30°C monotonically increases with the gas

phase concentration of C_2= (0, 0.33, 0.67 and 1%). Quantitative analysis indicates that the number of $C_3^=$ molecules formed varies as ~0.7-order in $C_2^=$ partial pressure for low $C_2^=$ concentrations (Figure S3.3). The number of $C_3^=$ molecules formed between 50-150^{o}C, however, is relatively constant and independent of the $C_2^=$ partial pressure for non-zero ethylene partial pressures. The different responses of the surface intermediates to ethylene partial pressures at low and high temperatures again reflects the presence of two distinct types of surface reaction intermediates that are weakly and strongly adsorbed.

The amount of $C_4^=$ desorbing during the titration is independent of $C_2^=$ partial pressure (see Figure S3.4). This trend suggests that the desorbing $C_4^=$ is related to desorption of molecularly adsorbed 2-butene since increasing $C_2^=$ partial pressure consumes more surface reaction intermediates to produce propylene as shown in Figure 3.15. The faster $C_4^=$ elution times with increasing $C_2^=$ partial pressure reflects displacement of molecularly adsorbed $C_4^=$ in the presence of gas phase $C_2^=$ and supports the conclusion that this 2-butene results from desorption of molecularly adsorbed $C_4^=$ from the catalyst.

3.2.4. Effect of pretreatment temperature on number of surface intermediates

The influence of $C_4^=$ adsorption temperature on the number of $C_3^=$ molecules formed during $C_2^=$ titration is presented in Figure 3.16. The number of $C_3^=$ molecules formed at 30°C decreases as the $C_4^=$ adsorption temperature is raised, especially above 70^{o}C. This reflects the facile recombination of the surface intermediates and desorption of $C_4^=$ during the adsorption step at elevated temperatures. The number of $C_3^=$ molecules formed during $C_2^=$ titration from the strongly bound surface intermediates at higher

temperatures (~50-250^{o}C) was also a strong function of the initial activation temperature. The number of $C_3^=$ molecules formed from the strongly bound intermediates initially increased with the pretreatment temperature and then sharply diminished to almost zero after the 300^{o}C pretreatment. The higher temperatures required for the formation of $C_3^=$ indicate that even more strongly bound surface intermediates are created from higher $C_4^=$ pretreatment temperatures.

3.2.5. Effect of ReO_x loadings on number of surface intermediates

The number of $C_3^=$ molecules formed from $C_2^=$ titration of surface intermediates created from $C_4^=$ adsorption at 30°C are shown in Figure 3.17 as a function of ReO_4 loadings. For most of the catalysts, almost all of the surface intermediates created by $C_4^=$ adsorption react within 10 minutes of C_2= titration and the total number of $C_3^=$ molecules produced monotonically increases with rhenia loading as shown in Figure 3.18. The percentage ratio of $C_3^=$ molecules produced to surface ReO_4 sites, however, strongly depends on rhenia loading. For low rhenia loadings (< 5% ReO_4), the $C_3^=$/Re percentage ratio monotonically increases with rhenia loading because of the presence of the less reactive surface ReO_4-I sites coordinated to basic alumina sites.[13] At higher rhenia loadings (> 7% ReO_4), the $C_3^=$/Re percentage ratio is independent of rhenia loading at ~6-8%. The $C_3^=$/Re percentage ratio is further increased by a factor of 1.4 (7.4% for 10ReAl *vs*. 10% for 10ReTaAl) by introduction of the surface TaO_x promoter that blocks formation of the less reactive surface ReO_4-I site.[13]

4. Discussion

4.1. Activation of surface ReO_x species

Activation of the surface ReO_x species on alumina yields oxygenated (CH_3CHO and HCHO) products and also forms surface olefinic intermediates. The appearance of the oxygenated products indicates that activation of the supported ReO_x/Al_2O_3 catalysts by propylene follows the pseudo-Wittig mechanism, as shown in scheme 3.1. [11] The pseudo-Witting mechanism involves removal of an oxo O atom from the surface ReO_4 species that allows for coordination of an olefin intermediate (e.g., $Re=CH_2$, $Re=CHCH_3$, etc.). The number of activated surface rhenia sites is a strong function of activation temperature: initially increasing from 30 to 170^oC and then decreasing with further increase in temperature. In the lower temperature range, only oxygenated products are formed reflecting mild removal of oxygen from the surface rhenia species. At higher temperatures, the removal of oxygen from the surface rhenia species becomes more aggressive, reflected by the formation of CO_2 and H_2O, and deeper reduction of the rhenia sites. This indicates that there is a preferred oxidation state and structure for activated surface rhenia sites on alumina when exposed to reactive olefins.

4.2 Nature of activated surface ReO_x sites

The activated rhenia species on alumina consist of Re^{+5} and Re^{+6} sites as shown by the *in situ* UV-vis bands in the 300-600 nm region (bands at 380, 450 and 560 nm) that closely match the Re^{+5} reference compounds (sees Figure 3.7 and 3.8) and those reported for Re^{+5} organometallic complexes.[17,18] Similar UV-vis bands in the 330-530nm region were observed for a variety of dioxorhenium(+5) complexes[17] and monodentate imido-

rhenium (+5) complexes.[18] The weak UV-vis band at 540 nm also corresponds to Re^{+6} species (see ReO_3 spectrum in Figure 3.8), which is detected with EPR spectroscopy.[13] The activated rhenia sites are coordinatively unsaturated and also bond to alkene intermediates ($Re{=}CH_2$. $Re{=}CHCH_3$, etc.). The alkene double bonds oxidize the partially reduced rhenia species back to Re^{+7}, which makes it difficult to spectroscopically detect the partially reduced rhenia species. Increasing the activation temperature, however, reacts and desorbs the alkene intermediates leaving behind partially reduced rhenia species that can now be spectroscopically detected. For example, compare the *in situ* UV-vis and XAS spectra at 70 and 150^{o}C (see Figures 3.8) showing the presence of partially reduced and oxygen deficient rhenia sites at 150^{o}C.

4.3 Nature of surface reaction intermediates

Adsorption of olefins on the supported ReO_x/Al_2O_3 catalysts results in both molecularly adsorbed alkenes and alkene intermediates. The molecular adsorbed olefins form surface alkene π-complexes with the catalyst surface. The exact identity of the surface alkene intermediates cannot be determined with IR spectroscopy, but the presence of ν(C=C) bands indicates that surface alkene intermediates are present. Presumably, $Re{=}CH_2$, $Re{=}CHCH_3$ and others would be present along with these π-complexes. Carbon NMR spectroscopy could potentially shed more light on the nature of the surface alkene intermediates, but the presence of the paramagnetic Re^{+6} species would interfere with the ^{13}C NMR signal.

4.4. Number of surface intermediates

One should take a great care in interpreting the number of sites under several conditions. The total number of active sites would never equal reactive intermediates at a condition since only a fraction of sites can react at that condition.

Removing physisorbed/chemisorbed 2-butene through evacuation (Ar flush) is *for the first time* shown to take away most or almost all of Re= $CHCH_2$. This result would not have been expected unless $CH_2CH=CHCH_2$ < > 2 Re=$CHCH_2$ is an important reaction step in creating active sites. Therefore, taking away $CH_2CH=CHCH_2$ results in less Re=$CHCH_2$ sites. Flowing ethylene simultaneously with 2-butene results in less active sites than first adsorption of 2-butene and followed by titration with ethylene probably because the surface in the latter case was not allowed to be saturated to the full extent with Re=$CHCH_2$ sites due to their immediate reaction with $CH_2=CH_2$. Regardless of their participation in the reaction, the same amount of Re=$CHCH_2$ sites leave at 30°C in 60 minutes with different C_2= partial pressures and different Ar flush times. The residual sites reacting at higher temperatures is the same for all C_4= adsorption/C_2= titration experiments at a certain ReO_x loading. The higher temperatures required to titrate the remaining surface intermediates indicate that these sites would have to overcome a certain activation barrier to react.

Pretreatment with C_4= at 70°C increases the total number of active sites to ~10% by increasing the residual sites at higher temperatures by a factor of 2 whereas TaO_x promotion achieve the same purpose at room temperature since it only creates ReO_x-II sites which anchor at acidic μ_2 and μ_3 AlO_x sites (discussed in the previous chapter). This is clearly evident from Figure 3.18 where the percentage of active sites is low where ReO_x-I sites at basic μ_1 AlO_x sites are present.

Our results *for the first time* indicate the inaccuracies in the evacuation/titration method employed in literature and explain the discrepancies in number of sites obtained across different studies.

5. Conclusions

The nature of catalytic active sites was extensively studied by *in situ* UV Vis, XAS (XANES/EXAFS), and HFHF EPR studies along with steady state and TPSR experiments. The detection of CH_3CHO and HCHO during activation clearly shows evidence of the pseudo-Wittig activation mechanism. The surface ReO_x species are *for the first time* experimentally shown to be activated by reduction to intermediate Re(+6) and Re(+5) species. This reduction is critical to reactivity as related by the data of *in situ* Raman, XAS, UV Vis and TPSR experiments. Upon exposure to olefins, active species reoxidize back to the +7 oxidation state. The importance of achieving optimal oxidation states is seen in production of CO_2 by over-reduction of the catalysts at high temperatures which immediately results in deactivation. Increasing the evacuation time (Ar flush) is *for the first time* shown to decrease the Re-alkylidene sites. A significant amount of surface intermediates (~90%) are titrated at room temperature although a small amount requires higher temperatures to be reacted. The number of the active sites is found to be dependent on a variety of conditions: the reaction temperature, evacuation (Ar flush time) between reactants, titrant partial pressure and type of ReO_4 species present (ReO_4-I or ReO_4-II).

References

1. Mol, J.C. *J. Mol. Catal. A. Chem*. **2004**, *213*, 39–45.

2. Disproportionation catalyst. British Petroleum Corporation. Great Britain Patent GB1054864 (A), September 8, 1964.

3. Balcar, H.; Zilkova, N.; Bastl, Z.; Dedecek, J.; Hamtil, R.; Brabec, L.; Zukal, A.; Cejka, J. *Studies in Surf. Sci. and Catal*. **2007**, *170*, 1145–1152.

4. Yide, X.; Xinguang, W.; Yingzhen, S.; Yihua, Z.; Xiexian, G. *J. Mol. Catal*. **1986**, *36*, 79–89.

5. Daniell, W.; Weingard, T; Knozinger, H. *J. Mol. Catal. A: Chem*. **2003**, *204-205*, 519–526.

6. Stoyanova, M.; Rodemerck, U.; Bentrup, U.; Dingerdissen, U.; Linke, D.; Mayer, R.-W.; Lansink Rotgerink, H.G.J.; Tacke, T. *App. Catal. A: Gen*. **2008**, *340*, 242–249.

7. Vuurman, M. A.; Wachs, I. E. *J. Phys. Chem.* **1992**, *96*, 5008-5016.

8. Chauvin, Y.; Commereuc, D. *J. Chem. Soc., Chem. Comm.*, **1992**, *6*, 462–464.

9. Salameh, A.; Coperet, C.; Basset, J.; Bohm, V.P.W.; Roper, M. *Adv. Synth. Catal*. **2007**, *349*, 238–242.

10. Mahmood, C. S.; Yarmo, M. A.; Hamid, S. B.D. *J. Mol. Catal. A. Chem*. **2000**, *161*, 11–16.

11. Demeter. X-ray Absorption Spectroscopy Using Feff and Ifeffit. v 0.9.21. < http://bruceravel.github.io/demeter/> Accessed April 16, 2015.

12. Lwin, S.; Keturakis, C.J.; Handzlik, J.; Sautet, P.; Li, Y.; Frenkel, A.I.; Wachs, I.E. *ACS Catalysis*. **2015**, *5*, 1432– 1444.

13. Lwin, S.; Kryzstek, J.; Stiegman, A.; Wachs, I. E. Unpublished results.

14. Propene < http://webbook.nist.gov/cgi/cbook.cgi?ID=C115071&Units=CAL&Type=IR-SPEC#IR-SPEC> Accessed April 16, 2015.

15. Silverstein, M. “Spectrometric Identification of Organic Compounds”, Wiley 7th Edition, 2005.

16. Davydov, A. “Molecular Spectroscopy of Oxide Catalyst Surfaces”, Wiley 3rd Edition, 2003.

17. Ram, M.S.; Johnson, C.S.; Blackbourn, R.L.; Hupp, J.T. *Inorg. Chem.* **1990**, 29, 238–244.

18. Booysen, I. N. MS thesis. Nelson Mandela Metropolitan University. 2007.

Figures

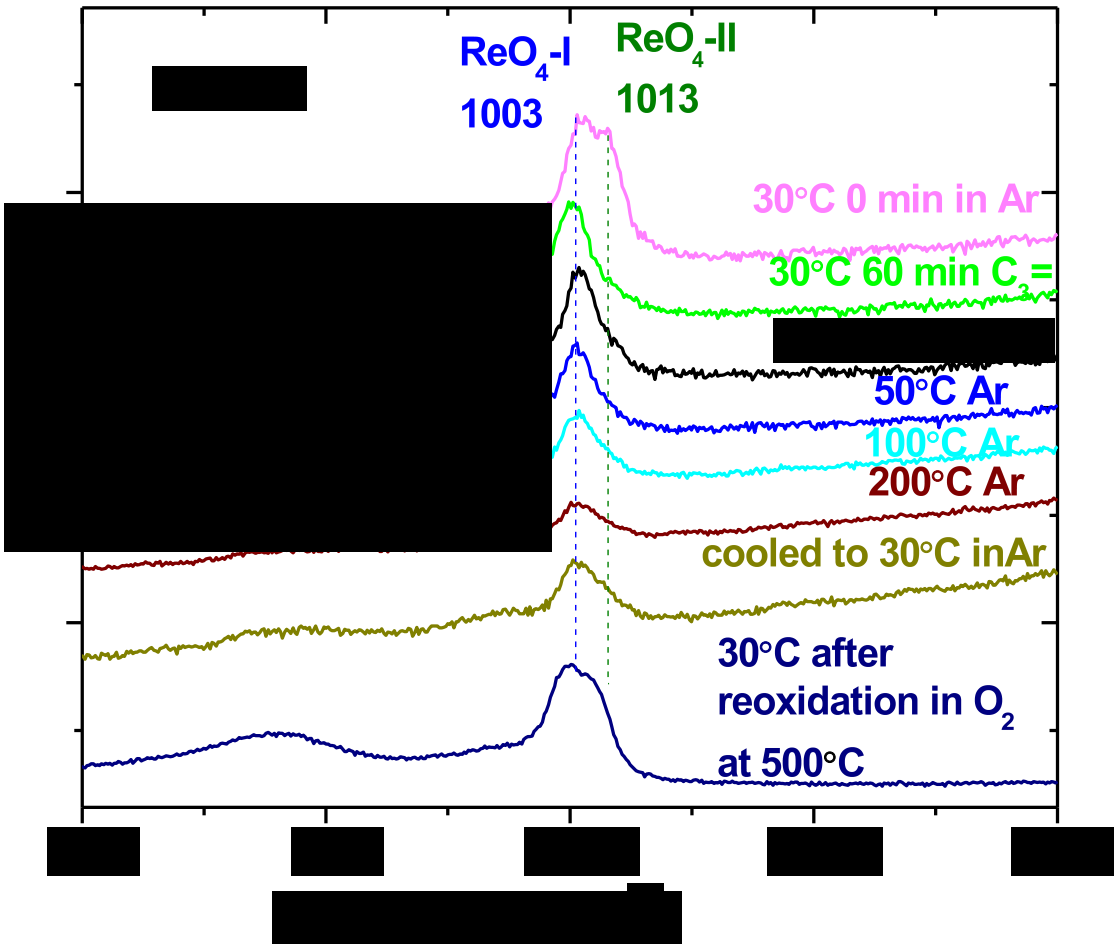

Figure 3.1. *In situ* Raman spectra of the 15.6ReAl catalyst before, during and after propylene adsorption/reaction/desorption. Spectra normalized using the 1013 cm^{-1} Raman band.

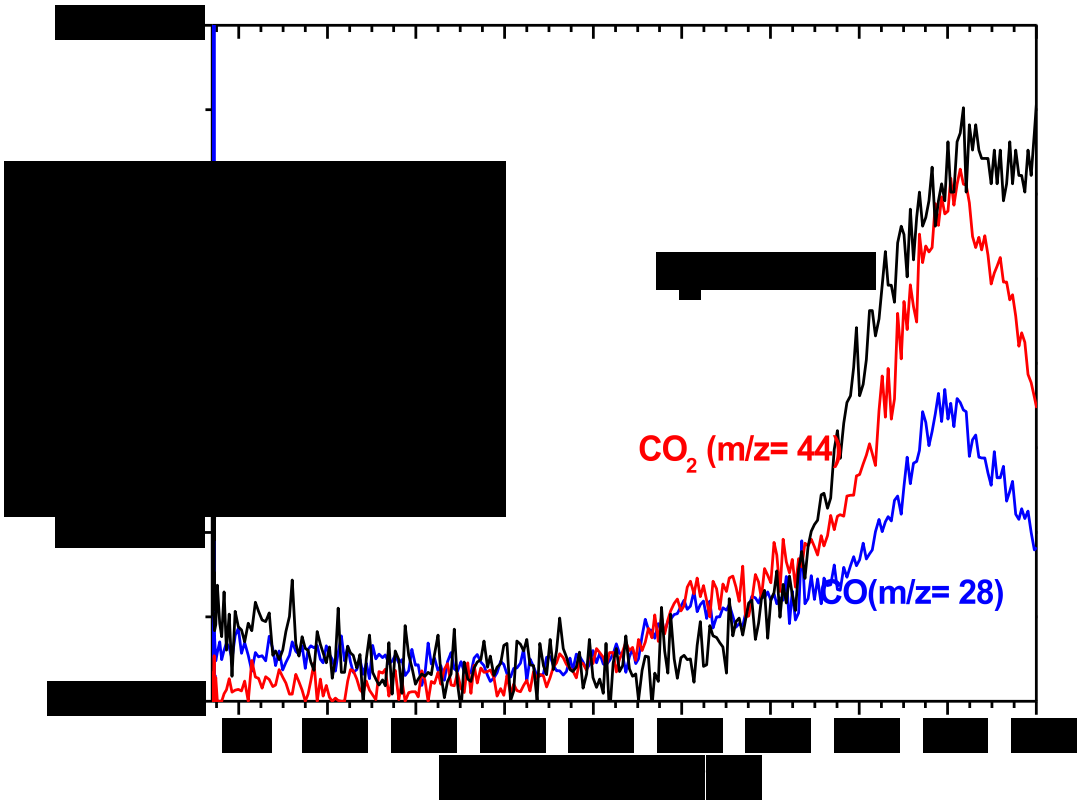

Figure 3.2. Combustion products during TPO (2% O_2/Ar) after $C_3^=$adsorption at 30°C for 60 minutes, flushing with Ar for minutes 60 minutes and desorption with Ar to 200°C.

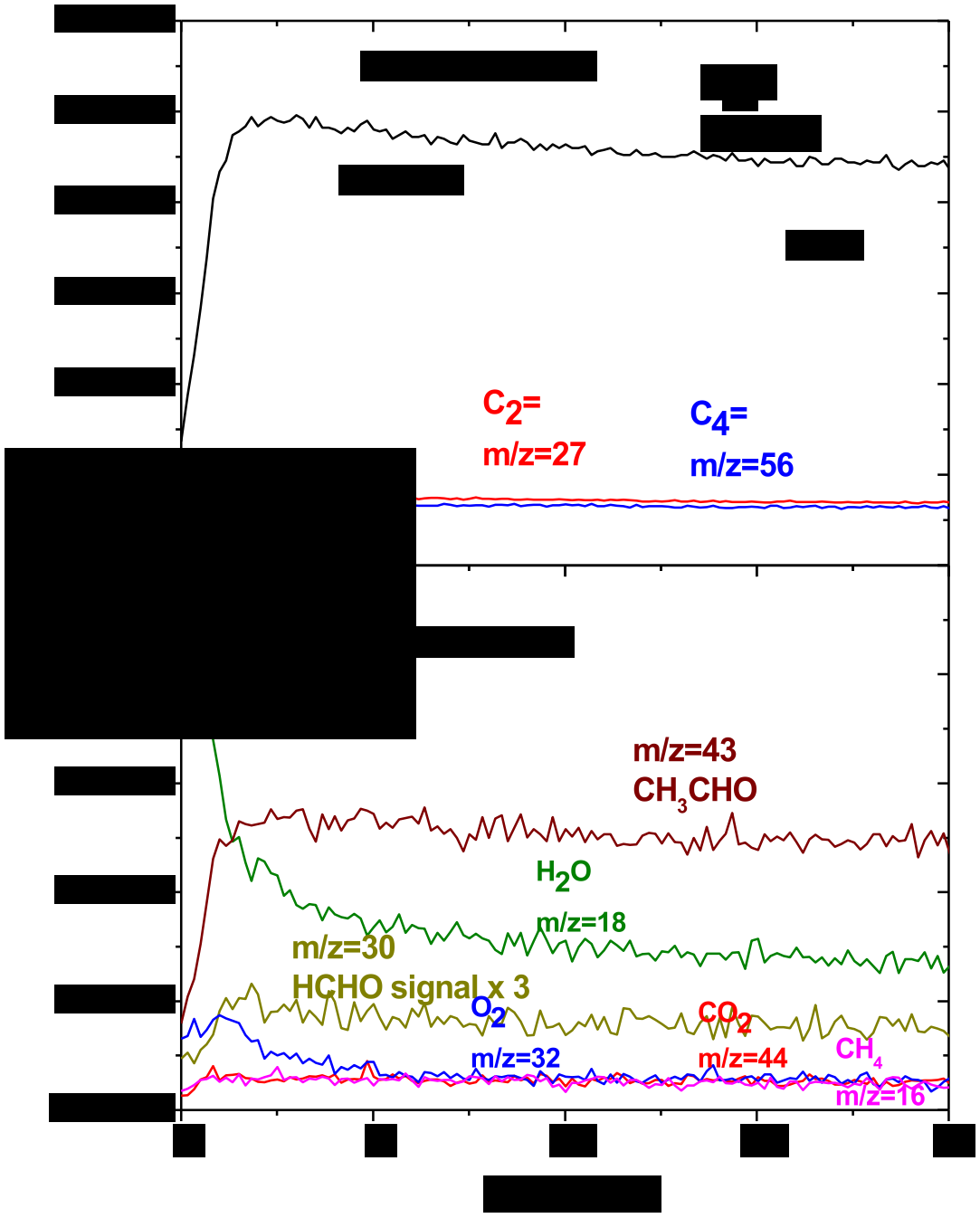

Figure 3.3. Time-resolved evolution of products during activation with $C_3^=$ at 30°C: main products (a) and oxygenated products (b)

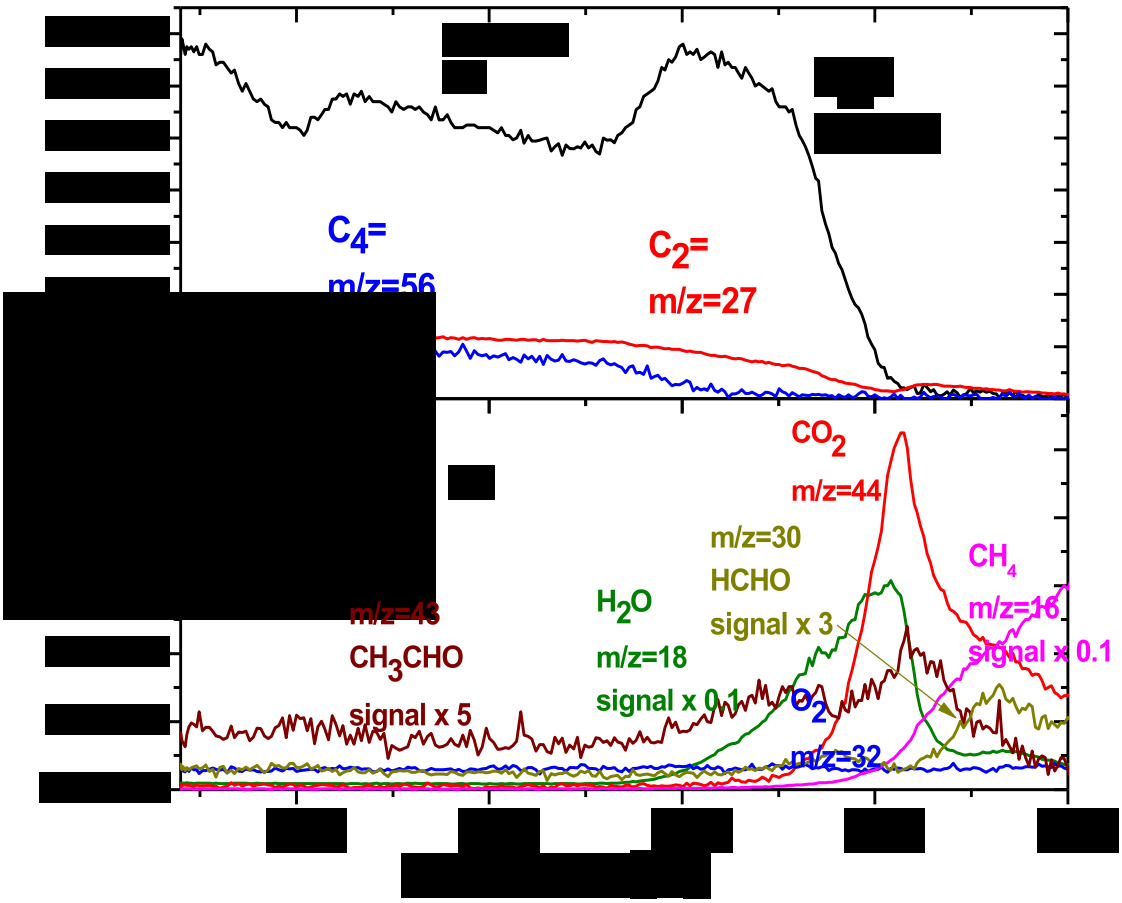

Figure 3.4. Profile of products during $C_3^{=}$/Ar-TPSR: main products (a) and oxygenated products (b).

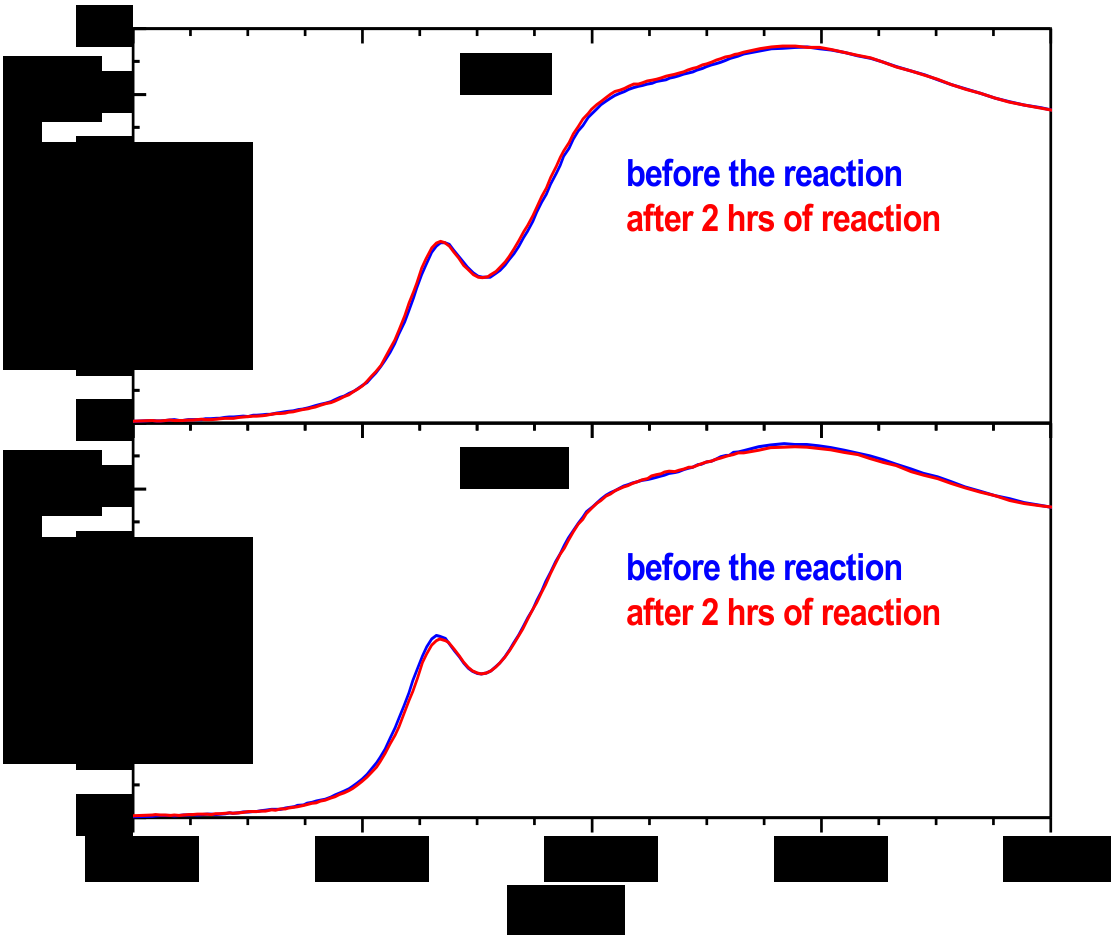

Figure 3.5. *In situ* Re L_1-edge XANES spectra of the 15.6ReAl catalyst before (blue) and during $C_3^=$ metathesis (red) at 70°C (top) and 150°C (bottom)

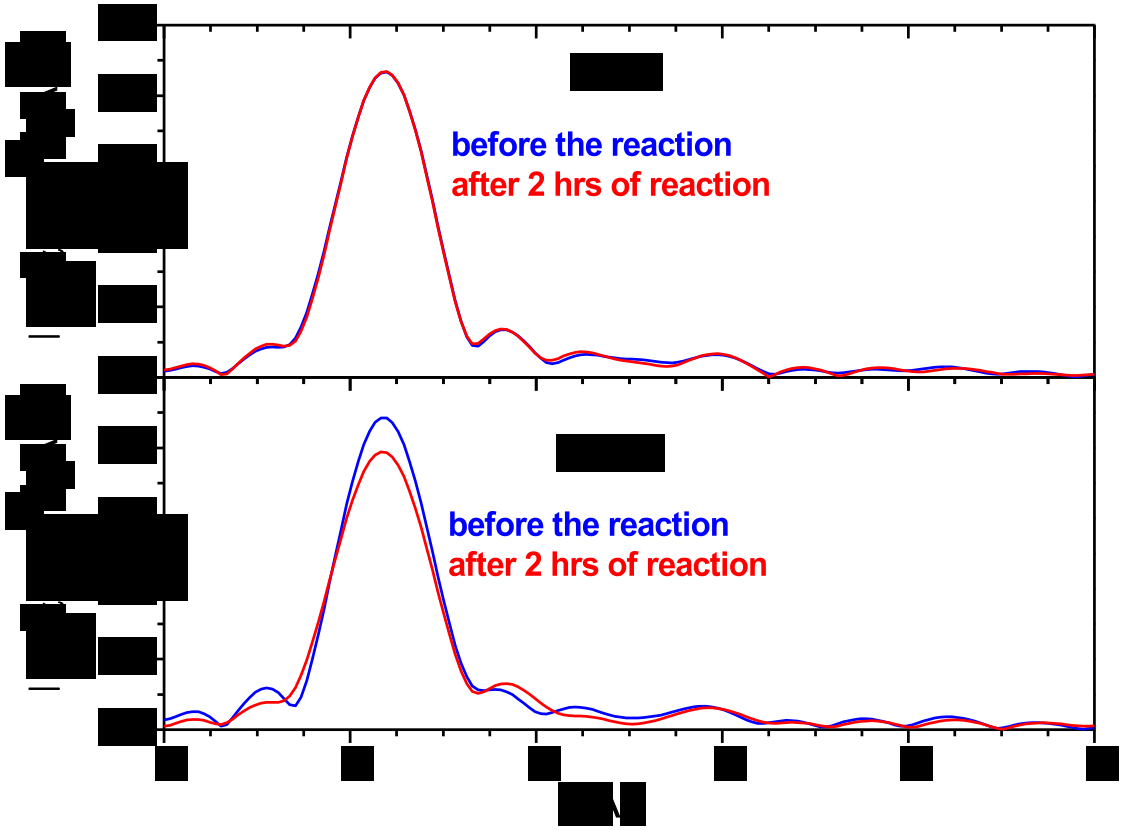

Figure 3.6. Magnitudes of Fourier-transformed k^2-weighted *in situ* Re L_1-edge EXAFS spectra in non-phase-corrected *R* space for the dehydrated supported 15.6 catalyst before (blue) and during reaction (red) at 70°C (top) and 150°C (bottom)

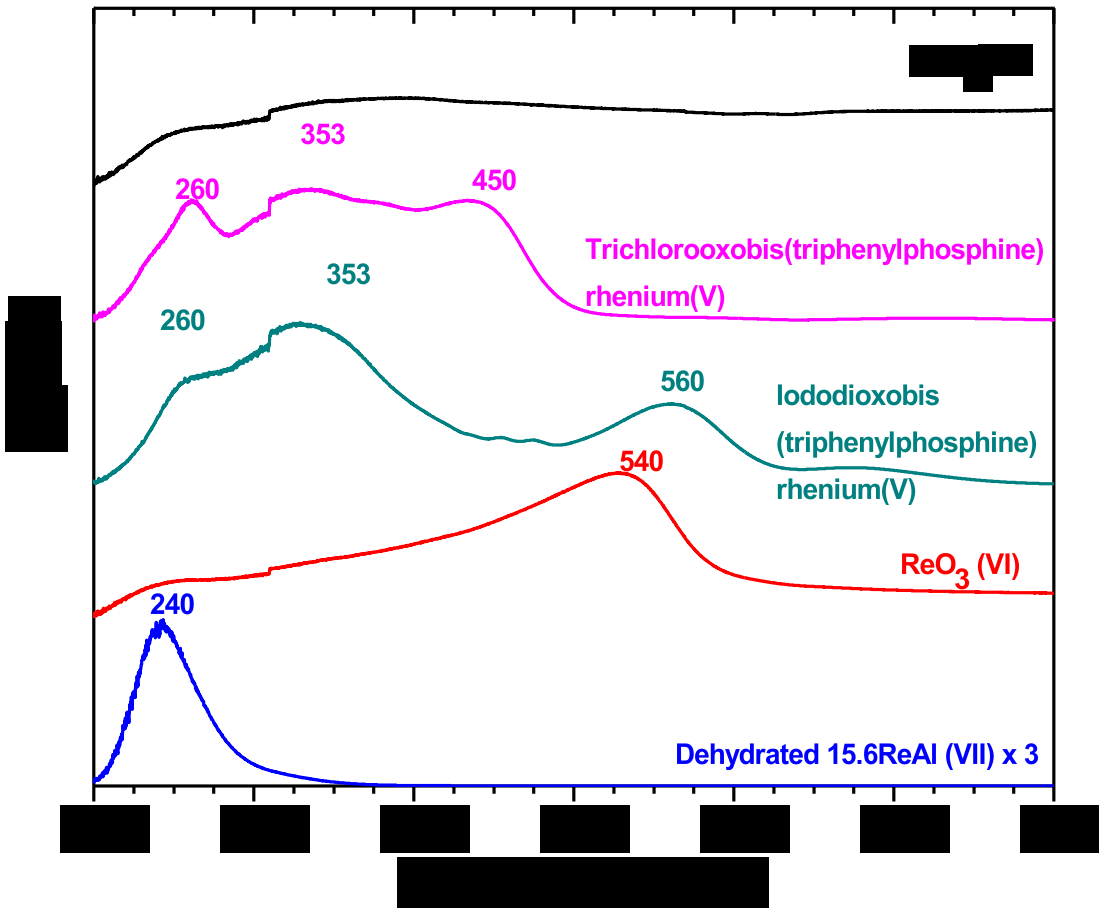

Figure 3.7. The UV-vis spectra of Re^{+4}, Re^{+5} and Re^{+6} reference compounds under ambient conditions and *in situ* spectrum of the dehydrated supported 15.6% ReO_x/Al_2O_3 catalyst. Signals adjusted so that they can be plotted on the same scale.

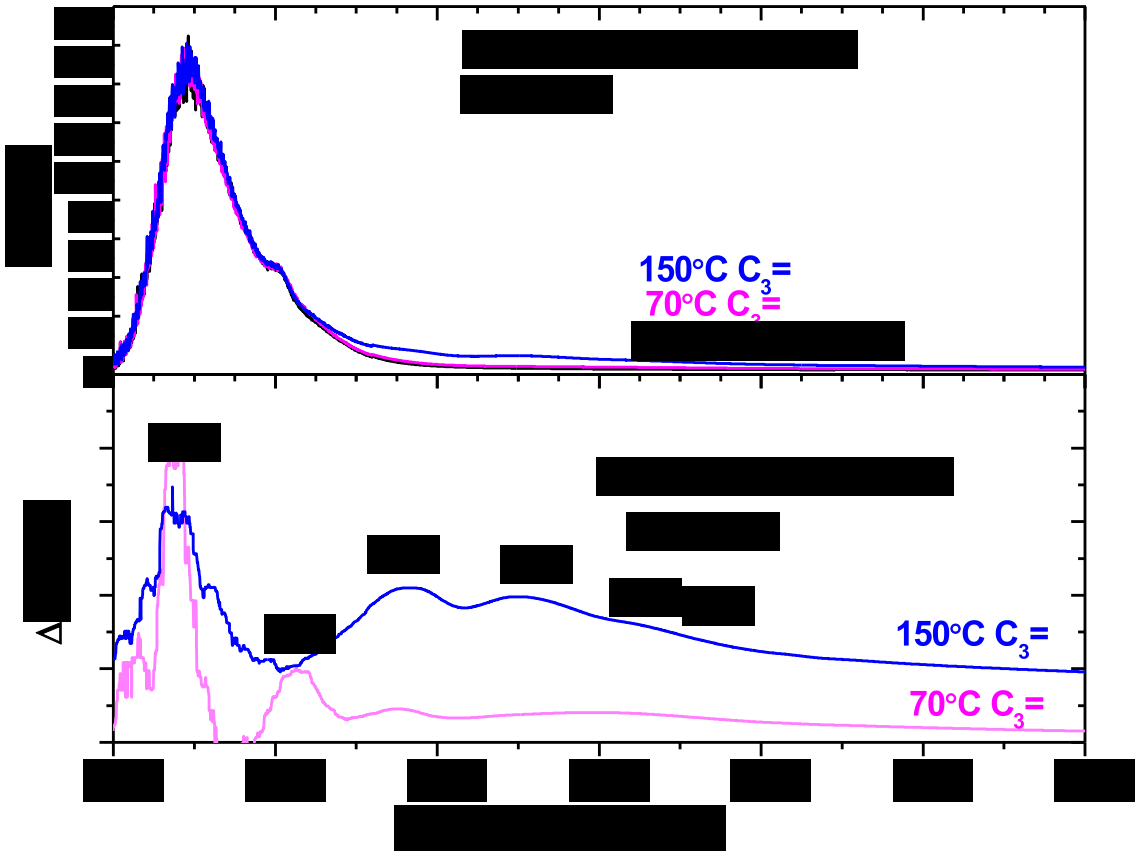

Figure 3.8. (a) *In situ* UV-vis spectra of the supported 15.6 ReAl catalyst before reaction in flowing He (70°C) and during $C_3^=$ metathesis at 70 and 150°C. (b) The UV-vis difference spectra obtained by subtraction of the spectrum in flowing He at 70°C prior to metathesis (bottom).

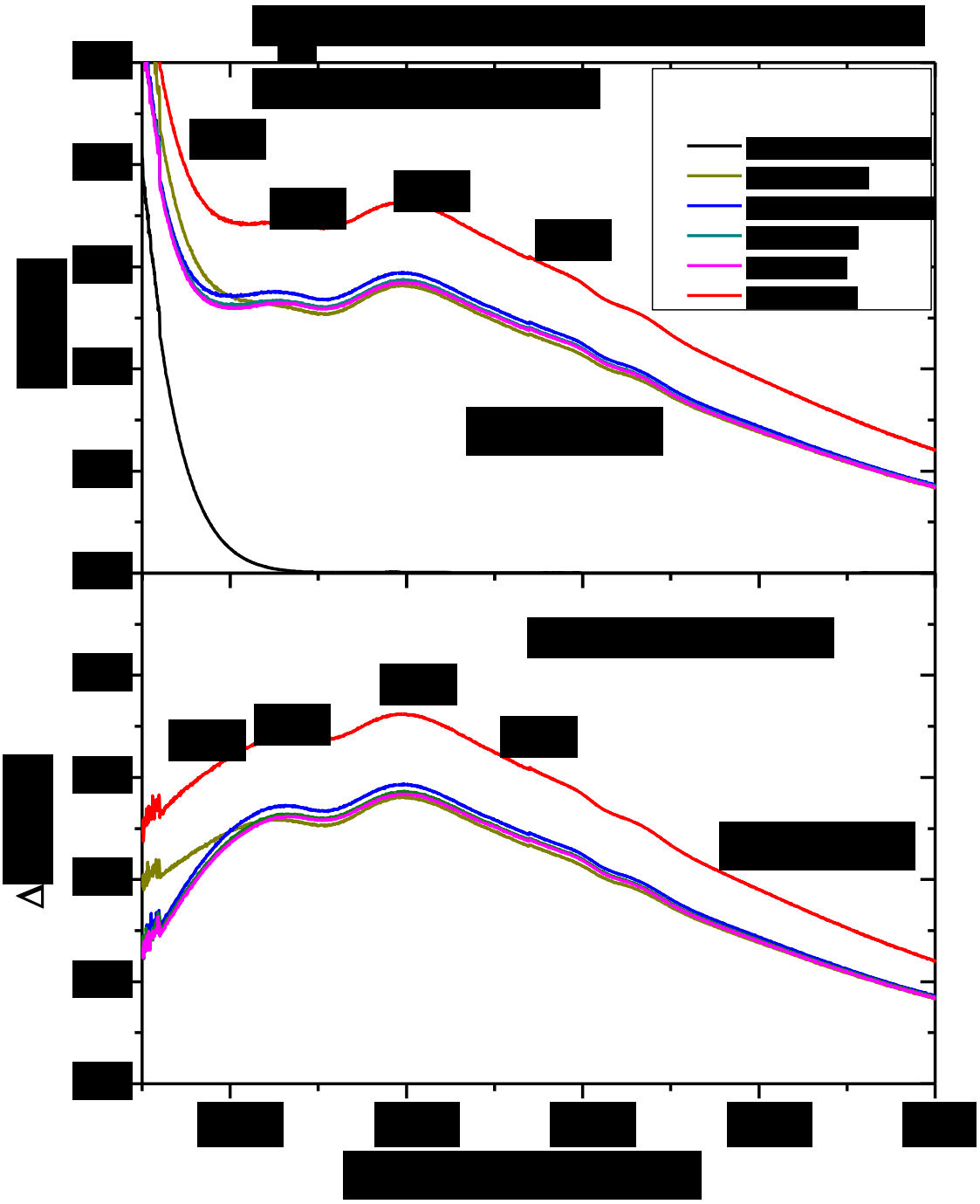

Figure 3.9. *In situ* UV-vis spectra of the supported 15.6 ReAl catalyst in the 350-800nm region during several adsorption/reaction/desorption cycles, (a) unsubtracted data and (b) subtracted data. The numbers in parentheses (0-5) indicate the order in which the experimental conditions were varied.

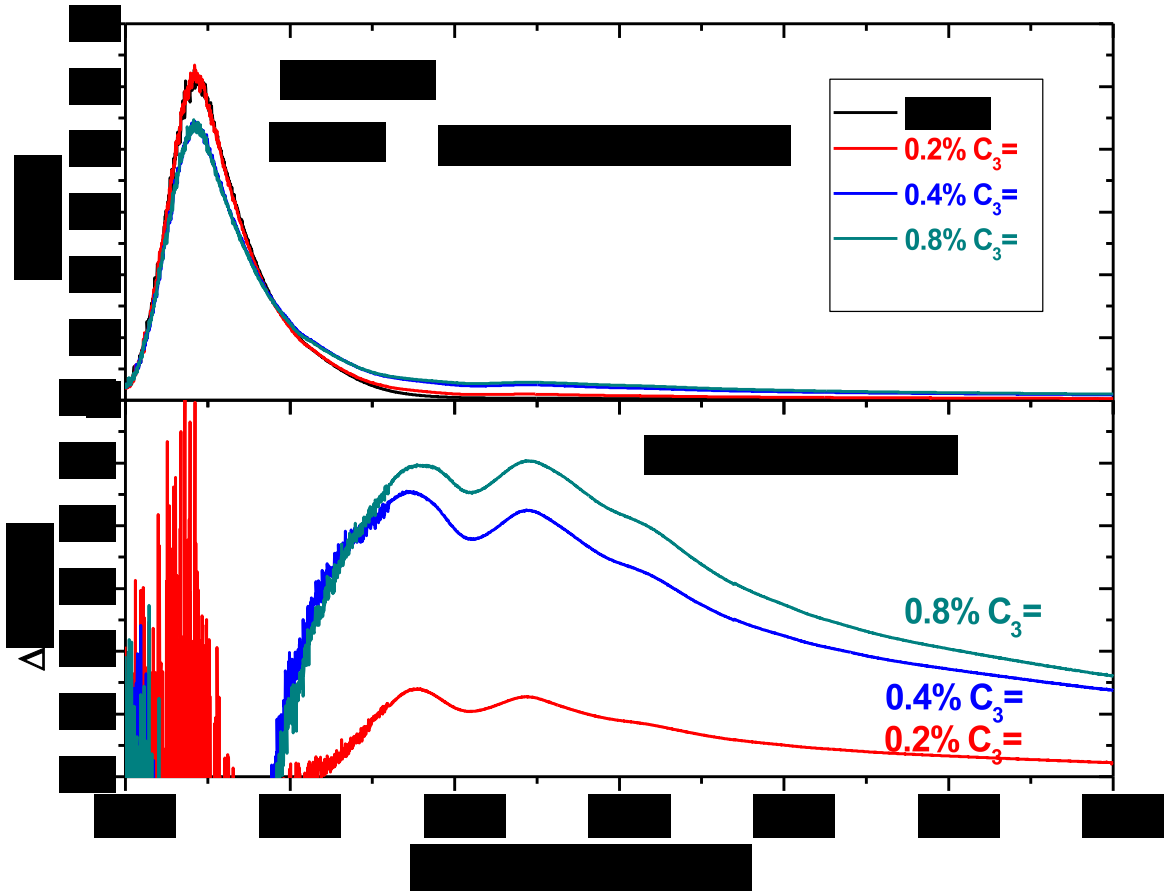

Figure 3.10. (a) *In situ* UV-vis spectra of the supported 15.6 ReAl catalyst at 150°C as a function of increasing propylene concentration. (b) The UV-vis difference spectra are obtained by subtraction of the spectrum in flowing He at 150°C prior to metathesis.

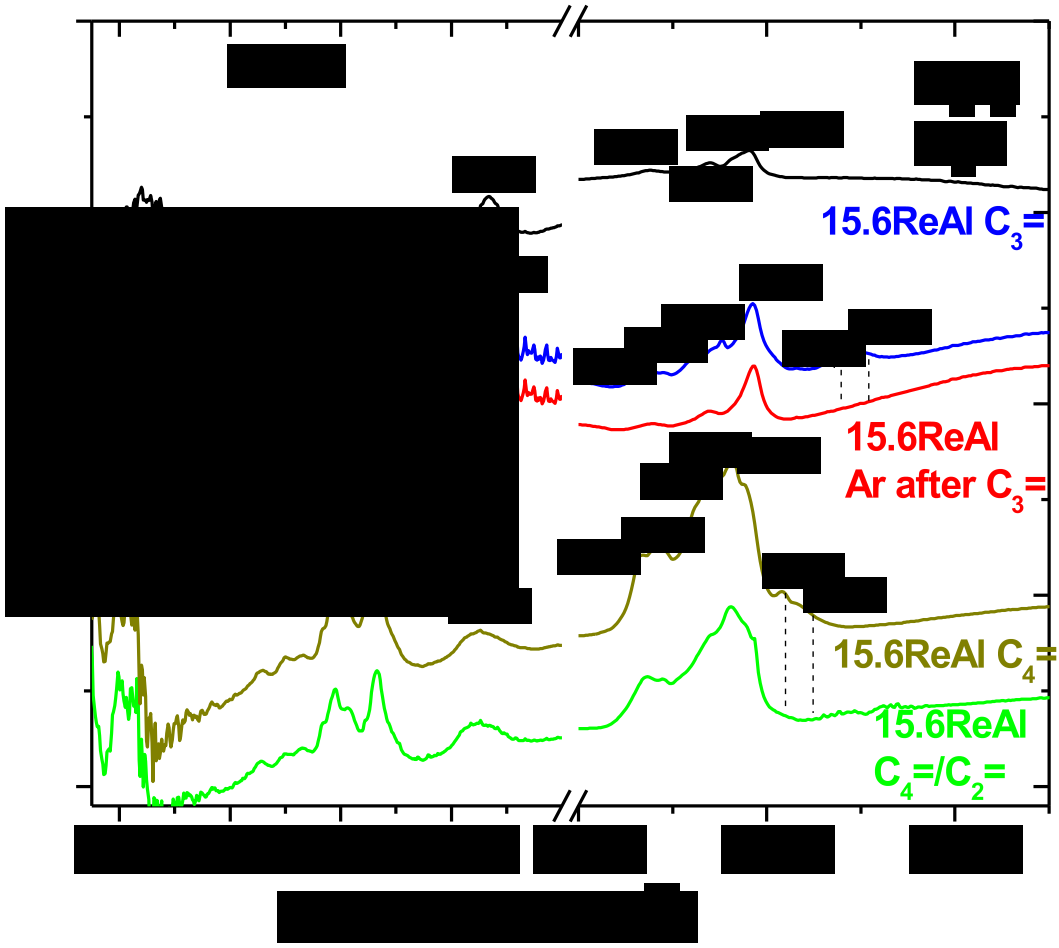

Figure 3.11. *In situ* difference IR spectra of the 15.6ReAl catalyst and pure Al_2O_3 support under various conditions at 25°C.

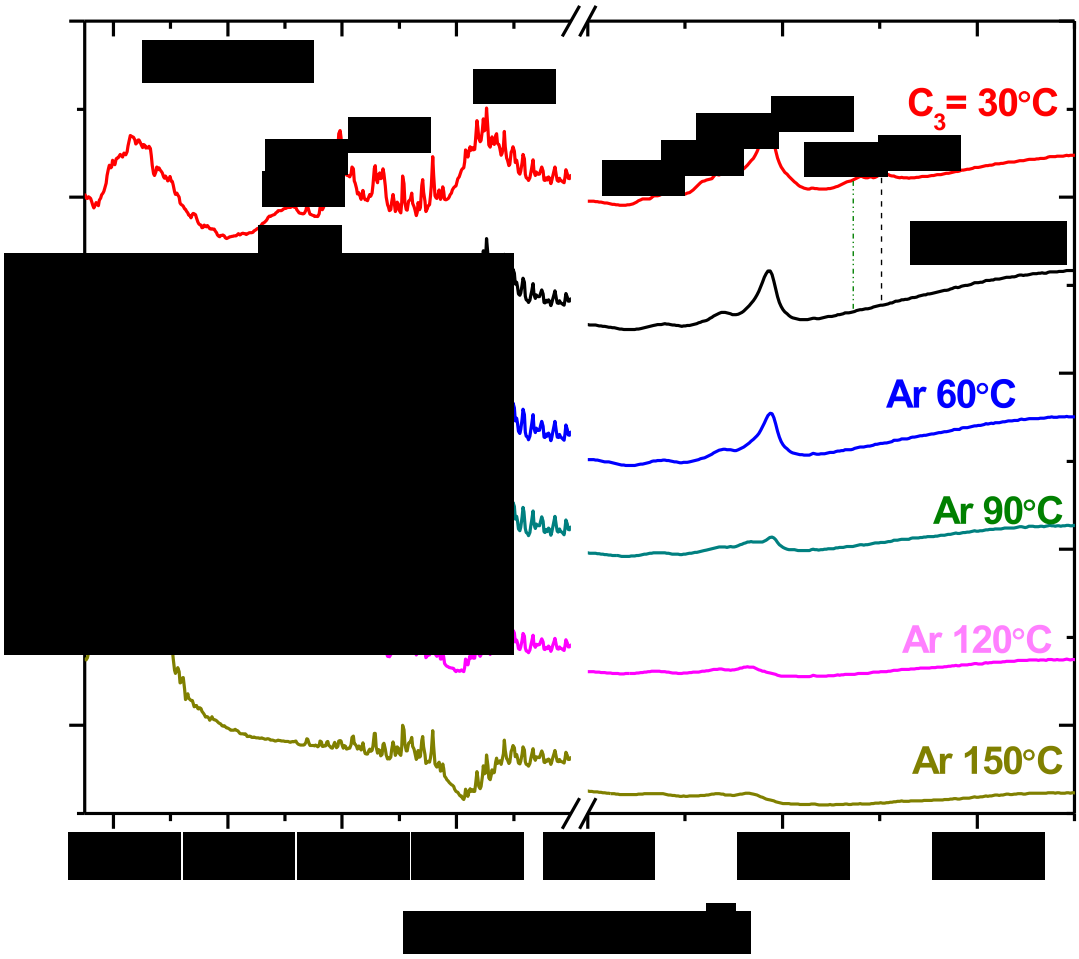

Figure 3.12. Temperature programmed *in situ* difference IR spectra of the 15.6ReAl catalyst in flowing Ar after $C_3^=$ adsorption at 30°C

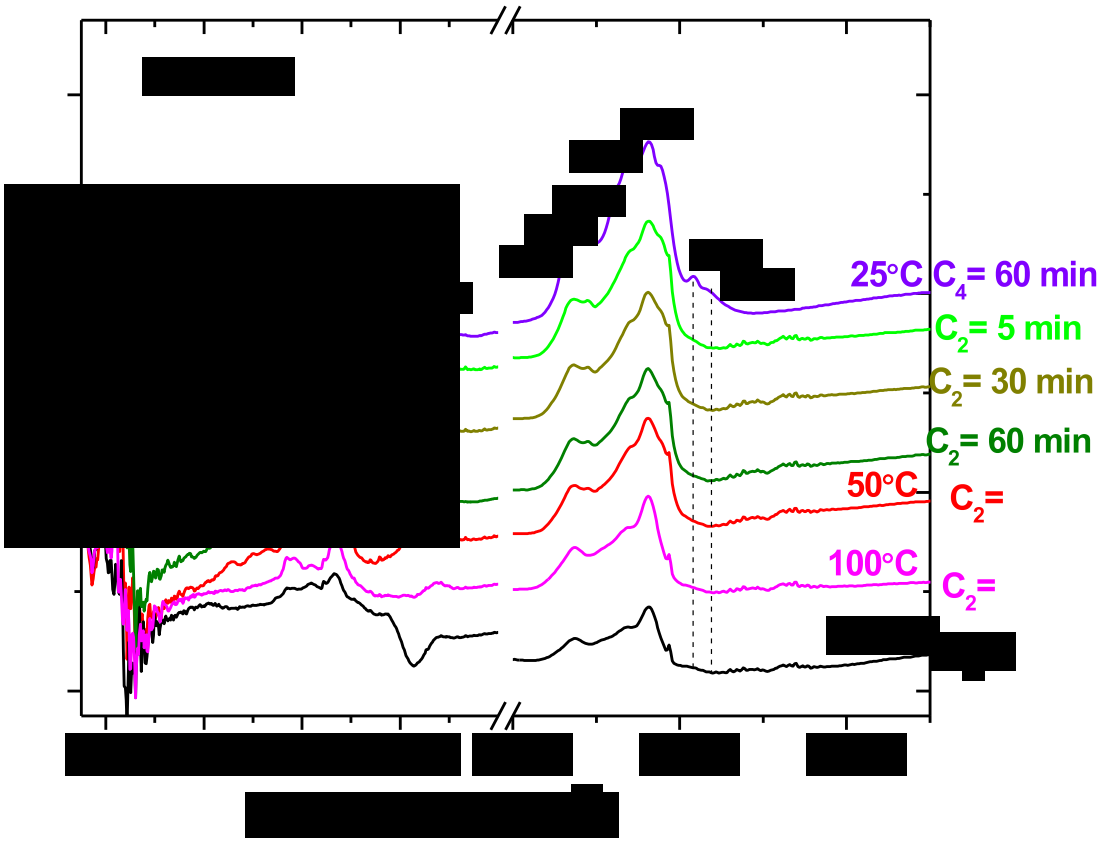

Figure 3.13. *In situ* difference IR spectra of the 15.6ReAl catalyst during $C_4^=$ adsorption and titration with $C_2^=$.

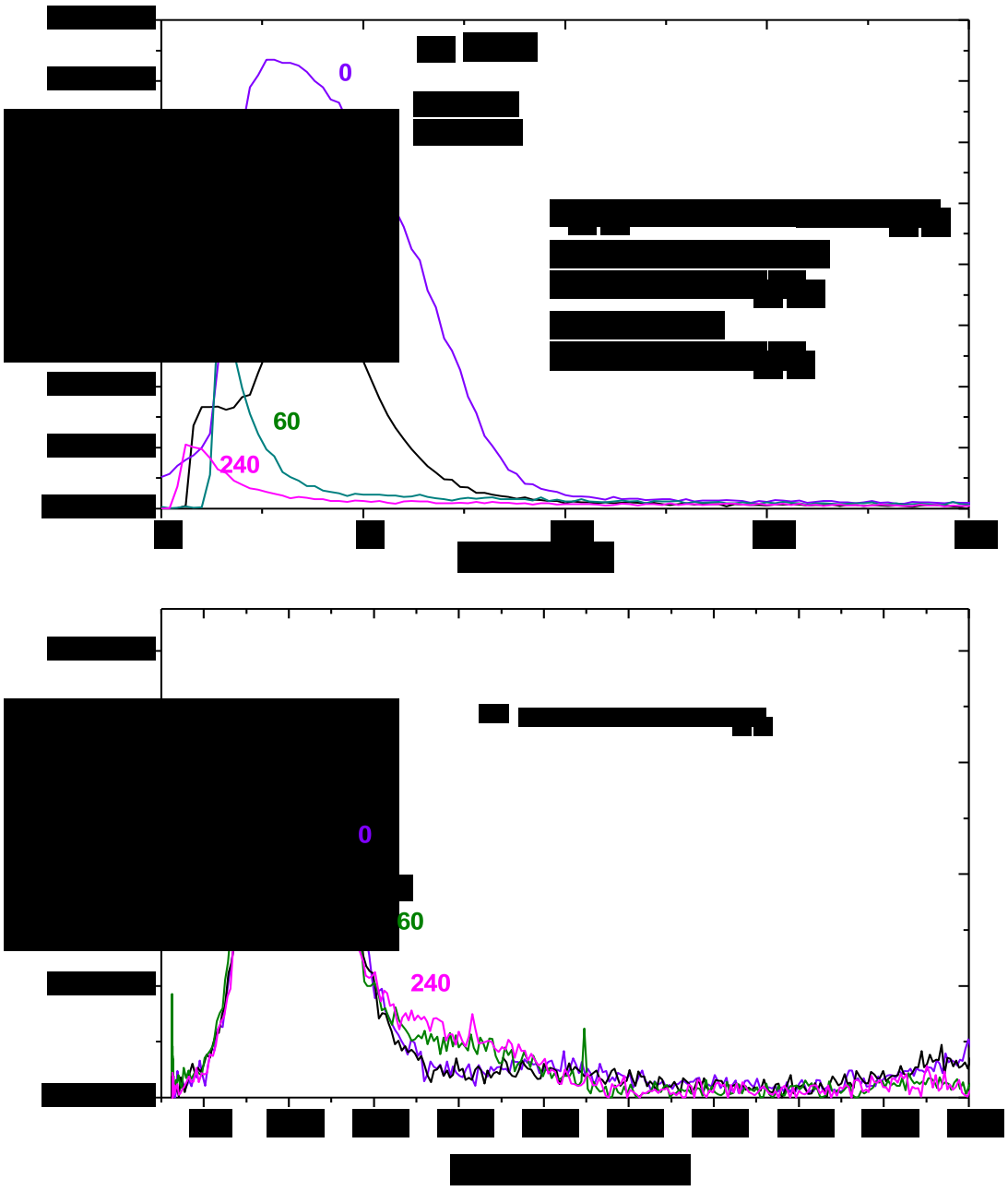

Figure 3.14. Production of $C_3^=$ from $C_2^=$ titration of surface intermediates resulting from $C_4^=$ adsorption (60 minutes at 30°C) as a function of Ar flushing time (0-240 minutes) between $C_4^=$ adsorption and $C_2^=$ titration, (a) as a function of time at 30°C (x-axis corresponds to the time of $C_2^=$ flow) and (b) during TPSR.

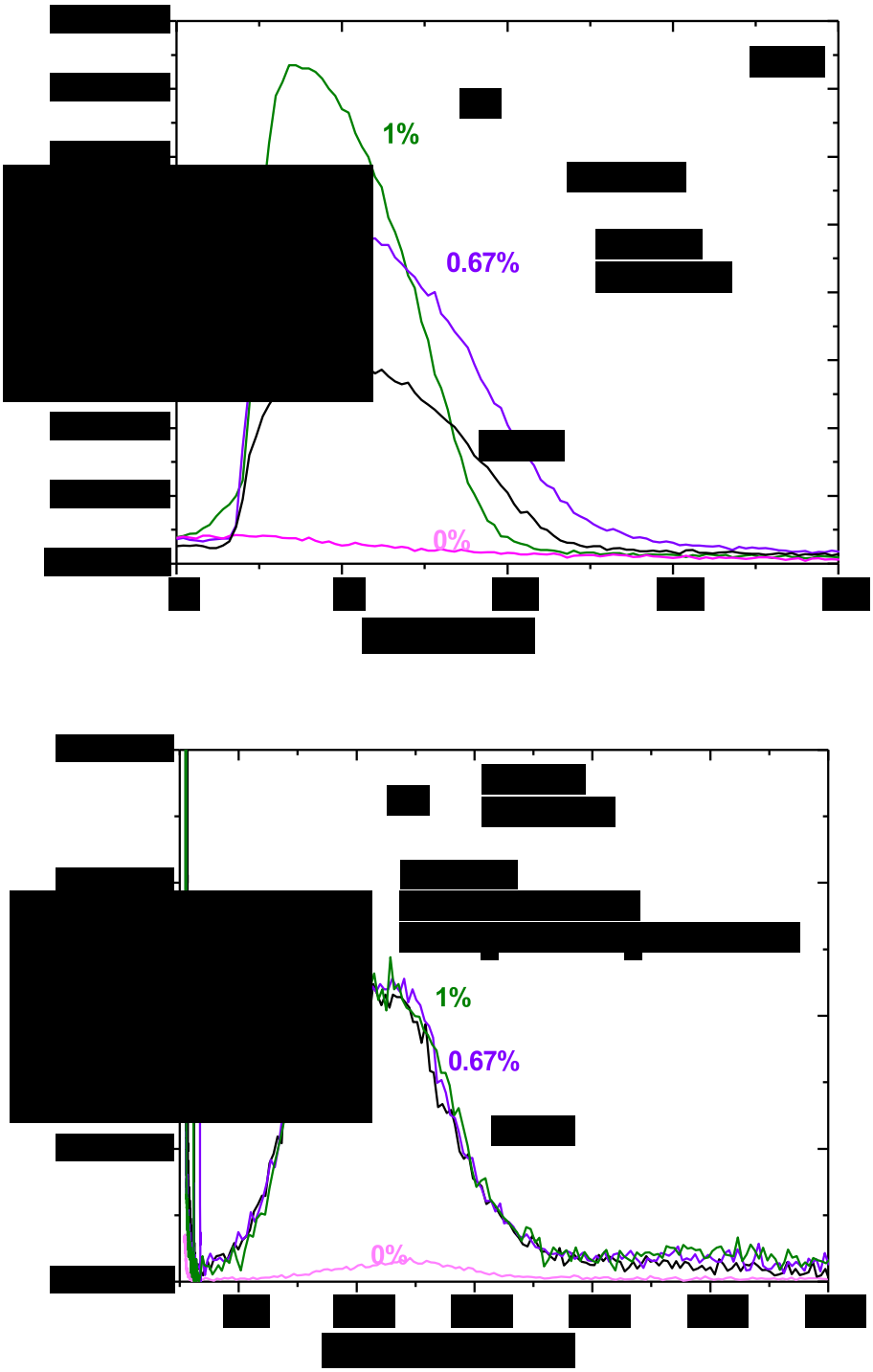

Figure 3.15. Production of $C_3^=$ from $C_2^=$ titration of surface intermediates resulting from $C_4^=$ adsorption (60 minutes at 30°C) as a function of $C_2^=$ partial pressure (a) as a function of time at 30°C (x-axis corresponds to the time of $C_2^=$ flow) and (b) during TPSR.

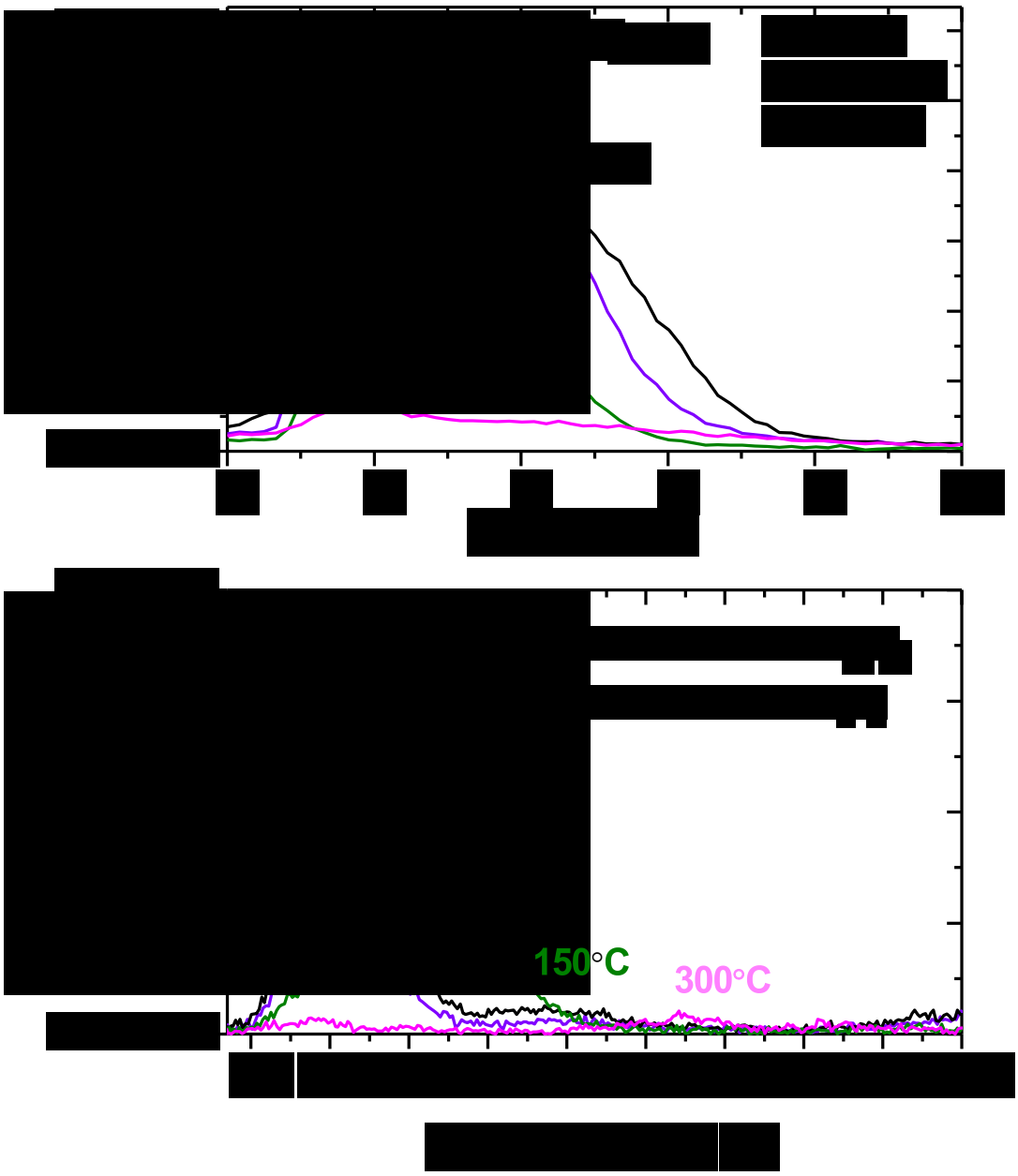

Figure 3.16. Evolution of $C_3^=$ during $C_2^=$ titration of surface intermediates resulting from $C_4^=$ adsorption (60 minutes at 30°C) as a function of $C_4^=$ activation temperature (30-300°C), (a) titration at 30°C (x-axis corresponds to the time of $C_2^=$ flow) and (b) titration during TPSR.

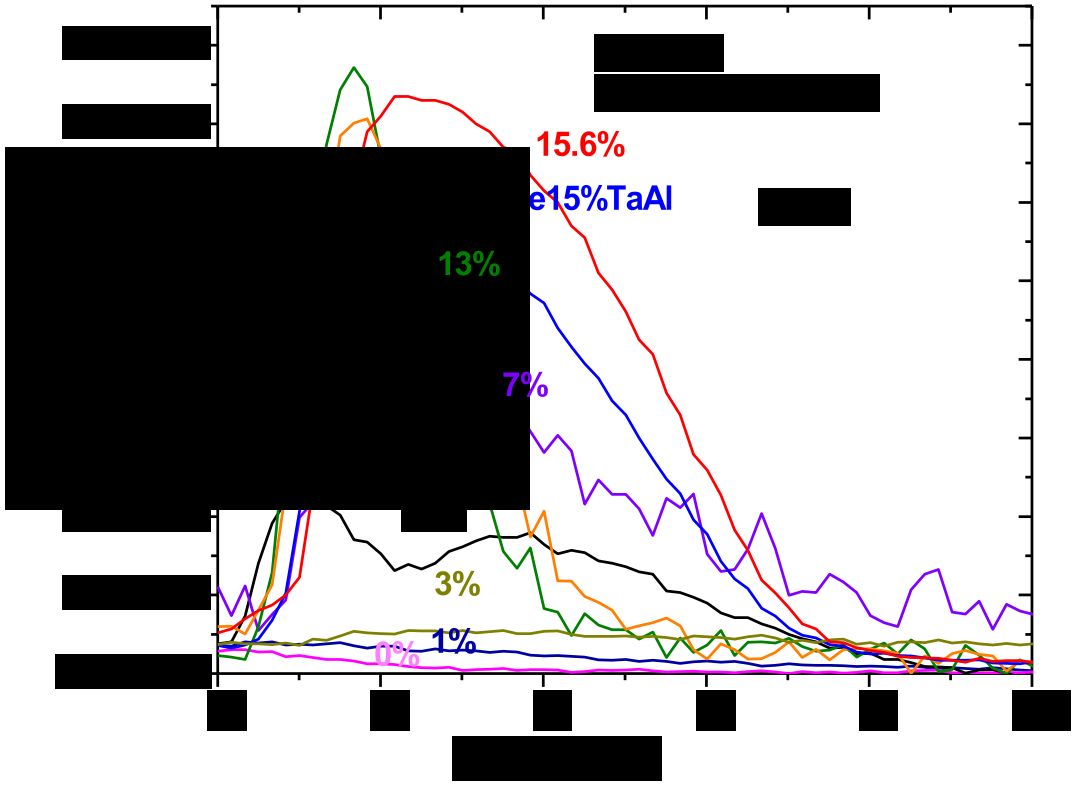

Figure 3.17. Evolution of $C_3^=$ during $C_2^=$ titration of surface intermediates resulting from $C_4^=$ adsorption (60 minutes at 30°C) as a function of ReO_x loading. The x-axis corresponds to the time of $C_2^=$ flow at 30°C.

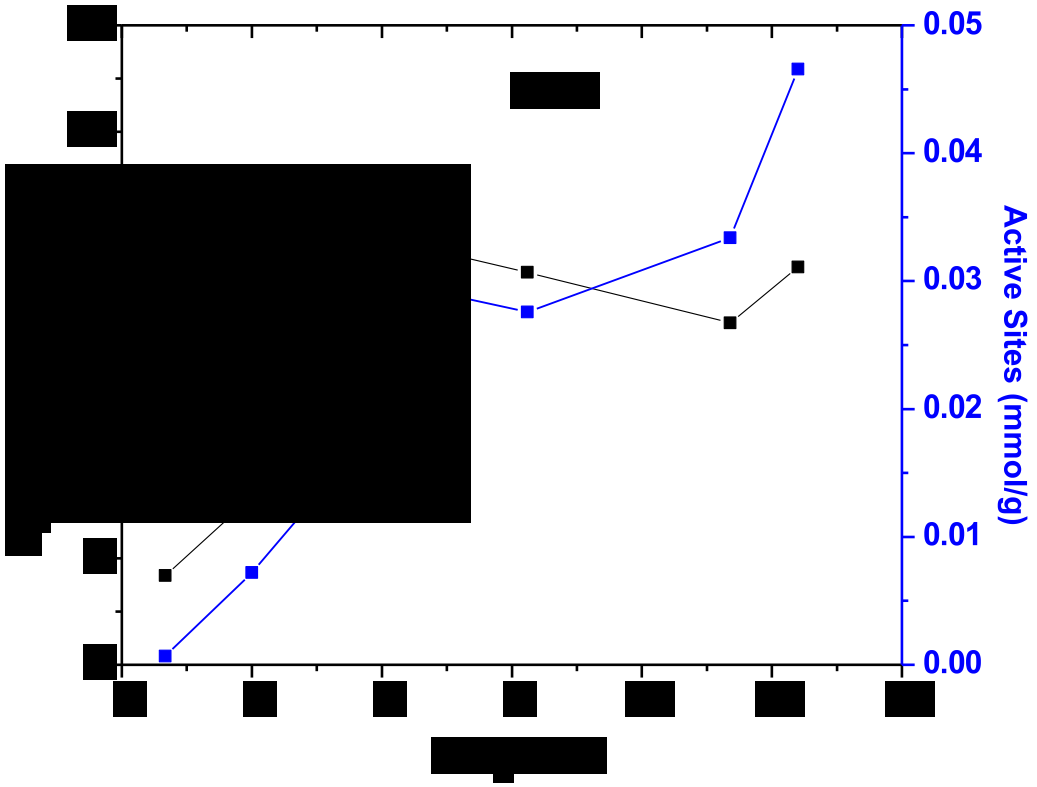

Figure 3.18. Number of $C_3^=$ molecules produced from titration of surface intermediates created by $C_4^=$ adsorption with $C_2^=$ as a function of ReO_4 loading on Al_2O_3. The y-axis is normalized by taking the number of $C_3^=$ molecules produced and dividing by the total number of ReO_4 sites to yield a percentage.

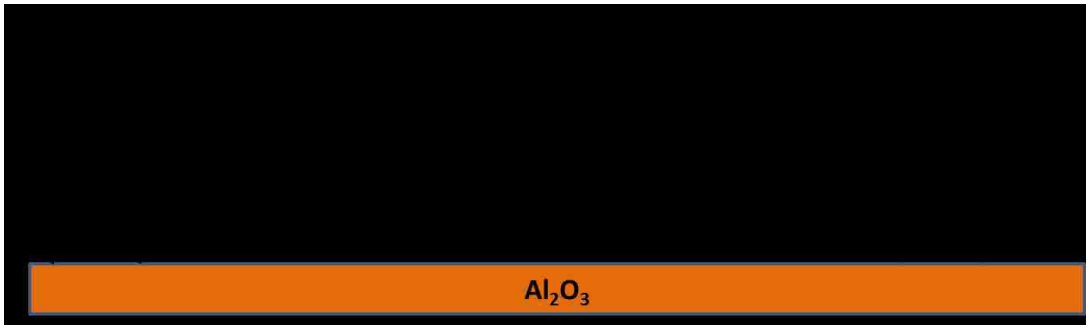

Scheme 3.1. Initial Formation of Active Re Alkylidene Species

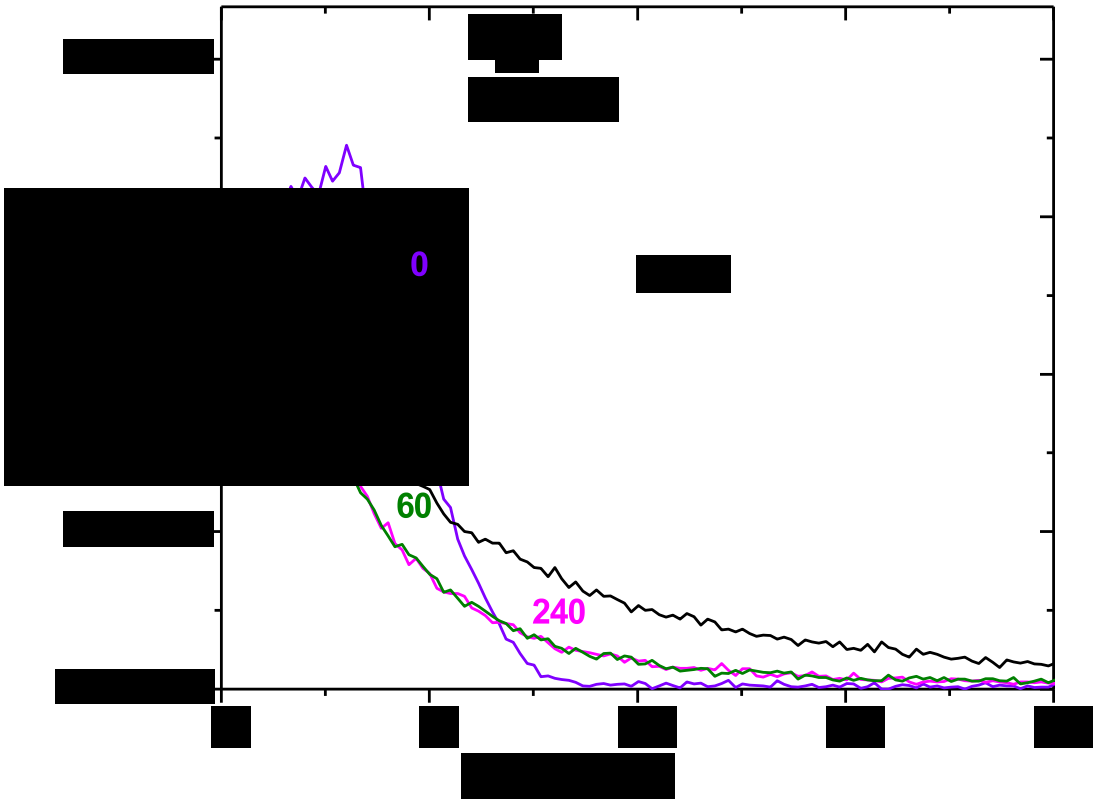

Figure S3.1. C_4= desorption profile during 0-240 minutes of Ar flush after its adsorption for 60 minutes. In the 0 minute experiment, 1%C_2=/Ar was flown immediately.

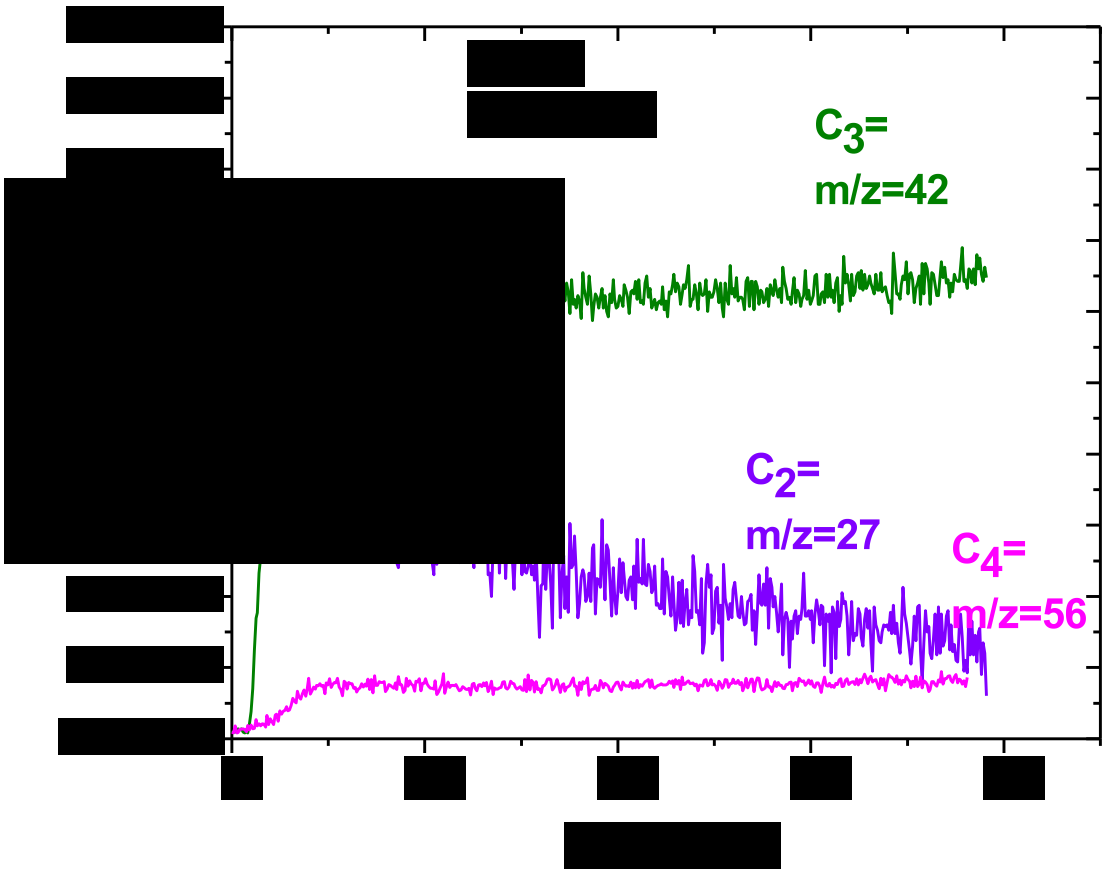

Figure S3.2. Time resolved evolution of products during metathesis of 1% $C_2^=$/Ar and 1% $C_4^=$/Ar to $C_3^=$ from the supported 15.6ReAl catalyst at 30°C.

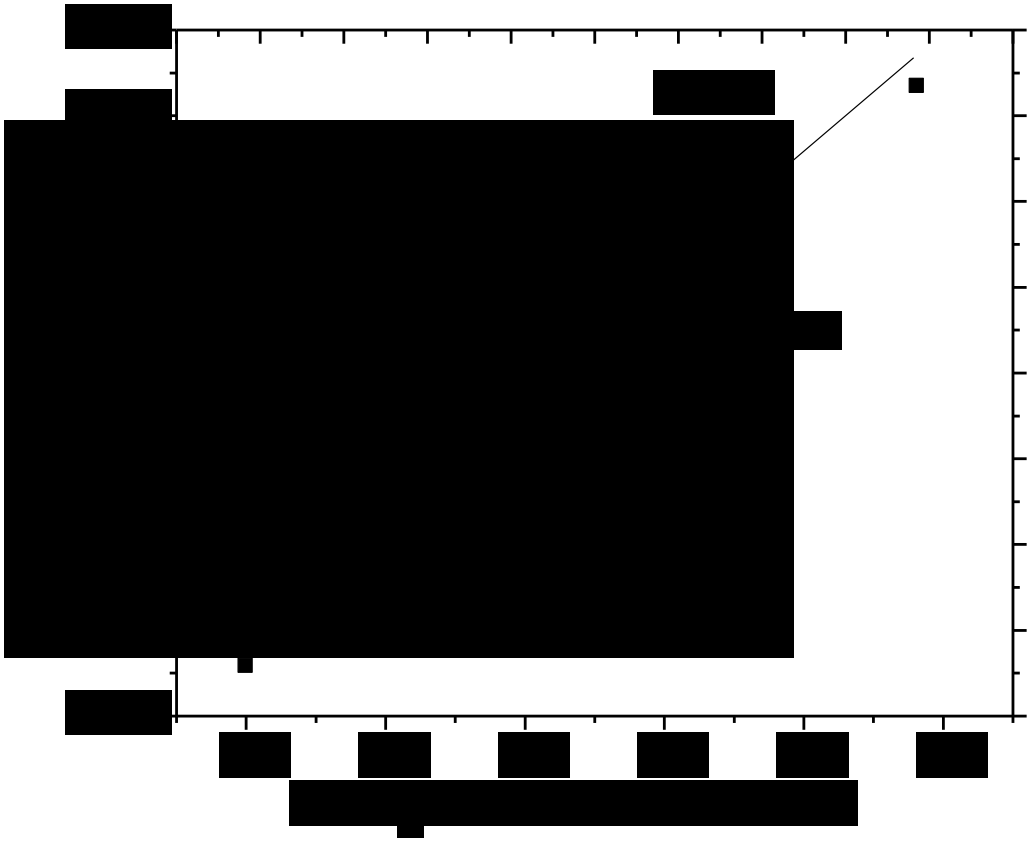

Figure S3.3. The effect of C_2= partial pressure on the number of sites (C_3= produced) after adsorption of C_4= at 30°C.

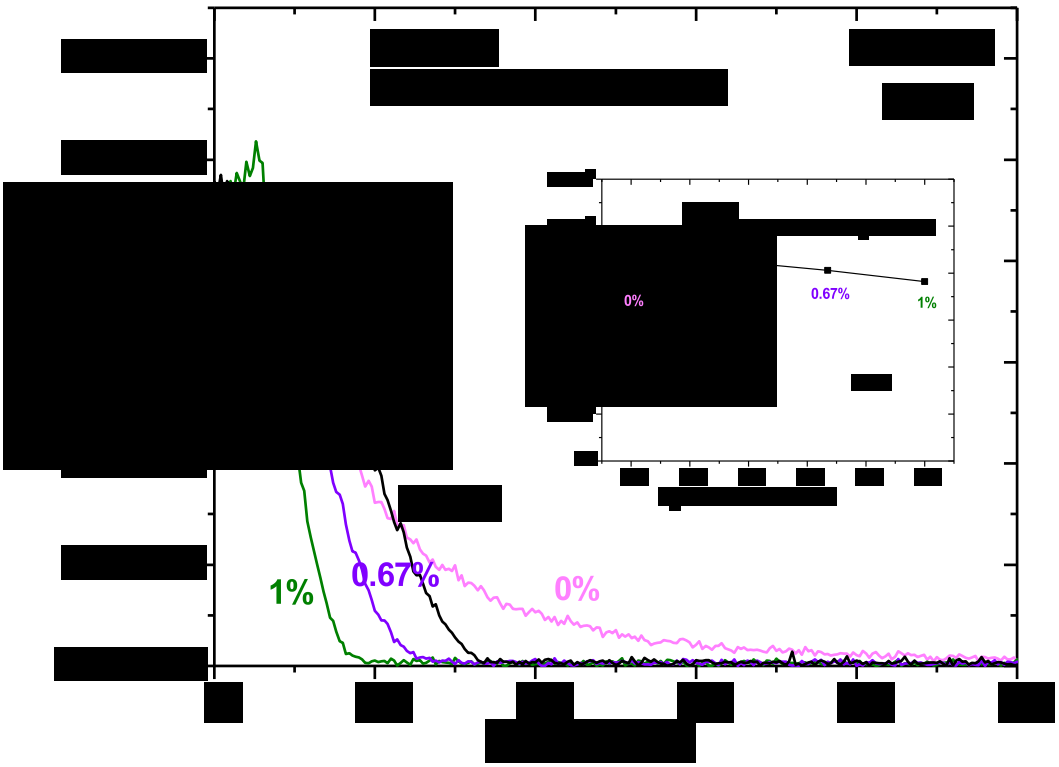

Figure S3.4. Evolution of $C_4^=$ during $C_2^=$ titration of surface intermediates resulting from $C_4^=$ adsorption (60 minutes at 30°C) as a function of $C_2^=$ partial pressure without Ar purge. The x-axis corresponds to the time of $C_2^=$ flow. Inset shows the integrated values for $C_4^=$ desorption.

CHAPTER 4

Mechanism and Kinetics of Olefin Metathesis by Supported ReO_x/Al_2O_3 Catalysts

Abstract

The adsorption, surface intermediates, reaction mechanism and kinetics of propylene metathesis by heterogeneous supported ReO_x/Al_2O_3 catalysts were investigated with *in situ* Raman spectroscopy, olefin titration, deuterium labeled olefins, temperature programmed surface reaction (TPSR) spectroscopy and steady-state reaction studies. The *in situ* Raman studies showed that the amount of adsorbed olefin increased with increasing olefin length ($C_2^= < C_3^= < C_4^=$). Olefin titration with the aid of isotopic deuterium labeled olefins demonstrated that surface $Re{=}CH_3$, $Re{=}CHCH_3$ and olefin π-complexes are present on the supported ReO_x/Al_2O_3 catalysts. The TPSR and steady-state experiments indicate for *the first time* that two olefin metathesis reaction pathways are present: unimolecular decomposition of surface metallacyclobutane complexes (1^{st}-order kinetics) at low temperatures (30-70^oC) and bimolecular reaction between two surface olefin π-complexes (2^{nd}- order) at elevated temperatures (> 70^oC). At intermediate temperatures, both reaction pathways are taking place and give rise to intermediate reaction orders between 1 and 2 in olefin partial pressure.

1. Introduction

Olefin metathesis has been a sustainable reaction to produce important chemicals for the past 50 years.[1] Supported ReO_x/Al_2O_3 catalysts for olefin metathesis were originally discovered by the British Petroleum (BP) in 1964.[2] The high reactivity and

selectivity of supported ReO_x/Al_2O_3 catalysts at ambient conditions allows performing metathesis of functionalized olefins, which is assisted by promoters.[3] The high price and volatility of rhenium limits the use of ReO_x catalysts only to production of fine chemicals,[3] but recent patent activity indicates a resurgence of interest in this system due to shortage of both linear and functionalized olefins.[4]

Although olefin metathesis by supported ReO_x/Al_2O_3 catalysts has been investigated over the years, conflicting reports still exist about the reaction mechanism and kinetics of this catalytic reaction. Supported ReO_x/Al_2O_3 catalysts can be activated upon exposure to propylene and 2-butene, but activation by ethylene is a slow process or even not possible.[5-7] Aldag *et al.*, however, concluded from C_2H_4/C_2D_4 studies that ethylene can initiate metathesis by supported ReO_x/Al_2O_3 catalysts at slightly higher temperatures.[8] The metathesis reaction was proposed to involve mobile adsorbates resulting in second-order kinetics with respect to the adsorbate concentration.[8] Spinicci *et al.* concluded that desorption of propylene from supported ReO_x/Al_2O_3 catalysts follows second-order kinetics with thermal-programmed desorption (TPD) studies.[9] Some kinetic studies suggested olefin metathesis proceeds via the Langmuir-Hinshelwood (L-H) kinetic model,[8,10,11] but Kapteijn *et al.* considered the L-H model inadequate and developed a first order-kinetic model based on intermediate alkylidene species ($Re=CH_2$ and $Re=CHCH_3$) with the product desorption being the rate-determining-step.[12] This mechanism is more in line with Chauvin's famous metallacyclobutane mechanism which was proposed for homogeneous and supported organometallic catalysts.[13]

The lack of agreement among researchers about the kinetics of olefin metathesis by supported ReO_x/Al_2O_3 catalysts is due to use of different catalysts (variable BET

surface areas and rhenia loadings) and reaction conditions (olefin partial pressures, and reaction temperatures) in the different studies. The motivation of this study is to resolve these issues by systematically applying *in situ* Raman spectroscopy, temperature programmed surface reaction (TPSR) spectroscopy and steady-state kinetics studies under various conditions to develop a comprehensive model of olefin metathesis by supported ReO_x/Al_2O_3 catalysts.

2. Experimental

2.1. Catalyst synthesis

The supported ReO_x/Al_2O_3 catalysts were prepared by impregnation of 65-70 wt% aqueous solution of perrhenic acid, $HReO_4$ (Sigma Aldrich) onto the Al_2O_3 support (Engelhard batch#H5433C). The full procedure of incipient-wetness impregnation, drying and calcination can be found in the previous chapter.

2.2. *In situ* Raman Spectroscopy

The Raman spectra the supported ReO_x/Al_2O_3 catalysts were obtained with a Horiba-Jobin Ybon LabRam HR instrument equipped with three laser excitations (532, 442 and 325 nm) and a liquid N_2-cooled CCD detector (Horiba-Jobin Yvon CCD-3000V). The 442 nm laser was chosen since it minimized sample fluorescence. Spectral resolution was approximately 1 cm^{-1} and the wavenumber calibration was checked using the silica standard line at 520.7 cm^{-1}. The lasers were focused on the samples with a confocal microscope using a 50X objective (Olympus BX-30-LWD). Typically, the spectra were collected at 30 s/scan and 5 scans with a 200 μm hole. Approximately 5-25 mg of each

catalyst in powder form was loaded into an environmental cell (Harrick, HVC-DR2) with a SiO_2 window and O-ring seals which was kept cool by flowing water. The catalysts were initially dehydrated at a heating rate of 10°C/min up to 500°C and held for an hour under a 30 mL/min flow of 10% O_2/Ar (Airgas, certified, 9.989% O_2/Ar balance). After cooling in Ar to 30°C, a spectrum was taken before 1% C_2= (ethylene), 1%C_3= (propylene) or 1%C_4= (trans-2-butene) in argon or helium (balance) was introduced (three separate experiments). After 60 minutes of each olefin flow at 30°C, another spectrum was taken.

2.3. Temperature Programmed Surface Reaction (TPSR) Spectroscopy

The temperature programmed surface reaction experiments were performed using an Altamira Instruments system (AMI-200). The outlet gases were connected to an online Dymaxicon Dycor mass spectrometer (DME200MS) for analysis. Typically ~ 100-200 mg of catalysts were loaded into the U-tube reactor. The cracking patterns were carefully adjusted with blank gas runs. The 15.6%ReO_x/Al_2O_3 (15.6ReAl) catalyst was used for the following experiments. As in other experiments, the catalysts were pre-treated with 10% O_2/Ar at 500°C for 30 minutes. They were then cooled down in Ar to the conditions of interest discussed below.

2.3.1. C_4H_8/C_2H_4 and C_2H_4/C_4H_8 TPSR Experiments

The catalyst was exposed to 1% C_4H_8 (2-butene)/Ar for 1 hour at 30°C. The gas flow was switched to 1% C_2H_4/Ar for 30 minutes and the temperature was ramped at 10^oC/min in 1% C_2H_4/Ar to 500°C. The reverse experiment was performed by first

exposing the catalyst to flowing 1% C_2H_4/Ar followed by titration and temperature ramp in 1% C_4H_8/Ar.

2.3.2. $C_4H_8/C_2H_4/C_4H_8$ TPSR Experiment

The catalyst was again exposed to 1% C_4H_8 (2-butene)/Ar for 1 hour at 30°C. The gas flow was switched to 1% C_2H_4/Ar for 30 minutes and then 1% C_4H_8/Ar for another 30 minutes. The reactor was finally heated at 10°C/min in flowing 1% C_4H_8/Ar to 500°C.

2.3.3. C_2H_4/C_3H_6 and C_4H_8/C_3H_6 TPSR Experiments

The catalyst was contacted with 1% C_3H_6/Ar for 1 hour at 30°C. After 30 minutes of 1% C_2H_4/Ar or 1% C_4H_8/Ar (separate experiments), the TPSR was performed in flowing 1% C_2H_4/Ar or 1% C_4H_8/Ar to 500°C. Only the TPSR results are reported since the product C_3H_6 MS signals overlaps with the desorbed C_3H_6 MS signals during titration at 30°C.

2.3.4. C_3H_6 Pretreatment/C_2H_4 Adsorption/Ar-TPSR Experiments

After the initial dehydration procedure, the catalyst was contacted with 1% C_3H_6/Ar for 45 minutes at 100, 125 or 150°C. The reactor was flushed with Ar for 45 minutes before it was cooled to room temperature (~30°C). The catalyst was exposed to flowing 1% C_2H_4/Ar at the same temperature for 45 minutes. After another 45 minutes of Ar to remove physically adsorbed hydrocarbons, the TPSR experiment was performed by ramping in flowing Ar at the rate of 10°C/min to 500°C. The results are shown in Supplemental Information.

2.3.5. C_3H_6 Desorption Ar-TPSR Experiments

The catalyst was contacted with pure C_3H_6 for 45 minutes at 100°C. The reactor was flushed with Ar for 45 minutes before it was cooled to room temperature (~30°C). C_3H_6 was adsorbed again at the same temperature for 45 minutes. After another 45 minutes of Ar to remove physically adsorbed species, it was heated in Ar to 50, 75, 100 or 125°C (separate experiments) to change the surface concentration of chemically adsorbed species. The catalyst was next cooled down in Ar to the room temperature again. Finally the TPSR was performed in Ar at the rate of 10°C/min to see the desorption pattern of different concentration of surface adsorbates. The desorption activation energies, E_d, were obtained by applying the Redhead equation.[14,15]

$$\frac{E_d}{RT_p^2} = \frac{\nu_n C_i^{n-1}}{\beta} e^{\left(\frac{-E_d}{RT_p}\right)} \quad (1)$$

where C_i is the initial surface concentration of the adsorbate (propylene in most of the cases in this chapter), T_p is the temperature of the maximum desorption rate, ν_n is the pre-exponential factor, β is the heating rate (K/min) and R is the universal gas constant. ν_n has units which is dependent on the desorption order and it is normally taken as $10^{13}s^{-1}$ for the first order desorption process. For the first order reaction, equation (1) reduces to

$$\frac{E_d}{RT_p^2} = \frac{\nu_1}{\beta} e^{\left(\frac{-E_d}{RT_p}\right)} \quad (2)$$

Therefore, the surface concentration of adsorbates does not play a role in the peak desorption temperature T_p for the first order process.

For n = 2, equation (1) becomes

$$\frac{E_d}{RT_p^2} = \frac{\nu_2 C_0}{\beta} e^{\left(\frac{-E_d}{RT_p}\right)} \tag{3}$$

Ehsasi and Christmann[15] described a simple method to obtain parameters for this equation which can be arranged to

$$\ln\left(C_0 T_p^2\right) = \frac{E_d}{RT_p} + \ln\left(\frac{\beta E_d}{\nu_2 R}\right) \tag{4}$$

As seen above, a plot of ln ($C_0T_p^2$) against $1/T_p$ should give a straight line with a slope of E_d/R and an intercept of ln ($\beta E_d/\nu_2 R$). The first C_0 value (atoms/cm^2) was the number of sites counted at high temperatures using the method described in the previous chapter. The latter C_0 values were correctly approximated by the decrease of the area under each curve. ν_2 would have the units of cm^2/ (atom s) or g/ (mmol hr) and is found from the intercept of the plot. Regardless of the order of the desorption process,

$$k_{rds} = \nu_n e^{\left(\frac{E_d}{RT_p}\right)} \tag{5}$$

k_{rds} therefore has the same unit as ν_n.

The apparent activation energy, E_{app}, can be obtained by the Arrhenius plot of ln (reactivity) vs (1/T) which can be obtained by steady state experiments over the temperature range of interest. The slope of the plot gives the value of ($-E_{app}/R$) and is the only parameter that does not depend on the reaction order. The enthalpy of adsorption, ΔH_{ads}, is the difference of the two adsorption energy, so it can be written as

$$\Delta H_{ads} = E_{app} - E_d \tag{6}$$

2.3.6. TPSR in C_3H_6, C_2H_4 or Ar Experiments after 100°C C_3H_6 Pretreatments

After contacts with C_3H_6 at 100°C and cooling down in Ar to room temperature as in the above experiments (no olefin was adsorbed again at room temperature), the TPSR experiments were performed with C_3H_6, C_2H_4 or Ar (separate experiments) at the ramp rate of 10°C/min to 500°C to see the simultaneous effect of gas phase reactants on T_p.

2.3.7. C_3H_6/C_3D_6 and C_3H_6/C_2D_4 TPSR Experiments

C_2D_4 (99% D atom) and C_3D_6 (99% D atom) were purchased from CDN Isotopes and used without further modifications. The catalyst was treated with C_3H_6 at 100°C for 45 minutes. After flushing and cooling with Ar to room temperature, C_3D_6 or C_2D_4 (separate experiments) was adsorbed for 45 minutes. After another 45 minutes of Ar to remove physically adsorbed hydrocarbons, the TPSR experiment was performed by ramping in Ar at the rate of 10°C/min to 500°C.

2.4. Steady-State Kinetics Experiments

The catalytic activity measurements were performed in a fixed-bed catalytic reactor under differential conditions (propylene conversion <15%). A separate molecular sieve moisture trap was installed in the inlet propylene gas line to purify the reactants. Both inlet and outlet gas lines were heated using external electric heaters to ~200°C to prevent condensation of the reactants and products. The catalysts were pretreated in 10% O_2/Ar at 500°C for 30 minutes before cooling down in Ar to either 70 or 150°C. Then a gas mixture of 1-10% C_3H_6/Ar was introduced at the rate of ~100mL/min. The desired concentration was achieved by diluting the 10% C_3H_6/Ar gas with Ar. The products were

analyzed using an online gas chromatograph (Agilent GC 6890) equipped with flame ionization (Agilent Serial #: USC250823H) and thermal conductivity (Restek Product #: PC3533) detectors. Conversion was normalized with propylene flow rate and catalyst weight to obtain reactivity, reported in mmol/g/hr. The turnover frequencies (TOF in s^{-1}) are obtained from dividing reactivity by number of active sites obtained independently from studies in the previous chapter.

3. Results

3.1. *In situ* Raman Spectroscopy

The *in situ* Raman spectra of the supported 9.4% ReO_x/Al_2O_3 catalyst exposed to flowing Ar, $C_2^=$/Ar, $C_3^=$/Ar and 2-$C_4^=$/Ar at 30°C are shown in Figure 4.1. The dehydrated catalyst in flowing Ar exhibits two bands from surface ReO_4-I (1003 cm^{-1}) and ReO_4-II (1013 cm^{-1}) dioxo species anchored to basic and acidic surface hydroxyls, respectively. The interaction of the olefins with the surface rhenia species increases with olefin size ($C_2^= < C_3^= < C_4^=$) as reflected by the decreasing intensity of the Raman Re=O oxo bands. The decrease in intensity of the Raman Re=O oxo bands is from both bonding of the olefins to the rhenia species and the corresponding darkening of the sample, with the latter dependent on the number of coordinated olefins. In all cases, olefins preferentially coordinate to the surface ReO_4-II species, which show a greater decrease in intensity upon olefin adsorption. .

3.2. Titration Studies and Temperature Programmed Surface Reaction (TPSR) Spectroscopy

3.2.1. C_4H_8/C_2H_4 and C_2H_4/C_4H_8 titration studies

The C_4H_8/C_2H_4 and C_2H_4/C_4H_8 titration results are presented in Figure 4.2 and demonstrate the importance of the order of introducing the different olefins. The notation C_4H_8/C_2H_4 refers to initial adsorption of C_2H_4 followed by titration with C_4H_8. For the C_4H_8/C_2H_4 titration, C_3H_6 is not formed at room temperature reflecting the absence of weakly adsorbed C_2H_4 on the catalyst and only a small amount of C_3H_6 is produced from strongly adsorbed C_2H_4 at high temperatures ($T>70^o$) . For the C_2H_4/C_4H_8 titration, significant amounts of C_3H_6 are formed at both room and high temperature reflecting the much higher adsorption ability of 2-butene on the catalyst. The titration results confirm the much weaker adsorption ability of $C_2^=$ than $C_4^=$ on supported ReO_x/Al_2O_3 catalysts, but also reveal that a minor amount of strongly adsorbed $C_2^=$ is also present on the catalyst that can react at elevated temperatures.

3.2.2. $C_4H_8/C_2H_4/C_4H_8$ titration studies

The results from the $C_4H_8/C_2H_4/C_4H_8$ titration are presented in Figure 4.3. As above, titration by $C_2^=$ of the surface intermediates formed upon $C_4^=$ adsorption produces $C_3^=$. Subsequent titration by $C_4^=$ of the remaining surface intermediates yields a very small amount of $C_3^=$ at room temperature, but significant amounts of $C_3^=$ are produced at elevated temperatures reflecting the presence of remaining strongly bound intermediates present on the catalyst from the room temperature C_2H_4/C_4H_8 titration. This titration series demonstrates that not all surface intermediates can be titrated by 2-$C_4^=$ at room temperature.

3.2.3. C_2H_4/C_3H_6 and C_4H_8/C_3H_6 titration studies

The reactivity of surface $Re{=}CH_2$ and $Re{=}CHCH_3$ intermediates formed by adsorption of propylene on the supported 15.6% ReO_x/Al_2O_3 catalyst was chemically probed by titration with $C_2^=$, which reacts with surface $Re{=}CHCH_3$ to yield $C_3^=$, and with 2-$C_4^=$, which reacts with surface $Re{=}CH_2$ to yield $C_3^=$. The room temperature titration stage was complicated by the simultaneous appearance of $C_3^=$ from both desorption and surface reaction. The C_2H_4/C_3H_6- and C_4H_8/C_3H_6-TPSR spectra are shown in Figure 4.4. Titration of surface $Re{=}CH_2$ with 2-$C_4^=$ forms a significant amount of $C_3^=$ as the temperature is increased while titration of $Re{=}CHCH_3$ with $C_2^=$ produces only a small amount of $C_3^=$ as the temperature is increased. This suggests that 2-$C_4^=$ does not efficiently react with surface $Re{=}CH_2$ intermediates at room temperature, but does at higher temperatures (in agreement with the $C_4^=/C_2^=/C_4^=$ titration above in Figure 4.3 only showing $C_3^=$ production at high temperatures). In contrast, the small amount of $C_3^=$ at high temperatures by titration of surface $Re{=}CHCH_3$ by $C_2^=$ suggests significant reaction at room temperature (in agreement with the $C_2^=/C_4^=$ titration above in Figure 4.2 showing significant $C_3^=$ at room temperature).

3.2.4. C_3H_6-TPSR

The influence of surface coverage of reaction intermediates on the olefin metathesis reaction was examined with $C_3^=$-TPSR. The surface coverage of the reaction intermediates created from $C_3^=$ adsorption, surface $Re{=}CH_2$ and $Re{=}CHCH_3$, was controlled by initially varying the pretreatment temperature from 50-125^{o}C before cooling

back down to room temperature and performing the TPSR experiment in flowing Ar (raising the pretreatment temperature monotonically decreases the surface concentration of intermediates). The resulting $C_3^=$-TPSR spectra are presented in Figure 4.5 and indicate that the peak temperature, Tp, is a strong function of the surface coverage of the reaction intermediates. A shift of Tp to higher temperatures with decreasing surface coverage is characteristic of 2nd– order surface kinetics.[14] The surface reaction intermediates created from $C_3^=$ adsorption also yield $C_2^=$ and $C_4^=$ reaction products with the exact same Tp values as $C_3^=$ (see Figure S4.2 in Supplemental Information). Thus, formation of all the olefin products follows 2nd–order surface kinetics and indicates a similar reaction mechanism.

The kinetic parameters for the 2nd–order surface reaction were determined by application of the Redhead equation for temperature programmed experiments.[14,15] Assuming an initial surface intermediate coverage of ~1% of the Re species (0.022 Re atoms/nm^2) that undergoes second order kinetics gives an activation of energy of 94 kJ/mol (see Figure S4.3 in Supplemental Information). This assumption is validated by TPSR experiments performed in the previous experiments. These 1% sites are leftovers from room temperature adsorption of C_4= or C_3= which cannot react at lower temperatures.

3.2.5. Ar/C_3D_6/C_3H_6 and Ar/C_2D_4/C_3H_6 TPSR

Additional mechanistic insights into the olefin metathesis reaction at high temperatures were provided with the aid of isotopically labeled olefins. Initial adsorption of $H_3CCH{=}CH_2$ at 100^{o}C followed by adsorption of $D_2C{=}CD_2$ at room temperature and

performing TPSR in flowing Ar produced the isotopic products shown in Figure 4.6. The striking feature is that all isotopic olefinic products appear at the same temperatures with a Tp=165^{o}C and a weak shoulder at ~100^{o}C suggesting a common reaction step. The same Tp temperatures for all the isotopically labeled olefin products demonstrates that breaking of C-H/C-D bonds does not take place during olefin metathesis. All three ethylene isotopomers ($H_2C=CH_2$, $H_2C=CD_2$ and $D_2C=CD_2$) are formed reflecting the presence of surface $Re=CH_2$ and $Re=CD_2$intermediates on the catalyst. Only two propylene isotopomers ($H_3CCH=CH_2$ and $H_3CCH=CD_2$) are produced from surface $Re=CD_2$, $Re=CH_2$ and $Re=CHCH_3$ intermediates on the catalyst. Only a small amount of $H_3CCH=CHCH_3$ is produced because of the greater concentration of surface carbenes ($Re=CD_2$/$Re=CH_2$) compared to surface alkylidenes ($Re=CHCH_3$).

Initial adsorption of $H_3CCH=CH_2$ at 100^{o}C followed by adsorption of $D_3CCD=CD_2$ at room temperature and performing TPSR in flowing Ar produced the high temperature isotopic products shown in Figure 4.7. All olefin products again appear at almost the same temperature suggesting a common reaction step and that breaking of C-H/C-D bonds does not take place during olefin metathesis. The 1:1 ratio of surface carbenes ($Re=CD_2$/$Re=CH_2$) to surface alkylidenes ($Re=CHCH_3$ and $Re=CDCD_3$) results in formation of all olefin isotopomers. The strongest signals are for fully deuterated olefin products indicating that the ratio of $C_3D_6/C_3H_6 > 1$ on the catalyst surface and accounts for the weak signals from the undeuterated olefin products. The production of the mixed isotopes ($H_3CCH=CD_2$, $D_3CCD=CH_2$ and $D_3CCD=CHCH_3$) reflects the presence of surface $Re=CH_2$, $Re=CD_2$, $Re=CHCH_3$ and $Re=CDCD_3$ intermediates on the catalyst.

3.3. Steady-State Kinetics

3.3.1 Reaction order

The kinetics for C_3H_6 metathesis to C_2H_4 and C_4H_8 by the supported ReO_x/Al_2O_3 catalyst was examined as a function of $C_3^=$ partial pressure and reaction temperature, and are presented in in Figure 4.8. The olefin metathesis reaction order in $C_3^=$ partial pressure is a strong function of temperature with ~0.9 at 70^{o}C and increases to ~1.8 at 150^{o}C.

3.3.2. Kinetic Parameters

As shown in Figure 4.9, the slope of the Arrhenius plot of ln (reactivity) vs (1/T) gives the value of ($-E_{app}/R$). Over the 30-150°C range, it is found to be 16.4 kJ/mol and insensitive to the reaction pathways.

3.3.2.1. Low temperature reaction pathway

The number of participating catalytic sites corresponds to the sum of the surface Re-alkylidenes and Re-metallacyclobutanes and was determined in the previous chapter to be ~7.5% of total ReO_x sites (0.019 mmol/g for 0.3g of catalyst or 0.165 Re atoms/nm^2). Knowing the number of participating active sites allows determining the TOF value and for propylene metathesis at 70^{o}C from the steady-state reactivity (mmol/g/hr), and is found to be TOF = 0.15 molecules/s. Given that the olefin metathesis reaction proceeds at 30°C, the Redhead equation was applied with an estimated value of Tp=30^{o}C to calculate the activation energy for the 1st-order reaction (E_{d1}) by employing the 1st-order pre-exponential factor (ν_1) of 10^{13}/s. The activation for propylene metathesis at low temperatures is determined to be E_{d1} = 86 kJ/mol and the apparent activation energy of 16

kJ/mol allows calculating the $C_3^=$ heat of adsorption (ΔH_{ads1}), which is found to be -70 kJ/mol. All the determined kinetic parameters are listed in table 4.1.

3.3.2.2. High temperature reaction pathway

The number of sites reacting at high temperatures corresponds to ~1% of total Re sites and thus the TOF is found to be 0.21 molecules/s using 1%C_3=/He as a reactant. Desorption of intermediates up to 150°C removes up to 50% of surface intermediates (Figure 4.5). Employing the methods described in section 2.3.5, the activation energy (E_{d2}) and pre-exponential factor (ν_2) for the 2nd-order reaction are calculated to be 94 kJ/mol and 7.8x 10^{12} g $mmol^{-1}$ hr^{-1} (or 6x 10^{-6} cm^2/(atom s))respectively. The $C_3^=$ heat of adsorption (ΔH_{ads2}) is -78kJ/mol. The kinetics parameters for the high temperature reaction pathway are presented in Table 4.2.

4. Discussion

4.1. Olefin adsorption and nature of surface intermediates

The adsorption of $C_2^=$-$C_4^=$ olefins on the supported ReO_x/Al_2O_3 catalysts form irreversibly adsorbed species since heating in inert Ar does not lead to complete olefin desorption from the catalyst and can be titrated with other olefins (see Figure S4.4). The olefins preferentially interact with the surface ReO_4-II sites on the alumina support and the extent of interaction of the olefins with the ReO_4-II sites increases with olefin length ($C_2^=$ < $C_3^=$ < $C_4^=$) (see Figure 4.1). In contrast to the general literature claim that $C_2^=$ does not adsorb or activate supported ReO_x/Al_2O_3 catalysts,[5-7] a minor amount of ethylene does adsorb and activates the catalyst in agreement with the early studies of Aldag *et al*.[8,10]

Surface $Re=CH_2$, $Re=CHCH_3$ intermediates and surface olefin π-complexes are present on the supported ReO_x/Al_2O_3 catalysts upon olefin exposure at room temperature as demonstrated by the olefin titration studies. The $C_2^=/C_4^=$ titration experiments reveal that adsorption of 2-butene on ReO_x/Al_2O_3 catalysts results in production of $C_3^=$ as well as $C_4^=$ from surface $Re=CHCH_3$ intermediate and surface 2-butene π-complex, respectively (see Figures 4.2, 4.3 and S3.4 of Chapter 3). The $C_2^=/C_3^=$ titration produced $C_3^=$ from reaction of ethylene with surface $Re=CHCH_3$ and $C_4^=/C_3^=$ titration yields $C_3^=$ from reaction of 2-butene with surface $Re=CH_2$ (see Figure 4.4).

4.2. Reaction mechanism(s) and kinetics

The olefin titration and steady-state kinetic studies revealed that olefin metathesis proceeds via two reaction pathways, low temperature (30^oC) and high temperature (> 70^oC), which exhibit 1^{st}-order and 2^{nd}-order kinetics, respectively. The 2^{nd}-order kinetics at high temperatures is further confirmed by the TPSR studies showing the strong coverage dependence of this reaction pathway at high temperature (see Figure 4.5). Only the mechanism(s) and kinetics of propylene metathesis will be discussed in the sections below.

4.2.1. Low temperature reaction pathway

Most of the reported propylene metathesis studies with supported ReO_x/Al_2O_3 catalysts have been performed at room temperature because of the high activity of this catalyst system.[4] The titration and kinetic studies also reflect the ease with which olefin metathesis can take place on supported ReO_x/Al_2O_3 catalysts at room temperature. The 1^{st}-order

reaction kinetics in propylene partial pressure at low temperatures is consistent with the Chauvin mechanism with the rate-determining-step involving decomposition of the surface metallacyclobutane intermediate.[13] According to this reaction mechanism, surface $Re{=}CH_2$ and $Re{=}CHCH_3$ intermediates are formed during catalyst activation by propylene and the reaction proceeds by reaction of $C_3^{=}$ to form 4- and 5-membered metallacyclobutane surface intermediates as shown by equations 7 and 9 below. The 4- and 5-membered metallacyclobutane surface intermediates unimolecularly decompose to $C_2^{=}/Re{=}CHCH_3$ and $C_4^{=}/Re{=}CH_2$, respectively as shown by equations 8 and 10 below, which is the rate-determining-step. The unimolecular decomposition rds accounts for the 1^{st}-order reaction kinetics and regenerates the active surface $Re{=}CH_2$ and $Re{=}CHCH_3$ intermediates as shown below.

(7)

(8)

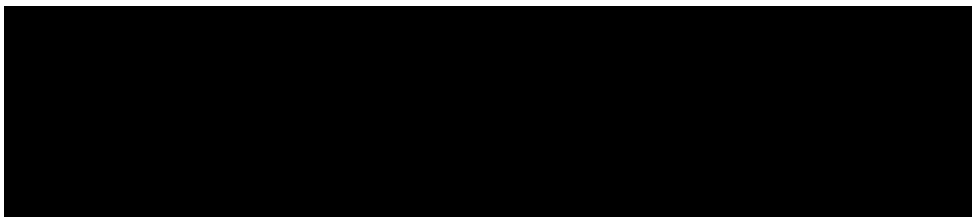

(9)

(10)

Combing all the relevant terms leads to the following equation equilibrium and rate determining steps.

C_3H_6 + [Re=C_1/C_2 carbenes] [redacted] [Re-C_4/C_5 MC]$_s$ K_{ads1} (11)

[Re-C_4/C_5 MC] [redacted] C_2H_4 + C_3H_6 + C_4H_8 + [Re=C_1/C_2 carbenes] k_{rds1} (12)

To simplify, [Re=C_1/C_2 carbenes]$_s$ and [Re-C_4/C_5 MC]$_s$ would be denoted as [*] and [C_3H_6*], respectively. Therefore,

$$K_{ads1} = \frac{[C_3H_6*]}{[*][C_3H_6]} \quad (13)$$

$$[*]_{01} = [C_3H_6*] + [*] \quad (14)$$

$[*]_{01}$ is the total number of active sites, either Re alkylidenes or Re-metallacyclobutanes under each conditions of interest for the first order conditions. Since most of the Re-alkylidenes reactant (i.e., convert to Re-metallacyclobutanes) at mild conditions (<100°C) as discussed in the previous chapter, the number of sites can be approximated by the amount of products formed.

Using equations (13) and (14) to solve for [C_3H_6*] gives

$$[C_3H_6*] = \frac{K_{ads1}[C_3H_6][*]_{01}}{1 + K_{ads1}[C_3H_6]} \quad (15)$$

$$r_1 = k_{rds1}[C_3H_6{*}] = \frac{k_{rds1}K_{ads1}[C_3H_6][*]_{01}}{1+K_{ads1}[C_3H_6]} = \frac{k_{rds1}K_{ads1}[*]_{01}P_{C_3=}}{1+K_{ads1}P_{C_3=}} \quad (16)$$

In the last step of equation (16), $[C_3H_6]$ is called $P_{C3=}$. Applying the lean adsorption assumption which is valid when partial pressure of propylene or number of active sites is low,[18] $K_{ads1}P_{C3=} << 1$, equation (16) for reactivity becomes

$$r_1 = k_{rds1}K_{ads1}[*]_{01}P_{C_3=} \sim k_1' P_{C_3=} \quad (17)$$

4.2.2. High temperature reaction pathway

The kinetic and TPSR studies reveal that the high temperature reaction pathway proceeds via a bimolecular mechanism involving reaction between two surface species. The apparent reaction order of 1.8 rather than 2 in propylene partial pressure at elevated temperatures may be reflecting the minor contribution of the 1st-order reaction kinetics at the higher reaction temperature. The 2nd-order reaction kinetics, however, can only be derived by assuming reaction between two adsorbed $C_3^=$ molecules since bimolecular reaction between surface $Re{=}CH_2$ and $Re{=}CHCH_3$ does not give rise to 2nd-order kinetics. This suggests that the surface intermediates present on the catalyst at high temperature are $C_3^=$ π-complexes and that the high temperature reaction pathway proceeds via 4-carbon complexes proposed by some of the early metathesis studies as shown below.[10] According to this bimolecular reaction mechanism, the olefins can exchange their individual components to yield the metathesis products. The kinetics for the bimolecular olefin metathesis reaction are derived by assuming reaction between two surface $C_3^=$ π-complexes.

$CH_3CH{=}CH_2 + Re$ [redacted] $Re{=}C_3H_6$ K_{ads2} (18)

$Re{=}C_3H_6 + Re{=}C_3H_6$ [redacted] $2Re + CH_2{=}CH_2 + CH_3CH{=}CHCH_3$ k_{rds3} (19)

$Re{=}C_3H_6 + Re{=}C_3H_6$ [redacted] $2Re + 2CH_3CH{=}CH_2$ k_{rds4} (20)

All olefins shared the same rate determining step (rds), as seen in Figures 4.7 and 4.8.

$k_{rds2}=k_{rds3}=k_{rds4}$ (21)

$[*]_{02} = [Re{=}C_3H_6]+ [*]$ (22)

$$K_{ads2} = \frac{[Re = C_3H_6]}{[*][C_3H_6]} \quad (23)$$

$$[*]_{02} = \frac{[Re = C_3H_6]}{[*][C_3H_6]} + [Re = C_3H_6] \quad (24)$$

$$[Re = C_3H_6] = \frac{K_{ads2}[C_3H_6][*]_{02}}{1 + K_{ads2}[C_3H_6]} \quad (25)$$

$$r_2 = k_{rds2}[Re = C_3H_6]^2 = \frac{k_{rds1}K^2_{ads2}[C_3H_6]^2[*]^2_{02}}{(1 + K_{ads2}[C_3H_6])^2} = \frac{k_{rds2}K^2_{ads2}[*]^2_{02}P^2_{C_3=}}{(1 + K_{ads2}P_{C_3=})^2} \quad (26)$$

In the last step of equation (26), $[C_3H_6]$ is called $P_{C3=}$. Applying the lean adsorption assumption leads to

$$r_2 = k_{rds2}K^2_{ads2}[*]^2_{02}P^2_{C_3=} \sim k'_2P^2_{C_3=} \quad (27)$$

The 2nd-order kinetics for olefin metathesis has been proposed before for both supported metal oxide heterogeneous and homogenous systems.[8-11,17] Kinetic fitting, however, is not direct proof of a reaction mechanism because of the ambiguity of simplified kinetics.[18] Similar temperature dependent pressure-reactivity profile has been observed by Kapteijn *et al*. from kinetic modeling. Their temperature dependent k_{rds} and

K_{ads} values, however, could easily be fitted to satisfy equation (16) when the surface concentration of the reactant is high (e.g., $K_{ads}P_{C3=}$ is not much less than 1). The temperature programmed desorption, which is done for *the first time* for this reaction system, is the only method demonstrating direct evidence of a bimolecular olefin metathesis reaction mechanism.

‘

4.3. Kinetics Parameters

The apparent activation energy (E_{app}) is calculated to be 16 kJ/mol and is the only parameter that is independent of the desorption process or the reactant partial pressure. This value is in relative agreement with those published in literature.[8,10,12] The much larger equilibrium adsorption constant K_{ads} value for the second-order reaction pathway, $K_{ads2} >> K_{ads1}$ in equation (18) vs (11), for means that this recombination is not easily reversible and, thus, dictates a higher desorption activation energy. This is also justified by the fact that relatively high temperatures are required to desorbed complexes as seen in *in situ* IR spectra in the previous chapter. The value of the second order pre-exponential factor obtained, ν_2, obtained in this study, $6x\ 10^{-6}$ $cm^2/(atom\ s)$, also indicates an acceptable collision frequency for non-ideal conditions and leads to the conclusion that very few pairs of $Re=C_3H_6$ produce C_2H_4 and C_4H_8 in this pathway. The value of 10^{-2} $cm^2/(atom\ s)$ is expected for ideal number of collisions and this number must be lower than 10^{-4} $cm^2/(atom\ s)$ for bimolecular surface reaction or desorption according to one of the guidelines of Boudart.[18] The high temperature for the second order reaction also results in larger desorption activation energy leading to a more exothermic reaction (more negative enthalpy values).

5. Conclusions

Propylene metathesis by supported ReO_x/Al_2O_3 catalysts occurs via surface $Re{=}CH_2$, $Re{=}CHCH_3$ and $C_3^{=}$ π-complexes. At low temperatures, metathesis proceeds by reaction of gas phase propylene with the surface $Re{=}CH_2$ and $Re{=}CHCH_3$ intermediates to form 4- and 5-membered metallacyclobutane complexes. The rate-determining-step is the unimolecular decomposition of the surface metallacyclobutanes to the $C_2^{=}$ and $C_4^{=}$ reaction products that regenerates the surface $Re{=}CH_2$ and $Re{=}CHCH_3$ intermediates. At high temperatures, metathesis proceeds by bimolecular reaction of $C_3^{=}$ π-complexes via formation of 4 membered carbon intermediates. Breaking of C-H/C-D bonds does not take place during olefin metathesis for both conditions. The kinetic parameters found for both pathways are within reasonable agreement with those in literature and satisfy the accepted kinetic guidelines. These new insights are able to solve the conflicting reports which existed in literature for decades.

References

1. Mol, J.C. *J. Mol. Catal. A. Chem*. **2004**, *213*, 39–45.
2. Disproportionation catalyst. British Petroleum Corporation. Great Britain Patent GB1054864 (A), September 8, 1964.
3. Mol, J. C.; van Leeuwen, P. W. N. M. **2008**. Metathesis of Alkenes. Handbook of Heterogeneous Catalysis. 14:3240–3256.
4. Lwin, S.; Wachs, I. E. ACS Catal. **2014**, *4*, 207–216.

5. Salameh, A.; Coperet, C.; Basset, J.; Bohm, V.P.W.; Roper, M. *Adv. Synth. Catal*. **2007**, *349*, 238–242.

6. McCoy, J.R.; Farona, M.F. *J. Mol. Catal*. **1991**, *66*, 51–58.

7. Olsthoorn, A.A.; Boelhouwer, C. *J. Catal*. **1976**, *44*, 207–216.

8. Aldag, A.W.; Lin, C. J.; Clark, A. *J. Catal.* **1978**, *51*, 278–285.

9. Spinicci, R.; Tofanari, A. *J. Therm. Analy*. **1983**, *27*, 391–400.

10. Aldag, A.W.; Clark, A. *J. Catal.* **1978**, *54*, 98–101.

11. Luckner, R. C.; McConchle, G. E.; Wills, G. E. *J. Catal.* **1973**, *28*, 83–88.

12. Kapteijn, F.; Bredt, L.H.G.; Homburg, E.; Mol, J.C. *Ind. Eng. Chem. Prod. Res. Dev.* **1981**, *20*, 457–466.

13. Hérisson, J.-L.; Chauvin, Y. *Makromol. Chem*. **1971**, *141*, 161–176.

14. Redhead, P.A. Vacuum **1962**, *12*, 203–211.

15. Ehsasi, M.; Christmann, K. Surf. Sci. **1988**, *194*, 172–198.

16. Burcham, L.J.; Badlani, M.; Wachs, I.E. *J. Catal*. **2001**, *203*, 104–121.

17. Hughes, W. B. *J. Am. Chem. Soc*. **1970**, *92*, 532–537.

18. Boudart, M. *AIChE*. **1972**, *18*, 465–478.

Figures

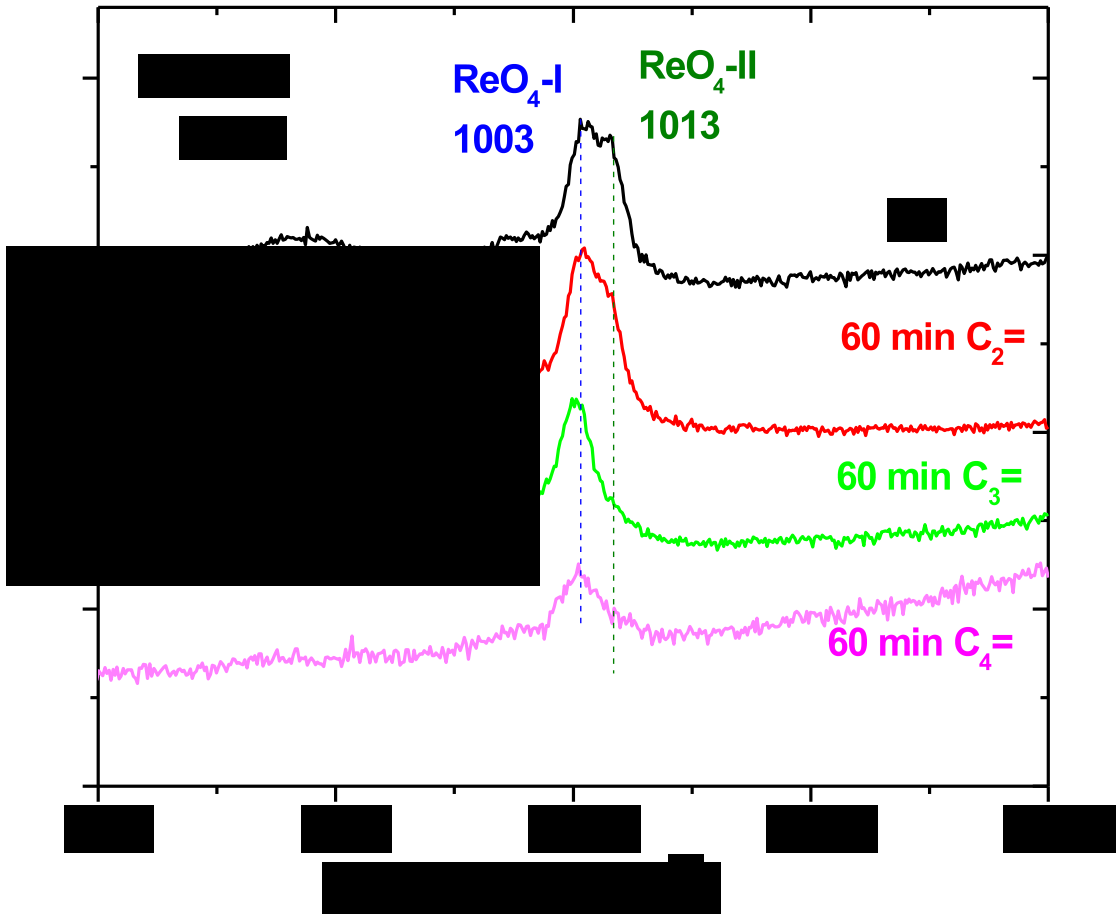

Figure 4.1. *In situ* Raman spectra of the supported 9.4% ReO_4/Al_2O_3 catalyst after 60 minutes under different flowing gases at 30°C

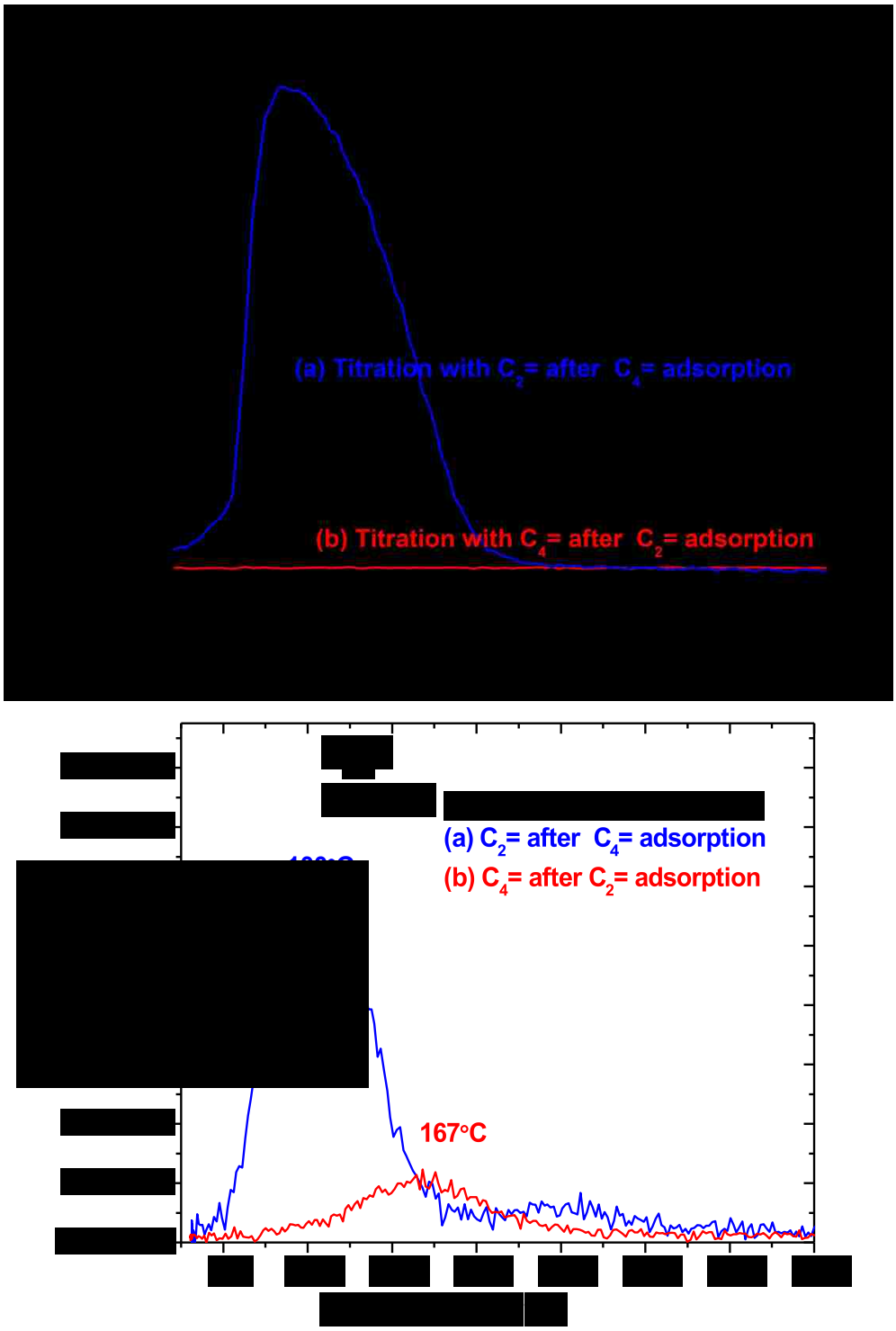

Figure 4.2. Formation of $C_3^=$ during titration experiments, $C_2^=/C_4^=$ (blue) and $C_4^=/C_2^=$ (red) at 30°C (top) and during TPSR (bottom)

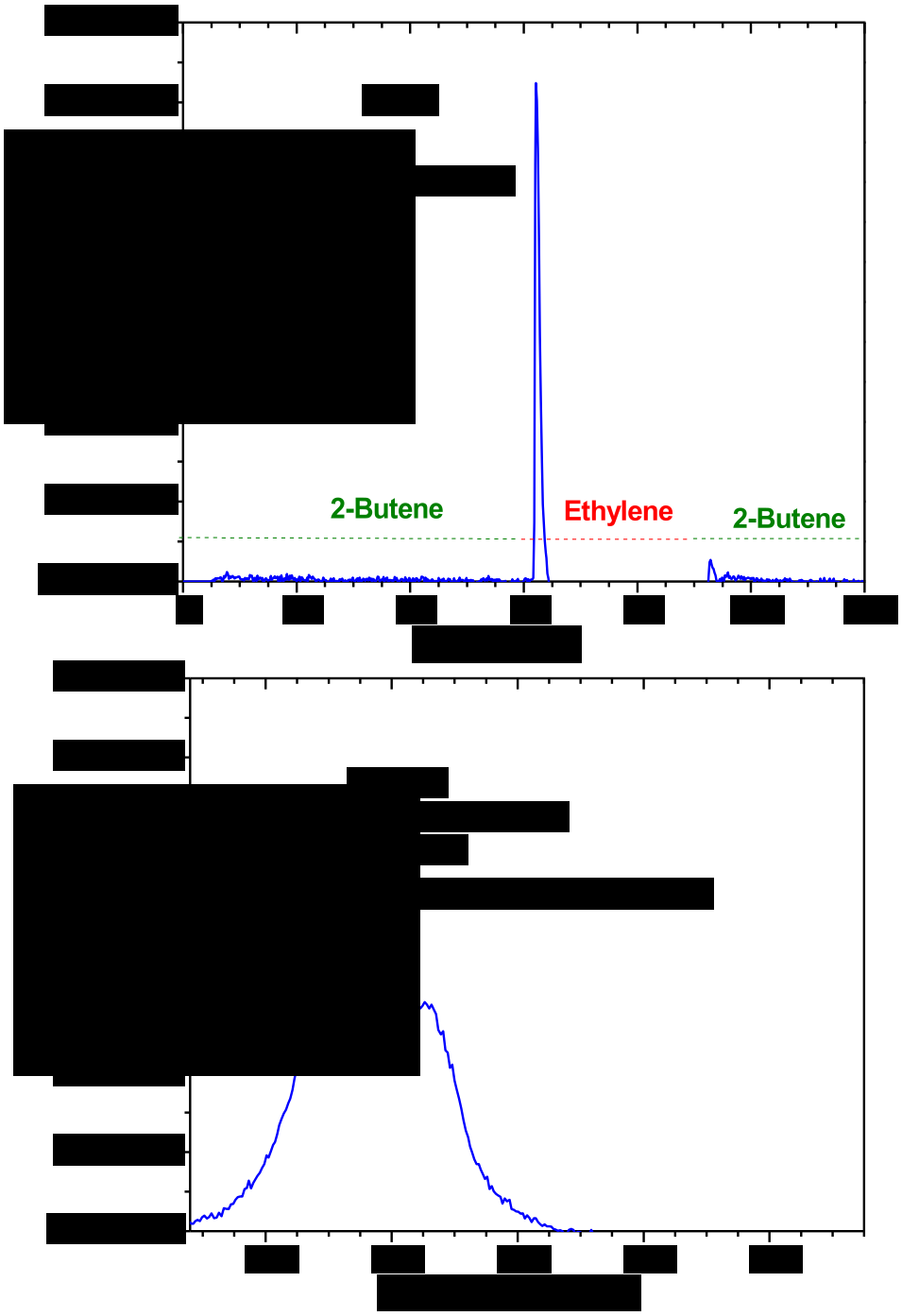

Figure 4.3. Formation of $C_3^=$ during titration experiments, $C_4^=/C_2^=/C_4^=$ at 30°C (top) and during TPSR (bottom)

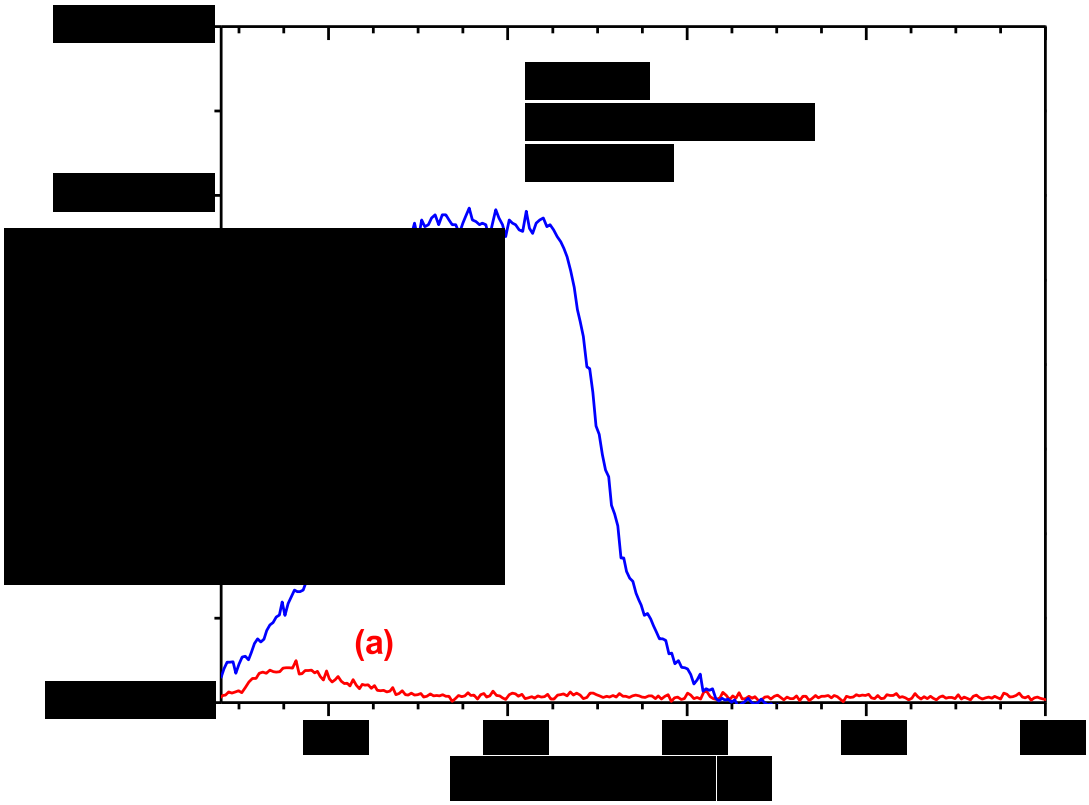

Figure 4.4. Formation of $C_3^=$ during titration experiments (a) $C_2^=/C_3^=$ TPSR (red) and (b) $C_4^=/C_3^=$ TPSR (blue).

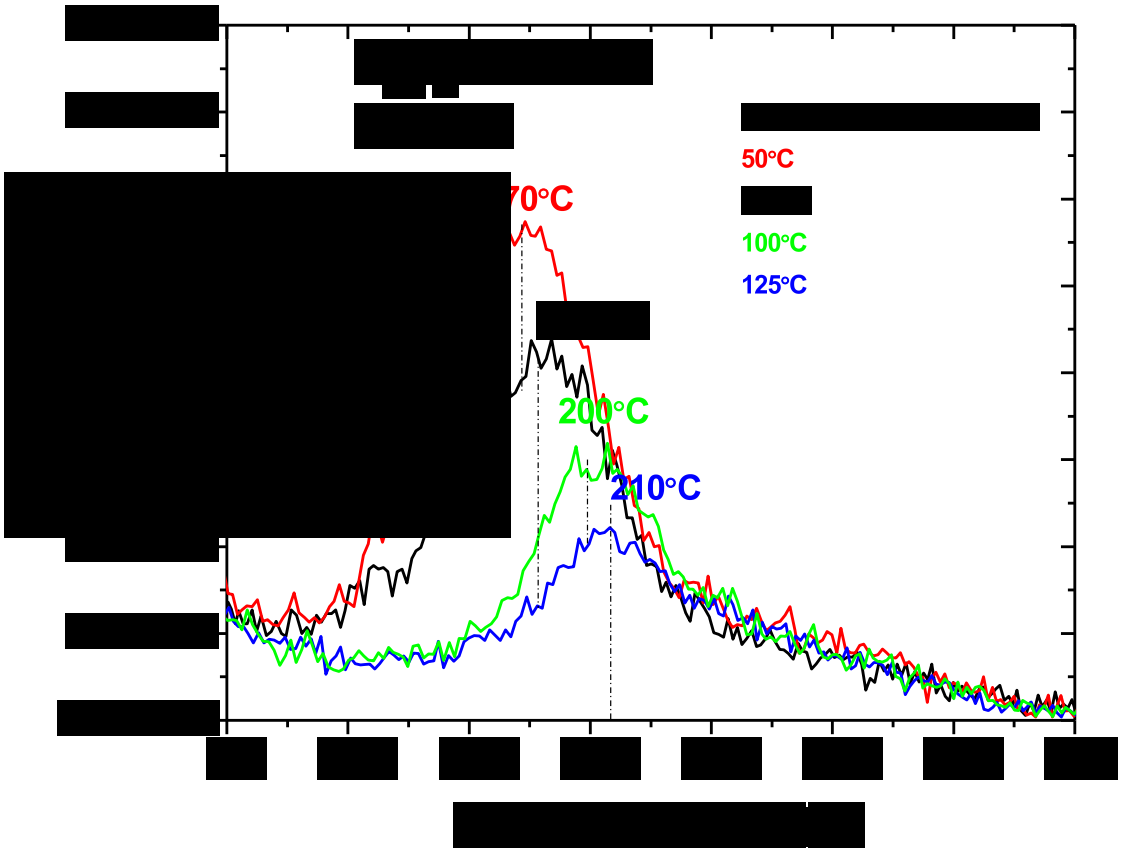

Figure 4.5. C_3H_6 signals in flowing Ar after various desorption temperature treatments. The full experimental procedure can be found in section 2.2.5. C_2H_4 and C_4H_8 signals follow the same T_p values as C_3H_6 (see Figure S4.2).

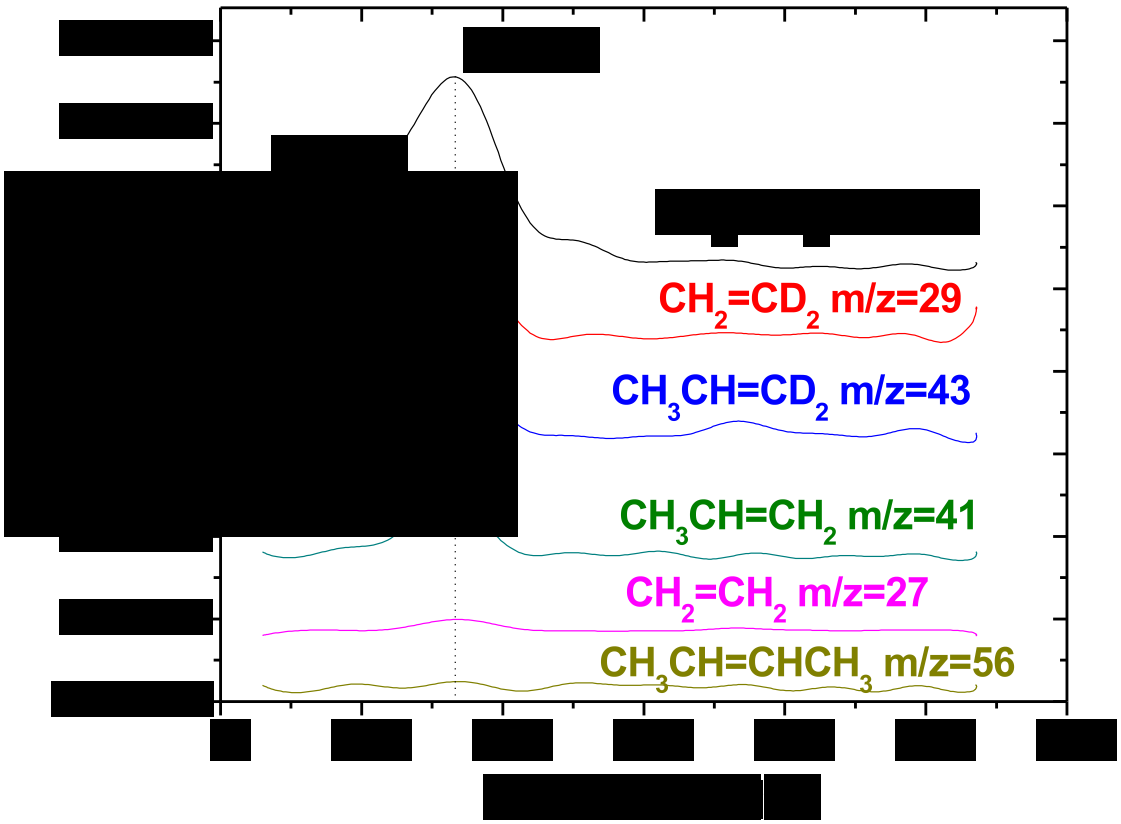

Figure 4.6. Isotopically labeled reaction products from $Ar/C_2D_4(30^oC)/C_3H_6(100^oC)$-TPSR.

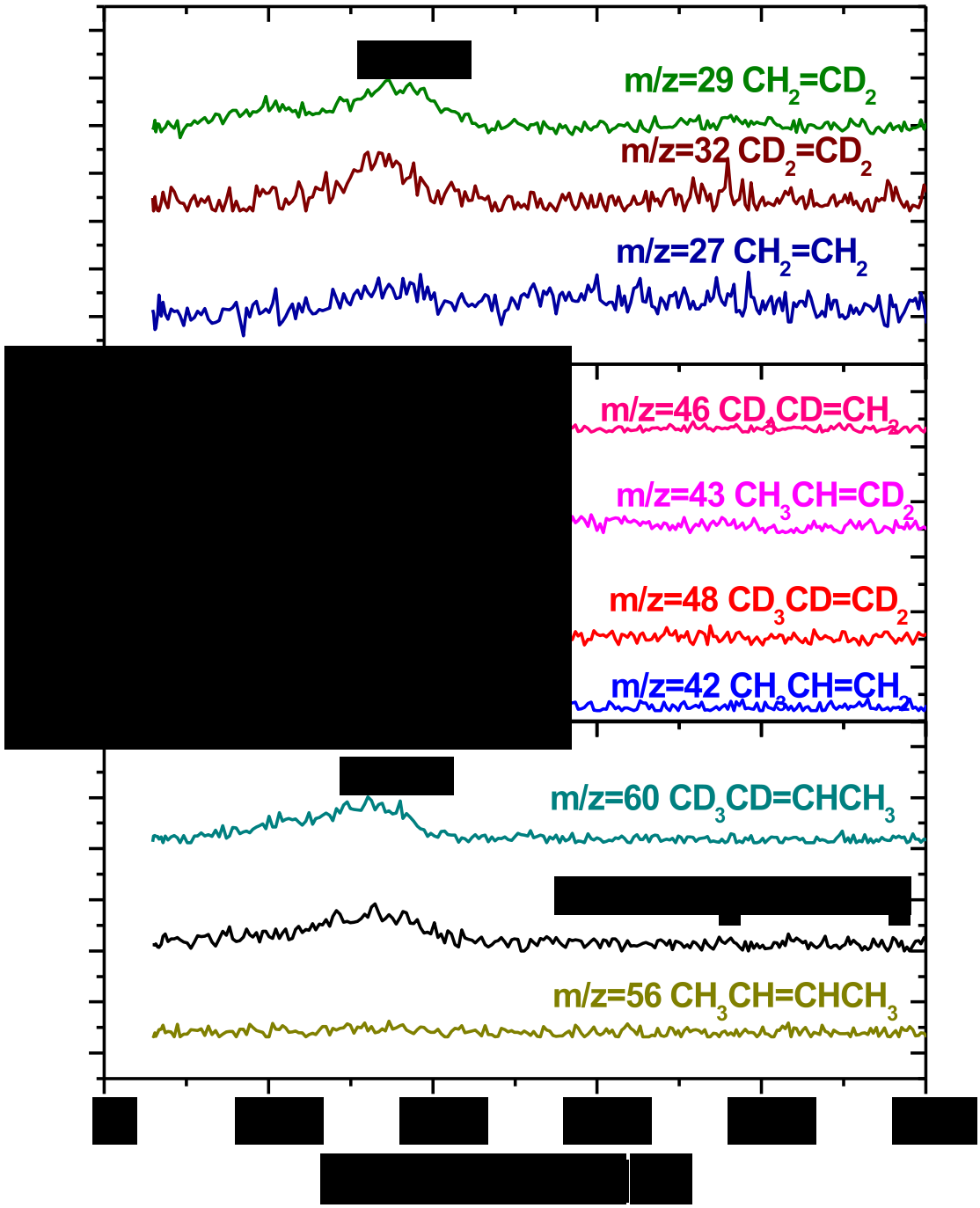

Figure 4.7. Isotopically labeled reaction products from Ar/C_3D_6(30°C)/C_3H_6(100°C)-TPSR..

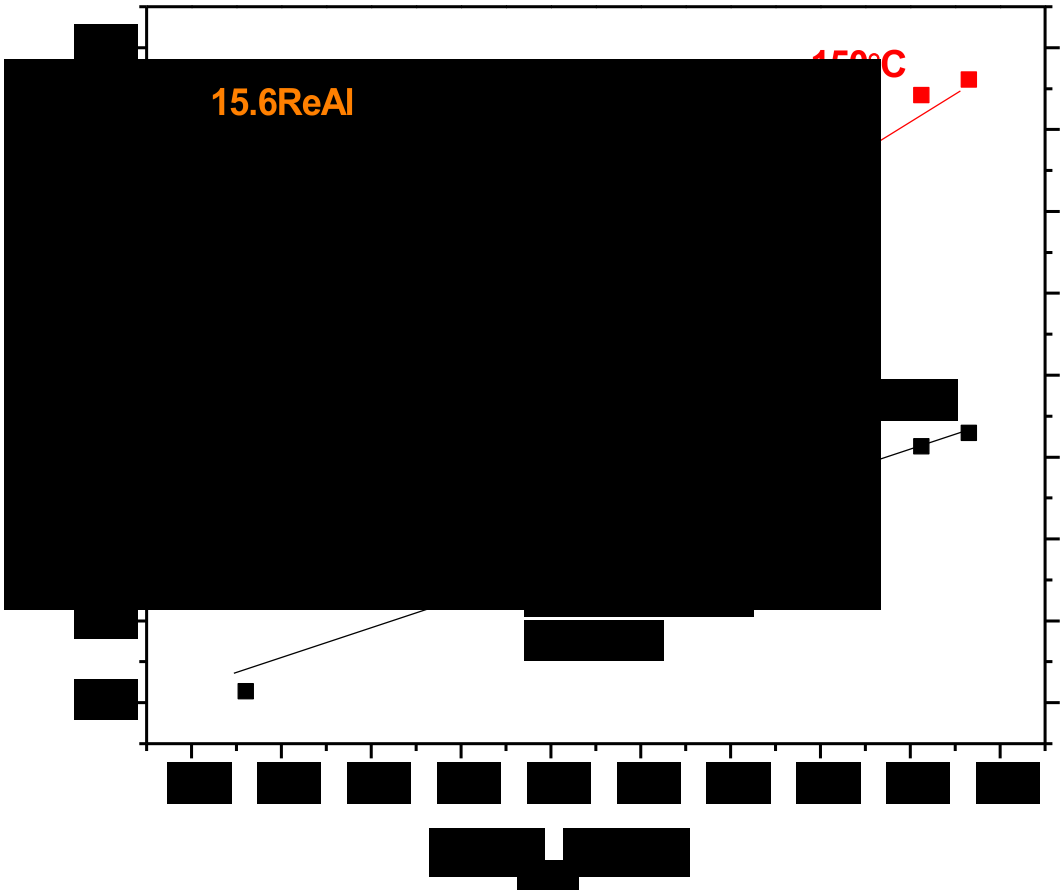

Figure 4.8. Propylene metathesis as a function of C_3H_6 partial pressure and temperature.

Figure 4.9. Arrhenius plot to calculate the apparent activation energy.

Table 4.1. Kinetics Parameters for the First-Order Desorption Process at 30-70°C under Lean Conditions (1% C_3H_6)

Parameter (units)	Value
$[*]_{01}$ (mmol/g)	0.019
k_{rds1} (s^{-1})	0.97
ν_1 (s^{-1})	10^{13}
K_{ads1} ($torr^{-1}$)	0.059
E_{app1} (kJ/mol)	16
E_{d1} (kJ/mol)	86
ΔH_{ads1} (kJ/mol)	-70

Table 4.2. Kinetics Parameters for the Second-Order Desorption Process at 150°C under Lean Conditions (1% C_3H_6)

Parameter (units)	Value
$[*]_{02}$ (mmol/g)	0.006
k_{rds2} (g $mmol^{-1}$ hr^{-1})	22
ν_2 (g $mmol^{-1}$ hr^{-1})	7.8E12
K_{ads2} ($torr^{-1}$)	32
E_{app2} (kJ/mol)	16
E_{d2} (kJ/mol)	94
ΔH_{ads2} (kJ/mol)	-78

Supplemental Information

S4.1. C_3H_6 Pretreatment/C_2H_4 Adsorption Ar-TPSR Experiments

The results of the Ar-TPSR experiments after x°C (x=100,125 and 150) C_3H_6 treatment/C_2H_4 room temperature adsorption are shown in Figure S4.1. The T_p shifts to higher temperatures with the higher C_3H_6 pretreatments suggesting that the peak temperatures have an inverse relationship with C_3H_6 coverage. No C_4H_8 was produced in this set of experiments. The 200, 300 and 400°C pretreatments cannot give products in the absence of a gas phase olefin and their results are not shown for brevity.

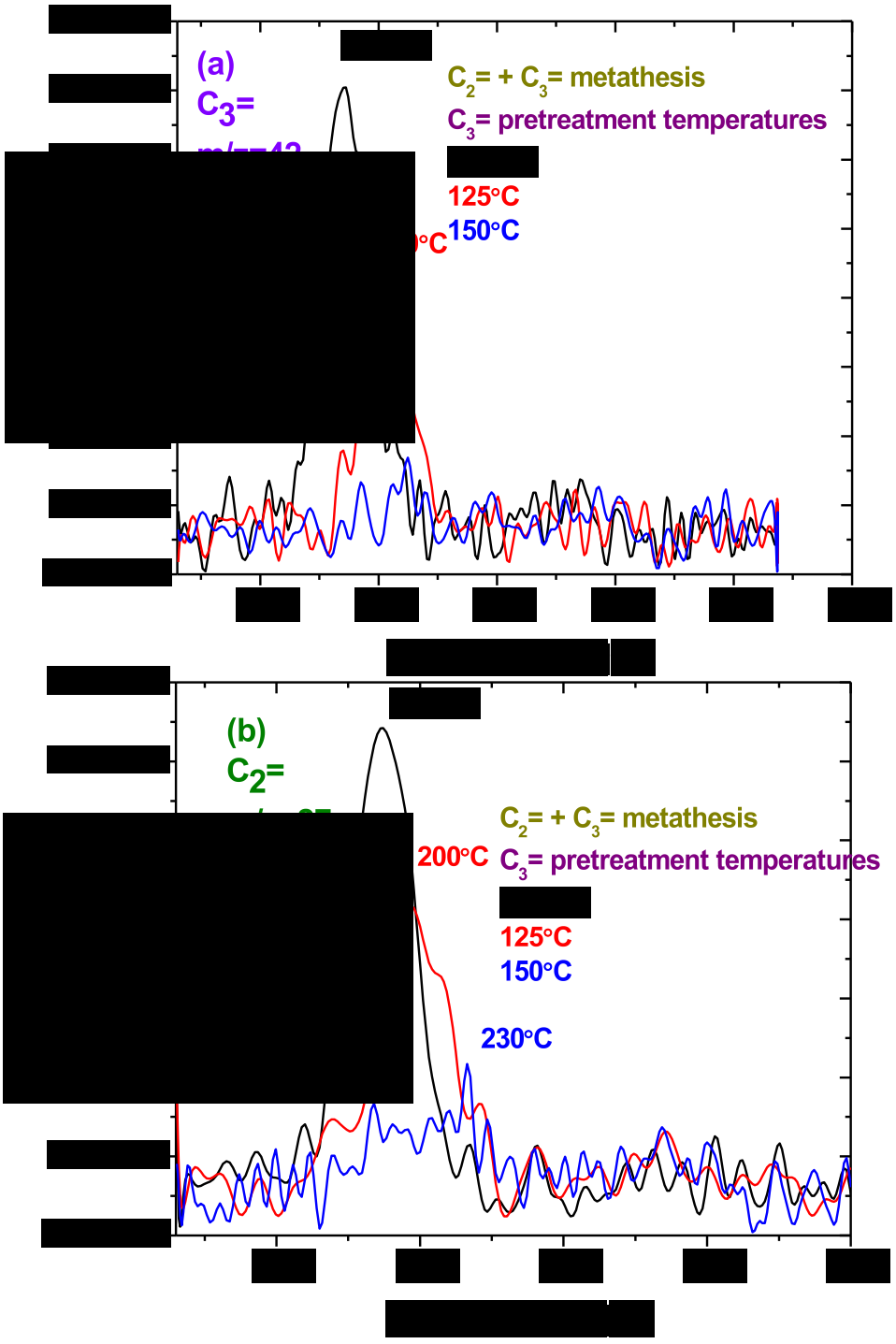

Figure S4.1. TPSR signals of (a) C_3H_6 and (b) C_2H_4 in flowing Ar after 100, 125 and 150°C C_3H_6 pre-treatment and room temperature C_2H_4 adsorption (separate experiments).

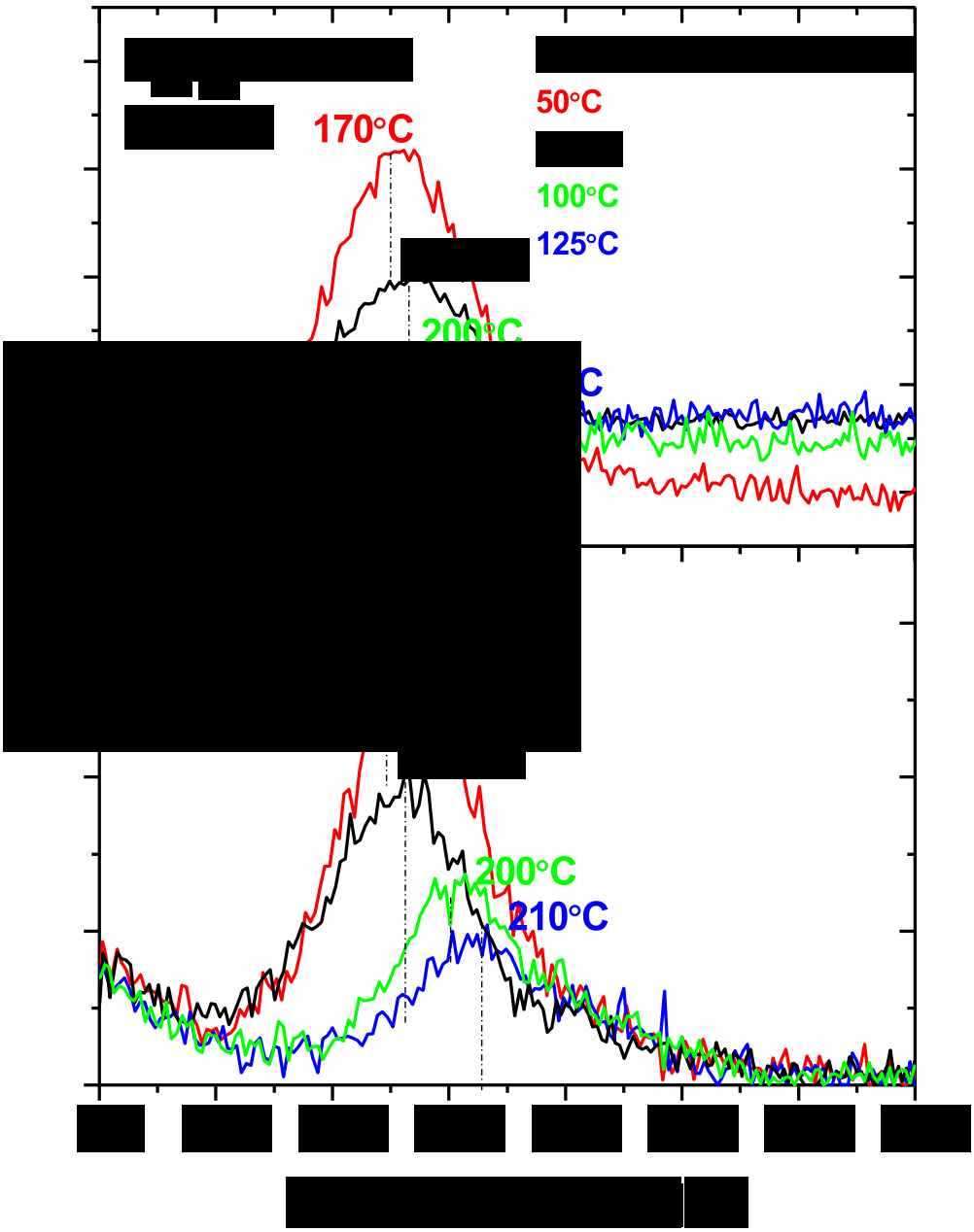

Figure S4.2. TPSR signals of (a) C_2H_4 (top) and (b) C_4H_8 (bottom) in flowing Ar after various desorption temperature treatments. The full experimental procedure can be found in section 2.3.5.

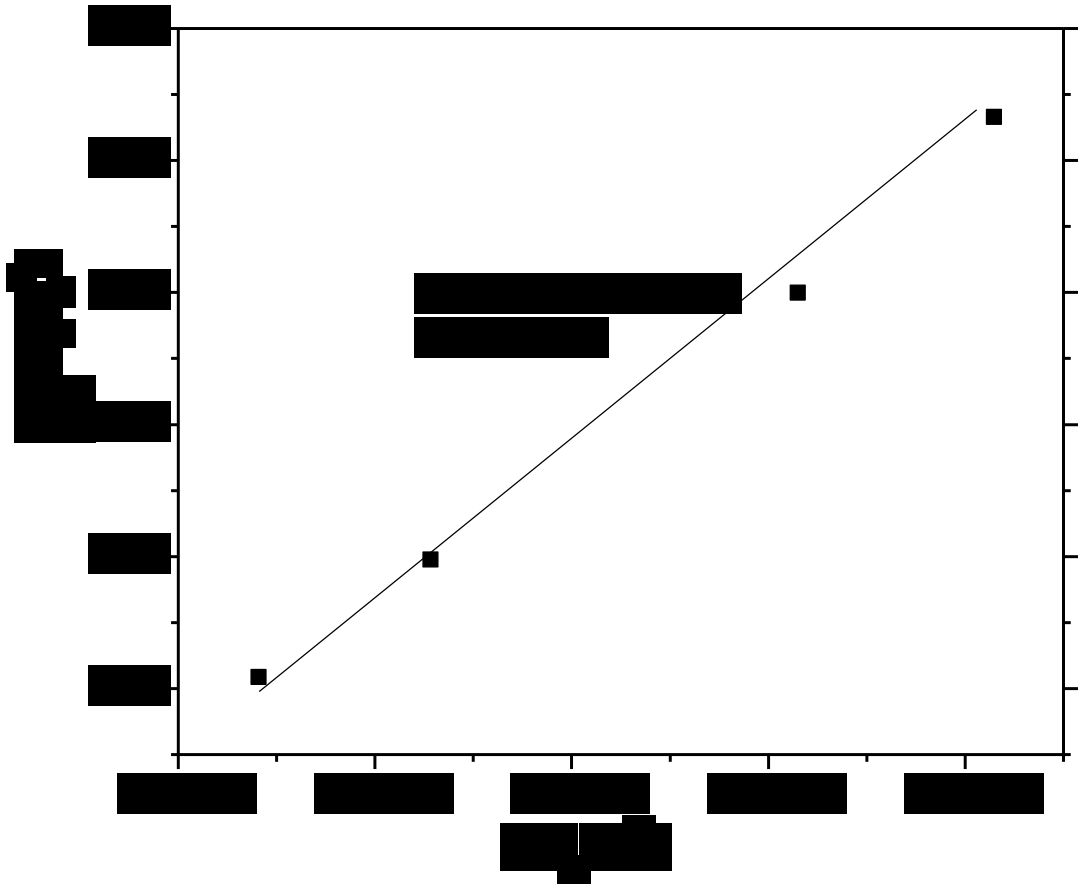

Figure S4.3. Plot of ln ($C_0T_p^2$) against $1/T_p$ to give a slope of E_a/R for the second order desorption kinetics.

4.2. TPSR in C_3H_6, C_2H_4 or Ar Experiments after 100°C C_3H_6 Pretreatments

The results are shown in Figure S4.4. These experiments were designed to observe effects of a gas phase reactant on T_p and possible recombination of surface intermediates under certain circumstances. C_3H_6 causes a decrease in T_p mostly likely due to creation of additional sites whereas C_2H_4 and Ar produce the same results although the amounts are different. No C_4H_8 was formed in the C_2H_4- and Ar- TPSR experiments indicating either C_3H_6 must readsorb on the surface to make C_4H_8 or recombination of $Re{=}CHCH_2$ with another $Re{=}CHCH_2$ does not occur when the catalyst was already pretreated with C_3H_6 at 100°C.

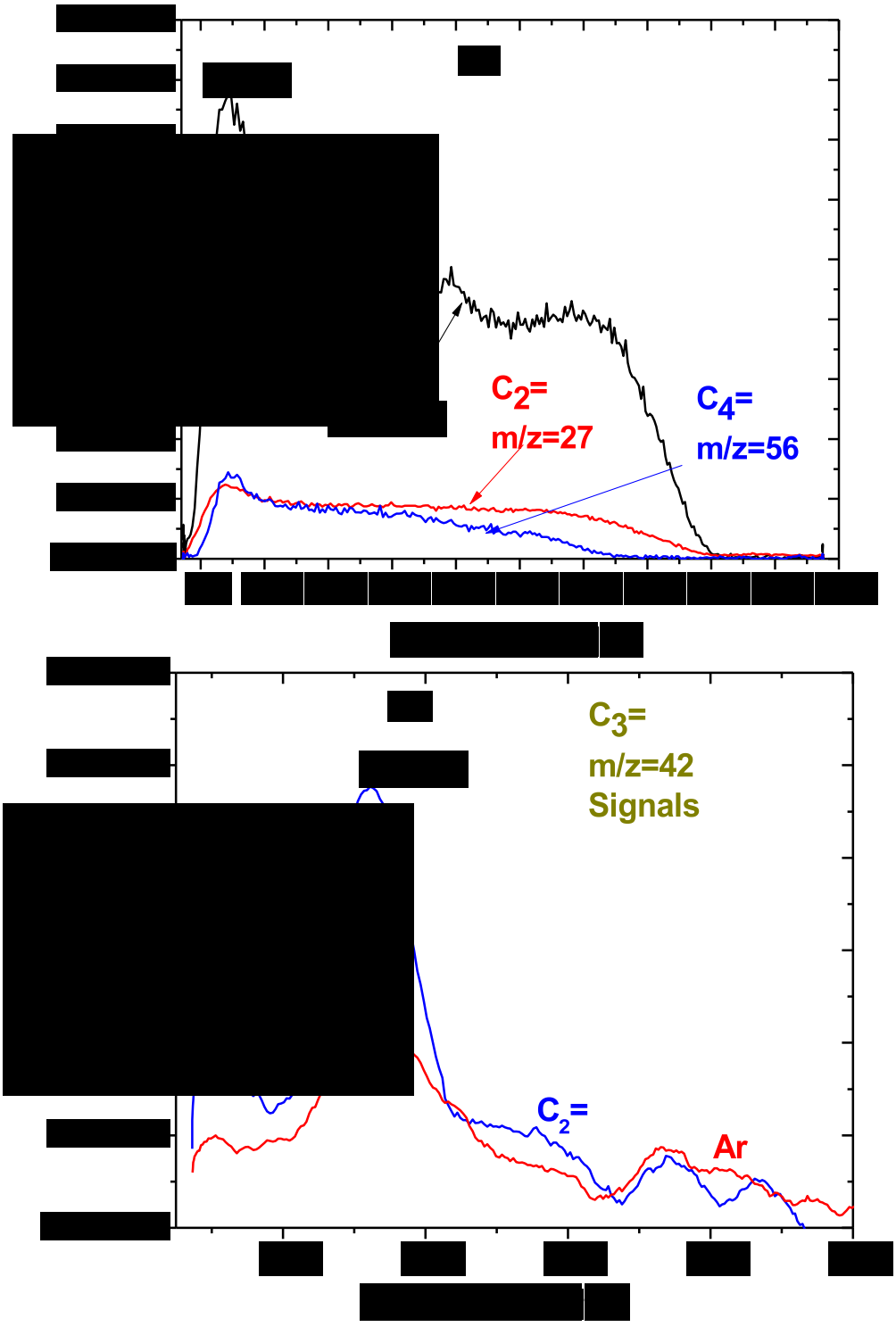

Figure S4.4. TPSR in flowing different gases after 100°C C_3H_6 pretreatment and cooling to room temperature in Ar: (a) in C_3H_6 and (b) in C_2H_4 (blue) and Ar (red).

CHAPTER 5

Conclusions and Proposed Future Studies

The main objectives of the research presented in this thesis are to (1) obtain insights about molecular structures of reactive sites, intermediates and kinetics by heterogeneous supported metal oxide metathesis catalysts and (2) develop a fundamental understanding that will allow the synthesis of better catalysts.

1. Conclusions

The supported ReO_x/Al_2O_3 system is best suited for developing a comprehensive understanding of olefin metathesis by a supported metal oxide system due to its low temperature of operation and isolated active sites which provides unprecedented insights with careful design of experiments. Substantial new information is achieved *for the first time* for this system during our study. DFT simulations with *in situ* ^{18}O-^{16}O Raman, XAS (XANES/EXAFS) and UV Vis experiments indicates that rhenium is present on the Al_2O_3 support as two different isolated tetrahedral dioxo ReO_4 species, namely ReO_4-I and ReO_4-II. The more reactive and reducible ReO_4-II species are anchored on acidic μ_2 and μ_3 Al_{VI} sites whereas the less reactive ReO_4-I species are formed on basic μ_1 Al_{IV} sites. A synthesis method using Ta_2O_5 as a sacrificial agent was developed *for the first time* to isolate ReO_4-II species. These reactive species go through the pseudo-Wittig mechanism before formation of rhenium carbene centers. The intermediate reduced Re(+5) and (+6) species are also detected *for the first time* through *in situ* UV Vis studies with well-defined references. Our site counting experiments indicate that the methods employed in literature

are under-counting the number of active sites. The number of sites is a variable that is found to be dependent on temperature, pressure and promoters. Adsorption of ethylene creates very little sites compared to that of 2-butene. The unimolecular first order reaction with Re carbenes and Re-cyclobutanes is more dominant at 30-70°C whereas the bimolecular second order with C_3H_6 π-complexes occurs at 100-200°C. At intermediate temperatures, both reaction pathways are taking place and give rise to intermediate reaction orders between 1 and 2 in olefin partial pressure. The dependence of products on the titrant reactant pressure at low temperatures for the first order kinetics and all isotopomers indicating the same peak temperature for the second order kinetics show that desorption/production formation is the rate limiting step for both conditions. Over 300°C or above, the catalysts deactivate due to over-reduction.

2. Proposed Future Studies

Olefin metathesis will continue to be a source of on purpose production for both functionalized and linear olefins for a foreseeable future. This thesis lays out a plethora of ideas for both catalyst design and operating conditions for those interested in this reaction. More synthesis methods with promotors and modifiers could be employed to synthesize further advanced supported metal oxide (ReO_x, MoO_x and WO_x) catalysts. Similar *in situ* and *operando* characterization studies along with steady state and TPSR experiments can be thoroughly designed for these systems to find the nature of active sites, reaction intermediates and kinetics. Further studies in these systems will bridge the gap between homogenous/organometallic and heterogeneous catalysts.

CURRICULUM VITAE

Soe Lwin
7 Asa Drive
Bethlehem, PA 18015
Phone: (484) 635-0877
Email: soe.lwin@lehigh.edu or soelwin2542@gmail.com

BACKGROUND SUMMARY

Chemical engineer with process engineering, safety and operations experience at a Fortune 500 oil and gas company. Extensive catalyst synthesis, surface characterization and reaction engineering experience during PhD career. Proven record of writing successful research grants with two approved proposals. PhD research resulted in two keynote presentations at major conferences. Received numerous personal and professional awards for academic, engineering and research excellence.

Full resume with dates of degrees, list of publications and references available upon request